

The Biogeochemistry and Biomarkers at Contrasting Sites of Terrestrial Serpentinization

by

© Melissa C. Cook

A thesis submitted to the School of Graduate Studies in partial fulfilment of the requirements for the degree of Doctor of Philosophy

Department of Earth Sciences
Memorial University of Newfoundland

July 2022

St. John's, Newfoundland and Labrador

Abstract

The range of aqueous and gaseous geochemistry and how it impacts potential metabolisms and microbial community composition at sites of serpentinization remains poorly understood. Therefore, the goal of this thesis was to characterize the aqueous and gaseous geochemistry and microbial communities at three distinct sites of serpentinization: The Cedars (CA, USA), Aqua de Ney (CA, USA), and the Tablelands (NL, CAN). The results demonstrate that there are many commonalities between these sites including ultra-basic, reducing fluids with high concentrations of methane. Isotopic data (i.e., $\delta^{13}\text{C}$ and $\delta^2\text{H}$), however, suggests that the methane from The Cedars is at least partially microbial, the Tablelands is non-microbial, and Aqua de Ney is abiogenic.

The geochemical results were used to create thermodynamic predictions (A_r) of reactions that could support microbial metabolisms. The A_r results demonstrate that although the values for each reaction are similar among sites, there is variation in available energy between reactions. Potential microbial metabolisms were tested in microcosm experiments and while there was little evidence of the expected metabolisms (i.e., carbon monoxide oxidation, hydrogen oxidation), microbial methanogenesis was observed in experiments from The Cedars.

Fluid and carbonate samples from The Cedars were analyzed for lipid biomarkers to determine the microbial community composition and identify lipids indicative of microbial methanogenesis. Although no archaeal lipids, including those indicative of methanogens, were detected in samples, chlorophyll *a* and pheophytin *a* were detected in carbonate samples but not fluids. These pigments could indicate the presence of cyanobacteria in carbonates at The Cedars.

Finally, Winterhouse Canyon Microbial Observatory (WHCMO) was established to understand the microbial community composition free from surface contributions. Results from the phospholipid fatty acid analysis suggested that the microbial community at WHCMO was largely eukaryotic and likely not representative of ultra-basic subsurface fluids. Winterhouse Canyon 2, a site where subsurface and surface fluids mix, was also sampled and the microbial community composition was determined to be largely non-eukaryotic and likely dominated by ultra-basic subsurface fluids. Overall, this thesis advanced the knowledge of serpentinizing systems by quantifying the range of geochemistry, the potential energy for metabolisms, and the microbial community composition and metabolisms.

Acknowledgements

First, I would like to thank Dr. Penny Morrill for all of the support and guidance you have provided as my supervisor. Your kindness and mentorship throughout this process has been invaluable. I wouldn't be the scientist I am today without you.

Next, thank you to my committee members, Dr. Mike Babechuk and Dr. Sue Ziegler, for your expertise and helpful edits on my thesis. I am also grateful for the intellectual, analytical, and field contributions of my collaborators, Dr. Jennifer G. Blank, Dr. Shino Suzuki, Dr. Kenneth H. Neelson, Dr. Todd Ventura, Jeremy Bentley, Amanda Rietze, Joshua Winter, Ian N. Coxon, and Emily Cumming.

This research was supported by grants from Natural Science and Engineering Research Council (NSERC) Discovery Grant and Canada Space Agency's Flights and Fieldwork for the Advancement of Science and Technology (FAST) awarded to Dr. Penny Morrill, as well as NSERC's Alexander Graham Bell Canada Graduate Scholarship-Doctoral (CGS-D) and financial support from Memorial University of Newfoundland.

I would also like to acknowledge the technical expertise of Dr. Geert van Biesen, Dr. Inês Nobre Silva, and Jamie Warren. Thanks as well to all of the current and past members of the DELTAS research group for your assistance throughout my time at MUN.

I would like to thank my fellow graduate students, particularly Roddy Campbell, Euri Papanicolaou, Anthony Valvasori, and Carly Mueller, for your support, for keeping me motivated throughout my degree, and for learning more about serpentinization than you probably ever wanted to.

Finally, I would like to thank my friends and family – particularly my parents Cheryl and Gary, my sister Tiffany, and my partner Mike – for your love and encouragement. I would not have made it to this point without you. I am eternally grateful.

Table of Contents

Abstract	ii
Acknowledgements	iv
List of Figures	viii
List of Tables	xiii
List of Abbreviations and Symbols	xv
Chapter 1. Introduction and Overview	1
1.1 The Serpentinization Reaction	1
1.2 Microbial Communities at Sites of Terrestrial Serpentinization	2
1.3 Ophiolite Field Settings in this Study	5
1.4 Thesis Objectives	7
1.5 Context of Research in Discipline	9
1.6 Co-authorship Statement	11
Chapter 2. A Geochemical Comparison of Three Terrestrial Sites of Serpentinization: the Tablelands, The Cedars, and Aqua de Ney	15
2.1 Introduction	17
2.2 Methods	25
2.3 Results	34
2.4 Discussion	47
2.5 Conclusions	62
2.6 Acknowledgments	63
2.7 References	64
2.8 Supplementary Information	76
Chapter 3. Assessing Geochemical Bioenergetics and Microbial Metabolisms at Three Terrestrial Sites of Serpentinization: the Tablelands (NL, CAN), The Cedars (CA, USA), and Aqua de Ney (CA, USA)	82
3.1 Introduction	84
3.2 Methods	89
3.3 Results	98
3.4 Discussion	106
3.5 Conclusions	116
3.6 Acknowledgments	118
3.7 References	119

3.8 Supplemental Information	127
Chapter 4. The Lipid Biomarker Record at The Cedars: A Terrestrial Site of Serpentinization	133
4.1 Introduction	135
4.2 Methods	142
4.3 Results	147
4.4 Discussion	155
4.6 Acknowledgments	162
4.7 References	163
4.8 Supplemental Information	172
Chapter 5. The Microbial Community Composition Within Ultra-basic Springs at an Active Site of Serpentinization: the Tablelands, NL, CAN	175
5.1 Introduction	177
5.2 Methods	182
5.3 Results	196
5.4 Discussion	207
5.6 Acknowledgments	221
5.7 References	222
5.8 Supplemental Information	231
Chapter 6. Summary	232
6.1 Conclusions	232
6.2 Outlook	235
References	238

List of Figures

Figure 1.1. Map of North America depicting the locations of The Cedars, Aqua de Ney, and the Tablelands. 5

Figure 2.1. Geologic maps of the three sites of terrestrial serpentinization chosen for this study: (A) the Tablelands, Canada, (B) The Cedars, U.S.A. and (C) Aqua de Ney, U.S.A. The sources from these maps came from (A) NL survey (<http://gis.geosurv.gov.nl.ca/>) and the federal Department of Natural Resources (<https://geogratis.gc.ca/>) and (B), (C) the U.S. Geologic Survey (<https://www.usgs.gov/products/maps/geologic-maps>). The contour interval is (A) 20 meters and (B), (C) 40 feet. 21

Figure 2.2. Images of sampling locations at the Tablelands (A) Winter House Canyon 2 (WHC2) and (B) Winter House Canyon 2 pool that has been emptied to collect recharge (WHC2-s), The Cedars (C) Grotto Pool Spring (GPS) and (D) Barnes Spring Complex (BSC), and Aqua de Ney (E) Ney Spigot and (F) Ney Well. 27

Figure 2.3. Hydrogen and oxygen isotope values of fluid samples from The Cedars, the Tablelands, and Aqua de Ney compared to the Global Meteoric Water Line (GMWL), $\delta^2\text{H} = 8 \delta^{18}\text{O} + 10$ (Harmon, 1961); Californian Local Meteoric Water Line (LMWL CA), $\delta^2\text{H} = 7.8 \delta^{18}\text{O} + 5.4$ (Coplen & Kendall, 2000); and the Oregon Local Meteoric Water Line (LMWL OR), $\delta^2\text{H} = 8.7 \delta^{18}\text{O} + 17.5$ (Kendall & Coplen, 2001). Error bars associated with sample points indicate \pm one standard deviation (1σ) of the reported values. 35

Figure 2.4. (A) Total inorganic carbon (TIC) concentrations (moles of $\text{C}\cdot\text{L}^{-1}$) in logarithmic scale versus $\delta^{13}\text{C}_{\text{TIC}}$ and (B) dissolved organic carbon (DOC) concentration (moles of $\text{C}\cdot\text{L}^{-1}$) versus $\delta^{13}\text{C}_{\text{DOC}}$ of groundwater, pooled/well water, and surface water from Tablelands, The Cedars, and Aqua de Ney. Error bars associated with sample points indicate \pm one standard deviation (1σ) of the reported values. 40

Figure 2.5. Natural gas plot showing the $\delta^{13}\text{C}$ values of methane, butane, and propane of dissolved and bubbling gases in groundwater and pooled water at the Tablelands, The Cedars, and Aqua de Ney. Dissolved gases are indicated by (d) in the site name while bubbling gases are indicated by (g) in the site name. **43**

Figure 2.6. Piper diagram illustrating the relationships in fluid composition between (A) ultra-basic and surface water endmembers and pooled waters at the Tablelands, The Cedars, and Aqua de Ney and (B) ultra-basic fluids from the Samail Ophiolite in Oman (Miller et al., 2016; Paukert et al., 2012), the Ojén peridotite massif and the Ronda peridotite massif (Giampouras et al., 2019), and Hakuba Happo (Suda et al., 2014). The amount of total dissolved solids (TDS), calculated using Geochemist’s Workbench, are indicated by the red circle..... **49**

Figure 2.7. A DC plot of $\delta^2\text{H}$ versus $\delta^{13}\text{C}$ for methane bubbling from the ultra-basic reducing spring at Aqua de Ney and for dissolved methane at the ultra-basic reducing springs at the Tablelands and The Cedars. Corresponding values for $\delta^2\text{H}$ versus $\delta^{13}\text{C}$ for methane from the Chimaera seep in Turkey (Etiope et al., 2011), the Samail Ophiolite in Oman (Miller et al., 2016), the Zambales ophiolite in the Philippines, Hakuba Happo in Japan (Suda et al., 2014), and CROMO in CA, U.S.A. (Wang et al., 2015) are also plotted. Empirically derived fields for microbial, thermogenic, and abiogenic methane production, as proposed by Etiope and Sherwood Lollar (2013) and references therein, are included for comparison..... **56**

Figure 2.8. Bernard Plot of lower molecular weight hydrocarbons from this study and published studies for the Tablelands (Cumming et al., 2019) and The Cedars (Morrill et al., 2013; Morrill unpublished data) compared to conventional fields for microbial and thermogenic gases (adapted from Hunt, 1996). Data points that plot between the two fields suggest a mixing of multiple

sources of methane or secondary process are occurring that affect the gaseous hydrocarbons of the lower springs. 58

Figure 2.9. Dual fractionation plot showing the fractionation factors between reactants and products for each site plotted along with the fields established by Cumming et al., 2019 for abiogenic CH₄, and microbial CH₄ formed via the carbonate reduction (CR) pathway and the and fermentation (AF) pathway. The $\alpha^{13}\text{C}(\text{TIC}-\text{CH}_4)$ data from this study was converted to $\alpha^{13}\text{C}(\text{CO}_2-\text{CH}_4)$ using the method described in Kohl et al., 2016). 60

Figure 3.1. Normalized headspace concentrations of methane (Eq. 3.13) in (A) The Cedars. (B) the Tablelands, and (C) Aqua de Ney methane oxidation microcosm experiments. Error bars indicate \pm one standard deviation (1σ) from the mean of triplicate treatments. There was no observable reduction of methane concentrations indicative of methane oxidation in the Tablelands or Aqua de Ney microcosms. In The Cedars microcosms, there was an overall increase in microbial methane concentrations, with a slight decrease between days 90-210 in the oxygen amended and live control microcosms. 101

Figure 3.2. Schematic of methane sources and sinks at terrestrial sites of serpentinization. The reactions with larger calculated chemical affinities (A_r) are represented by thicker arrows. 113

Figure 4.1. Topographic map of The Cedars, California, U.S.A (modified from the U.S. Geological Survey, Cazadera, CA, 2011). Springs discussed in this study are indicated by red stars. 143

Figure 5.1. Images of sampling locations at the Tablelands (A) Winterhouse Canyon 2 (WHC2) where the green star represents WHC2a, the yellow star WHC2b, and the red star WHC2c (B) Winter House Brook (WHB) and (C) Winterhouse Canyon Microbial Observatory 1 (WHCMO1) (pink), WHCMO2 (orange), and WHCMO3 (yellow). 184

Figure 5.2. Geologic map (modified from Berger et al., 1992) demonstrating the sampling locations (red stars) within the Tablelands massif. Map modified from Cook et al. (2021, Chapter 2). **185**

Figure 5.3. (A) The sterilized incubators and (B) the incubators after a year of exposure to the ultra-basic fluids at WHCMO. **188**

Figure 5.4. Piper diagram illustrating the relationships in fluid composition between WHC2a, WHC2b, WHC2c, WHCMO, and WHB. **198**

Figure 5.5. Hydrogen and oxygen isotope values of water samples from WHC2, WHB, and WHCMO compared to the Global Meteoric Water Line (GMWL), $\delta^2\text{H} = 8 \delta^{18}\text{O} + 10$ (Harmon, 1961) and Newfoundland Local Meteoric Water Line (LMWL) (Marche, 2016). The error bars are the standard deviations (1σ) of the duplicate samples. The error bar for the $\delta^2\text{H}_{\text{H}_2\text{O}}$ of water sampled from WHCMO is smaller than the plotted symbol..... **199**

Figure 5.6. Total concentrations of PLFAs extracted from samples from WHC2 (μg of C/g of carbonate) and WHCMO (μg of C/g of ultramafic substrate) presented on a logarithmic scale. The total PLFA extract from WHB (2018) was $4.7 \mu\text{g}$ of C/mL of water..... **201**

Figure 5.7. Microbial community composition at the Tablelands by phylogenetic groupings as assigned according to references in Table 5.5. **209**

Figure 5.8. (A) Relationship between the pH of ultra-basic springs within the Tablelands and the combined bacterial fraction (%) and (B) relationship between the E_h of the ultra-basic springs within the Tablelands and the combined bacterial fraction (%). Note that the combined bacterial fraction only includes non-specific, gram-negative, and gram-positive bacteria and only samples where data is available were plotted. **213**

Fig 5.9. Relationship between the total PLFA biomass extracted from WHC2a, WHC2b, WHC2c, and WHCMO (μg of C/g sample), the sum of energy densities (kcal/L H_2O) and E_h (mV)..... **218**

List of Tables

Table 2.1. Summary of environmental parameters and ion concentrations of groundwater, surface water, and pooled water at the Tablelands, The Cedars, and Aqua de Ney.....	38
Table 2.2. Composition of dissolved gases measured in groundwater and pooled water at the Tablelands, The Cedars, and Aqua de Ney.....	44
Table 2.3. Composition of bubbling gases measured at The Cedars and Aqua de Ney.*	46
Table 3.1. Reactions Used for Chemical Affinity Calculations and Corresponding Number of Electrons (e-) Transferred for Each Reaction.	90
Table 3.2. Environmental Parameters and Ion Concentrations in Spring Waters from the Tablelands, The Cedars, and Aqua de Ney.....	99
Table 3.3. Average Relative Oxygen and Hydrogen Concentrations in the Headspace of The Cedars' Live Oxygen-Containing and Control Treatments (Eq. 3.13).....	103
Table 3.4. Average Relative pH and E_h Measurements of Fluids of Live and Control Microcosms from The Cedars (Eq. 3.13).	104
Table 3.5. Average Relative Carbon Monoxide and Hydrogen Concentrations in the Headspace of Aqua de Ney Live Carbon Monoxide-Containing and Hydrogen-Containing Treatments (Eq. 3.13).	105
Table 3.6. Affinities (kcal/(mol·e ⁻)) of 10 Possible Reactions at 5 Terrestrial Sites of Serpentinization.	107
Table 4.1. Total Lipid Extracts (TLE) from filters and carbonate samples from four springs at The Cedars.	147
Table 4.2. Summary of lipids present within filter samples from BSC, GPS, and NS1 at The Cedars.	149
Table 4.3. Summary of lipids detected in TLE from carbonate sample from BSC.....	152

Table 5.1. Reactions Used for Chemical Affinity and Energy Density Calculations and Corresponding Number of Electrons (e-) Transferred for Each Reaction.....	194
Table 5.2. Summary of geochemical parameters of WHCMO, WHC2a, WHC2b, WHC2c, and WHB at the Tablelands.....	197
Table 5.3. Composition of dissolved gases measured in WHC2 and WHCMO.....	200
Table 5.4. Distribution of mol% of PLFAs detected in WHC2a, WHC2b, WHC2c, and WHB.	203
Table 5.5. Distribution of mol% of PLFAs detected in WHCMO1, WHCMO2, and WHCMO3.	205
Table 5.6. Summary of PLFA detected in this study and their interpretation for WHC2, WHB, and WHCMO.....	208
Table 5.7. Affinities (A_r) (in kcal/mol·e ⁻) of 8 possible reactions at the Tablelands organized by decreasing values of A_r	216
Table 5.8. Energy densities (E_r) (in kcal/L H ₂ O) of 8 possible reactions at the Tablelands organized by decreasing values of A_r	217

List of Abbreviations and Symbols

% – parts per hundred

‰ – parts per thousand

°C – degrees Celsius

α – isotopic fractionation factor

$\delta^{13}\text{C}$ – stable isotope composition of carbon

$\delta^2\text{H}$ – stable isotope composition of hydrogen

$\Delta_r G^\circ$ – standard Gibbs energy

ΔG° – standard molal Gibbs free energy of formation

^3H – tritium

AC – Austin Creek

ACN – acetonitrile

ANME – anaerobic methanotrophic archaea

A_R – chemical affinity

A_{rC_w} – chemical affinity of gases in aqueous phase

ATP – Adenosine triphosphate

BOIC – Bay of Islands Complex

BSC – Barnes Spring Complex

C_{2+} – sum of ethane, propane, and butane

CAPS – N-cyclohexyl-3-aminopropanesulfonic acid

CROMO – Coast Range Ophiolite Microbial Observatory

C_w – concentrations of gases in aqueous phase

DAG – diacylglycerols

DAGE – dialkyl glycerol diether

DCM – dichloromethane

DOC – dissolved organic carbon

e^- – electron

E^3H – electrolytic tritium

E_h – reduction/oxidation potential measurement

ESI – electrospray ionization

FAME – fatty acid methyl esters

f_{UB} – fraction of ultra-basic water

FID – Flame ionization detector

GC – gas chromatograph

GC-C-IRMS – gas chromatography combustion isotope ratio mass spectrometry

GDGT – glycerol dialkyl glycerol tetraethers

GFF – glass fiber filter

GMWL – global meteoric water line

GPS – grotto pool spring

Gram +ve – Gram positive bacteria

Gram -ve – Gram negative bacteria

ICP-MS – Inductively Coupled Plasma Mass Spectrometer

ICP-OES – Inductively Coupled Plasma Optical Emission Spectrometer

IPL – intact polar lipid

IRMS – isotope ratio mass spectrometer

K_r – equilibrium constant

K_{sp} – solubility product

LCHF – Lost City Hydrothermal Field

LMWL – local meteoric waterline

NDIR – non-destructive infrared

NL – Newfoundland

N-POC – non-purgeable organic carbon

ORP – oxidation reduction potential

PCC-1 – international peridotite standard

PLFA – phospholipid fatty acid

M – analyte of interest

Ma – 1 million years ago

MAGE – monoalkyl glycerol monoether

MBD – modified Bligh and Dyer

MCE – mixed cellulose ester

m/z – mass to charge ratio

PAF – 1-alkyl-2-acetyl-sn-glycero-3-phosphocholine

PMI – pentamethylcosane

Q_r – the activity product

R – ideal gas constant

rRNA – ribosomal ribonucleic acid

RSD – relative standard deviation

T – temperature

TAG – triacylglycerol

TCD – thermal conductivity detector

TIC – total inorganic carbon

TLE – total lipid extract

TU – tritium units

uHPLC-qToF-MS – ultra-high-performance liquid chromatography-quadrupole time of flight mass spectrometer

WHB – Winter House Brook

WHC2 – Winter House Canyon 2 pool

WHC2-s – Winter House Canyon groundwater spring

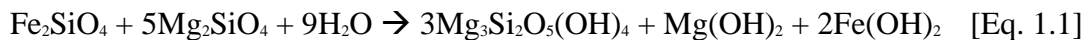
WHCMO – Winter House Canyon Microbial Observatory

Chapter 1. Introduction and Overview

1.1 The Serpentinization Reaction

The oceanic crust and upper mantle of the Earth are composed of mafic and ultramafic rocks. Tectonic activity can result in sections of this oceanic crust and upper mantle being obducted onto continental crust, creating an ophiolite. Many ophiolites are underlain by sedimentary organic matter that can be reduced resulting in the production of thermogenic methane that can be transported to the surface. Examples of ophiolites exist throughout the world including the Samail Ophiolite, located in the Sultanate of Oman, the Chimaera Ophiolite, located in Turkey, the Tablelands Ophiolite located in Canada, and Northern California's Coast Range Ophiolite and the Trinity Ophiolite located in the USA, to name a few.

When ultramafic minerals in these ophiolite sections are exposed to near-surface conditions the ultramafic minerals become thermodynamically unstable. These ultramafic minerals can be hydrated in an exothermic process called serpentinization. Serpentinization can be generally described by Eq. 1.1 and 1.2 where olivine and pyroxene are the ultramafic minerals which are altered to serpentine group minerals (Schulte et al., 2006).

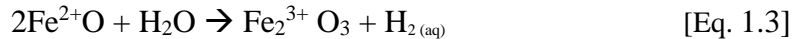


fayalite + forsterite + water \rightarrow serpentine + brucite + iron hydroxide



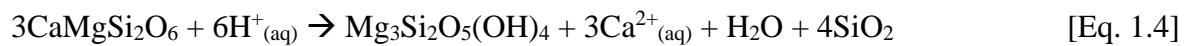
forsterite + pyroxene + water \rightarrow serpentine

As fluids move deeper into the subsurface, they are isolated from the atmosphere and become depleted in O_2 and CO_2 which results in H_2O becoming the main oxidant. This generates H_2 through the oxidation of ferrous iron in primary minerals (e.g., olivine, iron hydroxide) and results in the production of ferric iron in secondary minerals (e.g., magnetite). The H_2 generation can be generally described by Eq. 1.3 (Leong and Shock, 2020).



Iron (II) + water → Iron (III) + hydrogen

In the presence of the elevated temperatures, hydrogen gas, and iron catalysts produced by the serpentinization reactions, Ca-silicates are unstable leading to an increase in Ca^{2+} concentrations in the fluids. The production of Ca^{2+} ions consumes hydrogen ions causing the pH of the fluids to increase (pH > 11) (Eq. 1.4) (Frost & Beard, 2007).



diopside

serpentine

The fluids that result from serpentinization reactions are conducive to the production of abiotic methane through the reaction of hydrogen with inorganic carbon (Sleep et al., 2004). Furthermore, many ophiolites are underlain by, or adjacent to, organic bearing sediments which can be thermally degraded resulting in the production of thermogenic hydrocarbons such as methane.

1.2 Microbial Communities at Sites of Terrestrial Serpentinization

Although these fluids are rich in electron donors (i.e., hydrogen and methane) they contain very few electron acceptors (i.e., sulfate, nitrate, or oxygen) that are required by microorganisms for their metabolic activities (Morrill et al., 2013). The high pH of these fluids can also interfere with the production of adenosine triphosphate (ATP) and the inorganic carbon dissolved in these fluids is predominantly in the form of the carbonate ion, which is not usually biologically available (Krulwich et al., 2011; Suzuki et al., 2013). Despite these challenges, groundwaters associated with sites of serpentinization have been found to host diverse microbial communities. *Serpentinomonas*, a hydrogen-utilizing carbon-fixing *Betaproteobacteria* has been found at many terrestrial sites of serpentinization including the Tablelands, Canada (Brazelton et

al., 2013; Brazelton et al., 2012), The Cedars, USA (Suzuki et al., 2014), and Coast Range Ophiolite Microbial Observatory (CROMO), USA (Twing et al., 2017) by 16S rRNA gene sequencing. 16S rRNA gene sequences also revealed evidence of sulfur-cycling microorganisms in fluids sampled from CROMO (Sabuda et al., 2020). RNA and DNA analyses on fluids from CROMO have also suggested the presence of methane oxidizers (Seyler et al., 2020). 16S rRNA analyses on fluids from sites of terrestrial serpentinization have also revealed the presence of methanogens, archaea capable of producing methane. Methanogens were detected in fluids from the Del Puerto Ophiolite, USA (Blank et al., 2009) and an archaeal sequence that placed closely to the order *Methanosarcinales* in the phylogenetic tree was also detected at The Cedars (Suzuki et al., 2013). Therefore, in addition to a potential abiotic source of methane, methane at some serpentinite-hosted springs may be microbial in origin.

While microbial communities are typically inferred from genomic-based techniques, these techniques often rely on the amplification of extractable DNA from host cells. Lipids, however, constitute the main component of cellular membranes and do not rely on amplified signals. Furthermore, lipids can be preserved much longer in the rock record than DNA, which can be preserved for a few million years at most (Willerslev et al., 2004). While the preservation potential of lipids at sites of serpentinization is not well constrained, studies suggest certain lipids can be preserved in carbonate and carbonate-bearing rocks for hundreds of millions of years (Love et al., 2009; Saito et al., 2015; Saito et al., 2017). Phospholipid fatty acids (PLFAs) a type of lipids which form double layered membranes of Bacteria and Eukarya, by contrast, tend to degrade rapidly after cell death which provides information about the microbial community at the time of sampling (White et al., 1979). Therefore, unlike genomic-based techniques, lipid biomarkers can provide an overall picture of both the extant and extinct microbial communities

(Simoneit et al., 2004; Willerslev et al., 2004; Love et al., 2009; Saito et al., 2015; Saito et al., 2017).

Currently, there are limited lipidomic studies on sites of terrestrial serpentinization. Zwicker et al. (2018) analyzed lipid biomarkers in carbonate and rock samples from the Chimaera Ophiolite and found lipids likely indicative of methanogens and bacterial sulfate-reducers. Similarly, carbonate, travertine, and rock samples from the Samail Ophiolite also contained lipids likely indicative of methanogens and bacterial sulfate-reducers (Newman et al., 2020).

While lipidomic and genomic studies can provide indirect evidence for the presence or absence of microorganisms, they cannot determine whether these metabolisms (i.e., methanogenesis) are active in the system. Furthermore, they do not provide insight into the substrates that are utilized by these microorganisms. When these ultra-basic reducing fluids that are produced by the serpentinization reaction exit the subsurface, they can interact with the oxic atmosphere or surface waters and form pools. In addition to providing oxidized carbon and other electron acceptors to the system, the interaction of these fluids can create large redox gradients that provide energy for life. This potential energy can be quantified thermodynamically by calculating chemical affinities (A_r) (Eq. 1.5) (Canovas et al., 2017; Helgeson & Murphy, 1983).

$$A_r = RT \ln \left(\frac{K_r}{Q_r} \right) \quad [\text{Eq. 1.5}]$$

where R is the ideal gas constant, T is the temperature (in Kelvin), K_r is the equilibrium constant and Q_r is the activity product which is determined from analytical data of field samples.

By calculating the A_r , likely metabolisms can be identified and ranked by the energy available for that specific metabolism. Furthermore, these metabolisms can be tested through creation of microcosm experiments that contain native microbial communities. By monitoring the microcosms for substrate consumption and reaction products, direct evidence of microbial metabolisms can be obtained.

1.3 Ophiolite Field Settings in this Study

This thesis investigates the geochemistry, microbial metabolisms, and lipid biomarkers at three contrasting terrestrial sites of serpentinization: The Cedars, (CA, USA), Aqua de Ney (CA, USA), and the Tablelands, (NL, Canada) (Figure 1.1).



Figure 1.1. Map of North America depicting the locations of The Cedars, Aqua de Ney, and the Tablelands.

The Cedars, located in Sonoma County, California, USA, is a part of Northern California's Coast Range Ophiolite. The ophiolite is of Jurassic-age and was emplaced as part of the Franciscan Subduction Complex between 170-164 MA (Coleman, 2000; Shervais et al.,

2004) making The Cedars the youngest of the sites chosen for this thesis. Previous geochemical studies on fluids from The Cedars have shown that serpentinization is actively occurring based on the geology, ultra-basic reducing fluids (pH < 11, Eh > -585 mV), and the methane and hydrogen that bubbles from the springs (Barnes et al., 1967; Morrill et al., 2013). Geochemical studies on the methane from The Cedars (Kohl et al., 2016; Morrill et al., 2013; Wang et al., 2015) suggested it was at least partially microbial in source. Further 16S rRNA analyses by Suzuki et al. (2013) were only able to detect a single archaeal phylotype. Although the phylotype placed closely to *Methanosarcinales* in the phylogenetic tree, the sequence did not fit with any known methanogen (Suzuki et al., 2013).

Aqua de Ney, located in Siskiyou County, California, USA, is part of the Trinity Ophiolite Complex (Feth et al., 1961) that was emplaced between 431-404 Ma (Wallin & Metcalf, 1998). The groundwater at Aqua de Ney is unique among sites of serpentinization due to its high silica (4000 mg/L) and bicarbonate (15600 mg/L) concentrations. The fluid is also rich in sulfide in the form of H₂S (1000 mg/L) (Feth et al., 1961), however, the source of this sulfide remains unknown. The groundwater at Aqua de Ney bubbles with methane (>80 % by volume) (Mariner et al., 2003), however, the source of the methane remains poorly understood. It is also the only site of the three with the presence of a higher temperature (240 °C) geothermal system (Boschetti et al., 2017). There is currently no genomic data available on microbial communities at Aqua de Ney.

The Tablelands, located on the west coast of Newfoundland, Canada, is also known as Tablelands Massif or Table Mountain Massif. The Tablelands Massif is one of four Ordovician massifs that make up the Bay of Islands Complex (BOIC) (Suhr, 1992). The Tablelands ophiolite was emplaced during the Middle Ordovician between 500-485 Ma (Dunning & Krogh, 1985)

making it the oldest site chosen for this thesis. There are indicators that serpentinization is still occurring at the Tablelands including the ultra-basic pH (> 12) of the fluids, as well as the methane and hydrogen that are dissolved in the fluids (Morrill et al., 2014; Szponar et al., 2013). Studies have suggested that methane from this site is non-microbial (i.e., thermogenic or abiotic origin) (Cumming et al., 2019; Szponar et al., 2013). Genomic data from the Tablelands has suggested that microbial communities do exist in the ultra-basic fluids including those capable of hydrogen and carbon monoxide utilization (Brazelton et al., 2013; Brazelton et al., 2012; Morrill et al., 2014).

1.4 Thesis Objectives

The aqueous and gaseous geochemistry of an environment can impact nutrient availability and therefore, possible metabolisms and the microbial community composition. Despite the understanding of common geochemical indicators of active serpentinization (e.g., ultra-basic, reducing fluids and the production of methane and hydrogen gases), the range of aqueous and gaseous geochemistry at terrestrial sites of serpentinization is not well constrained. Therefore, the first objective of this thesis was to compare and contrast the fluids from the three distinct sites of serpentinization (i.e., The Cedars, Aqua de Ney, and the Tablelands). To accomplish this, fluids and gases from each site were geochemically characterized for their concentrations and in the case of the gases, their stable carbon and hydrogen isotope values. From there, possible variations between sites of terrestrial serpentinization could be identified and working hypotheses for the causes in variability in the geochemistry could be developed.

While microbial communities have been detected at The Cedars and the Tablelands, the chemical affinities supplied by the serpentinization reaction, as well as what metabolisms could be supported have not yet been quantified. The second objective of this thesis was to use the geochemistry that was established in objective one to create thermodynamic predictions of

potential microbial metabolisms supported in serpentinite-hosted ground waters, and in environments where serpentinite-hosted ground waters interact with oxic surface fluids and atmosphere. These chemical affinities could then be ranked in order of decreasing energy and thus the likeliness of them occurring at sites of serpentinization. These thermodynamic predictions were then tested in laboratory-based experiments using microcosms that contained fluids and native microbial communities from The Cedars, Aqua de Ney, or the Tablelands. Each microcosm was supplied with the required reactants of the metabolisms of interest and then analyzed for changes in concentrations of reactants and products.

Genomic and microcosm studies are frequently used to understand microbial communities that are present within serpentinite-hosted springs. These techniques, however, are limited. Microcosm studies, for example, rely on detecting products of microbial metabolisms, however, conditions created in the laboratory may not necessarily be representative of in situ conditions. Therefore, microorganisms may not survive under these simulated conditions and thus microbial metabolisms may not be observed. While genomic studies do not rely on simulated laboratory conditions, they require amplification of extractable DNA from host cells. Lipids, however, make up the cellular membranes of Archaea, Bacteria, and Eukarya. Lipidomic studies do not require amplification and lipids are well preserved in the rock record. Therefore, the third objective of this thesis was to use lipid biomarkers present in spring fluids and solid carbonates to create a profile of archaeal, bacterial, and eukaryotic communities that were present at a serpentinite-hosted spring, The Cedars. Interpreting lipid biomarkers can be challenging since they are not necessarily specific to a single microorganism. Therefore, the results of this study were then compared to previously published genomic studies to attempt to gain a better understanding of microbial communities (extant and extinct) at sites of

serpentinization. Specifically, because The Cedars is a site where the methane is, at least in part, microbial in origin, lipid biomarkers indicative of methanogens were considered.

While there have been some microbiological and geochemical studies to characterize the microbial communities at the Tablelands, there are no lipidomic studies. Furthermore, these studies have all been conducted on a pool (WHC2) where ultra-basic reducing fluids are thought to mix with oxic surface fluids. Although these mixed pools tend to harbour greater biomass (Schrenk et al., 2013), studies on fluids from the Samail Ophiolite in Oman have suggested that there are different microbial communities in the deep subsurface fluids than in the surficial hyperalkaline fluids (Rempfert et al., 2017). Therefore, the microorganisms that have been identified in samples from WHC2 may not be representative of the microbial communities in the subsurface. The fourth and final objective of this thesis was to characterize the microbial communities in the ultra-basic subsurface fluid at the Tablelands through establishing a microbial observatory. The microbial observatory was created by drilling three boreholes ~30 cm into the peridotite and inserting flow-through incubators filled with sterile crushed peridotite. These incubators remained in the boreholes for a year before they were removed and extracted for phospholipid fatty acids (PLFAs), the main lipid component of the cell membranes of Bacteria and Eukarya. PLFAs were also extracted from WHC2 and the nearby brook (WHB) to create a microbial community profile for the subsurface, mixed, and surface waters at the Tablelands. These were then used to determine how the microbial communities differ between sites and which sites harbour the greatest biomass.

1.5 Context of Research in Discipline

Serpentinization was likely prominent on early Earth when ultramafic rocks were more dominantly exposed at the surface (Sleep et al., 2004). Before the evolution of photosynthesis, the primary producers on early Earth would have relied on inorganic chemical sources of energy

such as serpentinization reactions. Furthermore, serpentinization reactions produce hydrogen gas which can support chemolithoautotrophic metabolisms such as methanogenesis and acetogenesis, by acting as an electron donor. Serpentinization could also supply a reduced carbon source in the form of abiotic hydrocarbons (McCollom & Seewald, 2007) and organic acids (Lang et al., 2018).

Orbital spectral imaging has also revealed the presence of ultramafic and serpentinized rocks on the surface of Mars (e.g., Nili Fossae and in the tectonically deformed Thaumasia Highlands) suggesting that serpentinization has occurred on Mars (Ehlmann et al., 2010; Viviano-Beck et al., 2017). Furthermore, methane has been detected in the Martian atmosphere (Formisano et al., 2004; Mumma et al., 2009) which could suggest the presence of life in the subsurface of Mars. However, conditions created by the serpentinization reaction are also conducive to the production of abiotic (i.e., non-microbial/geologic) methane so the presence of methane alone is not necessarily indicative of life. Therefore, it is necessary to understand the geochemical factors that lead to microbial methanogenesis, how to discern different methane sources, and how to identify microbial communities in these inaccessible environments.

Fluids that result from serpentinization reactions can discharge at ophiolites. These sites can act as analogues for these past and inaccessible sites of serpentinization. Furthermore, these sites also act as portals allowing us to study the subsurface biosphere. Through improving our understanding of the range of geochemistry and the metabolisms that sites of terrestrial serpentinization can sustain, we can further our understanding of life in the subsurface, on early Earth, and ultimately on other planetary bodies. By understanding not only how the microbial communities survive in these environments, but how they are preserved at sites of serpentinization can inform future missions to Mars and the search for life outside our planet.

1.6 Co-authorship Statement

Chapter 2. This chapter was accepted by the Journal of Geophysical Research – Biogeosciences (special issue on ophiolites and oceanic lithosphere) and therefore, follows the JGR manuscript submission guidelines:

Cook, M. C., Blank, J. G., Rietze, A., Suzuki, S., Nealson, K. H., & Morrill, P. L. (2021). A

Geochemical Comparison of Three Terrestrial Sites of Serpentinization: The Tablelands, The Cedars, and Aqua de Ney. *Journal of geophysical research. Biogeosciences*.

<https://doi.org/10.1029/2021JG006316>

As the first author of this thesis, I conducted all research pertaining to the objective of this manuscript including the literature review, research methodology, sample collection and analysis (except where stated below) and manuscript writing. Geochemical sampling at The Cedars took place in September 2017 with field assistance from Emily Cumming. Sampling at Aqua de Ney took place in June 2019 with field assistance from Dr. Penny Morrill and Dr. Jennifer G. Blank. Sampling at the Tablelands took place in July 2018 and July 2019 with field assistance from Dr. Penny Morrill, Emily Cumming, and Ben Taylor. Additional sampling at the Tablelands took place in October 2012 by Amanda Rietze. Jamie Warren, Dr. Geert van Biesen (CREAIT – Stable Isotope Laboratory), Dr. Inês Nobre Silva (CREAIT – ICPMS), and I did the sample analyses. I created the geologic maps in Chapter 2. Dr. Penny Morrill was responsible for the initial conceptualization of this project, provided valuable guidance on the direction of the research, and discussion of the results. Dr. Penny Morrill and the other co-authors provided editorial comments during the writing of the manuscript that greatly improved the quality of this manuscript.

Chapter 3. This chapter was accepted by the Journal of Geophysical Research – Biogeosciences (special issue on ophiolites and oceanic lithosphere) and therefore, follows the JGR manuscript submission guidelines:

Cook, M. C., Blank, J. G., Suzuki, S., Neelson, K. H., & Morrill, P. L. (2021b). Assessing Geochemical Bioenergetics and Microbial Metabolisms at Three Terrestrial Sites of Serpentinization: The Tablelands (NL, CAN), The Cedars (CA, USA), and Aqua de Ney (CA, USA). *Journal of geophysical research. Biogeosciences*, 126(6), n/a.

<https://doi.org/10.1029/2019JG005542>

As the first author of this thesis, I conducted all research pertaining to the objective of this manuscript including the literature review, research methodology, sample collection and analysis (except where stated below) and manuscript writing. Sampling for the microcosm experiments took place at The Cedars in September 2017 with field assistance from Emily Cumming. Sampling at Aqua de Ney took place in June 2019 with field assistance from Dr. Penny Morrill and Dr. Jennifer G. Blank. Sampling at the Tablelands took place in July 2018 with field assistance from Dr. Penny Morrill and Emily Cumming. Dr. Geert van Biesen (CREAIT – Stable Isotope Laboratory) and I did the sample analyses. Dr. Penny Morrill was responsible for the initial conceptualization of this project, provided valuable guidance on the direction of the research, and discussion of the results. Dr. Penny Morrill and the other co-authors provided editorial comments during the writing of the manuscript that greatly improved the quality of this manuscript.

Chapter 4. This chapter is a manuscript in preparation for journal submission:

Cook, M. C., Bentley, J.N, Ventura, G.T., Suzuki, S., Neelson, K.H., Morrill, P.L. (in prep). The Lipid Biomarker Record at The Cedars: A Terrestrial Site of Serpentinization.

As first author I conducted all research including the literature review, research methodology, sample collection, extraction, and analysis (except where noted below) and manuscript writing. Samples were collected from The Cedars in September 2017 with field assistance from Emily Cumming. I extracted and analyzed the samples in Dr. Todd Ventura's Organic Geochemistry laboratory at St. Mary's University (SMU) in Halifax, Nova Scotia. Samples were further analyzed by Jeremy N. Bentley (SMU) on uHPLC-qToF-MS under the supervision of Dr. Todd Ventura. Dr. Penny Morrill was responsible for the initial conceptualization of this project as outlined in grant proposals prior to starting the experiments. Dr. Penny Morrill and Jeremy N. Bentley provided valuable guidance on the direction of the research, discussion of the results, and editorial comments during the writing of the chapter.

Chapter 5. This chapter is a manuscript in preparation for journal submission:

Cook, M. C., Coxon, I. N., Szponar, N., Winter, J., Morrill, P.L. (in prep). The Microbial Community Composition Within Ultra-basic Springs at an Active Site of Serpentinization: the Tablelands, NL, CAN

As first author I conducted all research including the literature review, research methodology, sample collection and analysis (except where noted below) and manuscript writing. Samples were collected in July 2018 with field assistance from Dr. Penny Morrill, Emily Cumming, and Ben Taylor. The boreholes at the microbial observatory were drilled by Dr. Michael Babechuk and Dr. Penny Morrill. Dr. Geert van Biesen (CREAIT – Stable Isotope Laboratory), Dr. Inês Nobre Silva (CREAIT – ICPMS), and I analyzed the geochemical samples. Samples for PLFA (2010) were collected and extracted by Natalie Szponar. I collected the samples for PLFA (2018/2019). These samples were extracted by Joshua Winter. Samples for PLFA (2021) were collected and extracted by Ian N. Coxon. Samples for PLFAs were analyzed by Dr. Geert van

Biesen (CREAIT – Stable Isotope Laboratory). Ian N. Coxon, Natalie Szponar, Joshua Winter, and I analyzed the PLFA results. Dr. Penny Morrill was responsible for the initial conceptualization of this project as outlined in grant proposals prior to starting the experiments. Dr. Penny Morrill provided valuable guidance on the direction of the research, discussion of the results, and editorial comments during the writing of the chapter.

Chapter 2. A Geochemical Comparison of Three Terrestrial Sites of Serpentinization: the Tablelands, The Cedars, and Aqua de Ney

Melissa C. Cook¹, Jennifer G. Blank^{2,3}, Amanda Rietze¹, Shino Suzuki⁴, Kenneth H. Nealson⁵, Penny L. Morrill¹

¹Department of Earth Sciences, Memorial University of Newfoundland, St. John's, NL, Canada

²NASA Ames Research Center, Division of Space Sciences & Astrobiology, Moffett Field CA, USA

³Blue Marble Space Institute of Science, Mountain View, CA, USA

⁴Institute of Space and Astronautical Science, JAXA, Sagamihara Kanagawa, 252-5210, Japan

⁵Department of Earth Sciences, University of Southern California, Los Angeles, CA, USA

*This chapter was originally published in *Journal of Geophysical Research: Biogeosciences* 126:11. [Cook et al., 2021].*

Abstract

Although the Earth's subsurface hosts an abundance of microbial life, the influence of geochemistry on these communities remains poorly constrained. Ophiolites, sites where oceanic ultramafic minerals can be hydrated to serpentine minerals and metal oxides, create unique conditions capable of sustaining life. The fluid geochemistry of the Tablelands (NL, CAN), The Cedars (CA, U.S.A.), and Aqua de Ney (CA, U.S.A.), were studied to better characterize the range of fluid compositions observed at terrestrial sites of serpentinization. Fluids from these sites shared many commonalities including being ultra-basic and reducing as well as having elevated levels of Cl, Na, K, and Br as well as depleted concentrations of Mg. They also exhibited a wide range of geochemistry. Isotopic and compositional data suggested the CH₄ from The Cedars was a mixture of microbial and non-microbial sources while the CH₄ from the Tablelands was non-microbial in origin. Aqua de Ney was the only site where the CH₄ plotted in the abiogenic field. Despite being a known product of serpentinization, no H₂ was detected at Aqua de Ney, likely due to the formation of abiogenic CH₄ as well as the reaction of H₂ and SO₄²⁻ in the system to produce H₂S. These unique sites of terrestrial serpentinization help to better understand the range of geochemistry at sites of serpentinization and its influence on the microbial communities in the subsurface.

2.1 Introduction

2.1.1 The Subsurface Biosphere

Since the discovery of ecosystems in seafloor hydrothermal vent environments, it has been recognized that the subsurface of the Earth supports an abundance of microbial communities (Gold, 1992; Grassle, 1987; Lutz & Kennish, 1993). The primary producers in these settings, like those of Early Earth, cannot rely on photosynthetic sources of energy; they must, instead, rely on inorganic chemical sources of energy (i.e., lithoautotrophy). For lithoautotrophs to derive sufficient chemical energy for the required metabolisms, whether ancient or modern, their environment must be in a state of thermodynamic disequilibrium (Mitch Schulte et al., 2006). The most prominent source of chemical disequilibrium is the hydration of mafic and ultramafic rocks from the ocean crust (McCollom & Shock, 1997). This process, known as serpentinization, results in the alteration of olivine and pyroxene into serpentine minerals and iron-rich brucite. The iron-rich brucites can react with aqueous silica to form magnetite which is accompanied by the production of H_2 (Bach et al., 2006). Combined with the chemical disequilibrium created by the serpentinization reaction, H_2 can support chemoautotrophic biochemical processes, such as methanogenesis and acetogenesis, by acting as an electron donor (Brock, 1991; Nealson et al., 2005; Vance & Daswani, 2020). Because the resulting fluids are ultra-basic, reducing, and contain elevated concentrations of H_2 , these environments can also catalyze the formation of abiotic organic molecules, such as methane (Lang & Brazelton, 2020; McCollom & Seewald, 2007).

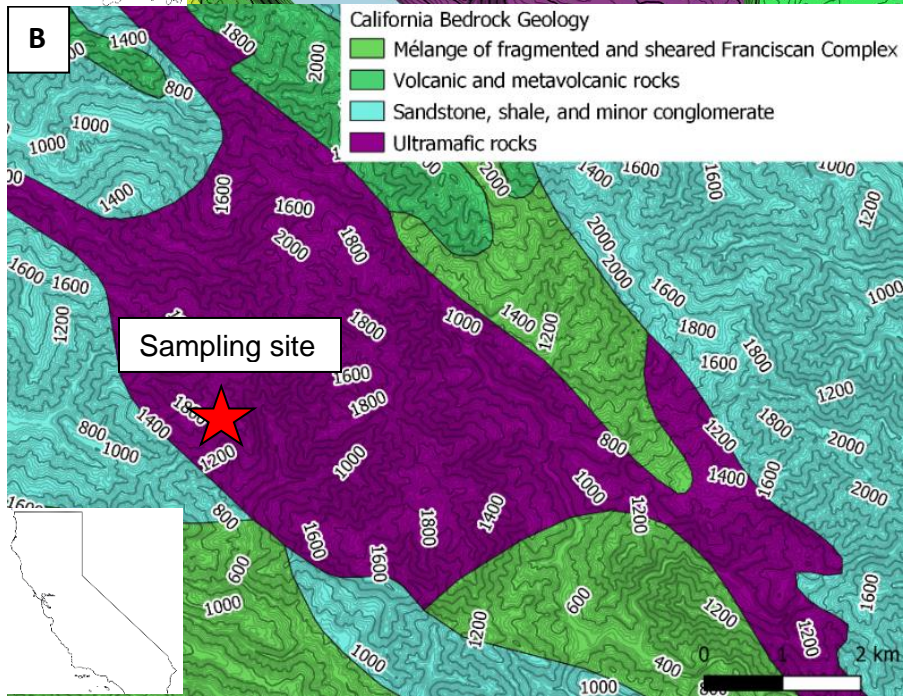
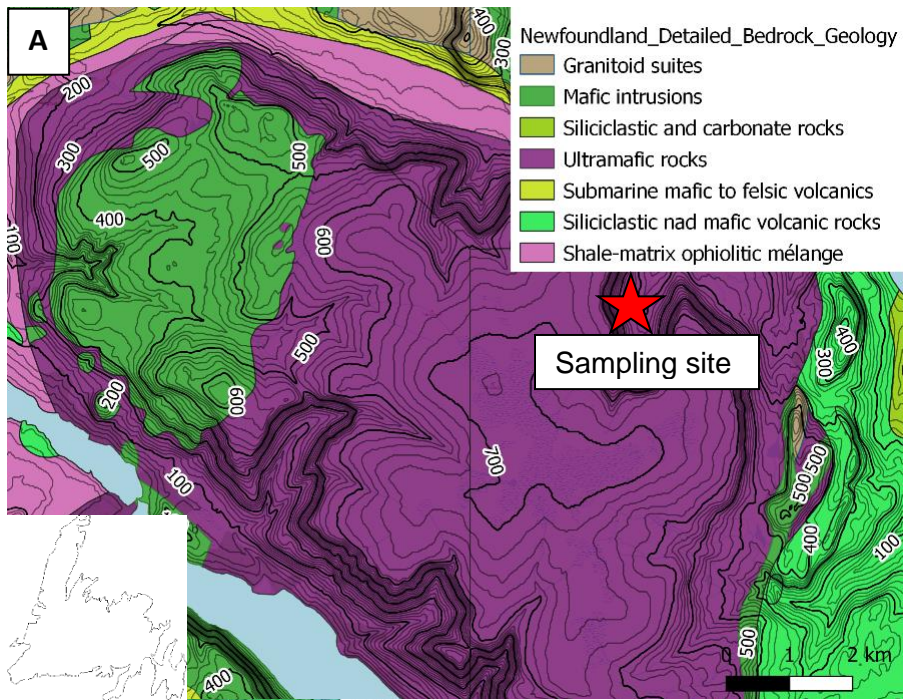
Despite the identification of a subsurface oceanic biosphere, its study remains challenging. Ophiolite suites, sections of former oceanic crust and upper mantle that have been emplaced on continental crust, provide one of the best natural windows into to these biospheres,

particularly if they discharge reducing ultra-basic fluids, derived from active serpentinization, that can be sampled and studied. Combinations of these fluids with more oxic and neutral surface waters mixes waters rich in electron donors and acceptors. This new mixed environment with a high redox gradient may support distinct microbial communities (McCollom & Seewald, 2013). Ophiolites exist throughout the world, and thus they offer potential to study a variety of subsurface microbiomes, as well as microbiomes associated with the interaction of subsurface and surface fluids.

The Samail Ophiolite, located in the Sultanate of Oman, is one of the most studied sites of terrestrial serpentinization. Rempfert et al. (2017) studied the geochemical compositions of subsurface fluids and found that even among fluids from the same ophiolite, there were large variations in the pH, concentration of H_2 , CH_4 , Ca, Mg, NO_3^- , SO_4^{2-} , trace metals, and DIC. They also found that the geochemistry of the fluids that result from serpentinization reactions was strongly correlated with the microbial community composition. Taxonomic and geochemical data from the Samail Ophiolite suggested that there were microbial communities capable of methanogenesis, acetogenesis, as well as the oxidation of methane and hydrogen. A microbial observatory was established in the Coast Range Ophiolite, CA, U.S.A. (CROMO, Coast Range Ophiolite Microbial Observatory) to monitor the biogeochemistry of the groundwater. When Crespo-Medina et al. (2014) geochemically characterized the fluids that result from serpentinization reactions sampled from the drillholes, there was also a variation in pH, oxidation reduction potential (ORP), H_2 , CH_4 and dissolved inorganic carbon (DIC) concentrations. Further genomic studies on fluids from CROMO have shown evidence of sulfur-cycling taxa as well as methanotrophs (Sabuda et al., 2020; Seyler et al., 2020).

Here, the geochemistry of fluids from three ophiolite settings in North America where serpentinization is active in the subsurface is evaluated. The measured ranges of compositional values are compared to characterize the potential of these fluids to support life in the subsurface, and in mixed surface environments of serpentinite-hosted springs.

Active serpentinization occurs in the presence of water-rock interactions where ultramafic rock is present. Indicators of active serpentinization include the presence of H₂ and CH₄ gases as well as the discharge of ultra-basic, reducing Ca-OH type fluids that have a high Ca:Mg ratio (Barnes et al., 1967; Sleep et al., 2004) and are believed to form in a closed system with respect to CO₂ (Bruni et al., 2002). It is also possible to get a second type of fluid that is formed through the weathering of already serpentinized ultramafic rocks; these Mg-HCO₃ fluids are moderately basic (pH < 10), rich in Mg (Barnes et al., 1967), and are thought to form in an open system where CO₂ is at equilibrium with atmosphere (Bruni et al., 2002). Despite the understanding of common indicators of active serpentinization, the range of geochemistry at sites of terrestrial serpentinization is not well constrained. Thus, the first objective of this study was to compare the geochemical properties of disparate sites of terrestrial serpentinization to identify geochemical parameters. To accomplish this, three sites of active terrestrial serpentinization were chosen for comparison: the Tablelands, (NL, Canada), The Cedars (CA, U.S.A.), and Aqua de Ney (CA, U.S.A.) (Figure 2.1). The second objective was to identify the variations between sites of terrestrial serpentinization by establishing the range of geochemistry at the three study sites. The final objective was to develop working hypotheses for the causes of the variability in the geochemistry at sites of terrestrial serpentinization.



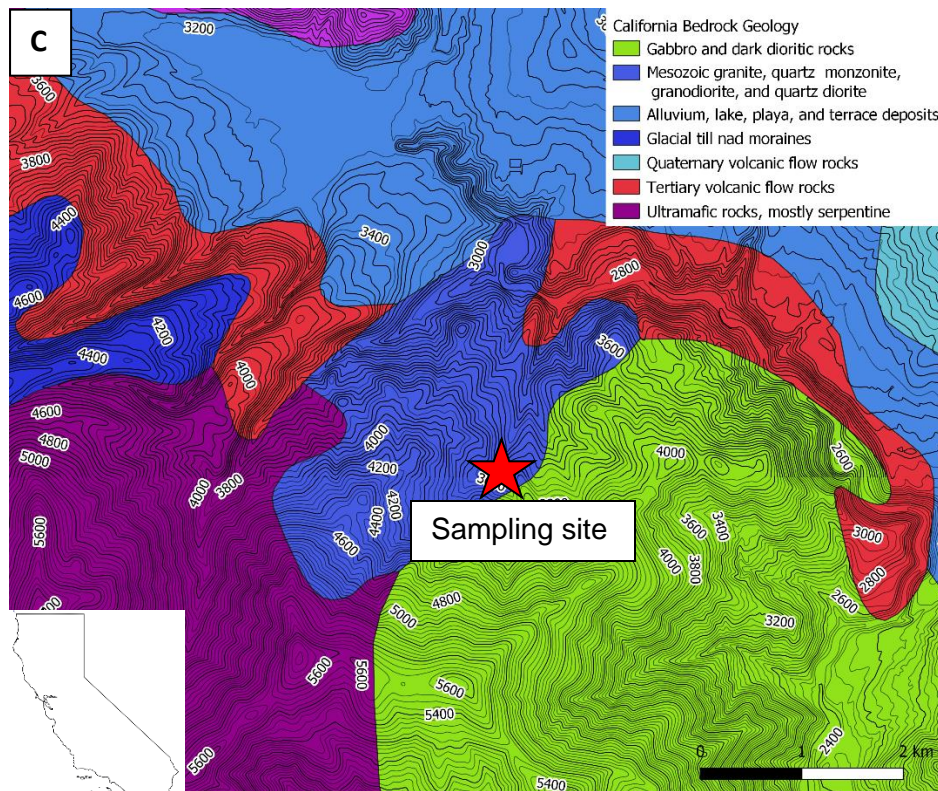


Figure 2.1. Geologic maps of the three sites of terrestrial serpentinization chosen for this study:

(A) the Tablelands, Canada, (B) The Cedars, U.S.A. and (C) Aqua de Ney, U.S.A. The sources

from these maps came from (A) NL survey (<http://gis.geosurv.gov.nl.ca/>) and the federal

Department of Natural Resources (<https://geogratis.gc.ca/>) and (B), (C) the U.S. Geologic Survey

(<https://www.usgs.gov/products/maps/geologic-maps>). The contour interval is (A) 20 meters and

(B), (C) 40 feet.

2.1.2 Ophiolite Field Settings in this Study

The Humber Arm Allochthon tectonic zone, located on the western coast of Newfoundland, Canada, is composed of a mixture of deep-sea sediments, mafic crustal material and mantle peridotites that originated from the ancient seafloor, referred as the Bay of Islands

ophiolite complex (BOIC) (Suhr, 1992; Suhr & Cawood, 1993). The BOIC is made up of four Ordovician ophiolites, one of which hosts the Tablelands, also referred to as Table Mountain Massif. Only the lower portion of the ophiolite (i.e., the ultramafic rocks and ultramafic to gabbroic lower crustal material) has been preserved at the Tablelands; the mantle peridotite has been classified as harzburgite and lherzolite (Suhr, 1992).

The Tablelands Ophiolite was emplaced during the Middle Ordovician, between 500-485 MA (Dunning & Krogh, 1985) during the Taconic orogeny that resulted in the accretion of peri-Laurentian marine arcs onto the Laurentian continental margin (van Staal et al., 2007). It is the oldest emplacement of the three study sites. There are indicators that serpentinization is still actively occurring at the Tablelands (Morrill et al., 2014; Szponar et al., 2013). Geochemical analyses of groundwater from the Tablelands have shown that methane and hydrogen are major components of the dissolved gas phases. Studies have also suggested that while groundwater from the Tablelands contains microorganisms, including those capable of carbon monoxide utilization, no evidence of microbial methanogenesis has been found (Cook, et al., 2021b (Chapter 3); Morrill et al., 2014). Indeed, Cumming et al. (2019) have proposed that methane from this site is likely of thermogenic or abiogenic origin.

The Cedars is located in Sonoma County, California, U.S.A., and is a part of Northern California's Jurassic-age, Coast Range Ophiolite (Shervais et al., 2005). This ophiolite is underlain by marine sediments, sandstones, and shales (Coleman, 2000). The peridotite at The Cedars has been extensively studied, in part due to its selection as the international peridotite standard (PCC-1) and is classified as a mixture of harzburgite and dunite which have varying proportions of olivine, orthopyroxene and clinopyroxene (Coleman, 2000). The peridotite has

been partially altered to serpentine minerals (between 5-20 %) in the central part of the body and to as much as 100 % along its contact with the surrounding rock (Coleman, 2004).

The Jurassic-age Coast Range ophiolite was emplaced as part of the Franciscan Subduction Complex, between 170-164 Ma (Coleman, 2000; Shervais et al., 2004), making it much younger than the Tablelands or Aqua de Ney (Coleman, 2000). Studies have shown that there are indicators that serpentinization is actively occurring and the groundwater at The Cedars bubbles with gases majorly composed of H₂ and CH₄ (Barnes et al., 1967). Both microbiological and geochemical studies have suggested that the CH₄ from The Cedars is at least partially microbial in source (Kohl et al., 2016; Morrill et al., 2013; Wang et al., 2015).

Aqua de Ney is located in Siskiyou County, California, U.S.A., and is a part of the Trinity Ophiolite Complex (Feth et al., 1961). This is underlain by a series of greenstones, limestones and shales and andesitic volcanic rocks (Feth et al., 1961). The ultramafic portion of the ophiolite is comprised of dunite (15-20 %), harzburgite and lherzolite (60-70 %) and plagioclase-bearing harzburgite and lherzolite (~15 %) (Dygert et al., 2016; Quick, 1981, 1982).

The Trinity Ophiolite Complex was emplaced between 431-404 Ma (Wallin & Metcalf, 1998) and its units are Silurian to Devonian in age. The groundwater is known to be unique; it is rich in silica (4 000 mg/L) which is likely due to the percolation through silica-rich volcanic rocks (Feth et al., 1961; García-Ruiz et al., 2017). The groundwater also contains elevated concentrations of the bicarbonate ion (15 600 mg/L) as well as sulfide in the form of H₂S (1000 mg/L) and ammonium nitrogen (148 mg/L) (Feth et al., 1961). Boschetti et al., (2017) proposed that the groundwater chemical and isotopic compositions have been affected by slab dehydration and serpentinization. It is also the only site of the three with the presence of a higher temperature (240 °C) geothermal system (Boschetti et al., 2017). The groundwater at Aqua de Ney bubbles

with methane (>80 % by volume) (Mariner et al., 2003). The source of the unusually high concentrations of methane at Aqua de Ney remains poorly understood.

2.2 Methods

2.2.1 Water Sampling

Water samples were collected from three similar settings in each of the ophiolite sites: reducing, ultra-basic groundwater springs, flowing oxic, surface waters that interacted with air, and pooled waters that were assumed to represent a mixture of the two. Groundwater samples were collected directly from their discharge points to minimize interaction with the atmosphere and represent the most pristine aqueous geochemistry of subsurface serpentine-hosted environment. Pooled water samples in contact with the atmosphere were open to contamination from shallow groundwater or oxic surface water. The pooled water sampling locations had large, vertical redox gradients that occur when serpentine-hosted springs water mix with surface water, shallow groundwater, and/or react with the atmosphere. Oxic flowing surface waters nearest to the ultra-basic groundwater springs and pools were sampled from the nearest brook or creek.

At the Tablelands, there was a pool of reducing ultra-basic water located in Winter House Canyon (referred to as WHC2) that is approximately 40 cm deep and 126 cm wide (Figure 2.2A). The surface of this pool was exposed to the atmosphere. The groundwater spring (referred to as WHC2-s) was sampled by isolating the ultra-basic discharge at the bottom of the pool and blocking the overland flow that contributes to the pool (Figure 2.2B). Winter House Brook (WHB), which flows along the bottom of the Winter House Canyon, was sampled to represent the oxic flowing surface water at the Tablelands. A groundwater sample at The Cedars was collected from the Grotto Pool Spring (GPS) (Figure 2.2C). GPS discharges above Austin Creek's water line and had been determined to be representative of deep ultra-basic reduced groundwater at The Cedars (Morrill et al., 2013). Barnes Spring Complex (BSC) had ultra-basic fluid pooling and potentially mixing with shallow groundwater and/or surface water (Figure

2.2D). Austin Creek (AC), which flowed alongside both GPS and BSC, was sampled as the flowing surface water sample.

Aqua de Ney was developed as a health spa in the early twentieth century, and some of the original cement features remain. Persisting infrastructure includes a well and a spigot with flowing water. Groundwater was sampled directly from the spigot to minimize mixing with surface water (Figure 2.2E). Pooled water was sampled from the Ney Well which was exposed to the atmosphere and located a few meters above Ney Creek (Figure 2.2F). Ney Creek was sampled a few meters upstream from the well to avoid possible influence of the well water.

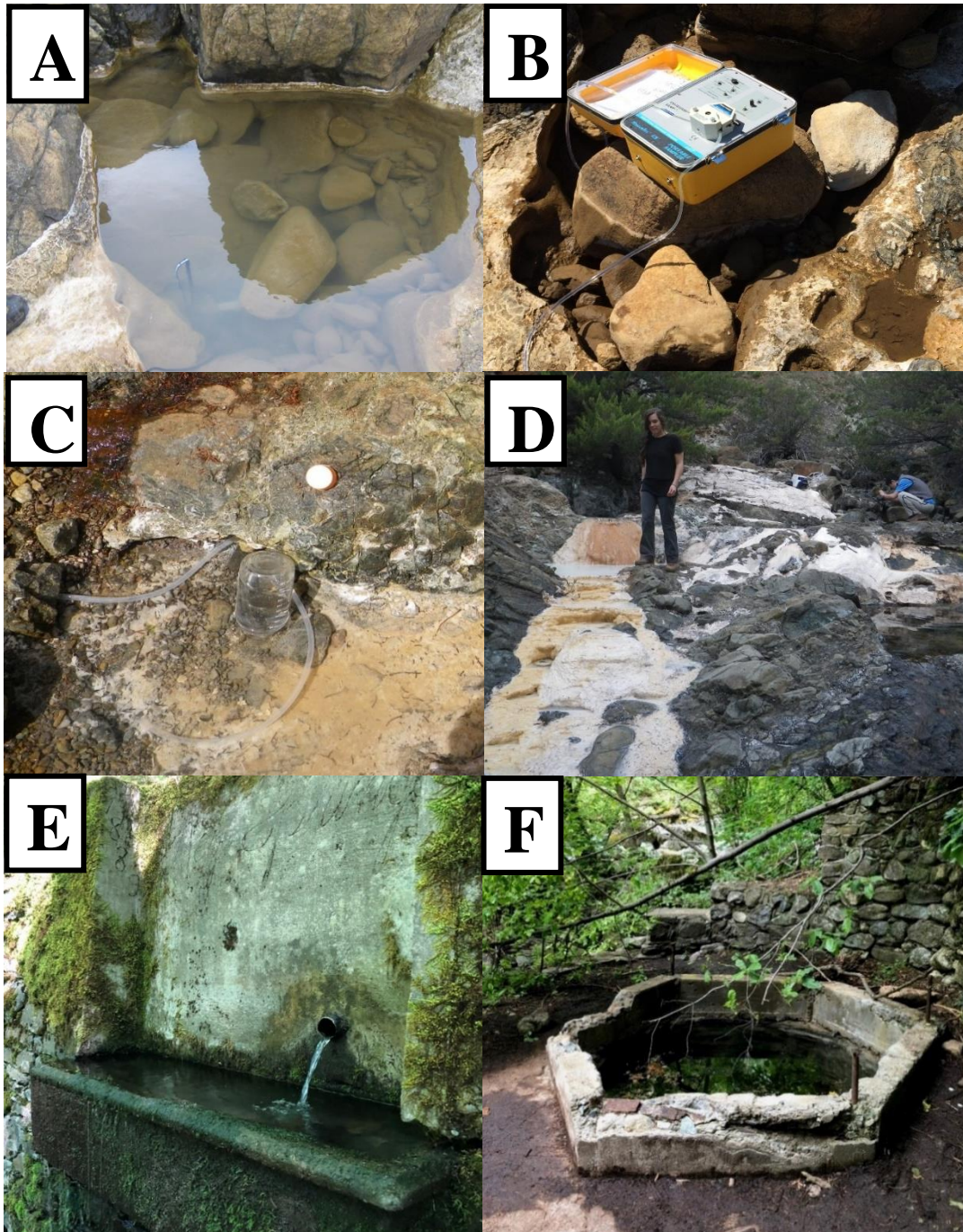


Figure 2.2. Images of sampling locations at the Tablelands (A) Winter House Canyon 2 (WHC2) and (B) Winter House Canyon 2 pool that has been emptied to collect recharge (WHC2-s), The Cedars (C) Grotto Pool Spring (GPS) and (D) Barnes Spring Complex (BSC), and Aqua de Ney (E) Ney Spigot and (F) Ney Well.

2.2.2 Sample Collection and *In Situ* Measurements

At the Tablelands, the groundwater was sampled by redirecting the overland flow of water away from the pool and then pumping all the water out of the pool. The discharging groundwater was sampled using a 60 mL syringe. At The Cedars, groundwater from GPS was sampled by inserting a tube directly into the spring effluent and using a syringe to extract fluid from the tube. At Aqua de Ney, groundwater was sampled directly from Ney Spigot using a 60 mL syringe. Pooled water from the Ney Well was sampled using a Masterflex® E/S™ portable peristaltic pump to extract fluid through Tygon® tubing held at the bottom of the well. Pooled water at the Tablelands (WHC2) and at The Cedars (BSC) was sampled directly using a 60 mL syringe.

At the time of sampling, fluids for trace ion geochemistry measurements were filtered through a 0.22 µm mixed cellulose ester (MCE) filter, collected in sterile 15 mL Falcon® tubes, and frozen until analysis. Samples for inductively coupled plasma mass spectrometer (ICP-MS) and inductively coupled plasma optical emission spectrometer (ICP-OES) analysis were acidified with nitric acid to a pH < 2. Water samples for total inorganic carbon (TIC) were collected with no headspace in 40 mL amber vials with a drop of concentrated HgCl₂ (to inhibit microbial activity) and a black butyl septum following the method described in Wilson et al. (2020). Samples collected for dissolved organic carbon (DOC) were filtered through a pre-combusted glass fiber filter (GFF). Thirty mL of fluid was collected in an amber 40 mL vial with 10 % H₃PO₄ and a Teflon septum following the method described in Wilson et al. (2020). These samples were stored cold and dark until analysis. Waters for δ²H and δ¹⁸O analysis were collected without headspace in 4 mL amber vials and stored dark and cold (Szponar et al., 2013). Waters for electrolytic tritium (E³H) analysis were collected in 500 mL Nalgene bottles with no headspace following the method described in Suzuki et al. (2017).

The pH and temperature of the fluid were measured in the field using an Oakton handheld waterproof field probe meter calibrated daily with 4, 7, and 10 pH buffers. The oxidation-reduction potential (ORP) of the fluid was measured in the field using an ORPTestr 10 m (Eutech Instruments). The ORP meter accuracy was confirmed with 4 and 7 pH buffers that were saturated with quinhydrone. These solutions had ORP values of 93 mV and 267 mV respectively. To create these solutions, 50 mL of each pH buffer was placed in a beaker and 0.1 g of quinhydrone was added to each beaker and stirred until the solution was saturated. Saturated quinhydrone solutions were used immediately to ensure no decomposition upon exposure to oxygen occurred. The ORP meter had a double junction platinum electrode such that a correction was required to convert ORP to E_h . Field measurements were therefore converted to E_h by adding 241.0 to the ORP (YSI, 2005).

Dissolved gases were collected using a 60 mL syringe following methods outlined in Cumming et al. (2019) that were adapted from Rudd et al. (1974). Thirty mL of fluid was taken up in a syringe that contained an equal amount of either helium or nitrogen gas. The syringe was sealed and shaken for 5 minutes to partition the dissolved gases into the gaseous phase. The gas phase was injected into a 30 mL serum vial displacing degassed Nanopure water. These vials were sealed with a blue butyl septum that was conditioned as described by Oremland et al. (1987). Mercuric chloride was added to the samples to terminate microbial activity and the samples were stored cold and dark. Bubbling gases were collected using a modified inverted plastic beaker with a sampling port and a 60 mL syringe with a needle attached. Gases were then injected in an evacuated serum vial sealed with a conditioned blue butyl septum.

2.2.3 Analytical Methods

2.2.3.1 Aqueous Geochemistry

Trace ion geochemistry was determined by ICP-MS except for sodium and potassium concentrations which were measured using a Thermo Scientific iCAP 6500 Series ICP-OES. Reference standards were used to ensure accuracy. Analytical error was $\pm 10\%$. Nitrate and sulfate concentrations were analyzed with a Thermo Fisher ICS 5000. Ions were separated using an AS23 column with an ASG23 guard column and a carbonate eluent with a 1.0 mL/min flow rate. Standards purchased from Sigma Aldrich were used to create calibration curves for nitrate and sulfate. Additionally, a standard containing 81 μM nitrate and 52 μM sulfate was injected during the analysis to check for instrument drift. The detection limits for nitrate and sulfate were 1.6 and 2.60 μM , respectively.

Samples for DOC and TIC were analyzed for concentrations and $\delta^{13}\text{C}$ at the Ján Veizer Stable Isotope Laboratory at the University of Ottawa using methods outlined in Murseli et al. (2019) and St-Jean (2003). Samples were analyzed using a modified OI Analytical Aurora Model 1030 Wet TOC Analyser with a model 1051 autosampler and a combustion unit. TIC concentrations were determined using non-destructive infrared (NDIR) detector coupled to a Thermo Finnigan Mat DeltaPlusXP isotope ratio mass spectrometer (IRMS). DOC concentration and $\delta^{13}\text{C}$ were also determined on the same system using the non-purgeable organic carbon (N-POC) method. Three internal standards were used to normalize the results. The analytical precision for concentration analysis was 0.5 ppm C (2σ) and 0.2 ‰ for the $\delta^{13}\text{C}$ analysis.

Water samples were analysed for $\delta^2\text{H}$ and $\delta^{18}\text{O}$ at Isotope Tracer Technologies, Inc., in Waterloo, Ontario, using a Picarro Cavity Ring Down Spectroscopy Analyzer (Model L2130-i). Three standards were used to normalize the results (V-SMOW, SLAP, and GISP). Results are reported relative to the V-SNOW reference standard. The reproducibility on $\delta^2\text{H}$ and $\delta^{18}\text{O}$ measurements was $\pm 1\%$ and $\pm 0.1\%$ respectively. Water samples for (E^3H) were analyzed at

Isotope Tracer Technologies, Inc., in Waterloo, Ontario, using liquid scintillation counting (LSC). The analytical error associated with this measurement was ± 0.2 TU (1σ).

2.2.3.2. Dissolved and Bubbling Gases

Hydrogen and oxygen gaseous concentrations were measured on an Agilent 6890A GC equipped with a micro thermal conductivity detector (TCD) using a Carbon 1010 capillary column (30 m x 0.32 mm inside diameter, 15 μ m film thickness) with nitrogen as a carrier gas. The oven temperature was 50 °C isothermal for 13 minutes. A mixed gas standard (Scott) was used to create the calibration curves for carbon dioxide and carbon monoxide. The gas standard contained 0.5 % oxygen, 0.5 % carbon monoxide, 0.5 % carbon dioxide and 0.5 % hydrogen in a balance of helium. The detection limits for hydrogen and oxygen in the gas phase were 10 and 15 μ M respectively. The precision on triplicate injections of the standard was always less than 5 % relative standard deviation (RSD).

Methane, carbon monoxide, and carbon dioxide concentrations were analyzed using an SRI 8610 gas chromatograph (GC) equipped with a Flame Ionization Detector (FID) and a methanizer using a Carboxen 1010 capillary column (30 m x 0.32 mm inside diameter, 15 μ m film thickness) with helium as the carrier gas following procedures outlined in Morrill et al. (2014). In short, the oven temperature was held constant at 40 °C for 16 min then increased by 15 °C/min to a final temperature of 125 °C, which was held constant for 3 min. A mixed gas standard (Scott) was used to create the calibration curves for carbon dioxide and carbon monoxide. The gas standard contained 0.5 % oxygen, 0.5 % carbon monoxide, 0.5 % carbon dioxide, and 0.5 % hydrogen in a balance of helium. A methane gas standard (Scott) of 1 % methane in a balance of helium was used to create the calibration curves for methane. The detection limits for methane, carbon dioxide, and carbon monoxide in the gas phase were 5, 10,

and 10 μM respectively (Morrill et al., 2014). The precision on triplicate injections of the standard was always less than 5 % (RSD).

The $\delta^{13}\text{C}$ of CH_4 and $\text{C}_1\text{-C}_6$ were measured by gas chromatography combustion isotope ratio mass spectrometry (GC-C-IRMS) (Agilent 6890N GC, Thermo ConFlo II interface, Thermo Delta V + IRMS) following methods outlined in Cumming et al. (2019). Gas samples were injected directly into the GC-C-IRMS system after being withdrawn from the sample serum vials with a gas-tight locking syringe. Injection sizes ranged from 4 μL to 500 μL . The separation of CO_2 and CH_4 was achieved using a Carboxen 1010 capillary column (30 m x 0.32 mm inside diameter, 15 μm film thickness) with a temperature program of 35 $^\circ\text{C}$ hold for 3.8 min, ramp at 25 $^\circ\text{C}/\text{min}$ to 110 $^\circ\text{C}$, hold for 5 min. Other low molecular weight hydrocarbons (C_2 , C_3 , $i\text{C}_4$, $n\text{C}_4$, $i\text{C}_5$, $n\text{C}_5$, $n\text{C}_6$) were separated using a RT-Q bond column (30 m x 0.32 mm ID, 10 μm film thickness) using a temperature program of 50 $^\circ\text{C}$ hold for 3.5 min, ramp 25 $^\circ\text{C}/\text{min}$ to 260 $^\circ\text{C}$, hold for 10 min. The total analytical error associated with the stable carbon isotope analysis by this method was ± 0.5 ‰ (1 σ). Isotope ratios were reported in delta notation ($\delta^{13}\text{C}$) and were calculated relative to international standards V-PDB for carbon isotopes:

$$\delta^{13}\text{C} = (\text{R}_{\text{sam}}/\text{R}_{\text{std}} - 1) \quad [\text{Eq. 2.1}]$$

where R_{sam} and R_{std} are the ratio of heavy to light isotopes (i.e., $^{13}\text{C}/^{12}\text{C}$) for the sample and standard, respectively (Coplen, 2011).

The $\delta^2\text{H}$ of H_2 , CH_4 , and low molecular weight hydrocarbons (C_2 , C_3 , $i\text{C}_4$, $n\text{C}_4$, $i\text{C}_5$, $n\text{C}_5$, $n\text{C}_6$) were measured on the same system as the $\delta^{13}\text{C}$ but using a Thermo Scientific micropyrolysis furnace (Py) in place of the combustion furnace. Gases were separated using the same columns and temperature programs described for $\delta^{13}\text{C}$ methods with a 5:1 split ratio. The

total analytical error associated with this method is $\pm 5\%$. Isotope ratios reported in delta notation ($\delta^2\text{H}$) and were calculated using Eq. 2.1 substituting $\delta^2\text{H}$ for $\delta^{13}\text{C}$.

2.3 Results

2.3.1 Isotope values of Waters

Tritium (^3H) was detected in the waters sampled from WHC2-s, BSC, and Ney Well (2.8 TU, 2.3 TU, and 1.9 TU, respectively). The ^3H values were less than modern precipitation ^3H values, which are generally between 5 to 15 TU (Clark & Fritz, 1997). This indicated that some of the ^3H decayed, or that the water samples were a mixture of sub modern waters (i.e., originating prior to the 1950's when atmospheric nuclear bomb testing began (Clark & Fritz, 1997)) with surface waters or recently recharged modern groundwater. Conversely, the ^3H concentration was below the detection limit (<0.8 TU) in the water from The Cedars groundwater spring, GPS, indicating that this water was sub modern and not mixed with a modern source of water (Suzuki et al., 2017).

Hydrogen and oxygen isotope values ($\delta^2\text{H}$ and $\delta^{18}\text{O}$) of the water from groundwater, pools, and surface water samples at the Tablelands, The Cedars, and Aqua de Ney were distinct. The hydrogen and oxygen isotope values of the waters from the Tablelands ranged from -56 to -62 ‰ and -9.0 to -10.2 ‰, respectively. The hydrogen and oxygen isotope values of the waters from The Cedars ranged from -42 to -40 ‰ and -7.3 to -6.9 ‰, respectively. The hydrogen and oxygen isotope of the waters from Aqua de Ney had the greatest range from -97 to -19 ‰ and -14.0 to 3.7 ‰, respectively. These values were plotted against the corresponding local meteoric water lines (Figure 2.3). The Tablelands data were compared with the Global meteoric water line, as no local meteoric water line data were available for Newfoundland. All samples, except for fluid from Ney Well, were well described by the corresponding meteoric water line indicating that the fluids at these sites were meteoric in origin. Interestingly, at Aqua de Ney

although the surface water sample (Ney River) and the groundwater (Ney Spigot) plotted along the Oregon meteoric water line, the sample from Ney Well plotted far below the line.

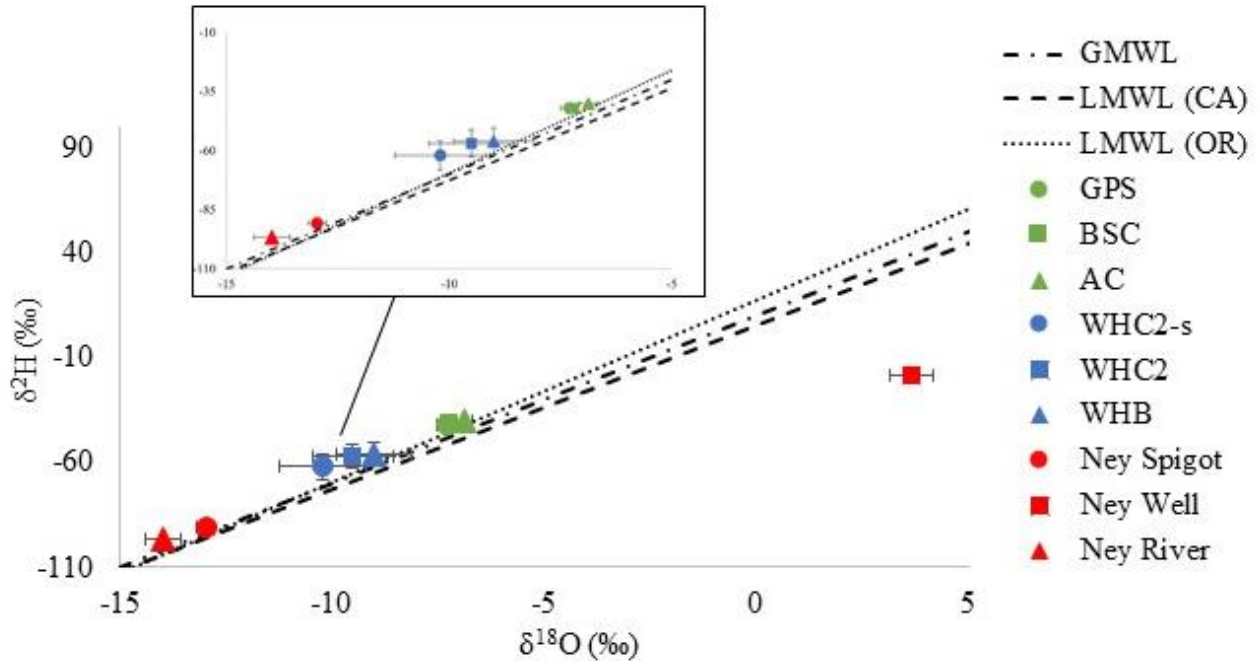


Figure 2.3. Hydrogen and oxygen isotope values of fluid samples from The Cedars, the Tablelands, and Aqua de Ney compared to the Global Meteoric Water Line (GMWL), $\delta^2\text{H} = 8 \delta^{18}\text{O} + 10$ (Harmon, 1961); Californian Local Meteoric Water Line (LMWL CA), $\delta^2\text{H} = 7.8 \delta^{18}\text{O} + 5.4$ (Coplen & Kendall, 2000); and the Oregon Local Meteoric Water Line (LMWL OR), $\delta^2\text{H} = 8.7 \delta^{18}\text{O} + 17.5$ (Kendall & Coplen, 2001). Error bars associated with sample points indicate \pm one standard deviation (1σ) of the reported values.

2.3.2 Aqueous Geochemistry

The aqueous geochemistry of groundwater discharging at the Tablelands, The Cedars, and Aqua de Ney is summarized in Table 2.1. The groundwater sampled at the Tablelands (WHC2-s) and at The Cedars (GPS) had ultra-basic pH values (>11) and were reducing ($E_h < -$

200 mV), however, the groundwater at Aqua de Ney (Ney Spigot) was not. The surface waters (i.e., AC, Ney River, and WHB) analyzed were slightly basic ($\text{pH} > 8$) and oxic ($E_h > 127$ mV). The fluid sampled from the pools at the Tablelands (WHC2) and The Cedars (BSC) were basic ($\text{pH} > 9.0$) and reducing ($E_h < -71$ mV), however, the fluid from Ney Well was ultra-basic ($\text{pH} = 12.9$) and reducing ($E_h = -224$ mV).

The groundwater at the Tablelands and The Cedars contained elevated levels of Na, K, Br and Cl as well as depleted levels of Mg relative to their respective surface water endmembers. The surface waters at all three sites were elevated in Mg concentrations relative to the groundwater. The Na, K in the pooled water at the Tablelands and The Cedars were most similar to those in the surface water samples. The Mg concentrations in the pooled water were more elevated than those in the groundwater but more depleted than those in the surface water. The well water at Aqua de Ney had the most anomalous geochemistry of all the sites tested. Ney well water had the highest concentrations of Na and K as well as the lowest Ca by at least an order of magnitude. The concentrations of Na, K, Mg, Br, and Cl have been plotted against the pH (see Supplementary Materials, Figure 2.S1).

In the fluids at the Tablelands and The Cedars, the NO_3^- and PO_4^{3-} concentrations were the highest in surface waters, however, at The Cedars the lowest concentrations of NO_3^- were measured in the groundwater and at the Tablelands the lowest concentration of NO_3^- was measured in the pool. At The Cedars, the lowest concentration of PO_4^{3-} was in the pool and at the Tablelands it was in the groundwater. The highest concentration of NH_4^+ at The Cedars was in the groundwater and the lowest was in the pool, however, at the Tablelands the NH_4^+ concentrations were the same in the groundwater and in the pooled water. Water from Ney Well had the highest concentration of NH_4^+ , PO_4^{3-} , and NO_3^- of all the sites studied. The

concentrations of NO_3^- , PO_4^{3-} , and SO_4^{2-} have been plotted against the pH (see Supplementary Materials, Figure 2.S2).

The TIC concentration and stable carbon isotope values in the waters sampled at the Tablelands were the lowest in the ultra-basic spring (3.48×10^{-5} moles of $\text{C}\cdot\text{L}^{-1}$, -18.6 ‰, respectively) and the highest in the oxic surface water (7.35×10^{-4} moles of $\text{C}\cdot\text{L}^{-1}$, -2.4 ‰) (Table 2.1, Figure 2.4A). While the $\delta^{13}\text{C}$ values at The Cedars were more depleted in ^{13}C compared to the Tablelands TIC, similar trends were still observed, with the highest TIC concentration and $\delta^{13}\text{C}$ values observed in the oxic surface waters at the site (4.30×10^{-3} moles of $\text{C}\cdot\text{L}^{-1}$, -16.9 ‰) compared to the spring waters sampled from GPS and BSC (4.79×10^{-5} moles of $\text{C}\cdot\text{L}^{-1}$, -44.4 ‰, and 3.64×10^{-5} moles of $\text{C}\cdot\text{L}^{-1}$, -33.9 ‰, respectively). Conversely, Aqua de Ney showed the opposite trend, where the highest TIC concentrations and $\delta^{13}\text{C}$ values were found in ultra-basic waters from Ney Well (6.52×10^{-2} moles of $\text{C}\cdot\text{L}^{-1}$, $+2.4$ ‰). The lowest TIC $\delta^{13}\text{C}$ was measured in samples from Ney Spigot (-15.5 ‰) and the lowest concentration was measured in samples from Ney Creek (4.62×10^{-4} moles of $\text{C}\cdot\text{L}^{-1}$). The range of the DOC concentration and stable isotope values was much smaller than that of the TIC for the Tablelands and The Cedars, unfortunately there was no data available for Aqua de Ney (Figure 2.4B).

Table 2.1. Summary of environmental parameters and ion concentrations of groundwater, surface water, and pooled water at the Tablelands, The Cedars, and Aqua de Ney.

Parameter	Groundwater			Pooled/Well Water			Surface Water		
	Tablelands	The Cedars	Aqua de Ney	Tablelands	The Cedars	Aqua de Ney	Tablelands	The Cedars	Aqua de Ney
	WHC2-s	GPS	Ney Spigot	WHC2	BSC	Ney Well	WHB	AC	Ney River
pH	12.2	11.9	7.6	13.1	11.8	12.9	8.1	8.7	8.5
Temp (°C)	-	17.1	13	9.6	17.4	11.6	13.1	18.7	14.4
E_h (mV)	-	-457	313	-71	-344	-224	127	309	-
Na (mM)	3.90 x 10 ¹	1.48 x 10 ¹	2.18 x 10 ⁻¹	8.79	1.96	5.24 x 10 ²	1.21 x 10 ⁻¹ (± 1.73 x 10 ⁻²)	1.07	1.80 x 10 ⁻¹ (± 6.90 x 10 ⁻²)
K (mM)	3.27 x 10 ⁻¹	1.59 x 10 ⁻¹	2.04 x 10 ⁻² (± 4.56 x 10 ⁻¹)	2.02 x 10 ⁻¹	3.07 x 10 ⁻²	3.63	1.04 x 10 ⁻² (± 6.33 x 10 ⁻³)	1.27 x 10 ⁻²	1.43 x 10 ⁻² (± 6.45 x 10 ⁻³)
NH₄⁺ (mM)	5.65 x 10 ⁻²	4.25 x 10 ⁻²	n.d.	5.65 x 10 ⁻²	1.75 x 10 ⁻³	7.82†	n.d.	3.44 x 10 ⁻³	0†
Ca (mM)	1.52	9.14 x 10 ⁻¹	2.66 x 10 ⁻¹	8.46 x 10 ⁻¹	1.23	2.57 x 10 ⁻³ (± 3.56 x 10 ⁻⁷)	1.43 x 10 ⁻²	1.41 x 10 ⁻¹	2.74 x 10 ⁻² (± 3.20 x 10 ⁻⁶)
Mg (mM)	1.23 x 10 ⁻²	3.70 x 10 ⁻⁴	3.00 x 10 ⁻¹	1.23 x 10 ⁻²	4.68 x 10 ⁻³ (± 6.24 x 10 ⁻⁴)	5.43 x 10 ⁻⁴ (± 1.21 x 10 ⁻⁴)	2.37 x 10 ⁻¹ (± 4.27 x 10 ⁻²)	1.64	2.33 x 10 ⁻¹
Fe (mM)	9.71 x 10 ⁻⁴	<d.l.	< d.l.	< d.l.	<d.l.	< d.l.	< d.l.	<d.l.	< d.l.
Mn (mM)	6.72 x 10 ⁻⁶	< d.l.	< d.l.	< d.l.	< d.l.	< d.l.	< d.l.	< d.l.	< d.l.
Cl (mM)	1.18 x 10 ¹	9.87	< 8.69 x 10 ⁻²	3.42 (± 4.77 x 10 ⁻¹)	1.59	9.36 x 10 ¹ (± 5.18 x 10 ⁵)	1.68 x 10 ⁻¹ (±3.09 x 10 ⁻²)	9.23 x 10 ⁻¹	< 8.69 x 10 ⁻²

Br (mM)	1.22 x 10 ⁻²	1.33 x 10 ⁻²	< d.l.	3.84 x 10 ⁻³	2.27 x 10 ⁻³	1.61 x 10 ⁻¹ (± 3.75 x 10 ¹)	3.35 x 10 ⁻⁴	1.54 x 10 ⁻³ (± 7.44 x 10 ⁻⁴)	<d.l.
SO₄²⁻ (mM)	3.79 x 10 ⁻³ φ	2.49 x 10 ⁻²	-	4.56 x 10 ⁻³	4.16 x 10 ⁻⁴	5.12 x 10 ⁻⁴	2.60 x 10 ⁻³	9.79 x 10 ⁻²	4.79 x 10 ⁻² ‡
H₂S (mM)	-	-	-	< d.l.	< d.l.	3.39 x 10 ¹	-	-	-‡
PO₄³⁻ (mM)	4.42 x 10 ⁻⁴ φ	3.79 x 10 ⁻⁴ *	-	4.32 x 10 ⁻³ *	3.05 x 10 ⁻⁴ *	1.47 x 10 ⁻² ‡	8.00 x 10 ⁻³ *	4.74 x 10 ⁻⁴ *	2.11 x 10 ⁻⁵ ‡
NO₃⁻ (mM)	1.24 x 10 ⁻³ φ	9.84 x 10 ⁻⁴	-	1.15 x 10 ⁻³	1.45 x 10 ⁻³	1.32	3.06 x 10 ⁻³	1.79 x 10 ⁻³	1.13 x 10 ⁻² ‡
Ca/Mg	124	2470	0.887	68.8	263	4.73	0.06	0.0860	0.118
TIC (moles of C·L⁻¹)	3.48 x 10 ⁻⁵	4.79 x 10 ⁻⁵	1.43 x 10 ⁻³	1.20 x 10 ⁻⁴ (± 1.33 x 10 ⁻⁵)	3.64 x 10 ⁻⁵	6.52 x 10 ⁻²	7.35 x 10 ⁻⁴	4.30 x 10 ⁻³ (± 4.85 x 10 ⁻⁴)	4.62 x 10 ⁻⁴
δ¹³C TIC (‰)	-18.6	-44.4	-15.5	-11.9	-33.4	2.4	-2.4	-16.9	-6.2
DOC (moles of C·L⁻¹)	-	1.89 x 10 ⁻⁴ (5.90 x 10 ⁻⁵)	-	1.46 x 10 ⁻⁴	1.18 x 10 ⁻⁴ (± 4.36 x 10 ⁻⁵)	-	3.13 x 10 ⁻⁵	5.71 x 10 ⁻⁵ (± 1.14 x 10 ⁻⁵)	-
δ¹³C DOC (‰)	-	-12.5	-	-15.1	-14.7 (± 1.7)	-	-29.8	-20.4	-
f_{UB}	1	1	0.00007	0.28	0.07	1	0	0	0
³H	2.8	<0.8 ^x	-	-	2.3 ^x	1.9	-	-	-

Standard deviations (1σ) of measurements were less than 10 % unless otherwise indicated. Parameters below limits of detection are indicated by the letters d.l. and parameters not measured are indicated by “-”. All data in this table were collected for this study except where noted: *(Rietze, 2015), †Feth et al. (1961), φMorrill et al. (2014), and Suzuki et al. (2017).

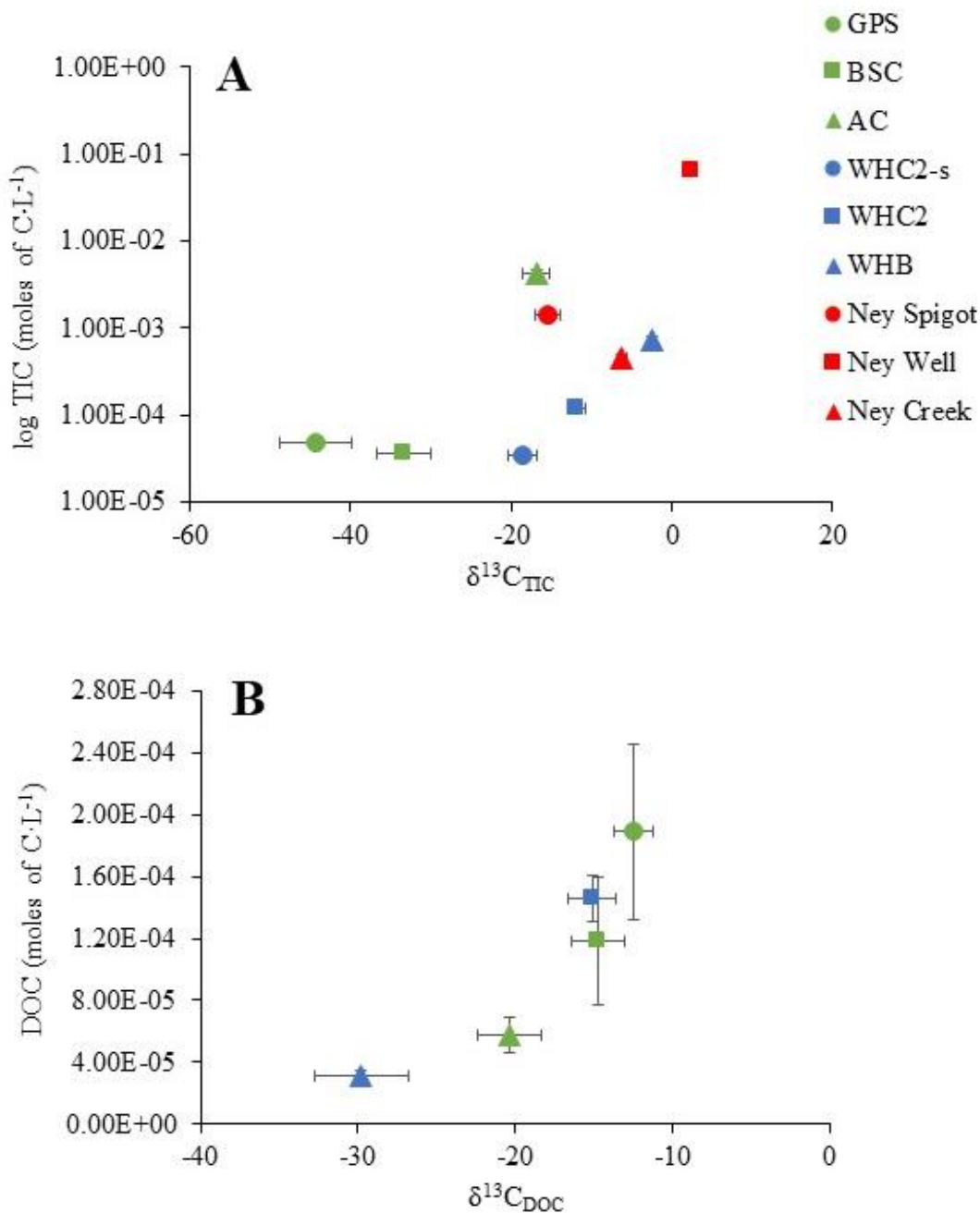


Figure 2.4. (A) Total inorganic carbon (TIC) concentrations (moles of C·L⁻¹) in logarithmic scale versus $\delta^{13}\text{C}_{\text{TIC}}$ and (B) dissolved organic carbon (DOC) concentration (moles of C·L⁻¹) versus $\delta^{13}\text{C}_{\text{DOC}}$ of groundwater, pooled/well water, and surface water from Tablelands, The Cedars, and Aqua de Ney. Error bars associated with sample points indicate \pm one standard deviation (1σ) of the reported values.

2.3.3 Gaseous Geochemistry

H₂ was detected in the dissolved and gaseous phases in both the groundwater spring and pool at The Cedars as well as in the dissolved phase in the groundwater spring and pool at the Tablelands (Tables 2.2 and 2.3). Conversely, H₂ was not detected in the groundwater spring or well water at Aqua de Ney. The $\delta^2\text{H}$ value of the H₂ was similar at The Cedars and the Tablelands, ranging from -790 to -752 ‰. In the groundwater spring at The Cedars (GPS), the dissolved phase H₂ was more enriched in ²H (-752 ‰) than the gaseous phase H₂ (-780 ‰), however, the dissolved and gaseous phase H₂ in the pool (BSC) (-775 ‰ and -772 ‰, respectively) were within error of each other. At the Tablelands, the H₂ in pool water was more enriched in ²H (-774 ‰) compared to the H₂ in the groundwater spring (-790 ‰).

CH₄ was detected at all sites (Tables 2.2 and 2.3). At The Cedars, it was found in the groundwater spring (GPS) and the pool (BSC) in both in the dissolved and gaseous phases. In the gas phase sampled from BSC, H₂ comprised approximately 5 % of the sample. At Aqua de Ney, CH₄ was detected in both the gaseous and aqueous phases in the well. In fact, CH₄ dominated the gas phase making up 84 % of the total volume. At the Tablelands, CH₄ was detected in the aqueous phase of the ultra-basic pool (WHC2) and groundwater spring (WHC2-s) at 8 μM and 363 μM, respectively. The dissolved CH₄ concentrations were similar in the groundwater spring of The Cedars and the Tablelands (36.3 μM and 34 μM, respectively) while the dissolved CH₄ concentration was much higher in the well at Aqua de Ney (1.92 x 10³ μM). The dissolved phase CH₄ concentration decreased in the pooled waters relative to the groundwater springs at the Tablelands (8 and 36.8 μM, respectively) and at The Cedars (22 and 34 μM, respectively).

Of all the sites studied, the $\delta^{13}\text{C}$ was the most negative in the bubbling CH₄ from the pooled water at The Cedars (BSC) (-63.8 ‰) followed by dissolved CH₄ in the groundwater

spring at The Cedars (GPS) (-57.8 ‰). The $\delta^{13}\text{C}$ of the gaseous CH_4 was within analytical error of the dissolved methane at both the pool and groundwater spring at The Cedars. At the Tablelands, the $\delta^{13}\text{C}$ of the dissolved methane was -27.6 ‰ in the ultra-basic pool (WHC2) and -27.0 ‰ in the groundwater spring (WHC2-s). At Aqua de Ney, the $\delta^{13}\text{C}$ of the bubbling methane in the well was the least negative of all the sites studied (-17.9 ‰).

The $\delta^2\text{H}$ of the dissolved and gaseous CH_4 in the groundwater spring (GPS) at The Cedars (-292 and -287 ‰ respectively), were within analytical error of each other. However, $\delta^2\text{H}_{\text{CH}_4}$ differed between the dissolved and gaseous-phases of the pool (BSC) at The Cedars (-305 and -355 ‰, respectively) with the dissolved-phase CH_4 being more enriched in ^2H compared to the gaseous-phase. The $\delta^2\text{H}_{\text{CH}_4}$ in the well at Aqua de Ney also differed between dissolved and gaseous-phases (-141 and -127 ‰, respectively); however, in this case the dissolved-phase CH_4 was more depleted in ^2H compared to the gaseous-phase. At the Tablelands the $\delta^2\text{H}_{\text{CH}_4}$ of the dissolved-phase sampled from the pool (WHC2) and the groundwater (WHC2-s) were within analytical error of each other (-176 and -175 ‰, respectively).

No higher chain alkanes (i.e., $\text{C}_2\text{-C}_6$) were detected in the dissolved-phase gases measured in the pools at the Tablelands or The Cedars. The dissolved-phase gas sample from the groundwater spring at The Cedars, however, contained ethane, propane, butane and pentane; the most abundant was ethane ($4.99 \times 10^{-1} \pm 3.33 \times 10^{-2} \mu\text{M}$) and the least abundant was isobutane ($8.60 \times 10^{-2} \mu\text{M}$). The gaseous-phase sample from the ultra-basic pool (BSC) at The Cedars, however, did contain propane, *i*-butane and *n*-butane (4.1×10^{-3} , 2.3×10^{-3} , and 4.9×10^{-3} % by volume respectively). The gaseous-phase sample from the groundwater spring contained ethane (65.4 % by volume) but no other higher-chain alkanes.

The $\delta^{13}\text{C}$ of methane, ethane, and propane for each site are shown in Figure 2.5 and in Tables 2.2 and 2.3. The $\delta^{13}\text{C}$ of the hydrocarbons at the Tablelands decreases with each additional carbon (-27 to -31.7 ‰). At both The Cedars and Aqua de Ney there is a ^{13}C enrichment between methane and ethane. There was little to no change in $\delta^{13}\text{C}$ of ethane and propane at The Cedars. Aqua de Ney has the most ^{13}C -enriched hydrocarbons and is the only site where ethane concentration was high enough to measure the $\delta^2\text{H}$. Similarly, to the change in $\delta^{13}\text{C}$ between C_1 and C_3 at Aqua de Ney (-17.9 to -8.8 ‰), there was also an enrichment in ^2H between C_1 and C_2 (from -127 to -53 ‰).

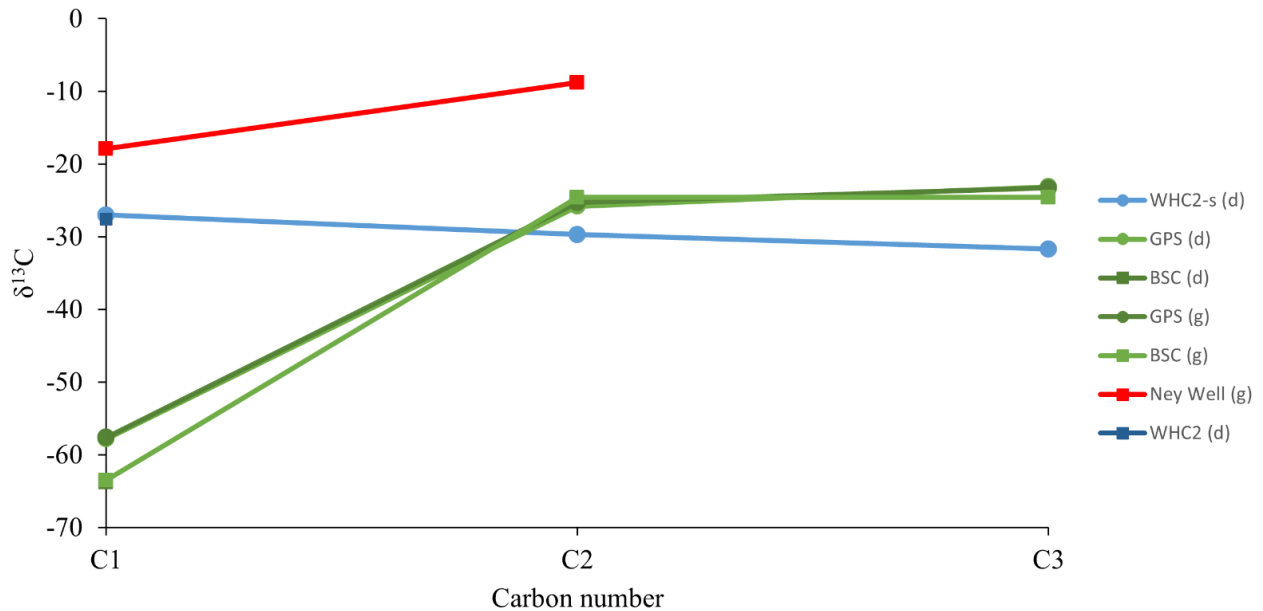


Figure 2.5. Natural gas plot showing the $\delta^{13}\text{C}$ values of methane, butane, and propane of dissolved and bubbling gases in groundwater and pooled water at the Tablelands, The Cedars, and Aqua de Ney. Dissolved gases are indicated by (d) in the site name while bubbling gases are indicated by (g) in the site name.

Table 2.2. Composition of dissolved gases measured in groundwater and pooled water at the Tablelands, The Cedars, and Aqua de Ney.

	Groundwater		Pooled/Well Water		
	WHC2-s	GPS	Ney Well	WHC2	BSC
CO₂ [μM]	-	31	< d.l.	< d.l.	44
O₂ [μM]	-	< d.l.	$2.27 \times 10^1 \pm 6.46 \times 10^1$	100	< d.l.
CO [μM]	< d.l.	< d.l.	< d.l.	45	< d.l.
H₂ [μM]	446	681	< d.l.	480	157
δ²H H₂ (‰)	-790 ± 4	-752 ± 3	< d.l.	-774	-775 ± 8
CH₄ [μM]	36.3	34	1.92×10^3	8	22
δ¹³C CH₄ (‰)	-27.0	-57.8 ± 0.7	-	-27.6 ± 0.06	-63.8 ± 0.4
δ²H CH₄ (‰)	-175 ± 1	-292 ± 2	-141 ± 2	-176	-305 ± 3
C₂ [μM]	1.26	$4.99 \times 10^{-1} \pm 3.33 \times 10^{-2}$	-	< d.l.	< d.l.
δ¹³C C₂	-29.7	-25.8	-	-	-
C₃ [μM]	1.04	2.27×10^{-1}	-	< d.l.	< d.l.
δ¹³C C₃ (‰)	-31.7	-23.1	-	< d.l.	n.d.
<i>i</i>C₄ [μM]	0.189	8.60×10^{-2}	-	< d.l.	< d.l.
<i>n</i>C₄ [μM]	0.344	$2.24 \times 10^{-1} \pm 5.0 \times 10^{-3}$	-	< d.l.	< d.l.
<i>i</i>C₅ [μM]	0.152	1.66×10^{-1}	-	< d.l.	< d.l.
<i>n</i>C₅ [μM]	0.236	$1.80 \times 10^{-1} \pm 4.0 \times 10^{-3}$	-	< d.l.	< d.l.

Standard deviations (1σ) of measurements were less than 10 % unless otherwise indicated. Parameters below limits of detection are indicated by the letters d.l. and parameters not measured are indicated by “-”. Data reported in this table were collected for this study except where noted: *Morill et al. (2013).

Table 2.3. Composition of bubbling gases measured at The Cedars and Aqua de Ney.*

	BSC	GPS	Ney Well
CO₂ (% by vol)	- ^x	-	< d.l.
O₂ (% by vol)	- ^x	-	-
CO (% by vol)	- ^x	< d.l.	< d.l.
H₂ (% by vol)	34 ^x	-	< d.l.
δ²H H₂ (‰)	-772	-780 ± 3.6	< d.l.
CH₄ (% by vol)	5.3 ± 1.2 ^x	7.1	84.4
δ¹³C CH₄ (‰)	-63.5 ± 1.6 ^x	-57.6	-17.9 ± 0.2
δ²H CH₄ (‰)	-355	-286.8	-126.5 ± 3.0
C₂ (% by vol)	< d.l. ^x	< d.l.	0.06
δ¹³C C₂	-24.6	-25.3	-8.8 ± 0.02
δ²H C₂ (‰)	- ^x	-	-52.9 ± 4.4
C₃ (% by vol)	4.1 x 10 ^{-3x}	0.01	< d.l.
δ¹³C C₃ (‰)	-24.6	-23.3	< d.l.
<i>i</i>C₄ (% by vol)	2.3 x 10 ^{-3x}	-	< d.l.
<i>n</i>C₄ (% by vol)	4.9 x 10 ^{-3x}	-	< d.l.
<i>i</i>C₅ (% by vol)	< d.l. ^x	-23	< d.l.
<i>n</i>C₅ (% by vol)	< d.l. ^x	-	< d.l.

*The gases in the Tablelands fluids were only in the dissolved phase. Standard deviations (1σ) of measurements were less than 10 % unless otherwise indicated. Parameters below limits of detection are indicated by the letters d.l. and parameters not measured are indicated by “-”. Data reported in this table were collected for this study except where noted: ^xMorill et al. (2013).

2.4 Discussion

2.4.1 Hydrochemical Analysis and Sample Grouping


The geochemical results (Table 2.1) demonstrated that while there was a wide range in values between the three studied sites of terrestrial serpentinization, there were also many commonalities. To better understand the geochemistry and to group the water types, the major ions were plotted on a Piper diagram (Piper, 1953) (Figure 2.6A). Figure 2.6A shows how all the flowing oxic surface waters (i.e., WHB, AC, and Ney River), despite their different geographical locations, plotted closely together in the Mg-HCO₃ Type water of the Piper diagram. It is notable that despite the different locations and sources of surface water, they share so many characteristics. In addition to the slightly basic pH (> 8.1), they are similarly depleted in SO₄²⁻, Cl, Na, K, and Ca and more enriched in Mg relative to their ultra-basic counterparts.

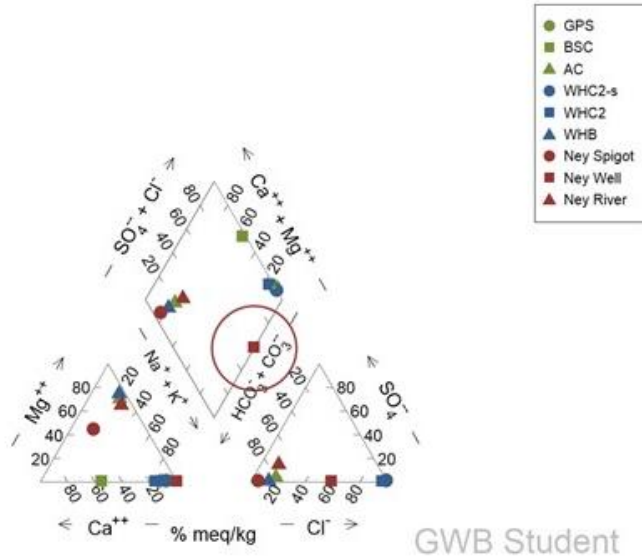
The groundwater springs of the Tablelands and The Cedars (WHC2-s and GPS, respectively) also grouped together in the Na-Cl Type water of the Piper diagram. Unexpectedly, the groundwater from Ney Spigot did not plot with the other groundwater samples, but instead plotted closely to the flowing surface waters in the Mg-HCO₃ type field. This suggests that, unlike the other groundwaters sampled in this study, the water flowing from Ney Spigot was likely surface water that had percolated through near the surface and had not been altered by serpentinization. The pooled groundwater, WHC2, at the Tablelands plotted with the ultra-basic groundwater spring waters in the Na-Cl Type water of the Piper diagram. This suggests that the major ion composition of WHC2 pooled water was not impacted by the exposure to the atmosphere and contributions from overland flow or precipitation. Conversely, the pooled groundwaters at The Cedars (BSC) had been impacted by exposure to the atmosphere and potential contamination by shallow groundwater, overland flow and/or precipitation, as it plotted

on the edge between the Na-Cl and Ca-Cl Type water fields on the Piper diagram. The water from Ney Well plotted on the other side of the Piper diagram from the groundwater group, on the edge between Na-Cl and Na-HCO₃ Type water fields.

To better understand how the aqueous geochemistry at other sites of serpentinization compared to the sites in this study, water samples from the Samail Ophiolite in Oman, the Ojén peridotite, and Hakuba Happo were also plotted on a Piper diagram (Figure 2.6B). Samples from Oman (Miller et al., 2016; Paukert et al., 2012) plotted in the Ca-Cl Type waters on the Piper diagram which was close to the pooled groundwater from The Cedars (BSC). Samples from Hakuba Happo (Suda et al., 2014) plotted in the Na-Cl Type waters close to the groundwater fluids from The Cedars (GPS) and the Tablelands (WHC2-s). Finally, samples from the Ojén peridotite massif and the Ronda peridotite massif (Giampouras et al., 2019) plotted between the Na-Cl and mixed Type waters on the Piper diagram.

A

TDS (mg/kg)

 1e4



B

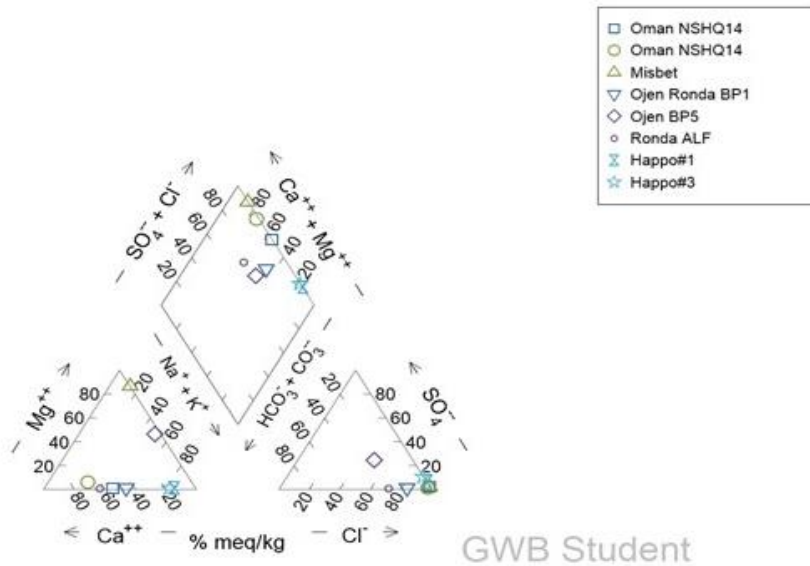


Figure 2.6. Piper diagram illustrating the relationships in fluid composition between (A) ultra-basic and surface water endmembers and pooled waters at the Tablelands, The Cedars, and Aqua de Ney and (B) ultra-basic fluids from the Samail Ophiolite in Oman (Miller et al., 2016; Paukert et al., 2012), the Ojén peridotite massif and the Ronda peridotite massif (Giampouras et al., 2019), and Hakuba Happo (Suda et al., 2014). The amount of total dissolved solids (TDS), calculated using Geochemist’s Workbench, are indicated by the red circle.

2.4.2 Aqua de Ney Well Water

The Ney Well water data plotted by itself on the Piper diagram signifying the fact that the water contained less Cl and more TIC relative to the other waters analyzed. However, these are not the only anomalies; almost every parameter measured for Ney Well water was unique, except for its E_h and pH. Processes in addition to serpentinization that are not occurring at The Cedars or the Tablelands can explain many of these unique data. These processes could include the contribution of residual fluid from a dehydrating slab, sulfate reduction, and evaporation.

Based on the $\delta^{11}\text{B}$, $\delta^7\text{Li}$, and B/Cl and Br/Cl ratios, Boschetti et al. (2017) suggested a hydrothermal origin ($\sim 240^\circ\text{C}$) for Aqua de Ney's water such that serpentinization and a deep dehydrating slab of oceanic crust (see Elder and Cashman (1992) for the tectonic setting) contributed to Aqua de Ney fluid geochemistry. The high concentration of K, Na, Cl, and Br and TIC may be due to the concentrating effect slab dehydration. The Ney Well water was also a great deal more enriched in ^2H and ^{18}O relative to Ney Creek and Ney Spigot, the well water values plotted below the LMWL (Figure 2.3) suggesting that they are non-meteoric in origin as suggested by Boschetti et al. (2017). The ^2H and ^{18}O data of water sampled from Aqua de Ney are well described ($r^2=0.9997$) by a linear regression with a slope of 4.4 and a y-intercept of -34.6 ‰. Boschetti et al. (2017) concluded that this lower slope likely reflects the effect of residual fluid entering the system from a dehydrating slab. Alternatively, it is possible that this slope could be indicative of an evaporitic environment. The Ney Well containment structure is a raised hexagonal concrete edifice ~ 2 m across and open to the atmosphere (Figure 2.2F). The water level is well below the concrete edge of the well such that water leaves this reservoir either through evaporation or seepage through the concrete. Evaporation could also explain some of the anomalies observed in conservative ion and TIC concentrations measured at Ney Well.

Unfortunately, the extent of the effect of evaporation on Ney Well has not been determined; to do this the well would have to be emptied and allowed to refill with discharging groundwater. The flow rate of the discharge would then need to be tested and the water sampled (as described in the methods for WHC2-s) to determine the impact, if any, evaporation has on the geochemistry.

A high Ca:Mg ratio is a common characteristic of Ca-OH type fluids associated with serpentinization as seen in The Cedars and the Tablelands groundwaters (which had ratios of 2470 and 124, respectively) (Barnes et al., 1967; Giampouras et al., 2019; Morrill et al., 2013). The Ca:Mg ratio in Ney Well water, however, is much lower (4.73). Saturation calculations were performed using the activities and the K_{sp} to determine whether preferential precipitation of Ca-carbonates could have scavenged these ions from the water. The results of the saturation calculations (see Supplementary Materials, Table 2.S1) suggested that both the Mg and Ca carbonates were undersaturated at Ney Well. By contrast, in the pooled water at the Tablelands, CaCO_3 was oversaturated while MgCO_3 was undersaturated and in the pooled water at The Cedars, both CaCO_3 and MgCO_3 were undersaturated.

To test for a possible marine origin, Cl:Br and SO_4^{2-} :Cl ratios of fluid from Ney Well were calculated and compared to known ratios of seawater. The Cl:Br ratio in the fluid from Ney Well (2.58×10^2) was within 10 % difference from that of seawater (2.85×10^2), consistent with the suggestion by (Boschetti et al., 2017) that Ney Well water is at least partially influenced by a fossil marine water. The Cl concentration in the fluid from Ney Well, while high, in meq/kg is low relative to the other ultra-basic endmembers (Figure 2.5). This was also noted by others including Feth et al. (1961) and Boschetti et al. (2017).

The presence of H₂S, as well as the trace to absent amounts of H₂, in the Ney Well water was also anomalous relative to the other ultra-basic serpentine hosted springs. However, these anomalies can be explained, at least in part, by the process of sulfate reduction whereby H₂ reacts with SO₄²⁻ to form H₂S. This process can occur abiotically but below 250 °C this reaction tends to be very slow (Shanks et al., 1981). Sulfate reduction can also be mediated by microorganisms (Muyzer & Stams, 2008). Lang et al. (2012) detected large variations in hydrogen, sulfate, and sulfide concentrations in fluids at Lost City Hydrothermal Field. They explained this phenomenon by a single high H₂ fluid that has been altered by microbial sulfate reduction (Lang et al., 2012). For this process to occur at Aqua de Ney, both H₂ and SO₄²⁻ would need to be present in the system. Although there were only trace concentrations of SO₄²⁻ detected at Aqua de Ney, nearby acid sulfate springs on Mt. Shasta have been reported to have an unusually high SO₄²⁻ concentration (Mariner et al., 1990; Nathenson et al., 2003). Although the origin of this SO₄²⁻ remains unknown, it has been proposed that the unusual geochemistry at springs on Mt. Shasta is a result of steam and gases flowing into water and dissolving the adjacent volcanic rock (Nathenson et al., 2003) and/or a contribution from magmatic SO₂. Due to the proximity of Mt. Shasta to Aqua de Ney, it is likely that Aqua de Ney may have a similar input of SO₄²⁻. Through a mass balance calculation, it was determined that if all the H₂ gas in the system were to react with all the available SO₄²⁻ to form H₂S, 3.39 x 10⁴ μM of H₂ would be present. While this concentration is higher than the amount of H₂ gas present in the groundwater at the sites of serpentinization sampled in this study (i.e. the Tablelands or The Cedars (446 and 681 μM respectively)) as well as at other sites of terrestrial serpentinization (e.g. Oman (Miller et al., 2016), CROMO (Crespo-Medina et al., 2014), Hakuba Happo (Suda et al., 2014), and the Voltri Massif (Brazelton et al., 2017)), the concentration of CH₄ was also higher at Ney Well compared

to the other sites. The predicted H₂ concentration is also similar to the concentration of CH₄ detected at Ney Well.

2.4.3 Groundwater and Pooled Water at The Cedars and the Tablelands

While the groundwater springs of The Cedars and the Tablelands represent the geochemistry of subsurface of serpentinite-hosted springs, the pooling groundwater of BSC and WHC2, which are open to the atmosphere and surface and shallow ground water contamination, represent the geochemistry resulting from high redox gradients where electron donor-rich groundwaters mix with electron acceptor-rich surface water. The different chemistries of these pools may be a result of the mixing of groundwater and surface water/shallow groundwater endmembers. A 2-component mixing model between the groundwater end member (represented by GPS and WHC-s for The Cedars and the Tablelands, respectively) and the surface water (represented by AC and WHB for The Cedars and the Tablelands, respectively) was created to determine the fraction of ultra-basic water (f_{UB}) contributing to each pool (after the method described in Szponar et al. (2013), see supplementary material for further information) (Table 2.1). The concentrations of conservative ions such as Br and Cl are positively correlated and are well described by a linear regression (Figures 2.S5 and 2.S6) suggesting conservative mixing between endmember fluids. Using this model, it was estimated that BSC was composed of 7 % ultra-basic groundwater and WHC was composed of 28 % ultra-basic groundwater. The fact that both these pools had similar pH values compared to their ultra-basic groundwater counterparts demonstrates the large buffering capacity of the ultra-basic groundwater.

Pool concentrations of non-conservative ions such as Mg, Fe, Mn, PO₄³⁻, NO₃⁻, and TIC were over predicted by the mixing model for both BSC and WHC2 (Table 2.S2), suggesting that these ions were consumed in the pools. The differences were greater for BSC than WHC2.

Although little is known about the processes that affect the aqueous concentrations of Mg, Fe, and Mn in these systems, it is likely that the decrease in their concentrations is due to the redox sensitivity of these elements (Pan et al., 2014). Complexation with other ions such as Cl would be minimal since the calculated activity coefficients (Table 2.S3) were close to 1 for fluids from the Tablelands and The Cedars. Phosphate, nitrate, and TIC are nutrients required for life, and were likely consumed for metabolic processes enabled by the presence of these electron acceptors provided by the oxic surface waters. The sulfate concentration was also over predicted in the BSC, but under predicted for WHC2. This difference can be explained by the redox values of the pools. BSC was more reducing (-344 mV) such that sulfate was likely being reduced, while WHC2 was less reducing (-71 mV) such that existing sulfides would be oxidized to sulfates. Concentrations of Ca were underpredicted in the pooled water at The Cedars and the Tablelands, which means that there was more Ca in the pools than can be explained by mixing of the two water sources. However, it is unlikely that Ca was being produced in the pools. Methane concentrations at the Tablelands were well predicted for WHC2 by the mixing models, however, methane concentrations at The Cedars were underpredicted for BSC by the mixing model.

2.4.4 Methane

Using hydrogen isotopic systematics of the $\text{CH}_4\text{-H}_2\text{-H}_2\text{O}_{(l)}$ system, equilibrium temperatures between these species were calculated and compared to measured temperatures to determine whether these gases were in isotopic equilibrium. These calculations were performed for the Tablelands and The Cedars but not Aqua de Ney since it had no detected H_2 gas. Equations from Horibe and Craig (1995) predicted equilibrium temperatures for $\text{H}_2\text{O}_{(l)}\text{-H}_2$ and $\text{CH}_4\text{-H}_2$ of 14 °C and -16 °C, respectively for the pooled water at the Tablelands (WHC2). The measured temperature of the water at WHC2 was 9.6 °C. The discrepancy between the measured

temperature and the predicted equilibrium temperature for CH₄-H₂ demonstrates that the CH₄ and H₂ were not in isotopic equilibrium. Similarly, predicted equilibrium temperatures for H₂O_(l)-H₂ and CH₄-H₂ at The Cedars were 6 °C and 8 °C, respectively, for GPS, well below the measured water temperature of 17.1 °C. Since serpentinization is an exothermic process, it is expected that the equilibrium temperatures of these gases to be higher than the measured temperature of the spring water if they formed in the subsurface; this, however, was not the case. Conversely, predicted equilibrium temperatures for H₂O_(l)-H₂ and CH₄-H₂ of 29 °C and 53 °C, respectively for BSC were higher than the measured pool temperature of 17.4 °C. While these may reflect a subsurface temperature, the calculated values differ substantially, with the greatest discrepancy occurring in the temperature calculated using CH₄ and H₂, indicating that the CH₄ and H₂ in BSC were also not in isotopic equilibrium. Therefore, kinetic isotope effects instead of equilibrium isotope effects more likely influenced the δ²H values of CH₄ sampled from the Tablelands and The Cedars.

δ²H and δ¹³C values of CH₄ sampled from each site in this study along with other sites of terrestrial serpentinization are plotted on the DC plot (Figure 2.7) along with the empirically derived microbial, thermogenic, and abiogenic fields. The relative positions of these fields have been derived from previous studies (Cumming et al., 2019; Etiope & Sherwood Lollar, 2013). This figure illustrates that while there is some overlap between the fields (specifically the abiogenic field and thermogenic field), non-microbial and microbial methane can still be differentiated (Cumming et al., 2019). CH₄ from both BSC and GPS at The Cedars plot in the microbial field. CH₄ from WHC2 and WHC2-s at the Tablelands as well as from CROMO plot where the thermogenic and abiogenic fields overlap. CH₄ from Ney Well, Chimaera, and the Zambales ophiolite plot solely in the abiogenic field.

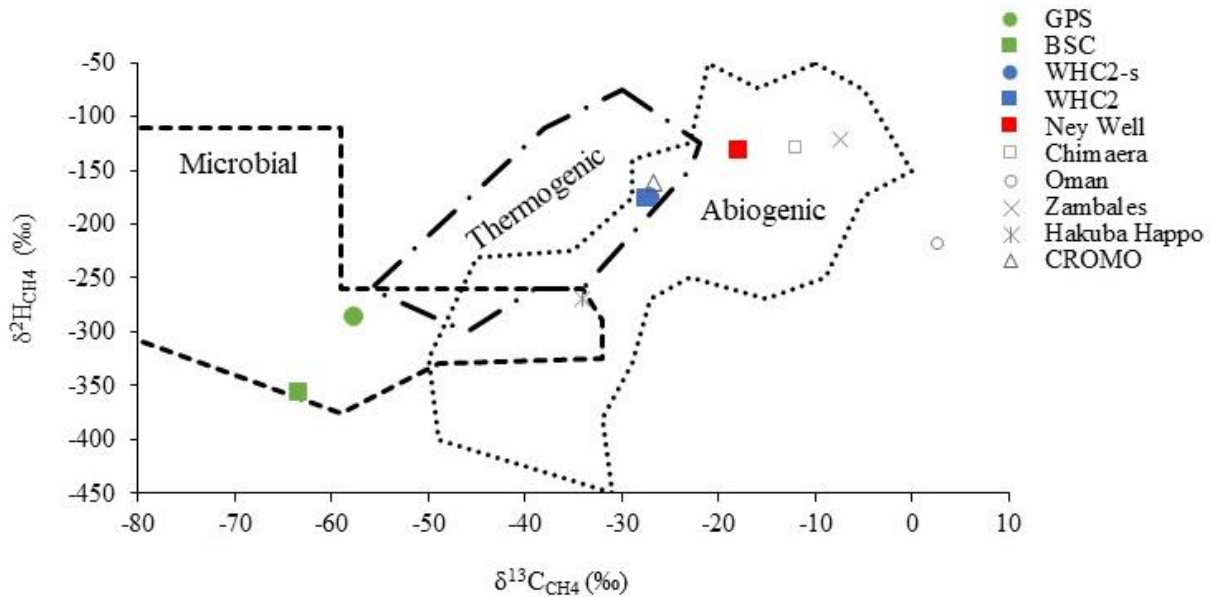


Figure 2.7. A DC plot of $\delta^2\text{H}$ versus $\delta^{13}\text{C}$ for methane bubbling from the ultra-basic reducing spring at Aqua de Ney and for dissolved methane at the ultra-basic reducing springs at the Tablelands and The Cedars. Corresponding values for $\delta^2\text{H}$ versus $\delta^{13}\text{C}$ for methane from the Chimaera seep in Turkey (Etiope et al., 2011), the Samail Ophiolite in Oman (Miller et al., 2016), the Zambales ophiolite in the Philippines, Hakuba Happo in Japan (Suda et al., 2014), and CROMO in CA, U.S.A. (Wang et al., 2015) are also plotted. Empirically derived fields for microbial, thermogenic, and abiogenic methane production, as proposed by Etiope and Sherwood Lollar (2013) and references therein, are included for comparison.

In conjunction with the DC plot, a Bernard plot (i.e., $\delta^{13}\text{C}$ values of CH_4 versus $\text{CH}_4/\text{C}_2 + \text{C}_3$) has been used to differentiate microbial and thermogenic sources of CH_4 . The data collected in this study was plotted along with previously published data from the Tablelands and The Cedars (Figure 2.8). The Tablelands data plots in the thermogenic field, Aqua de Ney data does

not plot in any field, and The Cedars data trends from the microbial field to the thermogenic field. Since there is no abiogenic field on the Bernard Plot, it cannot be used to differentiate non-microbial sources; however, Figure 2.8 supports the non-microbial nature of the methane from the Tablelands and Aqua de Ney. While the methane from The Cedars plots in the microbial field of the DC plot (Figure 2.7), on the Bernard Plot these data trend from the microbial field to the thermogenic field. This can happen if CH₄ is being oxidized or if there is mixing of CH₄ from two sources. Since GPS is reducing and the methane was sampled at the point of discharge, it is unlikely the CH₄ was substantially oxidized. It is more likely that there are two sources of CH₄ at The Cedars, one microbial and one non-microbial, and various amounts of mixing of CH₄ between the two sources is occurring. The mixing model (Figures 2.S3, 2.S4, and Table 2.S2) underpredicts the amount of CH₄ measured in BSC, also suggesting that there is an additional source of methane to the BSC pool. These data support a mixed source of methane in the BSC springs at The Cedars proposed by Morrill et al. (2013).

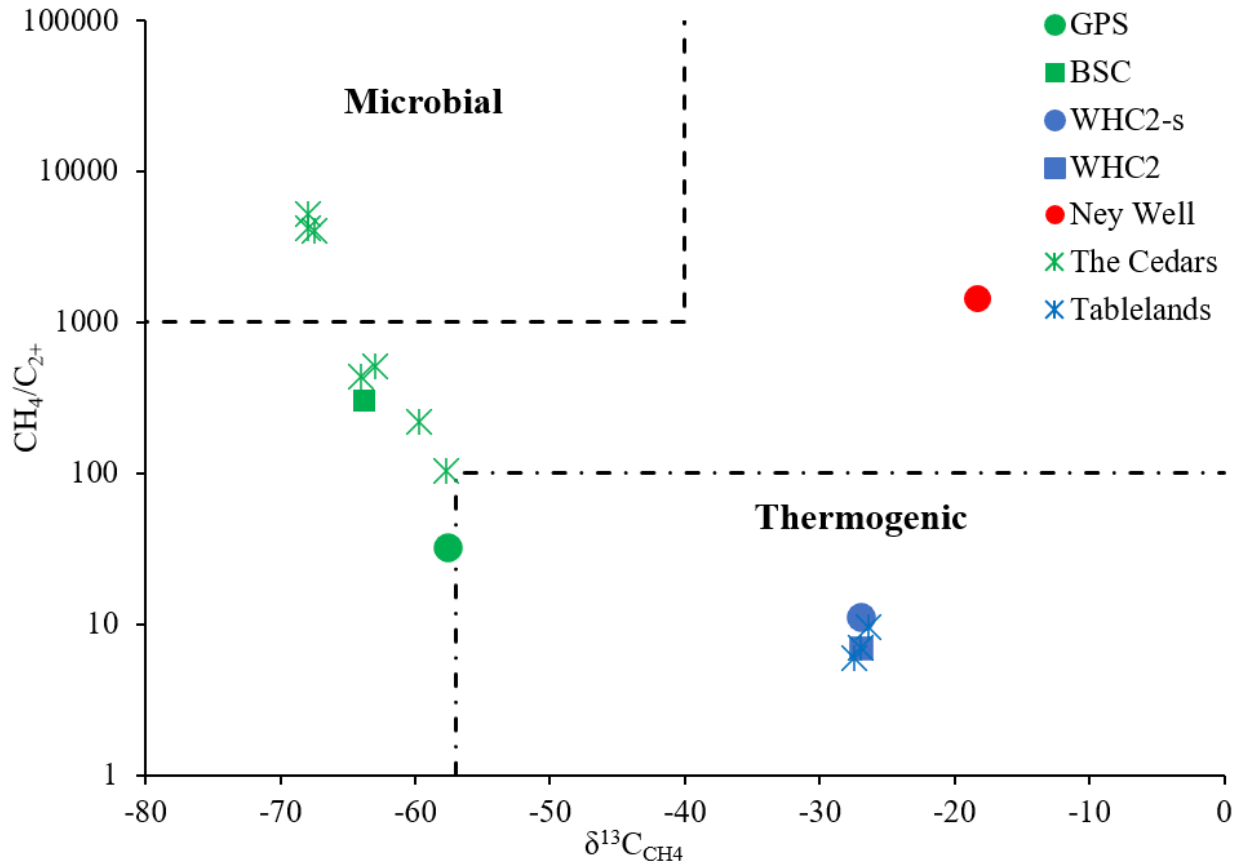


Figure 2.8. Bernard Plot of lower molecular weight hydrocarbons from this study and published studies for the Tablelands (Cumming et al., 2019) and The Cedars (Morrill et al., 2013; Morrill unpublished data) compared to conventional fields for microbial and thermogenic gases (adapted from Hunt, 1996). Data points that plot between the two fields suggest a mixing of multiple sources of methane or secondary process are occurring that affect the gaseous hydrocarbons of the lower springs.

The CH₄ at these three sites studied, as well as the other sites of terrestrial serpentinization plotted on Figure 2.7, demonstrate the wide range of δ¹³C and δ²H values that CH₄ can have at sites of serpentinization. The stable isotope values of CH₄ are directly affected

by the kinetic isotope effect associated with the reaction that forms the CH₄. In addition, other factors that can affect the stable isotope values of CH₄ include whether the reaction occurred in an open or closed system, the temperature at which the CH₄ was formed, post genetic processes such as CH₄ oxidation, and the isotope values of the reactants. Carbon and hydrogen reservoirs (e.g., TIC (Figure 2.S3), H₂O (Figure 2.3), CH₄ (Figure 2.7) and other hydrocarbons) of Aqua de Ney are the most enriched in the heavy isotopes relative to those of the Tablelands and The Cedars. This may be due to the fossil marine water contributions, dissolution of marine limestone, or magmatic contributions, which are known to be enriched in the heavy isotope compared to other crustal reservoirs (Clark & Fritz, 1997). Conversely, the more negative $\delta^{13}\text{C}$ TIC values at the Cedars will lead to a more negative value of CH₄.

The influence of the isotope values of the reactants can be removed by plotting isotopic fractionation factors (α) between reactants and products for both carbon and hydrogen. Figure 2.9 plots the fractionation factor of carbon isotope values between reactant carbon dioxide and product methane ($\alpha^{13}\text{C}(\text{CO}_2\text{-CH}_4)$) versus that of hydrogen isotope values between reactant water and product methane ($\alpha^2\text{H}(\text{H}_2\text{O-CH}_4)$) determined in this study with three statistically derived fields (Cumming et al., 2019). According to Cumming et al., (2019) a thermogenic field could not be developed due to the lack of data representing that pathway; therefore, it cannot be used to differentiate non-microbial sources. Nonetheless, Figure 2.9 demonstrates that with the removal of the starting isotope composition effect, the groundwater and pooled water from the Tablelands (WHC2-s and WHC2), Ney Well, and the groundwater from The Cedars (GPS) all in the abiogenic region, while pooled water from The Cedars (BSC) plots between the abiogenic and microbial fields. This intermediate result was also observed in the Bernard Plot (Figure 2.8).

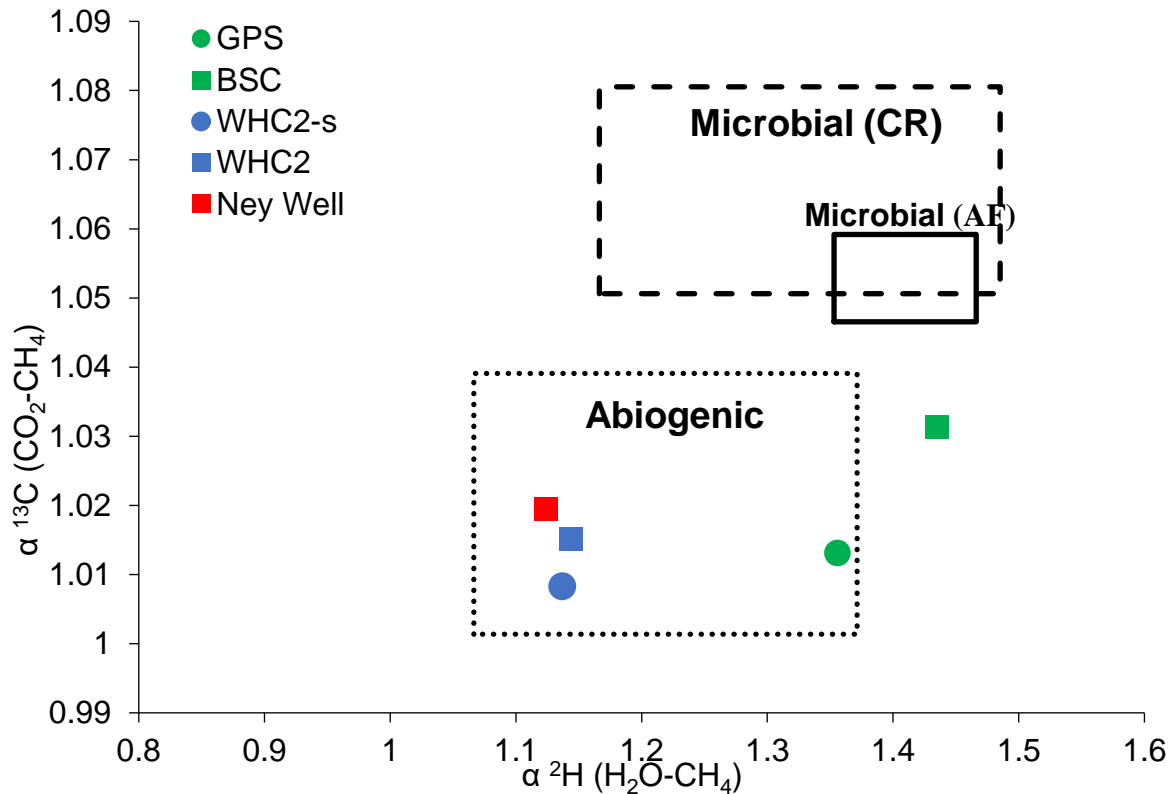


Figure 2.9. Dual fractionation plot showing the fractionation factors between reactants and products for each site plotted along with the fields established by Cumming et al., 2019 for abiogenic CH_4 , and microbial CH_4 formed via the carbonate reduction (CR) pathway and the and fermentation (AF) pathway. The $\alpha^{13}\text{C}(\text{TIC-CH}_4)$ data from this study was converted to $\alpha^{13}\text{C}(\text{CO}_2\text{-CH}_4)$ using the method described in Kohl et al., 2016).

Figures 2.7, 2.8, and 2.9 demonstrate the variety of CH_4 sources possible at sites of serpentinization. The CH_4 from Ney Well is abiogenic with ^{13}C enriched carbon and hydrogen reactants and relatively smaller fractionation factors compared to processes that create microbial methane. The abiotic nature of the CH_4 from Ney Well may be, in part, due to its higher temperatures (240 °C (Boschetti et al., 2017)) compared to the other sites in this study or due to

the presence of H₂S. If microbial sulfate reduction is occurring at Aqua de Ney, then it may be difficult for microbial methanogens to compete for resources. Thermodynamic calculations by Lang et al. (2012) suggested that sulfate reduction can supply 3 to 17 times more metabolic energy in unmixed anaerobic fluids than methanogenesis. While biomarkers from the Chimaera seep have suggested that both methanogens and sulfate reducers are both present at the site, likely active within variable microenvironments (Zwicker et al., 2018), this does not appear to be the case at Aqua de Ney. Conversely, there is little to no sulfate or sulfide in the spring waters of The Cedars where we see evidence of at least some microbial methanogenesis. At The Cedars, microbial methanogens do not have to compete with sulfate reducers for resources. However, microbial methane is not the only source of CH₄ at The Cedars. There is also a non-microbial source that seems to dominate the deeper groundwater springs as demonstrated in this study as well as Morrill et al. (2013). The CH₄ from the Tablelands continues to be a non-microbial enigma. This non-microbial CH₄ could be a result of the suppression of microbial methanogenesis due to the presence of sulfur in the spring water at the Tablelands (Cook et al., 2021b (Chapter 3)). However, determining the thermogenic or abiogenic nature of the Tablelands remains a challenge (as discussed in Cumming et al. (2019)), as all of the data lie within the overlapping zones of abiogenic and thermogenic hydrocarbons.

2.5 Conclusions

The range of geochemistry measured at the Tablelands, The Cedars, and Aqua de Ney provides a better understanding of the similarities and differences possible between sites of terrestrial serpentinization, as well as the microbial diversity hosted there. These sites represent very distinct endmembers of serpentinization in their sources of methane, age, and geochemistry. The Tablelands represents an older site of serpentinization where the methane is non-microbial in source. The Cedars represents a younger site of serpentinization where the methane is, at least partially, microbial in source. Finally, Aqua de Ney represents a site of serpentinization that has not only an elevated concentration of sulfur but also an evaporative environment and the methane is abiotic in source. Furthermore, despite hydrogen being a product of serpentinization reactions, no hydrogen was detected in samples from Aqua de Ney. It is likely that this is due to the hydrogen reacting with the sulfur forming the hydrogen sulfide that is present at Aqua de Ney. Despite the differences between the sites, many commonalities were still observed in the ultra-basic endmember fluids including low concentrations of electron acceptors (i.e., O_2 , NO_3^- , SO_4^{2-}) and ultra-basic reducing fluids. Because these sites are so unique, they can help us better understand the geochemical resources that support life in the subsurface and the biogeochemical signatures that this life produces. This may have important implications for the search for life beyond Earth, on other planets and moons where subsurface conditions may support microbial communities that are protected from harsh thermal and radiation conditions at the surface.

2.6 Acknowledgments

The authors would like to thank David McCrory and Roger Raiche for allowing access to The Cedars and Parks Canada for providing access to Tablelands. The authors would also like to thank Emily Cumming and Ben Taylor for their help in the field, Jamie Warren, Dr. Geert van Biesen (CREAIT – Stable Isotope Laboratory), and Dr. Inês Nobre Silva (CREAIT – ICPMS) for their expertise, and Dr. Mark Wilson for his help in the field as well as his wisdom and inspirational discussions. This research was funded by Natural Science and Engineering Research Council (NSERC) Discovery Grant and Canada Space Agency’s Flights and Fieldwork for the Advancement of Science and Technology (FAST) grant awarded to Dr. Penny Morrill and NSERC’s Alexander Graham Bell Canada Graduate Scholarship-Doctoral (CGS D) awarded to Melissa Cook. Saturation and f_{UB} calculations and mixing predictions can be found in the Supporting Information. Additional data that were used to create Figures and Tables are available through Memorial University’s research repository (<https://doi.org/doi:10.5683/SP3/BD9VRA>).

2.7 References

- Bach, W., Paulick, H., Garrido, C. J., Ildefonse, B., Meurer, W. P., & Humphris, S. E. (2006). Unraveling the sequence of serpentinization reactions: petrography, mineral chemistry, and petrophysics of serpentinites from MAR 15°N (ODP Leg 209, Site 1274). *Geophysical research letters*, 33(13), L13306-n/a.
<https://doi.org/10.1029/2006GL025681>
- Barnes, I., LaMarche, V. C., & Himmelberg, G. (1967). Geochemical Evidence of Present-Day Serpentinization. *Science (American Association for the Advancement of Science)*, 156(3776), 830-832. <https://doi.org/10.1126/science.156.3776.830>
- Boschetti, T., Toscani, L., Iacumin, P., & Selmo, E. (2017). Oxygen, Hydrogen, Boron and Lithium Isotope Data of a Natural Spring Water with an Extreme Composition: A Fluid from the Dehydrating Slab? *Aquatic geochemistry*, 23(5), 299-313.
<https://doi.org/10.1007/s10498-017-9323-9>
- Brazelton, W. J., Thornton, C. N., Hyer, A., Twing, K. I., Longino, A. A., Lang, S. Q., Lilley, M. D., Früh-Green, G. L., & Schrenk, M. O. (2017). Metagenomic identification of active methanogens and methanotrophs in serpentinite springs of the Voltri Massif, Italy. *PeerJ (San Francisco, CA)*, 5, e2945-e2945. <https://doi.org/10.7717/peerj.2945>
- Brock, T. D. (1991). *Biology of microorganisms* (6th ed.. ed.). Englewood Cliffs, N.J. : Prentice Hall.
- Bruni, J., Canepa, M., Chiodini, G., Cioni, R., Cipolli, F., Longinelli, A., Marini, L., Ottonello, G., & Vetusch Zuccolini, M. (2002). Irreversible water-rock mass transfer accompanying the generation of the neutral, Mg-HCO₃ and high-pH, Ca-OH spring waters of the Genova province, Italy. *Applied geochemistry*, 17(4), 455-474.
[https://doi.org/10.1016/S0883-2927\(01\)00113-5](https://doi.org/10.1016/S0883-2927(01)00113-5)

- Clark, I. D., & Fritz, P. (1997). *Environmental isotopes in hydrogeology*. Boca Raton, FL : Lewis Publishers.
- Coleman, R., G. (2000). Prospecting for ophiolites along the California continental margin. *Special papers (Geological Society of America)*, 349, 351. <https://doi.org/10.1130/0-8137-2349-3.351>
- Coleman, R. G. (2004). Geologic nature of the Jasper Ridge Biological Preserve, San Francisco Peninsula, California. *International Geology Review*, 46(7), 629-637.
<http://pubs.er.usgs.gov/publication/70027010>
- Cook, M. C., Blank, J. G., Suzuki, S., Nealson, K. H., & Morrill, P. L. (2021b). Assessing Geochemical Bioenergetics and Microbial Metabolisms at Three Terrestrial Sites of Serpentinization: The Tablelands (NL, CAN), The Cedars (CA, USA), and Aqua de Ney (CA, USA). *Journal of geophysical research. Biogeosciences*, 126(6), n/a.
<https://doi.org/10.1029/2019JG005542>
- Coplen, T. B. (2011). Guidelines and recommended terms for expression of stable-isotope-ratio and gas-ratio measurement results: Guidelines and recommended terms for expressing stable isotope results. *Rapid communications in mass spectrometry*, 25(17), 2538-2560.
<https://doi.org/10.1002/rcm.5129>
- Coplen, T. B., & Kendall, C. (2000). Stable Hydrogen and Oxygen Isotope Ratios for Selected Sites of the U.S. Geological Survey's NASQAN and Benchmark Surface-Water Networks.
- Crespo-Medina, M., Twing, K. I., Kubo, M. D. Y., Hoehler, T. M., Cardace, D., McCollom, T., & Schrenk, M. O. (2014). Insights into environmental controls on microbial communities

- in a continental serpentinite aquifer using a microcosm-based approach. *Frontiers in Microbiology*, 5, 604-604. <https://doi.org/10.3389/fmicb.2014.00604>
- Cumming, E. A., Rietze, A., Morrissey, L. S., Cook, M. C., Rhim, J. H., Ono, S., & Morrill, P. L. (2019). Potential sources of dissolved methane at the Tablelands, Gros Morne National Park, NL, CAN: A terrestrial site of serpentinization. *Chemical geology*, 514, 42-53. <https://doi.org/10.1016/j.chemgeo.2019.03.019>
- Dunning, G. R., & Krogh, T. E. (1985). Geochronology of ophiolites of the Newfoundland Appalachians. *Canadian journal of earth sciences*, 22(11), 1659-1670. <https://doi.org/10.1139/e85-174>
- Dygart, N., Liang, Y., & Kelemen, P. B. (2016). Formation of Plagioclase Lherzolite and Associated Dunite–Harzburgite–Lherzolite Sequences by Multiple Episodes of Melt Percolation and Melt–Rock Reaction: an Example from the Trinity Ophiolite, California, USA. *Journal of Petrology*, 57(4), 815-838. <https://doi.org/10.1093/petrology/egw018>
- Elder, D., & Cashman, S. M. (1992). Tectonic control and fluid evolution in the Quartz Hill, California, lode gold deposits. *Economic geology and the bulletin of the Society of Economic Geologists*, 87(7), 1795-1812. <https://doi.org/10.2113/gsecongeo.87.7.1795>
- Etioppe, G., Schoell, M., & Hosgörmez, H. (2011). Abiotic methane flux from the Chimaera seep and Tekirova ophiolites (Turkey): Understanding gas exhalation from low temperature serpentinization and implications for Mars. *Earth and planetary science letters*, 310(1), 96-104. <https://doi.org/10.1016/j.epsl.2011.08.001>
- Etioppe, G., & Sherwood Lollar, B. (2013). ABIOTIC METHANE ON EARTH. *Reviews of geophysics (1985)*, 51(2), 276-299. <https://doi.org/10.1002/rog.20011>

- Feth, J. H., Rogers, S. M., & Roberson, C. E. (1961). Aqua de Ney, California, a spring of unique chemical character. *Geochimica et cosmochimica acta*, 22(2), 75,IN71,77-76,IN72,86. [https://doi.org/10.1016/0016-7037\(61\)90107-7](https://doi.org/10.1016/0016-7037(61)90107-7)
- García-Ruiz, J. M., Nakouzi, E., Kotopoulou, E., Tamborrino, L., & Steinbock, O. (2017). Biomimetic mineral self-organization from silica-rich spring waters. *Science advances*, 3(3), e1602285-e1602285. <https://doi.org/10.1126/sciadv.1602285>
- Giampouras, M., Garrido, C. J., Zwicker, J., Vadillo, I., Smrzka, D., Bach, W., Peckmann, J., Jiménez, P., Benavente, J., & García-Ruiz, J. M. (2019). Geochemistry and mineralogy of serpentinization-driven hyperalkaline springs in the Ronda peridotites. *Lithos*, 350-351, 105215. <https://doi.org/10.1016/j.lithos.2019.105215>
- Gold, T. (1992). The deep, hot biosphere. *Proc Natl Acad Sci U S A*, 89(13), 6045-6049.
- Grassle, J. F. (1987). The Ecology of Deep-Sea Hydrothermal Vent Communities. In J. H. S. Blaxter & A. J. Southward (Eds.), *Advances in Marine Biology* (Vol. 23, pp. 301-362). Academic Press. [https://doi.org/https://doi.org/10.1016/S0065-2881\(08\)60110-8](https://doi.org/https://doi.org/10.1016/S0065-2881(08)60110-8)
- Harmon, C. (1961). Isotopic Variations in Meteoric Waters. *Science (American Association for the Advancement of Science)*, 133(3465), 1702-1703. <https://doi.org/10.1126/science.133.3465.1702>
- Horibe, Y., & Craig, H. (1995). D/H fractionation in the system methane-hydrogen-water. *Geochimica et cosmochimica acta*, 59(24), 5209-5217. [https://doi.org/10.1016/0016-7037\(95\)00391-6](https://doi.org/10.1016/0016-7037(95)00391-6)
- Kendall, C., & Coplen, T. B. (2001). Distribution of oxygen-18 and deuterium in river waters across the United States. *Hydrological processes*, 15(7), 1363-1393. <https://doi.org/10.1002/hyp.217>

- Kohl, L., Cumming, E., Cox, A., Rietze, A., Morrissey, L., Lang, S. Q., Richter, A., Suzuki, S., Nealson, K. H., & Morrill, P. L. (2016). Exploring the metabolic potential of microbial communities in ultra-basic, reducing springs at The Cedars, CA, USA: Experimental evidence of microbial methanogenesis and heterotrophic acetogenesis. *Journal of Geophysical Research: Biogeosciences*, *121*(4), 1203-1220.
<https://doi.org/10.1002/2015jg003233>
- Lang, S. Q., & Brazelton, W. J. (2020). Habitability of the marine serpentinite subsurface: a case study of the Lost City hydrothermal field. *Philos Trans A Math Phys Eng Sci*, *378*(2165), 20180429. <https://doi.org/10.1098/rsta.2018.0429>
- Lang, S. Q., Früh-Green, G. L., Bernasconi, S. M., Lilley, M. D., Proskurowski, G., Méhay, S., & Butterfield, D. A. (2012). Microbial utilization of abiogenic carbon and hydrogen in a serpentinite-hosted system. *Geochimica et cosmochimica acta*, *92*, 82-99.
<https://doi.org/10.1016/j.gca.2012.06.006>
- Lutz, R. A., & Kennish, M. J. (1993). Ecology of deep-sea hydrothermal vent communities: A review. *Reviews of geophysics* (1985), *31*(3), 211-242.
<https://doi.org/10.1029/93RG01280>
- Mariner, R. H., Evans, W. C., Presser, T. S., & White, L. D. (2003). Excess nitrogen in selected thermal and mineral springs of the Cascade Range in northern California, Oregon, and Washington: sedimentary or volcanic in origin? *Journal of volcanology and geothermal research*, *121*(1), 99-114. [https://doi.org/10.1016/S0377-0273\(02\)00414-6](https://doi.org/10.1016/S0377-0273(02)00414-6)
- Mariner, R. H., Presser, T. S., Evans, W. C., & Pringle, M. K. W. (1990). Discharge rates of fluid and heat by thermal springs of the Cascade Range, Washington, Oregon, and

- northern California. *Journal of Geophysical Research: Solid Earth*, 95(B12), 19517-19531. <https://doi.org/10.1029/JB095iB12p19517>
- McCollom, T. M., & Seewald, J. S. (2007). Abiotic synthesis of organic compounds in deep-sea hydrothermal environments. *Chem Rev*, 107(2), 382-401. <https://doi.org/10.1021/cr0503660>
- McCollom, T. M., & Seewald, J. S. (2013). Serpentinites, hydrogen, and life. *Elements (Quebec)*, 9(2), 129-134. <https://doi.org/10.2113/gselements.9.2.129>
- McCollom, T. M., & Shock, E. L. (1997). Geochemical constraints on chemolithoautotrophic metabolism by microorganisms in seafloor hydrothermal systems. *Geochimica et cosmochimica acta*, 61(20), 4375-4391. [https://doi.org/10.1016/s0016-7037\(97\)00241-x](https://doi.org/10.1016/s0016-7037(97)00241-x)
- Miller, H. M., Matter, J. M., Kelemen, P., Ellison, E. T., Conrad, M. E., Fierer, N., Ruchala, T., Tominaga, M., & Templeton, A. S. (2016). Modern water/rock reactions in Oman hyperalkaline peridotite aquifers and implications for microbial habitability. *Geochimica et cosmochimica acta*, 179(C), 217-241. <https://doi.org/10.1016/j.gca.2016.01.033>
- Morrill, P. L., Brazelton, W. J., Kohl, L., Rietze, A., Miles, S. M., Kavanagh, H., Schrenk, M. O., Ziegler, S. E., & Lang, S. Q. (2014). Investigations of potential microbial methanogenic and carbon monoxide utilization pathways in ultra-basic reducing springs associated with present-day continental serpentinization: the Tablelands, NL, CAN. *Frontiers in Microbiology*, 5. <https://doi.org/10.3389/fmicb.2014.00613>
- Morrill, P. L., Kuenen, J. G., Johnson, O. J., Suzuki, S., Rietze, A., Sessions, A. L., Fogel, M. L., & Nealson, K. H. (2013). Geochemistry and geobiology of a present-day serpentinization site in California: The Cedars. *Geochimica et cosmochimica acta*, 109, 222-240. <https://doi.org/10.1016/j.gca.2013.01.043>

- Murseli, S., Middlestead, P., St-Jean, G., Zhao, X., Jean, C., Crann, C. A., Kieser, W. E., & Clark, I. D. (2019). The Preparation of Water (DIC, DOC) and Gas (CO₂, CH₄) Samples for Radiocarbon Analysis at AEL-AMS, Ottawa, Canada. *Radiocarbon*, *61*(5), 1563-1571. <https://doi.org/10.1017/RDC.2019.14>
- Muyzer, G., & Stams, A. J. M. (2008). The ecology and biotechnology of sulphate-reducing bacteria. *Nature Reviews. Microbiology*, *6*(6), 441-454. <https://doi.org/http://dx.doi.org/10.1038/nrmicro1892>
- Nathenson, M., Thompson, J. M., & White, L. D. (2003). Slightly thermal springs and non-thermal springs at Mount Shasta, California: Chemistry and recharge elevations. *Journal of volcanology and geothermal research*, *121*(1), 137-153. [https://doi.org/10.1016/S0377-0273\(02\)00426-2](https://doi.org/10.1016/S0377-0273(02)00426-2)
- Nealson, K. H., Inagaki, F., & Takai, K. (2005). Hydrogen-driven subsurface lithoautotrophic microbial ecosystems (SLiMEs): do they exist and why should we care? *Trends in microbiology (Regular ed.)*, *13*(9), 405-410. <https://doi.org/10.1016/j.tim.2005.07.010>
- Oremland, R. S., Miller, L. G., & Whiticar, M. J. (1987). Sources and flux of natural gases from Mono Lake, California. *Geochimica et cosmochimica acta*, *51*(11), 2915-2929. [https://doi.org/10.1016/0016-7037\(87\)90367-X](https://doi.org/10.1016/0016-7037(87)90367-X)
- Pan, Y., Koopmans, G. F., Bonten, L. T. C., Song, J., Luo, Y., Temminghoff, E. J. M., & Comans, R. N. J. (2014). Influence of pH on the redox chemistry of metal (hydr)oxides and organic matter in paddy soils. *Journal of soils and sediments*, *14*(10), 1713-1726. <https://doi.org/10.1007/s11368-014-0919-z>
- Paukert, A. N., Matter, J. M., Kelemen, P. B., Shock, E. L., & Havig, J. R. (2012). Reaction path modeling of enhanced in situ CO₂ mineralization for carbon sequestration in the

- peridotite of the Samail Ophiolite, Sultanate of Oman. *Chemical geology*, 330-331, 86-100. <https://doi.org/10.1016/j.chemgeo.2012.08.013>
- Piper, A. M. (1953). *A graphic procedure in the geochemical interpretation of water analysis / by Arthur M. Piper*. District of Columbia: U.S. Dept. of the Interior, Geological Survey, Water Resources Division, Ground Water Branch, 1953.
- Quick, J. E. (1981). Petrology and petrogenesis of the Trinity peridotite, An upper mantle diapir in the eastern Klamath Mountains, northern California. *Journal of Geophysical Research: Solid Earth*, 86(B12), 11837-11863. <https://doi.org/10.1029/JB086iB12p11837>
- Quick, J. E. (1982). The origin and significance of large, tabular dunite bodies in the Trinity peridotite, northern California. *Contributions to mineralogy and petrology*, 78(4), 413-422. <https://doi.org/10.1007/BF00375203>
- Rempfert, K. R., Miller, H. M., Bompard, N., Nothaft, D., Matter, J. M., Kelemen, P., Fierer, N., & Templeton, A. S. (2017). Geological and Geochemical Controls on Subsurface Microbial Life in the Samail Ophiolite, Oman. *Frontiers in Microbiology*, 8, 56-56. <https://doi.org/10.3389/fmicb.2017.00056>
- Rietze, A. (2015). *Investigating geochemistry and habitability of continental sites of serpentinization: the Cedars, California, USA and the Tablelands, Newfoundland, CAN* Memorial University of Newfoundland].
- Rudd, J. W. M., Hamilton, R. D., & Campbell, N. E. R. (1974). Measurement of Microbial Oxidation of Methane in Lake Water. *Limnology and oceanography*, 19(3), 519-524. <https://doi.org/10.4319/lo.1974.19.3.0519>
- Sabuda, M. C., Brazelton, W. J., Putman, L. I., McCollom, T. M., Hoehler, T. M., Kubo, M. D. Y., Cardace, D., & Schrenk, M. O. (2020). A dynamic microbial sulfur cycle in a

serpentinizing continental ophiolite. *Environ Microbiol*, 22(6), 2329-2345.

<https://doi.org/10.1111/1462-2920.15006>

Schulte, M., Blake, D., Hoehler, T., & McCollom, T. (2006). Serpentinization and Its Implications for Life on the Early Earth and Mars. *Astrobiology*, 6(2), 364-376.

<https://doi.org/10.1089/ast.2006.6.364>

Seyler, L. M., Brazelton, W. J., McLean, C., Putman, L., Hyer, A., Kubo, M. D., Hoehler, T., Cardace, D., & Schrenk, M. O. (2020). Carbon Assimilation Strategies in Ultrabasic Groundwater: Clues from the Integrated Study of a Serpentinization-Influenced Aquifer.

mSystems, 5(2), e00607-00619. <https://doi.org/10.1128/mSystems.00607-19>

Shanks, W. C., Bischoff, J. L., & Rosenbauer, R. J. (1981). Seawater sulfate reduction and sulfur isotope fractionation in basaltic systems: Interaction of seawater with fayalite and magnetite at 200–350°C. *Geochimica et cosmochimica acta*, 45(11), 1977-1995.

[https://doi.org/10.1016/0016-7037\(81\)90054-5](https://doi.org/10.1016/0016-7037(81)90054-5)

Shervais, J. W., Kimbrough, D. L., Renne, P., Hanan, B. B., Murchey, B., Snow, C. A., Zoglman Schuman, M. M., & Beaman, J. (2004). Multi-Stage Origin of the Coast Range Ophiolite, California: Implications for the Life Cycle of Supra-Subduction Zone Ophiolites.

International Geology Review, 46(4), 289-315. [https://doi.org/10.2747/0020-](https://doi.org/10.2747/0020-6814.46.4.289)

[6814.46.4.289](https://doi.org/10.2747/0020-6814.46.4.289)

Shervais, J. W., Murchey, B. L., Kimbrough, D. L., Renne, P. R., & Hanan, B. (2005).

Radioisotopic and biostratigraphic age relations in the Coast Range Ophiolite, Northern California

implications for the tectonic evolution of the western Cordillera. *Geological Society of America bulletin*, 117(5-6), 633-653. <https://doi.org/10.1130/B25443.1>

- Sleep, N. H., Meibom, A., Th, F., Coleman, R. G., & Bird, D. K. (2004). H₂-Rich Fluids from Serpentinization: Geochemical and Biotic Implications. *Proceedings of the National Academy of Sciences - PNAS*, *101*(35), 12818-12823.
<https://doi.org/10.1073/pnas.0405289101>
- St-Jean, G. (2003). Automated quantitative and isotopic (¹³C) analysis of dissolved inorganic carbon and dissolved organic carbon in continuous-flow using a total organic carbon analyser. *Rapid communications in mass spectrometry*, *17*(5), 419-428.
<https://doi.org/10.1002/rcm.926>
- Suda, K., Ueno, Y., Yoshizaki, M., Nakamura, H., Kurokawa, K., Nishiyama, E., Yoshino, K., Hongoh, Y., Kawachi, K., Omori, S., Yamada, K., Yoshida, N., & Maruyama, S. (2014). Origin of methane in serpentinite-hosted hydrothermal systems: The CH₄-H₂-H₂O hydrogen isotope systematics of the Hakuba Happo hot spring. *Earth and planetary science letters*, *386*, 112-125. <https://doi.org/10.1016/j.epsl.2013.11.001>
- Suhr, G. (1992). Upper mantle peridotites in the Bay of Islands Ophiolite, Newfoundland: Formation during the final stages of a spreading centre? *Tectonophysics*, *206*(1), 31-53.
[https://doi.org/10.1016/0040-1951\(92\)90366-E](https://doi.org/10.1016/0040-1951(92)90366-E)
- Suhr, G., & Cawood, P. A. (1993). Structural history of ophiolite obduction, Bay of Islands, Newfoundland. *Geological Society of America bulletin*, *105*(3), 399-410.
[https://doi.org/10.1130/0016-7606\(1993\)105<0399:SHOOOB>2.3.CO2](https://doi.org/10.1130/0016-7606(1993)105<0399:SHOOOB>2.3.CO2)
- Suzuki, S., Ishii, S., Hoshino, T., Rietze, A., Tenney, A., Morrill, P. L., Inagaki, F., Kuenen, J. G., & Nealson, K. H. (2017). Unusual metabolic diversity of hyperalkaliphilic microbial communities associated with subterranean serpentinization at The Cedars. *ISME J*, *11*(11), 2584-2598. <https://doi.org/10.1038/ismej.2017.111>

- Szponar, N., Brazelton, W. J., Schrenk, M. O., Bower, D. M., Steele, A., & Morrill, P. L. (2013). Geochemistry of a continental site of serpentinization, the Tablelands Ophiolite, Gros Morne National Park: A Mars analogue. *Icarus (New York, N.Y. 1962)*, 224(2), 286-296. <https://doi.org/10.1016/j.icarus.2012.07.004>
- Vance, S. D., & Daswani, M. M. (2020). Serpentinite and the search for life beyond Earth. *Philosophical transactions of the Royal Society of London. Series A: Mathematical, physical, and engineering sciences*, 378(2165), 20180421-20180421. <https://doi.org/10.1098/rsta.2018.0421>
- Wallin, E. T., & Metcalf, R. V. (1998). Supra-Subduction Zone Ophiolite Formed in an Extensional Forearc: Trinity Terrane, Klamath Mountains, California. *The Journal of geology*, 106(5), 591-608. <https://doi.org/10.1086/516044>
- Wang, D., T. , Gruen, D. S., Sherwood Lollar, B., Kai-Uwe, H., Lucy, C. S., James, F. H., Alexander, N. H., John, W. P., Penny, L. M., Martin, K., Kyle, B. D., Eoghan, P. R., Chelsea, N. S., Daniel, J. R., Jeffrey, S. S., Jennifer, C. M., Harold, F. H., Michael, D. K., Dawn, C., Tori, M. H., & Shuhei, O. (2015). Nonequilibrium clumped isotope signals in microbial methane. *Science (American Association for the Advancement of Science)*, 348(6233), 428-431. <https://doi.org/10.1126/science.aaa4326>
- Wilson, J., Munizzi, J., & Erhardt, A. M. (2020). Preservation methods for the isotopic composition of dissolved carbon species in non-ideal conditions. *Rapid communications in mass spectrometry*, 34(21), e8903-n/a. <https://doi.org/10.1002/rcm.8903>
- YSI. (2005). *Measuring ORP on YSI 6-Series Sondes: Tips, Cautions and Limitations*. <https://www.yei.com/File%20Library/Documents/Technical%20Notes/T608-Measuring-ORP-on-YSI-6-Series-Sondes-Tips-Cautions-and-Limitations.pdf>

Zwicker, J., Birgel, D., Bach, W., Richoz, S., Smrzka, D., Grasmann, B., Gier, S., Schleper, C., Rittmann, S. K. M. R., Koşun, E., & Peckmann, J. (2018). Evidence for archaeal methanogenesis within veins at the onshore serpentinite-hosted Chimaera seeps, Turkey. *Chemical geology*, 483, 567-580. <https://doi.org/10.1016/j.chemgeo.2018.03.027>

2.8 Supplementary Information

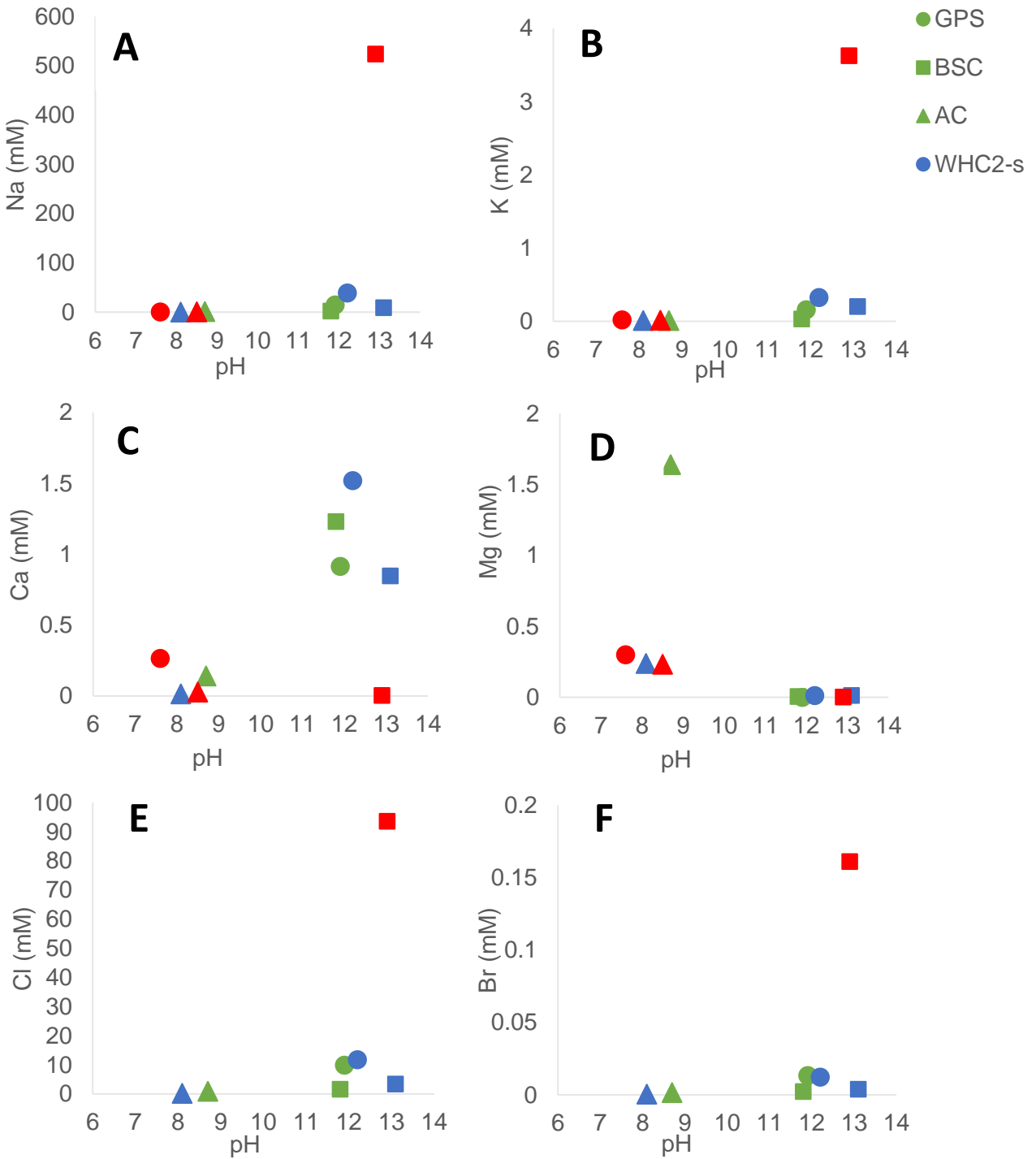


Figure 2.S1. Sodium (A), potassium (B), calcium (C), magnesium (D), chloride (E), and bromide (F) concentrations in millimolar versus pH of groundwater, pooled/well water, and surface water from Tablelands, The Cedars, and Aqua de Ney.

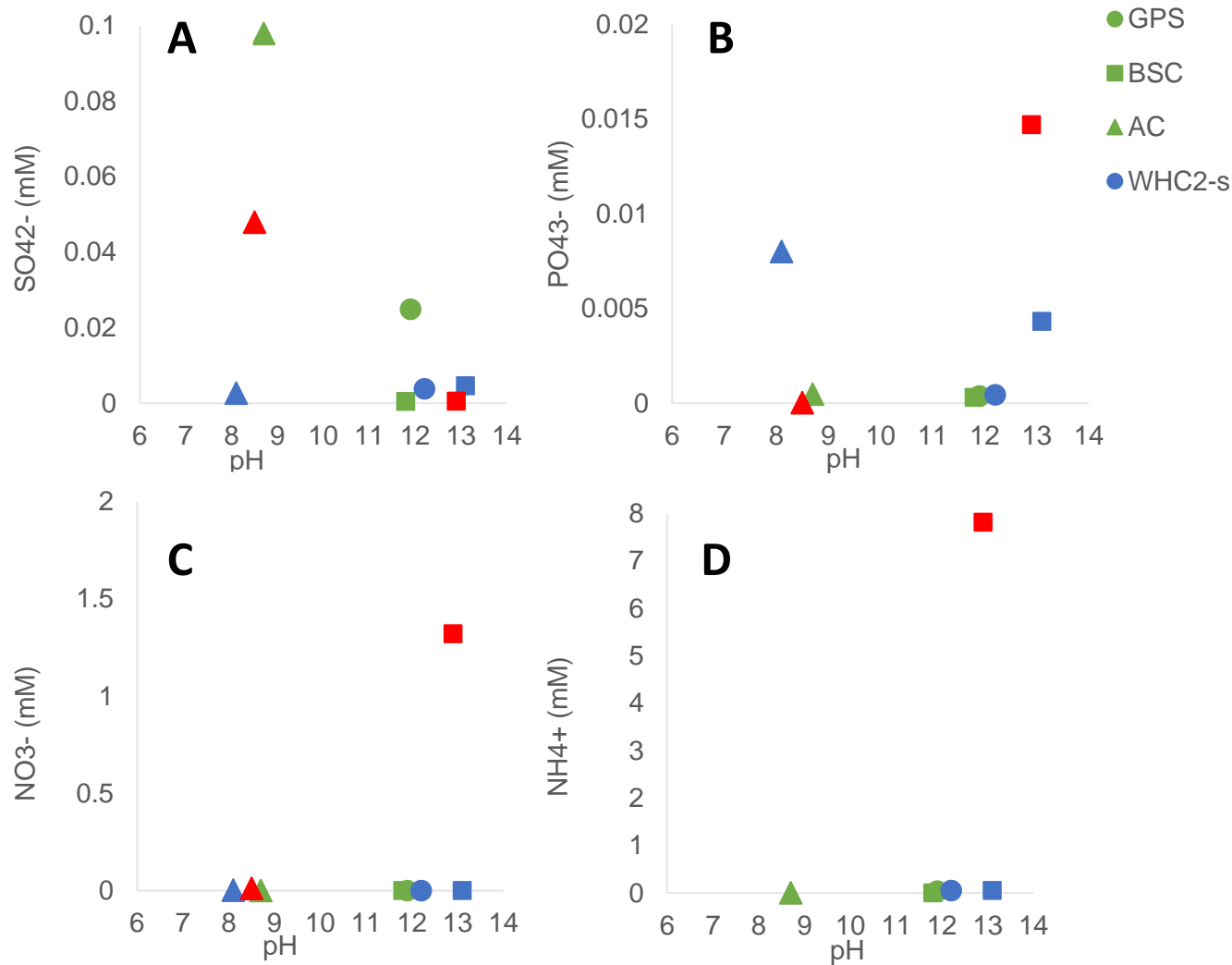


Figure 2.S2. Sulfate (A), phosphate (B), nitrate (C), and ammonium (D) concentrations in millimolar versus pH groundwater, pooled/well water, and surface water from Tablelands, The Cedars, and Aqua de Ney.

Mixing equations used to calculate the extent of mixing between in the groundwater endmember (f_{UB}) and the surface water endmember ($1 - f_{UB}$):

$$Cl_{(mixed)} = f_{UB} \times [Cl]_{UB} + [(1 - f_{UB}) \times Cl_{fresh}]$$

$$f_{UB} = (Cl_{mixed} - Cl_{fresh}) / (Cl_{UB} - Cl_{fresh})$$

Where the freshwater was 0% ultra-basic ($1 - f_{UB} = 0$) and the ultra-basic spring was 100% ultra-basic ($f_{UB} = 1$).

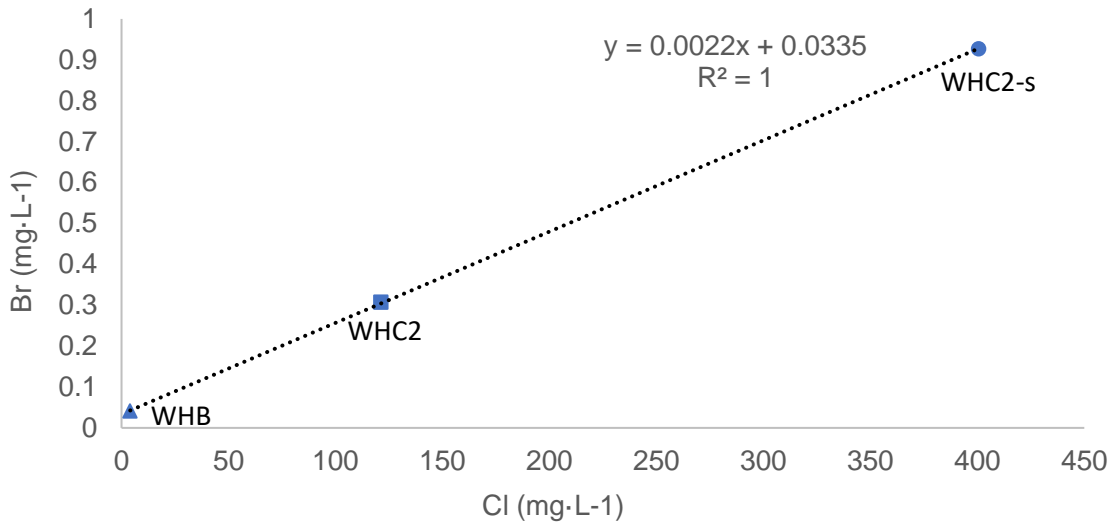


Figure 2.S3. Dissolved ion concentrations (mg·L⁻¹) of chloride and bromide as conservative tracers used to determine the mixing of groundwater and surface water (f_{UB}) in pooled water from the Tablelands.

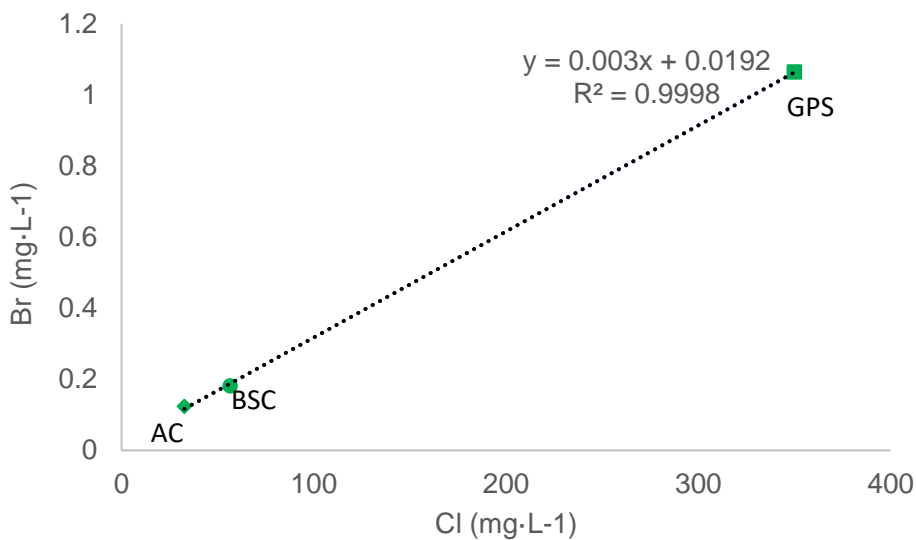


Figure 2.S4. Dissolved ion concentrations ($\text{mg}\cdot\text{L}^{-1}$) of chloride and bromide as conservative tracers used to determine the mixing of groundwater and surface water (f_{UB}) in pooled water from The Cedars.

Table 2.S1. Saturation calculations of CaCO_3 and MgCO_3 in groundwater and pooled water from the Tablelands, The Cedars, and Aqua de Ney.

	Q (MgCO_3)	K_{sp} (MgCO_3)	Saturated?	Q (CaCO_3)	K_{sp} (CaCO_3)	Saturated?
WHC2-s	4.33×10^{-10}	6.82×10^{-6}	Undersaturated	5.35×10^{-8}	4.47×10^{-9}	Oversaturated
WHC2	1.32×10^{-10}	6.82×10^{-6}	Undersaturated	9.14×10^{-9}	4.47×10^{-9}	Oversaturated
GPS	2.31×10^{-8}	6.82×10^{-6}	Undersaturated	9.36×10^{-12}	4.47×10^{-9}	Undersaturated
BSC	2.52×10^{-10}	6.82×10^{-6}	Undersaturated	6.63×10^{-8}	4.47×10^{-9}	Undersaturated
Ney Well	1.75×10^{-10}	6.82×10^{-6}	Undersaturated	8.29×10^{-10}	4.47×10^{-9}	Undersaturated
Ney Spigot	7.14×10^{-8}	6.82×10^{-6}	Undersaturated	5.63×10^{-8}	4.47×10^{-9}	Oversaturated

Table 2.S2. Mixing Predictions for Non-Conservative Parameters in pooled water at the Tablelands and The Cedars based on f_{UB} .

	WHC2C		BSC	
	% Difference	Well predicted?	% Difference	Well predicted?
Ca	-64	Underpredicted	112	Overpredicted
Mg	174	Overpredicted	-145	Underpredicted
Fe	-	-	199	Overpredicted
Mn	-	-	-	-
Cl	0	Well predicted	-	-
Br	-5	Well predicted	-3	Well predicted
SO₄²⁻	-43	Underpredicted	4.	Well predicted
H₂S	-	-	198	Overpredicted
PO₄³⁻	31	Overpredicted	-	-
NO₃⁻	76	Overpredicted	42	Overpredicted
Na	22	Overpredicted	18	Overpredicted
K	-68	Underpredicted	4	Well predicted
CH₄	15	Well predicted	-162	Underpredicted

“-” signifies that parameter was not able to be calculated due to insufficient data.

Table 2.S3. Activity coefficients (γ) calculated for specific cations and anions in groundwater, pooled/well water, and surface water from the Tablelands, The Cedars, and Aqua de Ney.

	Groundwater			Pooled/Well water			Surface Water		
	WHC2-s	GPS	Ney Spigot	WHC2	BSC	Ney Well	WHB	AC	Ney River
Ca	0.42	0.60	0.40	0.30	0.67	0.16	0.81	0.64	0.46
Mg	0.42	0.60	0.45	0.30	0.67	0.16	0.81	0.66	0.46
Cl	0.80	0.88	0.78	0.73	0.90	0.90	0.95	0.89	0.84
Br	0.80	0.88	0.78	0.73	0.90	0.90	0.95	0.89	0.84
SO₄²⁻	0.42	0.60	0.37	0.30	0.67	0.16	0.81	0.63	0.46
HS⁻	0.80	0.88	0.78	0.73	0.90	0.90	0.95	0.90	0.84

PO₄³⁻	0.14	0.31	0.10	0.06	0.40	0.009	0.62	0.35	0.17
NO₃⁻	0.80	0.88	0.78	0.73	0.90	0.90	0.95	0.88	0.84
Na	0.80	0.88	0.78	0.73	0.90	0.90	0.95	0.89	0.84
K	0.80	0.88	0.76	0.73	0.90	0.90	0.95	0.89	0.84
CO₃²⁻	0.41	0.88	0.37	0.30	0.67	0.16	0.81	0.63	0.46

Chapter 3. Assessing Geochemical Bioenergetics and Microbial Metabolisms at Three Terrestrial Sites of Serpentinization: the Tablelands (NL, CAN), The Cedars (CA, USA), and Aqua de Ney (CA, USA)

Melissa C. Cook¹, Jennifer G. Blank^{2,3}, Shino Suzuki⁴, Kenneth H. Nealson⁵ and Penny L. Morrill¹

¹Department of Earth Sciences, Memorial University of Newfoundland, St. John's, NL, Canada.

²NASA Ames Research Center, Division of Space Sciences & Astrobiology, Moffett Field CA, USA

³Blue Marble Space Institute of Science, Mountain View, CA, USA

⁴Institute of Space and Astronautical Science, JAXA, Sagami-hara Kanagawa, 252-5210, Japan

⁵Department of Earth Sciences, University of Southern California, Los Angeles, CA, USA

This chapter was originally published in Journal of Geophysical Research: Biogeosciences 126:6. [Cook et al., 2021b].

Abstract

The subsurface process of serpentinization creates an extreme environment for microbial life. This environment includes reducing, ultra-basic groundwater that is limited in electron acceptors. Despite these challenging conditions, there is a great deal of potential energy available to support microbial metabolisms both in the anaerobic subsurface and in aerobic surface environments where serpentinization associated groundwater discharges. In this study, the available energy was quantified through the calculation of chemical affinities, A_r , for three sites of active serpentinization in North America: the Tablelands (NL, CAN), The Cedars (CA, USA), and Aqua de Ney (CA, USA). The results showed that A_r values for each reaction were similar for all sites studied; however, the available energy varied a great deal from reaction to reaction. For example, the reaction of carbon monoxide oxidation provided the most energy to the system followed closely by hydrogen oxidation and methanotrophy. Potential microbial metabolisms were tested, simulating surface and subsurface conditions, in a laboratory-based setting using microcosms with materials from each site. During these microcosm experiments, carbon monoxide oxidation was not observed, and there was little evidence of methane oxidation. This suggests that either microorganisms that can take advantage of these metabolisms were not present or that they were not active under the specific conditions created in the microcosm experiments. Unexpectedly, microbial methanogenesis was observed in methane oxidation microcosms using material collected from The Cedars. The microbial production of methane occurred despite the addition of electron acceptors demonstrating the broad tolerance of methanogens at The Cedars for less reducing conditions.

3.1 Introduction

Serpentinization, the subsurface process through which ultramafic rocks are hydrated, results in the production of serpentine minerals as well as a suite of secondary minerals including hydroxides and magnetite. Serpentinization can occur within ophiolite sequences, which are sections of oceanic crust and upper mantle that have been emplaced tectonically onto continental crust. Terrestrial sites of serpentinization share many geochemical characteristics including the production of hydrogen and methane gas, highly reducing fluids with an ultra-basic pH (> 11) and high concentrations of dissolved calcium ions (Coleman and Keith, 1971; Sleep et al., 2004). The inorganic carbon dissolved in the fluids is predominantly in the form of carbonate ions, which are usually not biologically available. While the fluids at these sites typically contain an abundance of electron donors (i.e., hydrogen and methane), the fluids contain very low concentrations of electron acceptors (i.e., sulfate, nitrate, or oxygen) which are required for metabolic activity) (Morrill et al., 2013; Suzuki et al., 2013). Additionally, the high pH of these fluids can interfere with the production of adenosine triphosphate (ATP) (Krulwich et al., 2011). Therefore, the geochemical conditions created by serpentinization create an extreme environment for life.

Despite this extreme environment, groundwaters associated with serpentinization host diverse microbial communities. Knowledge of the taxonomies and metabolic capabilities of native microbial communities at terrestrial sites of serpentinization are needed to understand the habitability of these systems as well as the metabolic strategies, the limitations to carbon fixation at high pH, the coupling of abiotic and biological processes, and the magnitude of microbial contribution to biogeochemical cycling (Schrenk et al., 2013). Recent studies have begun to provide a more comprehensive overview of native microbial communities and their role in

biogeochemical cycling of various elements in serpentine-hosted springs. Sabuda et al. (2020) found evidence of sulfur-cycling taxa including *Dethiobacter*, *Desulfitispora*, and '*Desulforudis*' in fluids sampled from Coast Range Ophiolite Microbial Observatory (CROMO). A hydrogen-utilizing carbon-fixing *Betaproteobacteria*, *Serpentinomonas*, has been found at many terrestrial sites of serpentinization including the Tablelands, Canada (Brazelton et al., 2011; Brazelton et al., 2013), The Cedars, USA (Suzuki et al., 2014), CROMO, USA (Twing et al., 2017), and the Leka ophiolite complex, Norway (Daae et al., 2013). Evidence of microorganisms involved in methane cycling has also been identified at some terrestrial sites of serpentinization. For example, RNA and DNA sequence data from fluids sampled at CROMO support the presence of methanotrophs (Seyler et al., 2020); at the Santa Elena Ophiolite methanotrophic bacteria from the families *Methylococcaceae*, *Methylobacteriaceae*, and *Methylocystaceae* have been identified (Sánchez-Murillo et al., 2014). Daae et al. (2013) found evidence of methylotrophs and methane oxidizers using 16S rRNA analyses of borehole samples from the Leka Ophiolite in Norway. Methanogens have been detected using 16S rRNA sequencing in fluids from the Del Puerto Ophiolite, USA (Blank et al., 2009), in the fluids from the Samail ophiolite, Oman (Rempfert et al., 2017), and in fluids from the Santa Elena Ophiolite (Sánchez-Murillo et al., 2014). At The Cedars, an archaeal sequence was detected that placed closely to the order *Methanosarcinales* in the phylogenetic tree (Suzuki et al., 2013). Geochemical evidence (Morrill et al., 2013), and later microcosm experiments (Kohl et al., 2016), confirmed microbial production of methane at The Cedars.

While genomic data suggest that serpentinizing environments host diverse communities, the base of the food chain in these settings is not well understood. The ultra-basic, highly reducing conditions limit carbon availability in these systems for autotrophic metabolisms.

Oxidized carbon species in the fluids can be reduced to hydrocarbons or precipitated as carbonate. Organic acids have been proposed as an alternative source of carbon to support the autotrophic metabolisms in the extreme environment generated by serpentinization (Lang et al., 2018); this is consistent with microcosm laboratory experiments of Kohl et al. (2016) in which microbial methanogenesis was detected after introducing methanol, formate, and acetate to native microbial communities from The Cedars. It has also been hypothesized that the hydrogen produced through the serpentinization process could serve as geochemical fuel for biotic and abiotic organic synthesis in these systems, resulting in fluids that are high in dissolved reduced carbon compounds (i.e., methane, short chain n-alkanes, and formate) (Lang et al., 2018).

Oxidized carbon and other electron acceptors can be introduced to the system through the percolation of surface waters into the groundwater system, or the interaction of groundwater with the oxic atmosphere or surface waters when serpentinization associated groundwaters discharge and pool at the surface. These pools are portals that allow for mixing of oxic and anoxic waters, creating large redox gradients that provide potential energy for life. To quantify the energy in these systems that could be exploited by microbial life, chemical affinities (A_r), or reaction potentials, can be calculated (Helgeson & Murphy, 1983; Canovas et al., 2017). The chemical affinity for a specific reaction represents the amount of energy provided for metabolism and growth of an organism for that reaction. These predictions can be tested through laboratory-based experiments. Specifically, microcosm experiments allow for control of the environment and for reactants to be supplied in order to promote a variety of metabolisms. By monitoring the change in concentrations within these microcosms, it is possible to determine substrates and products of active metabolic reactions. Chemical affinities for a series of reactions were calculated and ranked for the Samail ophiolite in Oman (Canovas et al., 2017). The authors

found that carbon monoxide oxidation and hydrogen oxidation reactions produced the most energy, while methanogenesis and anaerobic methanotrophy with sulfate reactions produced the least. Whether other sites of serpentinization will have the same energetics and similar microorganisms able to metabolize the available energy is unknown.

This study calculates chemical affinity values and tests for metabolisms at three contrasting sites of active serpentinization: the Tablelands (NL, CAN), The Cedars (CA, USA), and Aqua de Ney (CA, USA). The Tablelands Massif in Newfoundland, Canada, is a part of the Bay of Islands ophiolite complex and the Humber Arm Allochthon which was emplaced between 500-400 Ma (Dunning & Krogh, 1985). The Cedars, in Sonoma County in Northern California, USA, is part of the Coast Range Ophiolite that was emplaced as part of the Franciscan Subduction Complex between 170-164 Ma (Coleman, 2000). Aqua de Ney is part of the Trinity Ophiolite Complex that was emplaced between 431-404 Ma (Wallin & Metcalf, 1998). The spring itself is in Siskiyou County, Northern California, USA.

While each of these sites has ultra-basic ($\text{pH} > 11$), reducing groundwater (i.e., with oxidation-reduction potential, E_h , values < -71 mV) enriched in CH_4 discharging from serpentinized peridotite, previously published geochemical studies of each of these active terrestrial sites of serpentinization reveal that these sites represent three distinct sites of serpentinization with respect to methane source and available electron donors and acceptors. The Cedars bubbles with hydrogen and methane-rich gases and has a microbial source of methane (Morrill et al., 2013; Wang et al., 2015; Kohl et al., 2016). Aqua de Ney bubbles with putative abiotic methane and is enriched in sulfide and ammonia with relatively elevated levels of dissolved electron acceptors (Feth et al., 1961). The Tablelands has a non-microbial source of

methane (Szponar et al., 2013; Cumming et al., 2019) and, like The Cedars, is relatively electron acceptor-poor.

The first research goal of this study was to calculate, and then rank, affinities for putative aerobic and anaerobic metabolic reactions at the three distinct sites of serpentinization. Since affinity calculations require knowledge of concentrations of reactants and products, we obtained these values using a combination of laboratory analyses and literature review. We hypothesized that the metabolic reactions with the highest calculated affinities would be the reactions most likely to occur at the respective site of terrestrial serpentinization. Therefore, the second research goal of this study was to use the calculated affinities to predict microbial metabolic reactions that would be observed in the system. The third objective was to test these predictions through a series of microcosm experiments using material sampled from each site supplying microcosms with reactants of the metabolisms of interest and then analyzing for changes in concentrations of reactants and products.

3.2 Methods

3.2.1 Chemical Affinity Calculations

Chemical affinities (A_r) of ten reactions (Table 3.1) likely to occur at sites of terrestrial serpentinization were calculated using the following equation:

$$A_r = RT \ln \left(\frac{K_r}{Q_r} \right) \quad [\text{Eq. 3.1}]$$

where R is the ideal gas constant, T is the temperature (in Kelvin), K_r is the equilibrium constant and Q_r is the activity product. The equilibrium constant (K_r) is calculated using the Gibbs free energy ($\Delta_r G^\circ$) of the reaction:

$$K_r = e^{-\Delta_r G^\circ / RT} \quad [\text{Eq. 3.2}]$$

The Gibbs energy for each reaction was calculated using standard molal Gibbs free energies of formation ($\Delta_r G^\circ$) values from Amend and Shock (2001). The activity product (Q_r) was calculated using the activities of each chemical species. The activity product calculations were based on data from field samples collected at The Cedars, the Tablelands, and Aqua de Ney (Table 3.2). Activities were calculated using the Debye-Hückel equation (cf. Table 3.S1). A temperature of 18 °C was used in all affinity calculations, a value within 10 °C of the temperature of the spring water at each site. A sensitivity test was also performed to determine the affect using a temperature of 18 °C had on the A_r value and it was determined to be insignificant.

Table 3.1. Reactions Used for Chemical Affinity Calculations and Corresponding Number of Electrons (e-) Transferred for Each Reaction.

Eq #	Reaction Name	Stoichiometric Equation	e ⁻
3.3	Hydrogen oxidation	$\text{H}_{2(\text{aq})} + 0.5\text{O}_{2(\text{aq})} \leftrightarrow \text{H}_2\text{O}$	2
3.4	Water-gas shift	$\text{CO}_{(\text{aq})} + \text{H}_2\text{O}_{(\text{aq})} \leftrightarrow \text{CO}_{2(\text{aq})} + \text{H}_2$	2
3.5	Carbon monoxide oxidation	$\text{CO}_{(\text{aq})} + 0.5\text{O}_{2(\text{aq})} \leftrightarrow \text{CO}_{2(\text{aq})}$	2
3.6	Carbon monoxide reduction	$3\text{H}_{2(\text{aq})} + \text{CO}_{(\text{aq})} \leftrightarrow \text{CH}_{4(\text{aq})} + \text{H}_2\text{O}$	6
3.7	Methanogenesis (CO ₂)	$\text{CO}_{2(\text{aq})} + 4\text{H}_{2(\text{aq})} \leftrightarrow \text{CH}_{4(\text{aq})} + 2\text{H}_2\text{O}$	8
3.8	Methanogenesis (formate)	$3\text{H}_2 + \text{HCOO}^- + \text{H}^+ \leftrightarrow \text{CH}_4 + 2\text{H}_2\text{O}$	6
3.9	Methanogenesis (acetate)	$\text{CH}_3\text{COO}^- + \text{H}_2\text{O} \leftrightarrow \text{CH}_4 + \text{CO}_3^{2-} + \text{H}^+$	4
3.10	Methanotrophy (nitrate)	$8\text{NO}_3^- + 8\text{H}^+ + 5\text{CH}_{4(\text{aq})} \leftrightarrow 4\text{N}_{2(\text{aq})} + 5\text{CO}_{2(\text{aq})} + 14\text{H}_2\text{O}$	40
3.11	Methanotrophy (sulfate)	$\text{CH}_{4(\text{aq})} + \text{SO}_4^{2-}{}_{(\text{aq})} \leftrightarrow \text{HCO}_3^-{}_{(\text{aq})} + \text{HS}^- + 2\text{H}_2\text{O}$	8
3.12	Aerobic methanotrophy	$\text{CH}_{4(\text{aq})} + 2\text{O}_{2(\text{aq})} \leftrightarrow \text{CO}_{2(\text{aq})} + 2\text{H}_2\text{O}$	8

Chemical affinities of ten possible reactions in ultra-basic reducing pools were calculated using field data from site BS5 at The Cedars, site WHC at the Tablelands, and the well of Aqua de Ney Spring. These values were calculated in kcal per mole of electrons transferred in each reaction so that a comparison between reactions was possible.

3.2.2 Gas Sampling

Dissolved gases were sampled using a modified gas phase equilibration technique detailed in Cumming et al. (2019). In short, 20 mL of fluid from each spring was withdrawn using a 60 mL syringe and shaken vigorously with an equal volume of helium to strip the gases

from the fluid. The entire gas phase of two syringes was then injected into a 30 mL glass serum vial that was prefilled with degassed water and sealed with a blue butyl septum. The dissolved gases in the helium displaced the water in the serum vial and samples were then fixed with mercuric chloride to ensure there was no microbial growth in the bottles.

3.2.3 Microcosm Experiments

3.2.3.1 Collection of Samples for Microcosm Experiments

A detailed site description of all springs sampled can be found in Chapter 2 (Cook et al., 2021). Fluid and precipitated carbonate samples for The Cedars microcosm experiments were collected from Barnes Spring 5 (BS5) in September 2017. Fluid and sediment samples for the Tablelands microcosm experiments were collected from Winter House Canyon (WHC) in July 2018. Fluids for the Aqua de Ney microcosm experiments were collected from the spring in June 2019. Fluids containing native microbial communities were collected in pre-combusted 1 L glass Kimble bottles prefilled with nitrogen gas and capped with lids lined with black-butyl septa. To maintain an anaerobic sample the 1 L bottles were submerged in the pool of spring water. While the bottle was inverted the cap was removed and water displaced most of the nitrogen gas. While the bottle was still submerged, its cap was replaced while ~50 mL of nitrogen gas remained. Carbonate and sediment slurry samples were collected using an adapted 60 mL syringe and stored in sterile 50 mL Falcon® tubes without headspace. Samples were stored in the dark at ambient temperature until they were returned to the laboratory whereupon they were transferred to an anaerobic glove box with a nitrogen atmosphere.

3.2.3.2 Microcosm Setup and Sampling

The design of the microcosms for this experiment replicated the design of other successful microcosms experiments (Kohl et al., 2016; Morrill et al., 2014). Microcosms consisted of a sealed bottle containing spring water, proximal sediments (when available), nutrient medium, and buffer solution. The bottles (160 mL serum vials, with butyl septa tops) were filled approximately one third with solution and the remaining headspace contained nitrogen gas. Microcosms for the methane oxidation experiments were prepared in an anaerobic glovebox filled with a nitrogen atmosphere. Microcosms for the hydrogen and carbon monoxide utilization experiments were prepared on the laboratory benchtop in an aerobic environment. The E_h and pH of the water were tested at the time of microcosm construction. For each methane oxidation experiment, a total of 54 microcosms were assembled. For each of the hydrogen utilization and the carbon monoxide utilization experiments, a total of 9 microcosms were assembled. All microcosms received 30 mL of fluid from the corresponding site. Microcosms from The Cedars and the Tablelands received 2 mL of carbonate or sediment slurry from the site of interest. Microcosms from Aqua de Ney received no carbonate or sediment because none was available. Each vial was then given 14 mL of essential nutrients in the form of a mineral medium solution for chemolithotrophs called DSMZ Medium 81 to ensure that the microcosms were not nutrient limited throughout the experiments. The exact composition of this Medium and how much each microcosm received is detailed in Tables 3.S2A and 3.S2B. Microcosms also received 14 mL of a 15 mmol·L⁻¹ N-cyclohexyl-3-aminopropanesulfonic acid (CAPS) buffer solution to maintain the overall pH of the systems as close as possible to field pH values. Prepared vials were sealed with blue butyl septa that were conditioned as described by Oremland et al. (1987).

There were three treatment groups for the methane oxidation experiments in this study. Each group received a different electron acceptor: nitrate, sulfate, or oxygen. Each treatment group received 2 mL of a 10 mmol·L⁻¹ solution containing the corresponding electron acceptor, or in the case of the oxygen-containing treatment group, 2 mL of air. All solutions were filtered through 0.22 µm mixed cellulose ester (MCE) filters. Each treatment group included live experiments and killed controls; each type of experiment was conducted in triplicate. The killed controls received the same solutions as the live experiments plus 0.5 mL of a saturated solution of mercuric chloride. A live control treatment group received all the same solutions as the live experiments except for the electron acceptor solution. After construction, 3 mL of 100 % methane at atmospheric pressure was added to each microcosm vial such that methane made up approximately 3 % of the headspace volume. The microcosm set-up is summarized in Table 3.S3A.

For the hydrogen utilization experiment, all microcosms received 1 mL of 100 % hydrogen at atmospheric pressure after construction such that hydrogen made up approximately 1 % of the headspace volume. All microcosms for the carbon monoxide utilization experiment received 2 mL of 100 % carbon monoxide at atmospheric pressure such that carbon monoxide made up approximately 2 % of the headspace volume. The microcosms for the carbon monoxide and hydrogen utilization killed experiments each additionally received 0.5 mL of a saturated solution of mercuric chloride. A live control treatment group did not receive carbon monoxide or hydrogen. The microcosm set-up is summarized in Table 3.S3B and Table 3.S3C.

Twenty-four hours after the initial setup, the headspace of the Tablelands, The Cedars, and Aqua de Ney methane oxidation microcosms were sampled for methane and carbon dioxide

concentrations. These gases in the headspace were sampled three more times (at 90, 210, and 270 days) in The Cedars microcosms, three more times (at 30, 60, and 90 days) in the Tablelands microcosms, and two more times (at 14 and 60 days) in the Aqua de Ney microcosms. The increases in sampling frequency in each subsequent experiment were based on observations in gas production from previous experiments.

Hydrogen and oxygen concentrations in the headspace of The Cedars methane oxidation microcosms were analyzed at the beginning and end of the experiment. In the methane oxidation microcosms from the Tablelands and Aqua de Ney, hydrogen and oxygen concentrations were not analyzed at the end of the experiments because no changes in methane or carbon dioxide concentrations were observed.

Hydrogen and methane concentrations in the headspace of the Aqua de Ney hydrogen utilization microcosms were analyzed three times (at 0, 14, and 60 days). Carbon monoxide, carbon dioxide, and methane concentrations in the headspace of the Aqua de Ney carbon monoxide utilization microcosms were analyzed three times (at 0, 14, and 60 days). Both experiments were terminated after 60 days because no changes in hydrogen, carbon monoxide, carbon dioxide or methane concentrations were observed.

At the time of termination, an aliquot of fluid from each of The Cedars methane oxidation microcosms was removed using a 5 mL syringe and transferred into a sterile 15 mL Falcon® tube. These samples were frozen immediately until analysis for their sulfate or nitrate concentration. The E_h and pH of the fluid were also measured in each individual microcosm at the end of each experiment. No further analyses were performed on microcosm fluids from the

Tablelands or Aqua de Ney since no carbon dioxide was produced and no changes in methane concentrations were observed.

3.2.4 Analytical Methods

3.2.4.1 Methane, Carbon Dioxide, and Carbon Monoxide Concentrations

The headspace in the microcosms was analyzed using an SRI 8610 gas chromatograph (GC) equipped with a Flame Ionization Detector (FID) and a methanizer using a Carboxen 1010 capillary column (30 m x 0.32 mm inside diameter, 15 μm film thickness) with helium as the carrier gas following procedures described in Morrill et al. (2014). Briefly, the oven temperature was held constant at 40 °C for 16 min and then increased by 15 °C/min to a final temperature of 125 °C, which was held constant for 3 min. A mixed gas standard (Scott™) was used to create the calibration curves (with a minimum of 3 data points) for carbon dioxide and carbon monoxide. The gas standard contained 0.5% oxygen, 0.5 % carbon monoxide, 0.5 % carbon dioxide and 0.5 % hydrogen in a balance of helium. A methane gas standard (Scott™) of 1 % methane in a balance of helium was used to create the calibration curves for methane. Detection limits for methane, carbon dioxide, and carbon monoxide in the gas phase were 5, 10, and 10 μM respectively. Precision on triplicate injections of the standard was always less than 5 % relative standard deviation (RSD) (2σ).

3.2.4.2 Hydrogen and Oxygen Concentrations

Hydrogen and oxygen gas concentrations were analyzed on an Agilent 6890A GC equipped with a micro thermal conductivity detector (TCD) using a Carboxen 1010 capillary column (30 m x 0.32 mm inside diameter, 15 μm film thickness) with nitrogen as a carrier gas.

The oven temperature was 50 °C isothermal for 13 minutes. The mixed gas standard (Scott™) was also used to create the calibration curves for hydrogen and oxygen by injecting different volumes at atmospheric pressure. The detection limits for hydrogen and oxygen in the gas phase were 10 and 15 µM respectively. Precision on triplicate injections of the standard was always less than 5 % RSD (2σ).

3.2.4.3 Nitrate and Sulfate Concentrations

Nitrate and sulfate concentrations were analyzed on a Thermo Fisher ICS 5000. Ions were separated using an AS23 column with an ASG23 guard column and a carbonate eluent with a 1.0 mL/min flow rate. Sulfate and nitrate standards purchased from Sigma Aldrich were used to create calibration curves for nitrate and sulfate. Additionally, a standard containing 81 µM nitrate and 52 µM sulfate was injected during the analysis to check for instrument drift. The detection limits for nitrate and sulfate were 1.6 and 2.60 µM respectively.

3.2.4.4 pH and E_h Measurements of Microcosms

The pH of the fluid was measured using an Oakton handheld waterproof field probe calibrated daily with 4, 7, and 10 pH buffers. The redox potential (ORP) of the fluid was measured in the field at the time of sampling using an ORPTestr 10 m (Eutech Instruments). The ORP meter's accuracy was confirmed with check standards (4 and 7 pH buffers saturated with quinhydrone). These solutions had ORP values of 93 mV and 267 mV, respectively. To create these solutions, 50 mL of each pH buffer was placed in a beaker and 0.1 g of quinhydrone was added to each beaker and stirred until the solution was saturated with quinhydrone. Saturated quinhydrone solutions were used immediately to ensure no decomposition upon exposure to

oxygen occurred. The ORP meter had a double junction platinum electrode such that a correction was required to convert ORP to E_h . Field measurements were therefore converted to E_h by adding 241.0 to the ORP (YSI, 2005).

3.2.4.5 Calculations to Determine the Microbial Effect

To determine whether changes in measured parameters such as CH_4 , H_2 , O_2 , CO , NO_3^- , SO_4^{2-} , pH and E_h , were due to biological reactions, abiotic changes in measured parameters were removed by subtracting the relative average value of the killed controls from the live treatments and controls at each time point sampled using the following equation:

$$\Delta CH_{4t} = \left(\frac{[X]_t}{[X]_0} \right)_L - \left(\frac{[X]_t}{[X]_0} \right)_K \quad [\text{Eq. 3.13}]$$

Where X was the measured parameter, $\left(\frac{[X]_t}{[X]_0} \right)_L$ was the average relative value for X of the live triplicate microcosm experiments for each treatment group, and $\left(\frac{[X]_t}{[X]_0} \right)_K$ was the average relative value for X of all the killed microcosms.

3.3 Results

3.3.1 Aqueous Geochemistry

The aqueous geochemistry of groundwater discharging at the Tablelands, The Cedars, Aqua de Ney is summarized in Table 3.2. The fluids at all sites were ultra-basic pH (> 11) and reducing ($E_h < -71$ mV). The fluid at the Tablelands contained dissolved levels of hydrogen, methane, and carbon monoxide gas, while The Cedars and Aqua de Ney bubbled with gases. The gas at The Cedars was rich in hydrogen and methane, while the gas at Aqua de Ney was rich in methane and hydrogen sulfide. The total inorganic carbon (TIC) was very low at the Tablelands and The Cedars ($< 1.20 \times 10^{-4}$ moles \cdot L $^{-1}$ of C), however, the TIC at Aqua de Ney was much higher (6.52×10^{-2} moles \cdot L $^{-1}$ of C). The fluids at Aqua de Ney also contained higher levels of nitrate and phosphate than the other sites.

Table 3.2. Environmental Parameters and Ion Concentrations in Spring Waters from the Tablelands, The Cedars, and Aqua de Ney.

Measured Parameters	Tablelands	The Cedars	Aqua de Ney
pH	13.1	11.8	12.9
Temp (°C)	9.6	17.4	11.6
E_h (mV)	-71	-344	-224
H₂(M)	5.29 x 10 ⁻⁴	5.37 x 10 ⁻⁵	≤ 1.0 x 10 ⁻⁵
O₂ (M)	1.0 x 10 ⁻⁴	≤ 1.5 x 10 ⁻⁵	≤ 1.5 x 10 ⁻⁵
CO (M)	4.5 x 10 ⁻⁵	≤ 1.0 x 10 ⁻⁵	≤ 1.0 x 10 ⁻⁵
CO₂ (M)	4.5 x 10 ⁻⁵	4.4 x 10 ⁻⁵	≤ 1.0 x 10 ⁻⁵
SO₄²⁻ (M)	4.56 x 10 ⁻⁶	4.16 x 10 ^{-7*}	5.12 x 10 ⁻⁷
H₂S (M)	≤ 5.0 x 10 ⁻⁷	≤ 5.0 x 10 ⁻⁷	3.39 x 10 ^{-2†}
NO₃⁻ (M)	1.15 x 10 ⁻⁶	1.45 x 10 ⁻⁶	1.32 x 10 ⁻³
CH₃COO⁻ (M)	2.01 x 10 ^{-6*}	1.50 x 10 ^{-6*}	n.d.
HCOO⁻ (M)	9.97 x 10 ^{-5*}	4.75 x 10 ^{-5*}	n.d.
CH₄ (M)	8.0 x 10 ⁻⁶	2.2 x 10 ⁻⁵	3.20 x 10 ⁻²
TIC (moles L⁻¹ C)	1.20 x 10 ⁻⁴ (± 1.33x10 ⁻⁵)	3.64 x 10 ⁻⁵ (± 2.05x10 ⁻⁶)	6.52 x 10 ⁻² (± 5.74x10 ⁻³)
δ¹³C CH₄ (‰)	-27.6**	-62.9*	n.d.
δ²H CH₄ (‰)	-171**	-355*	n.d.

The Tablelands data were collected in July 2018, The Cedars data were collected in Sept. 2017, and Aqua de Ney data were collected in June 2019. While the fluid at The Cedars and Aqua de Ney bubble with gas, only the dissolved concentrations reported in this table were used in chemical affinity calculations. Standard deviations of parameter measurements were less than 10 % unless otherwise indicated. Data reported in this table was collected for this study except where noted: *Rietze (2015), †Feth et al. (1961), and **Cumming et al. (2019). Parameters that were not measured are indicated by the letters n.d.

3.3.2 Microcosm Methane Concentrations

Figure 3.1A demonstrates that methane was produced biologically in all of The Cedars live treatments and live control microcosms. Conversely, when Eq. 3.13 was applied to the

methane concentration data from the Tablelands and Aqua de Ney microcosms, there was no observable biological change in the methane concentrations outside of experimental precision (Figures 3.1B and C).

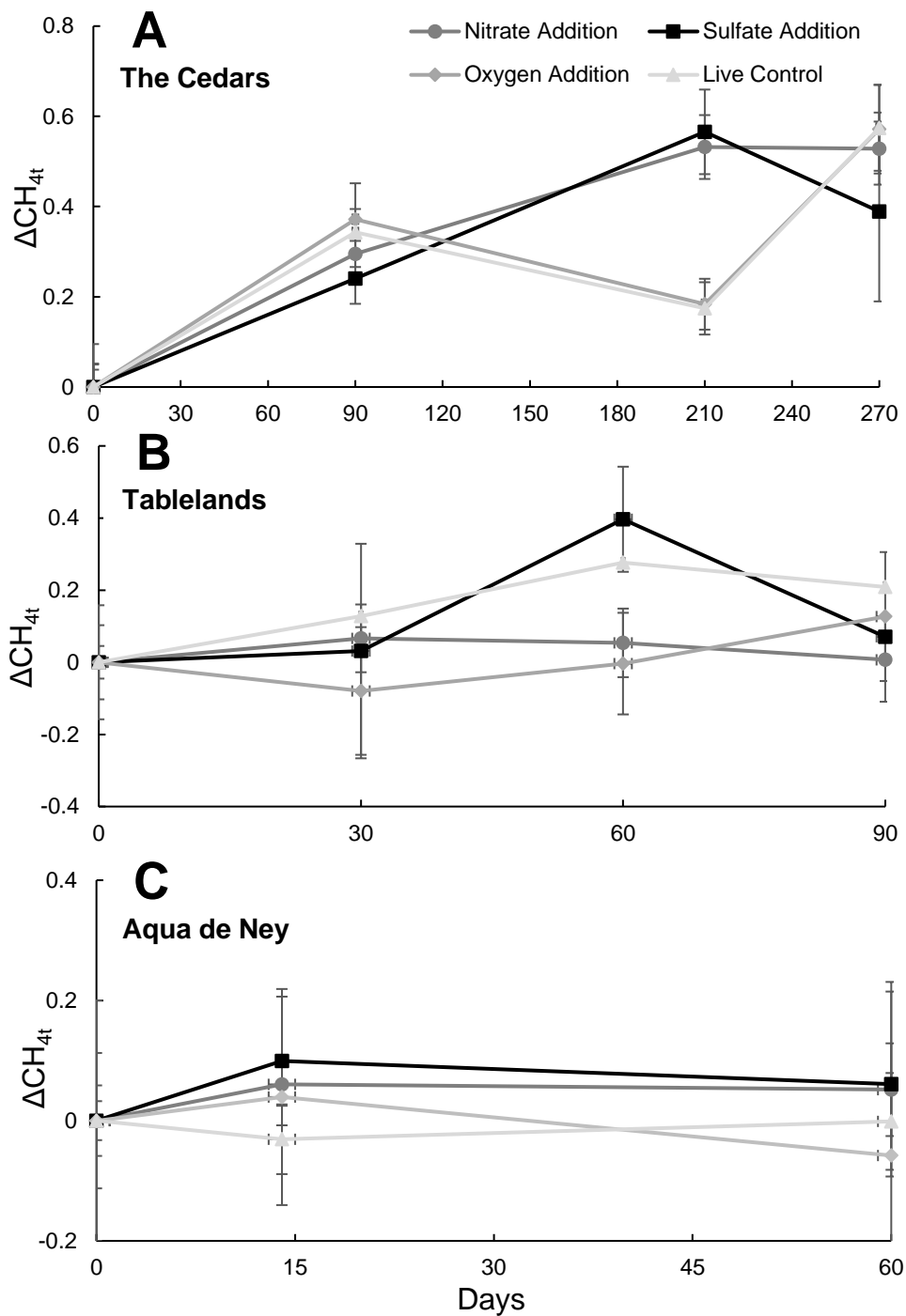


Figure 3.1. Normalized headspace concentrations of methane (Eq. 3.13) in (A) The Cedars. (B) the Tablelands, and (C) Aqua de Ney methane oxidation microcosm experiments. Error bars indicate \pm one standard deviation (1σ) from the mean of triplicate treatments. There was no

observable reduction of methane concentrations indicative of methane oxidation in the Tablelands or Aqua de Ney microcosms. In The Cedars microcosms, there was an overall increase in microbial methane concentrations, with a slight decrease between days 90-210 in the oxygen amended and live control microcosms.

3.3.3 The Cedars' CH₄ Oxidation Microcosms' Hydrogen, Oxygen, Nitrate, and Sulfate Concentrations

Hydrogen and oxygen concentrations in the headspace of the live and killed oxygen-containing treatment groups and the live control treatment group from The Cedars were measured at the beginning and at the end of the experiment (Table 3.3). While there was no observable change outside of experimental precision in the oxygen concentration in the live oxygen-containing treatments, there was biological oxygen consumption observed in the live control. Conversely, hydrogen was produced biologically in both the live oxygen-containing and live control treatments. Biological consumption of electron acceptors, nitrate and sulfate was calculated using Eq. 3.13. There was no change in the average relative nitrate (-0.0082 ± 0.018) or sulfate (-0.0034 ± 0.013) concentrations attributable to biological activity observed outside of experimental precision. No carbon monoxide was detected in the headspace of any of the live or killed treatments groups throughout the duration of the experiment.

Table 3.3. Average Relative Oxygen and Hydrogen Concentrations in the Headspace of The Cedars' Live Oxygen-Containing and Control Treatments (Eq. 3.13).

Sample Group	ΔO_{2t}	ΔH_{2t}	$\Delta NO_3^-_t$	$\Delta SO_4^{2-}_t$
Live O₂ – Killed	0.22 (± 1.51)	0.31 (± 0.11)	n.d.	n.d.
Live Control – Killed	-0.59 (± 0.20)	0.34 (± 0.12)	n.d.	n.d.
Live NO₃⁻ – Killed	n.d.	n.d.	-0.0082 (± 0.018)	n.d.
Live SO₄²⁻ – Killed	n.d.	n.d.	n.d.	-0.0034 (± 0.013)

Note: Standard deviations (1σ) among triplicate experiments are given in parentheses. Parameters that were not measured are indicated by the letters n.d.

3.3.4 The Cedars' CH₄ Oxidation Microcosms' pH and E_h Measurements

The initial pH and E_h of the fluid from The Cedars at the time of microcosm construction were 11.7 and +214 mV, respectively. The final average pH of the killed microcosms was 9.47 and the final pH of the live control, oxygen, nitrate, and sulfate-containing treatment groups were 10.23, 9.91, 9.93, and 9.71, respectively. The average E_h of the killed microcosms was +337 mV and the average E_h of the live control, oxygen, nitrate, and sulfate-containing treatment groups were +225, +251, +214, and +194 mV, respectively. The average change in pH and E_h values between the two time points for the live and control microcosms have been summarized in Table 3.4. The E_h in all of the live and killed microcosms became less reducing throughout the duration of the experiment, however, the change in E_h was less in the live sulfate-containing and nitrate-containing treatment groups relative to their killed controls. The pH of the microcosms decreased in all microcosms and the pH of each live treatment group was similar to the respective killed controls. The small changes in E_h and pH in the live and killed microcosms throughout the duration of the experiment demonstrate that these systems are well buffered, likely due to the CAPS buffer that was added to each microcosm (Table 3.4).

Table 3.4. Average Relative pH and E_h Measurements of Fluids of Live and Control Microcosms from The Cedars (Eq. 3.13).

Sample Group	ΔpH	ΔE_h (mV)
Live Control - Killed	-0.03 (± 0.04)	-10 (± 1)
Live O₂ - Killed	0.01 (± 0.03)	-8 (± 0.2)
Live NO₃⁻ - Killed	0.00 (± 0.03)	-5 (± 1)
Live SO₄²⁻ - Killed	-0.03 (± 0.03)	-3 (± 1)

Note: Standard deviations (1σ) among triplicate experiments are given in parentheses.

3.3.5 Hydrogen and Carbon Monoxide Utilization Experiments

Hydrogen concentrations were measured in the headspace of the live and killed Aqua de Ney hydrogen utilization microcosms. Carbon monoxide concentrations were measured in the headspace of the live and killed Aqua de Ney carbon monoxide utilization microcosms. To determine if any of the changes were biological, abiotic changes were removed using Eq. 3.13. No biological changes in hydrogen or carbon monoxide concentration were observed (Table 3.5). No production of methane or carbon dioxide in the headspace of any microcosms throughout the experiment was observed; methane and carbon dioxide were below the detection limits ($<5 \mu\text{M}$ and $<10 \mu\text{M}$ respectively) in all microcosms.

Table 3.5. Average Relative Carbon Monoxide and Hydrogen Concentrations in the Headspace of Aqua de Ney Live Carbon Monoxide-Containing and Hydrogen-Containing Treatments (Eq. 3.13).

Sample Group	T₀	T₁₄	T₆₀
Live CO – Killed	0 (± 0.54)	-0.02 (± 0.52)	0.035 (± 0.57)
Live H₂ – Killed	0 (± 0.24)	-0.17 (± 0.31)	-0.18 (± 0.26)

Note: Standard deviations (1σ) among triplicate experiments are given in parentheses.

3.4 Discussion

3.4.1 Available Energy for Life at Sites of Serpentinization

The theoretical energy for certain metabolic reactions is similar among the sites studied here as well as at other sites of serpentinization. Table 3.6 ranks the chemical affinities determined in this study for The Cedars, the Tablelands, and Aqua de Ney to the chemical affinities calculated from data reported in Sabuda (2017) for Coast Range Ophiolite Microbial Observatory (CROMO) located near Lower Lake, California, and the chemical affinities reported in Canovas et al. (2017) for the Samail Ophiolite in Oman. As demonstrated in Table 3.6, the energy produced follows the same trend at all sites, with carbon monoxide oxidation providing the greatest potential energy for all of the sites, followed by hydrogen oxidation and methanotrophy. Autotrophic methanogenesis with carbon dioxide and carbon monoxide would yield the least amount of energy, if any, at all sites since A_r values that are less than or equal to 3 kcal/(mol·e⁻) suggesting that the system is at equilibrium with respect to the other constituents and there will not be energy available to support microbial activity (Shock et al., 2010). Although Aqua de Ney had much higher TIC and nitrate concentrations than the Tablelands or The Cedars and contained no detectable hydrogen, there was very little variation in affinity results between sites. The similarity in the order of reactions and their chemical affinities suggests that despite the geochemical differences between these sites, their similarities (high pH, reducing environment and scarce electron acceptors) have a larger impact on the overall potential energy supply to the system.

Table 3.6. Affinities (kcal/(mol·e⁻)) of 10 Possible Reactions at 5 Terrestrial Sites of Serpentinization.

Reaction	Tablelands ^a	The Cedars ^b	Aqua de Ney ^c	CROMO ^d	Samail Ophiolite ^e
CO oxidation	32	31	31	-	-
$\text{CO}_{(\text{aq})} + 0.5\text{O}_{2(\text{aq})} \leftrightarrow \text{CO}_{2(\text{aq})}$					
Hydrogen oxidation	28	27	26	30	35
$\text{H}_{2(\text{aq})} + 0.5\text{O}_{2(\text{aq})} \leftrightarrow \text{H}_2\text{O}$					
Aerobic methanotrophy	24	24	24	26	27
$\text{CH}_{4(\text{aq})} + 2\text{O}_{2(\text{aq})} \leftrightarrow \text{CO}_{2(\text{aq})} + 2\text{H}_2\text{O}$					
Methanogenesis (acetate)	23	24	-	-	-
$\text{CH}_3\text{COO}^- + \text{H}_2\text{O} \leftrightarrow \text{CH}_4 + \text{CO}_3^{2-} + \text{H}^+$					
Methanotrophy (nitrate)	18	19	22	19	22
$8\text{NO}_3^- + 8\text{H}^+ + 5\text{CH}_{4(\text{aq})} \leftrightarrow 4\text{N}_{2(\text{aq})} + 5\text{CO}_{2(\text{aq})} + 14\text{H}_2\text{O}$					
CO reduction	6	5	4	3	3-5
$3\text{H}_{2(\text{aq})} + \text{CO}_{(\text{aq})} \leftrightarrow \text{CH}_{4(\text{aq})} + \text{H}_2\text{O}$					
Water-gas shift	4	4	5	4	4-9
$\text{CO}_{(\text{aq})} + \text{H}_2\text{O}_{(\text{aq})} \leftrightarrow \text{CO}_{2(\text{aq})} + \text{H}_2$					
Methanogenesis (CO ₂)	4	3	2	2	3
$\text{CO}_{2(\text{aq})} + 4\text{H}_{2(\text{aq})} \leftrightarrow \text{CH}_{4(\text{aq})} + 2\text{H}_2\text{O}$					
Methanotrophy (sulfate)	1	1	1	1	2
$\text{CH}_{4(\text{aq})} + \text{SO}_4^{2-}(\text{aq}) \leftrightarrow \text{HCO}_3^-(\text{aq}) + \text{HS}^- + 2\text{H}_2\text{O}$					
Methanogenesis (formate)	-42	-43	-	-	-
$3\text{H}_2 + \text{HCOO}^- + \text{H}^+ \leftrightarrow \text{CH}_4 + 2\text{H}_2\text{O}$					

Bolded values were calculated in this study.

Values calculated in this study used data from ^a Szponar et al. (2013), ^b Rietze (2015), ^c Feth et al. (1961), ^d Sabuda (2017).

^e Values taken from Canovas et al. (2017). Heterotrophic methanogenesis was either not calculated or organic acid acetate and formate concentrations were not measured for Aqua de Ney, CROMO, and the Samail Ophiolite.

To determine if the microcosm conditions changed the chemical affinities determined using field data, the chemical affinities were calculated again based on the aqueous chemistry of the microcosms. To do this we calculated the concentrations of the gases available in the microcosms in the aqueous phase (C_w). This was done using Henry's law constant and the known gaseous concentration in the headspace of the microcosms. These data have been summarized in Table 3.S4A. Subsequently, these values were used to calculate the chemical affinity of gases in the aqueous phase $A_r(C_w)$. These affinity values have also been reported (Table 3.S4B). The calculated $A_r(C_w)$ values were very similar to the A_r values calculated based on field data from each site: the overall conclusions were not affected.

3.4.2 Carbon Monoxide-Based Metabolisms

Non-photosynthetic life gains energy through electron flow, with the electrons being harvested from either inorganic or organic electron donors. The source of electrons for the microbial food web at sites of serpentinization is poorly constrained at this point. For most aquatic systems, the carbon source for the base of the microbial food web is bicarbonate that is reduced to organic carbon by lithotrophs and/or phototrophs. However, serpentinizing systems are limited in bicarbonate; in ultra-basic environments, the dominant species of inorganic carbon is the carbonate ion, for which there is no known transport pathway across the cell membrane (Sorokin & Kuenen, 2005). If the base of the food web in serpentinizing ecosystems is autotrophic, then the inorganic source of carbon could be carbon monoxide.

The chemical affinity calculations demonstrate that microbial utilization of carbon monoxide (oxidation or reduction) will produce energy for microbial metabolism. In fact, the A_r values for carbon monoxide oxidation were the greatest of all of the A_r values calculated for every site that was considered. We hypothesized that the metabolic reactions with the highest calculated affinities would be the reactions most likely to be occurring at the respective site of terrestrial serpentinization. Previous experiments performed with fluid and sediment from the Tablelands observed microbial carbon monoxide oxidation (Morrill et al., 2014). However, despite the favourable A_r values, carbon monoxide oxidation was not observed in experiments with materials collected from Aqua de Ney (this study) or The Cedars (Kohl et al., 2016). Both the Cedars and Aqua de Ney experiments followed the same experimental procedures and analyses described in Morrill et al. (2014) where carbon monoxide utilization was observed. The carbon monoxide analytical method used can detect a drop of carbon monoxide by as little as 5 % (i.e., a decrease of 5.00×10^{-5} M of carbon monoxide from the initial concentration could be detected) of the total carbon monoxide concentration. Given that this change is much lower than that observed in Morrill et al. (2014) (i.e., a drop in carbon monoxide concentrations greater than 59 %), this suggests that the method is sensitive enough to detect carbon monoxide utilization in these experiments. If carbon monoxide utilizing microorganisms were present in the spring fluids, they were either not active, not active in the very specific environments that were created in the microcosms, or their carbon monoxide consumption was very slow. Fones et al. (2019) found that the rate of CO oxidation to CO₂ was significantly slower in ultra-basic peridotite waters than in waters with a lower pH. They also found that CO assimilation to biomass was much

lower in microcosms that contained ultra-basic peridotite waters ($\text{pH} > 10.6$) and basic peridotite waters ($\text{pH} < 8.5$) relative to contact wells (wells that were near the contact between gabbro-dominated and peridotite-dominated lithologies). It is possible that the CO monoxide utilization was too slow in microcosms constructed during this study to be measured.

The lack of observed carbon monoxide utilization in the microcosm experiments is not proof that carbon monoxide oxidation does not, or cannot, occur in the natural system. It could be that the reaction was not possible in the simulated environment of the microcosm or over the duration of its experiment. For example, in The Cedars microcosms, the lack of carbon monoxide oxidization may have been caused by the lack of an oxidizing environment. Despite the addition of oxygen to The Cedars' microcosms, the experiments remained reducing.

3.4.3 Methanotrophy-Based Microcosms

The chemical affinity calculations also predicted that methanotrophy could provide energy for life in the serpentinization systems that we considered. Methanotrophy that uses oxygen as the electron acceptor was predicted to provide the greatest energy, followed by nitrate, and then sulfate. Despite the relatively high A_r values for methanotrophy, the laboratory experiments using material from the Tablelands, and Aqua de Ney showed no evidence of this reaction occurring regardless of the electron acceptor that was added (i.e., methane concentrations did not decrease, and there were no changes in the nitrate, sulfate in the live microcosms). One possible reason for this may be that methanotrophic bacteria were not present in the fluids that we used for the experiments.

A genomic study by Brazelton et al. (2011) was unable to detect methanotrophs in samples from the Tablelands.

The microcosms using material from The Cedars showed very little evidence of methane oxidation, with the exception of days 90-210 where a slight decrease in methane concentrations were observed in the oxygen containing, and live control microcosms. The oxygen concentration in the live control group decreased throughout the duration of The Cedars microcosm experiment, which may have been due to methane oxidation, but it is also likely that this decrease in oxygen was due to general respiration reactions.

3.4.4 Microbial Methanogenesis

Interestingly, in The Cedars methanotrophy microcosm experiments, while the average relative methane concentrations in the killed microcosms did not change, the average relative methane concentrations in the live microcosms increased instead of decreased. The increase in the average relative methane concentrations suggests that microbial methanogenesis dominated over methanotrophy. This is not the first time spontaneous microbial methane generation has been observed live microcosm experiments with material from The Cedars. Kohl et al. (2016) also observed microbial methane generation in unamended microcosms composed of fluid and sediment from The Cedars.

It is also remarkable that methanogens survived in the less reducing environment created through the addition of electron acceptors despite their sensitivity to oxygen (Jarrell, 1985). Additionally, in these environments methanogens also managed to

produce methane; in fact, the methane production in the live control, which received no electron acceptors, and the oxygen-containing live microcosms was very similar, suggesting that the presence of oxygen did not hinder methanogenesis. While this result is unusual as methanogens were once thought to be strictly anaerobic, this is not the first study to report such findings. Fetzer and Conrad (1993) found that methanogenesis was not inhibited at oxygen concentrations below 0.005 % and E_h potentials as high as +420 mV. Fetzer and Conrad tested methanogenesis over a range of E_h potentials and found that there was no significant effect on methanogenesis, and that methane production was initiated at E_h potentials of +50 mV. More recently, studies have suggested that not only can microbial methane be produced in oxic environments (e.g., in oxygenated water columns of oligotrophic lakes), this could be an important source of atmospheric methane that is not accounted for in our current global methane budget models (Günthel et al., 2019; Hans-Peter et al., 2011).

3.4.5 Methane Cycling in Serpentinite-Hosted Springs

Based on our affinity calculations, there is energy available for methane cycling (Figure 3.2) at the serpentinite-hosted spring locations studied. Methane consumption via aerobic methanotrophy was predicted to provide the most energy of all the methane-based reactions considered. This was followed closely by methane production via acetotrophic methanogenesis. However, autotrophic methanogenesis with either carbon dioxide or carbon monoxide as the carbon source, as well as the water-gas shift reaction, was predicted to provide little to no energy at all. Methanogenesis using formate as the carbon source was predicted not to provide any energy. Based on the other similarities in

A_r values between sites, acetotrophic methanogenesis may also provide significant energy in other serpentinizing systems as well. However, despite the available energy, methanogens are rarely found in the metagenomes of sites of continental serpentinization.

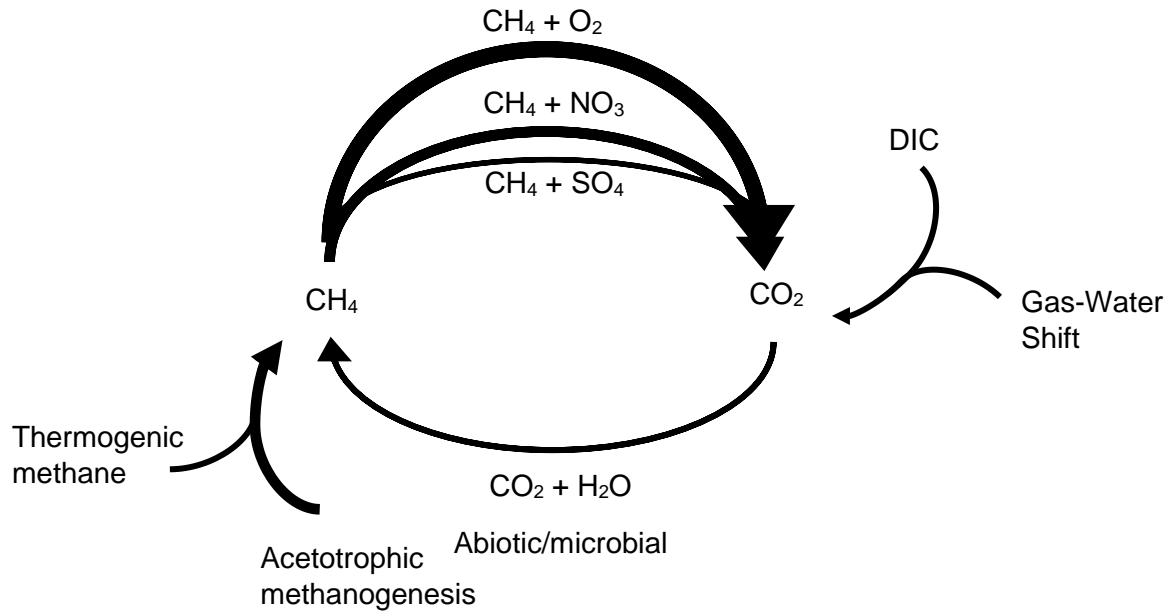


Figure 3.2. Schematic of methane sources and sinks at terrestrial sites of serpentinization. The reactions with larger calculated chemical affinities (A_r) are represented by thicker arrows.

Isotopic and aqueous geochemical data from the Tablelands suggest that the methane is non-microbial in origin at this site (Cumming et al., 2019; Szponar et al., 2013), which is supported by a lack of microbial methane production in microcosm studies (Morrill et al., 2014), and the lack of methanogens in the metagenome (Brazelton et al., 2011). Similarly, stable carbon and hydrogen isotope and clumped isotope compositions of methane from Aqua de Ney suggest the methane is abiotic rather than

microbial (Blank et al., 2017). Twing et al. (2017) were also unable to detect the presence of any methanogens in wells at CROMO using a combination of metagenomics and 16S rRNA gene sequencing.

Conversely, isotopic and aqueous geochemical data from The Cedars suggest, at least in part, a microbial origin for the methane present there (Morrill et al., 2013; Wang et al., 2015). Microcosms with ^{13}C -labeled substrates demonstrated that methanogens at The Cedars were capable of converting bicarbonate, acetate, formate, and methanol to methane (Kohl et al., 2016). Microbial methane was also generated in carbon monoxide amended microcosms, however, no change in the carbon monoxide concentrations were observed (Kohl et al., 2016). In fluids from the Samail Ophiolite in Oman, *Methanobacterium*, a methanogen that generates methane using hydrogen with formate, carbon monoxide, or carbon dioxide, was detected (Miller et al., 2016; Rempfert et al., 2017).

Genomic data from Brazelton et al. (2011) showed no evidence of methanotrophs in serpentinite-hosted springs of the Tablelands which could explain why there was little evidence of methanotrophy in the microcosm experiments. However, while evidence of methanotrophic archaea and bacteria in continental sites of serpentinization is relatively limited at this time, there are some sites where they have been identified in fluids that result from serpentinization reactions. For example, 16s rRNA and mcrA sequences belonging to the ANME-1a group of anaerobic methanotrophic archaea were detected in fluid from the Cabeço de Vide Aquifer in Portugal (Tiago and Veríssimo, 2013). 16s rRNA sequences belonging to the families *Methylococcaceae*, *Methylbacteriaceae*, and

Methylocystaceae were found in fluids from the Santa Elena Ophiolite in Costa Rica (Sánchez-Murillo et al., 2014). Metagenomic and experimental evidence of methanotrophic bacteria belonging to the family *Methylococcaceae* were found in fluids from the Voltri Massif in Italy (Brazelton et al., 2017). 16s rRNA evidence indicated the presence of methanotrophs in fluids from the Samail Ophiolite in Oman (Miller et al., 2016; Rempfert et al., 2017). A combination of metagenomic, metatranscriptomics, and untargeted metabolomics techniques were used to elucidate the presence of methanotrophs in fluids from CROMO (Seyler et al., 2020). This is interesting because calculated chemical affinities for methanotrophy in fluids from the Samail Ophiolite and CROMO were quite similar to those in fluids from Aqua de Ney. While the limitations of a microcosm study cannot be ruled out, the potential reason we did not observe CH₄ oxidation at Aqua de Ney or the Tablelands is that methanotrophs may not be present in the waters of these sites. This has been confirmed at the Tablelands (Brazelton et al., 2011), but needs to be confirmed at Aqua de Ney through genomic studies.

3.5 Conclusions

In summary, chemical affinities (A_r) for key metabolic reactions associated with methane cycling and carbon monoxide-based metabolisms were calculated for four contrasting sites of serpentinization: the Tablelands (NL, CAN), The Cedars (CA, USA), Aqua de Ney (CA, USA), and CROMO (CA, USA) and compared to previously calculated A_r values for the Samail Ophiolite, Oman. It was observed that while the A_r values varied a great deal from reaction to reaction, the A_r values for each reaction were similar across all sites studied. The calculations suggested that the oxidation of carbon monoxide should provide the most energy at all the sites, followed by hydrogen oxidation, methanotrophy with oxygen as the electron acceptor, methanogenesis with acetate as the electron donor, methanotrophy with nitrate as an electron acceptor, and carbon monoxide reduction. It was also noted that methanogenesis via carbon dioxide reduction, methanotrophy with sulfate as the electron acceptor, and methanogenesis with formate as the electron donor would yield little to no energy at all of the sites studied. Despite having the greatest A_r values, neither carbon monoxide nor hydrogen oxidation were observed, and there was little evidence of methane oxidation, when these potential metabolisms were tested in a laboratory-based setting using microcosms with materials from the Tablelands, The Cedars, or Aqua de Ney. While it is possible that the lack of observable methane, hydrogen, and carbon monoxide were due to the limitations of the microcosm studies, it is also possible that the organisms that can take advantage of these metabolisms were not present. Microbial acetotrophic methanogenesis was predicted to provide sufficient energy to the serpentinizing systems considered in this study, and yet methane at most sites of serpentinization is abiotic or thermogenic – i.e., putative non-

microbial. The Cedars is an exception with microcosms showing that microbial methanogenesis prevailed despite adverse, less reducing conditions. These results lead to new research questions about the carbon substrates used for methanogenesis as well as highlights the uniqueness of the methanogens and microbial community in general at The Cedars.

3.6 Acknowledgments

The authors would like to thank David McCrory and Roger Raiche for allowing access to The Cedars and Parks Canada for providing access to the Tablelands. The authors would also like to thank Emily Cumming and Dr. Mark Wilson for their help in the field, Jamie Warren, Dr. Geert van Biesen (CREAIT – Stable Isotope Laboratory), and Dr. Inês Nobre Silva (CREAIT – ICPMS) for their expertise, and Dr. Michael Babechuk for his inspirational discussions. This research was funded by Natural Science and Engineering Research Council (NSERC) Discovery Grant and Canada Space Agency's Flights and Fieldwork for the Advancement of Science and Technology (FAST) grant awarded to Dr. Penny Morrill and NSERC's Alexander Graham Bell Canada Graduate Scholarship-Doctoral (CGS D) awarded to Melissa Cook. Activity coefficients, activities of chemical species used in A_r calculations, and the experimental set-up can be found in the Supporting Information. This data is available through Memorial University's research repository (<https://doi.org/10.5683/SP2/ICSESD>).

3.7 References

- Amend, J. P., & Shock, E. L. (2001). Energetics of overall metabolic reactions of thermophilic and hyperthermophilic Archaea and Bacteria. *FEMS Microbiology Reviews*, 25(2), 175-243. <https://doi.org/10.1111/j.1574-6976.2001.tb00576.x>
- Blank, J. G., Etiope, G., Stamenković, V., Rowe, A. R., Kohl, I., Li, S., & Young, E. D. (2017). *Methane at the Aqua de Ney hyperalkaline spring (N. California USA), a site of active serpentinization*. Paper presented at the Astrobiology Science Conference 2017, Mesa, Arizona, USA.
- Blank, J. G., Green, S. J., Blake, D., Valley, J. W., Kita, N. T., Treiman, A., & Dobson, P. F. (2009). An alkaline spring system within the Del Puerto Ophiolite (California, USA): A Mars analog site. *Planetary and Space Science*, 57(5), 533-540. <http://www.sciencedirect.com/science/article/pii/S0032063308003978>
- Boudier, F., Sueur, E. L., & Nicolas, A. (1989). Structure of an atypical ophiolite: The Trinity complex, eastern Klamath Mountains, California. *Geological Society of America Bulletin*, 101(6), 820-833.
- Brazelton, W. J., Schrenk, M. O., Kelley, D. S., & Baross, J. A. (2006). Methane- and Sulfur-Metabolizing Microbial Communities Dominate the Lost City Hydrothermal Field Ecosystem. *Applied and Environmental Microbiology*, 72(9), 6257-6270. <https://doi.org/10.1128/AEM.00574-06>
- Brazelton, W. J., Mehta, M. P., Kelley, D. S., & Baross, J. A. (2011). Physiological Differentiation within a Single-Species Biofilm Fueled by Serpentinization. *mBio*, 2(4), e00127-00111. <https://mbio.asm.org/content/mbio/2/4/e00127-11.full.pdf>
- Brazelton, W. J., Morrill, P. L., Szponar, N., & Schrenk, M. O. (2013). Bacterial Communities Associated with Subsurface Geochemical Processes in Continental

- Serpentinite Springs. *Applied and Environmental Microbiology*, 79(13), 3906-3916. <https://aem.asm.org/content/aem/79/13/3906.full.pdf>
- Brazelton, W. J., Thornton, C. N., Hyer, A., Twing, K. I., Longino, A. A., Lang, S. Q., Lilley, M. D., Früh-Green, G. L., & Schrenk, M. O. (2017). Metagenomic identification of active methanogens and methanotrophs in serpentinite springs of the Voltri Massif, Italy. *PeerJ (San Francisco, CA)*, 5, e2945-e2945. <https://doi.org/10.7717/peerj.2945>
- Canovas, P. A., Hoehler, T., & Shock, E. L. (2017). Geochemical bioenergetics during low-temperature serpentinization: An example from the Samail ophiolite, Sultanate of Oman. *Journal of Geophysical Research: Biogeosciences*, 122(7), 1821-1847. <https://agupubs.onlinelibrary.wiley.com/doi/abs/10.1002/2017JG003825>
- Coleman, R. G. (2000). Prospecting for ophiolites along the California continental margin. *Special Papers-Geological Society of America*, 351-364.
- Cumming, E. A., Rietze, A., Morrissey, L. S., Cook, M. C., Rhim, J. H., Ono, S., & Morrill, P. L. (2019). Potential sources of dissolved methane at the Tablelands, Gros Morne National Park, NL, CAN: A terrestrial site of serpentinization. *Chemical Geology*, 514, 42-53. <http://www.sciencedirect.com/science/article/pii/S0009254119301299>
- Daae, F. L., Økland, I., Dahle, H., Jørgensen, S. L., Thorseth, I. H., & Pedersen, R. B. (2013). Microbial life associated with low-temperature alteration of ultramafic rocks in the Leka ophiolite complex. *Geobiology*, 11(4), 318-339. <https://doi.org/10.1111/gbi.12035>

- Dunning, G., & Krogh, T. (1985). Geochronology of ophiolites of the Newfoundland Appalachians. *Canadian Journal of Earth Sciences*, 22(11), 1659-1670.
- Feth, J., Rogers, S., & Roberson, C. (1961). Aqua de Ney, California, a spring of unique chemical character. *Geochimica et Cosmochimica Acta*, 22(2-4), 75-86.
- Fetzer, S., & Conrad, R. (1993). Effect of redox potential on methanogenesis by *Methanosarcina barkeri*. *Archives of Microbiology*, 160(2), 108-113.
<https://doi.org/10.1007/BF00288711>
- Fones, E. M., Colman, D. R., Kraus, E. A., Nothaft, D. B., Poudel, S., Rempfert, K. R., Spear, J. R., Templeton, A. S., & Boyd, E. S. (2019). Physiological adaptations to serpentinization in the Samail Ophiolite, Oman. *The ISME Journal*, 13(7), 1750-1762. <https://doi.org/10.1038/s41396-019-0391-2>
- Günthel, M., Donis, D., Kirillin, G., Ionescu, D., Bizic, M., McGinnis, D. F., Grossart, H.-P., & Tang, K. W. (2019). Contribution of oxic methane production to surface methane emission in lakes and its global importance. *Nature communications*, 10(1), 5497-5410. <https://doi.org/10.1038/s41467-019-13320-0>
- Hans-Peter, G., Katharina, F., Claudia, D., Werner, E., & Kam, W. T. (2011). Microbial methane production in oxygenated water column of an oligotrophic lake. *Proceedings of the National Academy of Sciences - PNAS*, 108(49), 19657-19661.
<https://doi.org/10.1073/pnas.1110716108>
- Helgeson, H. C., & Murphy, W. M. (1983). Calculation of mass transfer among minerals and aqueous solutions as a function of time and surface area in geochemical processes. I. computational approach. *Journal of the International Association for*

- Mathematical Geology*, 15(1), 109-130. journal article.
<https://doi.org/10.1007/BF01030078>
- Jarrell, K. F. (1985). Extreme Oxygen Sensitivity in Methanogenic Archaeobacteria. *BioScience*, 35(5), 298-302. <https://doi.org/10.2307/1309929>
- Kelley, D. S., Karson, J. A., Jakuba, M., Bradley, A., Larson, B., Ludwig, K., Glickson, D., Buckman, K., Bradley, A. S., Brazelton, W. J., Roe, K., Elend, M. J., Früh-Green, G. L., Delacour, A., Bernasconi, S. M., Lilley, M. D., Baross, J. A., Summons, R. E., Sylva, S. P., . . . Proskurowski, G. (2005). A Serpentinite-Hosted Ecosystem: The Lost City Hydrothermal Field. *Science (American Association for the Advancement of Science)*, 307(5714), 1428-1434.
<https://doi.org/10.1126/science.1102556>
- Kohl, L., Cumming, E., Cox, A., Rietze, A., Morrissey, L., Lang, S. Q., et al. (2016). Exploring the metabolic potential of microbial communities in ultra-basic, reducing springs at The Cedars, CA, USA: Experimental evidence of microbial methanogenesis and heterotrophic acetogenesis. *Journal of Geophysical Research: Biogeosciences*, 121(4), 1203-1220.
<https://agupubs.onlinelibrary.wiley.com/doi/abs/10.1002/2015JG003233>
- Krulwich, T. A., Sachs, G., & Padan, E. (2011). Molecular aspects of bacterial pH sensing and homeostasis. *Nature Reviews Microbiology*, 9(5), 330-343.<https://doi.org/10.1038/nrmicro2549>
- Lang, S. Q., Früh-Green, G. L., Bernasconi, S. M., Brazelton, W. J., Schrenk, M. O., & McGonigle, J. M. (2018). Deeply-sourced formate fuels sulfate reducers but not

- methanogens at Lost City hydrothermal field. *Scientific Reports*, 8(1), 755.
<https://doi.org/10.1038/s41598-017-19002-5>
- Miller, H. M., Matter, J. M., Kelemen, P., Ellison, E. T., Conrad, M. E., Fierer, N., et al. (2016). Modern water/rock reactions in Oman hyperalkaline peridotite aquifers and implications for microbial habitability. *Geochimica et Cosmochimica Acta*, 179, 217-241.
<http://www.sciencedirect.com/science/article/pii/S0016703716300205>
- Morrill, P. L., Brazelton, W. J., Kohl, L., Rietze, A., Miles, S. M., Kavanagh, H., et al. (2014). Investigations of potential microbial methanogenic and carbon monoxide utilization pathways in ultra-basic reducing springs associated with present-day continental serpentinization: the Tablelands, NL, CAN. *Frontiers in Microbiology*, 5(613). Original Research.
<https://www.frontiersin.org/article/10.3389/fmicb.2014.00613>
- Morrill, P. L., Kuenen, J. G., Johnson, O. J., Suzuki, S., Rietze, A., Sessions, A. L., et al. (2013). Geochemistry and geobiology of a present-day serpentinization site in California: The Cedars. *Geochimica et Cosmochimica Acta*, 109, 222-240.
<http://www.sciencedirect.com/science/article/pii/S0016703713000768>
- Oremland, R. S., Miller, L. G., & Whiticar, M. J. (1987). Sources and flux of natural gases from Mono Lake, California. *Geochimica et Cosmochimica Acta*, 51(11), 2915-2929.
- Rempfert, K. R., Miller, H. M., Bompard, N., Nothaft, D., Matter, J. M., Kelemen, P., et al. (2017). Geological and Geochemical Controls on Subsurface Microbial Life in

- the Samail Ophiolite, Oman. *Frontiers in Microbiology*, 8(56). Original Research.
<https://www.frontiersin.org/article/10.3389/fmicb.2017.00056>
- Rietze, A. (2015). *Investigating geochemistry and habitability of continental sites of serpentization: the Cedars, California, USA and the Tablelands, Newfoundland, CAN*. Memorial University of Newfoundland.
- Sabuda, M. C. (2017). *Biogeochemistry of Environmental Gradients in Serpentinization-Influenced Groundwater at the Coast Range Ophiolite Microbial Observatory, California*: Michigan State University.
- Sabuda, M.C., Brazelton, W.J., Putman, L.I., McCollom, T.M., Hoehler, T.M., Kubo, M.D.Y., Cardace, D., & Schrenk, M.O. (2020). A dynamic microbial sulfur cycle in a serpentinizing continental ophiolite. *Environmental Microbiology*, 22(6), 2329-2345.
- Sánchez-Murillo, R., Gazel, E., Schwarzenbach, E.M., Crespo-Medina, M., Schrenk, M.O., Boll, J., & Gill, B.C. (2014). Geochemical evidence for active tropical serpentization in the Santa Elena Ophiolite, Costa Rica: An analog of a humind early Earth? *Geochemistry, Geophysics, Geosystems*, 15(5), 1783-1800.
- Schrenk, M. O., Brazelton, W. J., & Lang, S. Q. (2013). Serpentinization, carbon, and deep life. *Reviews in Mineralogy and Geochemistry*, 75(1), 575-606.
- Schulte, M., Blake, D., Hoehler, T., & McCollom, T. (2006). Serpentinization and Its Implications for Life on the Early Earth and Mars. *Astrobiology*, 6(2), 364-376.
<https://doi.org/10.1089/ast.2006.6.364>
- Seyler, L.M., Brazelton, W.J., McLean, C., Putman, L.I., Hyer, A., Kubo, M.D.Y., Hoehler, T., Cardace, D., & Schrenk, M.O. (2020). Carbon assimilation strategies

- in ultrabasic groundwater: clues from the integrated study of a serpentinization-influenced aquifer. *mSystems*, 5(2), e00607-19.
- Shock, E. L., Holland, M., Meyer-Dombard, D. A., Amend, J. P., Osburn, G. R., & Fischer, T. P. (2010). Quantifying inorganic sources of geochemical energy in hydrothermal ecosystems, Yellowstone National Park, USA. *Geochimica et Cosmochimica Acta*, 74(14), 4005-4043.
<http://www.sciencedirect.com/science/article/pii/S0016703710001201>
- Sorokin, D. Y., & Kuenen, J. G. (2005). Haloalkaliphilic sulfur-oxidizing bacteria in soda lakes. *FEMS Microbiology Reviews*, 29(4), 685-702.
<https://doi.org/10.1016/j.femsre.2004.10.005>
- Suzuki, S., Ishii, S. i., Hoshino, T., Rietze, A., Tenney, A., Morrill, P. L., et al. (2017). Unusual metabolic diversity of hyperalkaliphilic microbial communities associated with subterranean serpentinization at The Cedars. *The ISME Journal*, 11(11), 2584-2598. <https://doi.org/10.1038/ismej.2017.111>
- Suzuki, S., Ishii, S. i., Wu, A., Cheung, A., Tenney, A., Wanger, G., et al. (2013). Microbial diversity in The Cedars, an ultrabasic, ultrareducing, and low salinity serpentinizing ecosystem. *Proceedings of the National Academy of Sciences*, 110(38), 15336-15341. <https://www.pnas.org/content/pnas/110/38/15336.full.pdf>
- Suzuki, S., Kuenen, J. G., Schipper, K., van der Velde, S., Ishii, S. i., Wu, A., et al. (2014). Physiological and genomic features of highly alkaliphilic hydrogen-utilizing Betaproteobacteria from a continental serpentinizing site. *Nature Communications*, 5(1), 3900. <https://doi.org/10.1038/ncomms4900>

- Szponar, N., Brazelton, W. J., Schrenk, M. O., Bower, D. M., Steele, A., & Morrill, P. L. (2013). Geochemistry of a continental site of serpentinization, the Tablelands Ophiolite, Gros Morne National Park: A Mars analogue. *Icarus*, 224(2), 286-296. <http://www.sciencedirect.com/science/article/pii/S0019103512002783>
- Tiago, I., Veríssimo, A. (2013). Microbial and function diversity of a subterrestrial high pH groundwater associated to serpentinization. *Environ Microbiol.*, 15(6), 1687-1706. doi: 10.1111/1462-2920.12034
- Twing, K. I., Brazelton, W. J., Kubo, M. D. Y., Hyer, A. J., Cardace, D., Hoehler, T. M., et al. (2017). Serpentinization-Influenced Groundwater Harbors Extremely Low Diversity Microbial Communities Adapted to High pH. *Frontiers in Microbiology*, 8(308). Original Research. <https://www.frontiersin.org/article/10.3389/fmicb.2017.00308>
- Wallin, E. T., & Metcalf, R. V. (1998). Supra-Subduction Zone Ophiolite Formed in an Extensional Forearc: Trinity Terrane, Klamath Mountains, California. *The Journal of geology*, 106(5), 591-608. <https://doi.org/10.1086/516044>
- Wang, D. T., Gruen, D. S., Sherwood Lollar, B. , Hinrichs, K.-U., Stewart, L. C., Holden, J. F., et al. (2015). Nonequilibrium clumped isotope signals in microbial methane. *Science*, 348(6233), 428-431. <https://science.sciencemag.org/content/sci/348/6233/428.full.pdf>
- YSI. (2005). *Measuring ORP on YSI 6-Series Sondes: Tips, Cautions and Limitations*. <https://www.ysi.com/File%20Library/Documents/Technical%20Notes/T608-Measuring-ORP-on-YSI-6-Series-Sondes-Tips-Cautions-and-Limitations.pdf>

3.8 Supplemental Information

Table 3.S1. Activity coefficients (γ) and activities calculated using the Debye-Hückel equation.

Analyte	The Cedars		The Tablelands		Aqua de Ney	
	γ	Activity	γ	Activity	γ	Activity
H ₂	1	5.37 x 10 ⁻⁵	1	5.29 x 10 ⁻⁴	1	1.00 x 10 ⁻⁵
O ₂	1	1.00 x 10 ⁻⁴	1	1.00 x 10 ⁻⁵	1	1.00 x 10 ⁻⁵
H ₂ O	1	1	1	1	1	1
CO	1	1.00 x 10 ⁻⁵	1	1.00 x 10 ⁻⁵	1	1.00 x 10 ⁻⁵
CO ₂	1	4.4 x 10 ⁻⁵	1	4.5 x 10 ⁻⁵	1	1.00 x 10 ⁻⁵
CH ₄	1	2.2 x 10 ⁻⁵	1	8.0 x 10 ⁻⁶	1	3.20 x 10 ⁻²
SO ₄ ²⁻	0.67	2.79 x 10 ⁻⁷	0.49	2.24 x 10 ⁻⁶	0.25	5.12 x 10 ⁻⁴
HCO ₃ ⁻	0.67	5.89 x 10 ⁻⁶	0.49	1.15 x 10 ⁻⁴	0.25	7.78 x 10 ⁻²
HS ⁻	0.90	4.52 x 10 ⁻⁷	0.84	4.19 x 10 ⁻⁷	0.71	3.39 x 10 ⁻²
NO ₃ ⁻	0.90	1.31 x 10 ⁻⁶	0.83	9.48 x 10 ⁻⁷	0.71	1.32 x 10 ⁻³
N ₂	1	2.30 x 10 ⁻³	1	1.80 x 10 ⁻³	1	2.00 x 10 ⁻³
CH ₃ COO ⁻	0.92	1.35 x 10 ⁻⁶	0.87	1.66 x 10 ⁻⁶	-	-
CHO ₂	0.92	4.28 x 10 ⁻⁵	0.87	8.25 x 10 ⁻⁵	-	-

Table 3.S2A. DSMZ Mineral Medium 81 for Chemolithotrophic Growth.

Solution A	Concentration in microcosm (g/L)
KH ₂ PO ₄	0.495
Na ₂ HPO ₄ x 2 H ₂ O	0.625
Distilled Water	-
Solution B	Concentration in microcosm (g/L)
NH ₄ Cl	0.215
MgSO ₄ x 7 H ₂ O	0.108
CaCl ₂ x 2 H ₂ O	0.002
MnCl ₂ x 4 H ₂ O	0.001
NaVO ₃ x H ₂ O	0.001
Trace element solution SL-6	<i>See Table S2B</i>
Distilled water	-
Solution C	Concentration in microcosm (g/L)
Ferric ammonium citrate	0.011
Distilled water	-

Table 3.S2B. DSMZ Mineral Medium 27 – Trace Element Solution SL-6 for Microorganisms.

Compound	Concentration in Microcosm (g/L)
ZnSO ₄ x 7 H ₂ O	1.08 x 10 ⁻⁴
MnCl ₂ x 4 H ₂ O	3.23 x 10 ⁻⁵
H ₃ BO ₃	3.23 x 10 ⁻⁴
CoCl ₂ x 6 H ₂ O	2.15 x 10 ⁻⁴
CuCl ₂ x 2 H ₂ O	1.08 x 10 ⁻⁵
NiCl ₂ x 6 H ₂ O	2.15 x 10 ⁻⁵
Na ₂ MoO ₄ x 2 H ₂ O	3.23 x 10 ⁻⁵
Distilled Water	-

Table 3.S3A. Experimental set-up of methane oxidation microcosm experiments.

Site	Experiment	Treatment	Sediment Slurry	Fluid	Headspace	Mineral media	CAPS buffer	CH ₄	Electron Acceptor	Initial pH	HgCl ₂
The Cedars	Control	Live	2 mL	30 mL	N ₂	19 mL	14 mL	3 mL	-	11.7	-
	Oxygen Addition	Live	2 mL	30 mL	N ₂	19 mL	14 mL	3 mL	2 mL O ₂	11.7	-
		Killed	2 mL	30 mL	N ₂	19 mL	14 mL	3 mL	2 mL O ₂	11.7	200 µL
	Nitrate Addition	Live	2 mL	30 mL	N ₂	19 mL	14 mL	3 mL	2 mL NO ₃ ⁻	11.7	-
		Killed	2 mL	30 mL	N ₂	19 mL	14 mL	3 mL	2 mL NO ₃ ⁻	11.7	200 µL
	Sulfate Addition	Live	2 mL	30 mL	N ₂	19 mL	14 mL	3 mL	2 mL SO ₄ ²⁻	11.7	-
Killed		2 mL	30 mL	N ₂	19 mL	14 mL	3 mL	2 mL SO ₄ ²⁻	11.7	200 µL	
The Tablelands	Control	Live	2 mL	30 mL	N ₂	19 mL	14 mL	3 mL	-	11.9	-
	Oxygen Addition	Live	2 mL	30 mL	N ₂	19 mL	14 mL	3 mL	2 mL O ₂	11.9	-
		Killed	2 mL	30 mL	N ₂	19 mL	14 mL	3 mL	2 mL O ₂	11.9	200 µL
	Nitrate Addition	Live	2 mL	30 mL	N ₂	19 mL	14 mL	3 mL	2 mL NO ₃ ⁻	11.9	-
		Killed	2 mL	30 mL	N ₂	19 mL	14 mL	3 mL	2 mL NO ₃ ⁻	11.9	200 µL
	Sulfate Addition	Live	2 mL	30 mL	N ₂	19 mL	14 mL	3 mL	2 mL SO ₄ ²⁻	11.9	-
Killed		2 mL	30 mL	N ₂	19 mL	14 mL	3 mL	2 mL SO ₄ ²⁻	11.9	200 µL	
Aqua de Ney	Control	Live	-	30 mL	N ₂	19 mL	14 mL	3 mL	-	12.5	-
		Live	-	30 mL	N ₂	19 mL	14 mL	3 mL	2 mL O ₂	12.5	-

Oxygen Addition	Killed	-	30 mL	N ₂	19 mL	14 mL	3 mL	2 mL O ₂	12.5	600 μL
Nitrate Addition	Live	-	30 mL	N ₂	19 mL	14 mL	3 mL	2 mL NO ₃ ⁻	12.5	-
	Killed	-	30 mL	N ₂	19 mL	14 mL	3 mL	2 mL NO ₃ ⁻	12.5	600 μL
Sulfate Addition	Live	-	30 mL	N ₂	19 mL	14 mL	3 mL	2 mL SO ₄ ²⁻	12.5	-
	Killed	-	30 mL	N ₂	19 mL	14 mL	3 mL	2 mL SO ₄ ²⁻	12.5	600 μL

Table 3.S3B. Experimental set-up of carbon monoxide oxidation microcosm experiments.

Site	Experiment	Treatment	Sediment Slurry	Fluid	Headspace	Mineral Media	CAPS buffer	Electron Donor	Initial pH	HgCl ₂
Aqua de Ney	Control	Live	-	30 mL	Air	14 mL	14 mL	-	12.5	-
		Killed	-	30 mL	Air	14 mL	14 mL	-	12.5	600 µL
	Carbon monoxide	Live	-	30 mL	Air	14 mL	14 mL	CO	12.5	-
		Killed	-	30 mL	Air	14 mL	14 mL	CO	12.5	600 µL

Table 3.S3C. Experimental set-up of hydrogen oxidation microcosm experiments.

Site	Experiment	Treatment	Sediment Slurry	Fluid	Headspace	Mineral Media	CAPS buffer	Electron Donor	Initial pH	HgCl ₂
Aqua de Ney	Control	Live	-	30 mL	Air	14 mL	14 mL	-	12.5	-
		Killed	-	30 mL	Air	14 mL	14 mL	-	12.5	600 µL
	Hydrogen Oxidation	Live	-	30 mL	Air	14 mL	14 mL	H ₂	12.5	-
		Killed	-	30 mL	Air	14 mL	14 mL	H ₂	12.5	600 µL

Table 3.S4A. Aqueous concentrations of gases in microcosms calculated using Henry's constant.

Compound	K_H (mol·kg ⁻¹ ·bar ⁻¹)	Molar concentration gas phase	Molar concentration aqueous phase (C_w)
CH ₄	0.0014	0.001	3.47 x 10 ⁻⁵
CO	0.00086	0.001	2.13 x 10 ⁻⁵
H ₂	0.00078	0.0003	5.80 x 10 ⁻⁶

Table 3.S4B. Chemical affinities at the Tablelands, The Cedars, and Aqua de Ney calculated using aqueous gas concentrations ($A_r C_w$) compared with chemical affinities (A_r).

Eq#	Reaction	The Tablelands		The Cedars		Aqua de Ney	
		A_r (C_w)	A_r	A_r (C_w)	A_r	A_r (C_w)	A_r
3.S1	Hydrogen oxidation	27	28	27	27	26	26
3.S2	Water-gas shift	5	4	5	4	5	5
3.S3	Carbon monoxide oxidation	32	32	31	31	31	31
3.S4	Carbon monoxide reduction	5	6	5	5	5	4
3.S5	Methanogenesis (CO ₂)	3	4	2	3	2	2
3.S6	Methanogenesis (formate)	-43	-42	-43	-43		-
3.S7	Methanogenesis (acetate)	22	23	24	24		-
3.S8	Methanotrophy (nitrate)	19	18	19	19	21	22
3.S9	Methanotrophy (sulfate)	1	1	1	1	0	1
3.S10	Aerobic methanotrophy	24	24	24	24	24	24

Chapter 4. The Lipid Biomarker Record at The Cedars: A Terrestrial Site of Serpentinization

Abstract

The Cedars is a site of terrestrial serpentinization where previous studies have suggested the methane is, at least in part, microbial in origin. The Cedars hosts a series of ultra-basic reducing springs where fluids that result from serpentinization reactions discharge from the subsurface and form carbonate deposits. Two ultra-basic springs (GPS1 and NS1) and a pool (BSC) where the ultra-basic fluids discharge and are exposed to the atmosphere were chosen for this study. Fluids and carbonate samples from these sampling locations were extracted and analyzed for lipid biomarkers to provide an overall description of the archaeal and bacterial microbial community at The Cedars. No lipids indicative of Archaea were detected in the carbonate or fluids analyzed in this study. Furthermore, the majority of lipids identified were diacylglycerols (DAGs) suggesting the microbial communities at The Cedars were largely composed of Bacteria or Eukarya. Despite evidence of microbial methanogenesis, no lipids indicative of methanogens were identified in carbonate or fluid samples which suggests either methanogens were not present, or the lipids were below the limits of detection. Chlorophyll *a* and pheophytin *a*, pigments associated with photosynthetic organisms, were however detected in the carbonate sample from the BSC pool but not in the fluids. These pigments could suggest the presence of cyanobacteria living in surface pools created by serpentine-hosted springs where CaCO₃ precipitates at The Cedars. It is possible that cyanobacteria that could be contributing to the overall methane budget at The Cedars and could help explain the absence of lipids indicative of methanogens.

4.1 Introduction

4.1.1 Serpentinization

Serpentinization, a process where ultramafic rocks primarily composed of olivine and pyroxenes are altered to serpentines, was likely more prevalent during early Earth when there were more exposed ultramafic rocks (Sleep et al., 2004). In addition to the production of serpentine, the process also results in the production of a suite of secondary minerals (e.g., brucite and magnetite), and hydrogen gas (Abrajano et al., 1988; Schulte et al., 2006). It is hypothesized that the hydrogen produced by serpentinization could have been the source of electrons that fueled early microbial life (Schulte et al., 2006). Furthermore, research has suggested that serpentinization has also occurred, or is occurring, on extra-terrestrial planetary bodies such as Mars, Titan, and Enceladus (Ehlmann et al., 2010; Vance et al., 2007). Although studying these environments is challenging, serpentinization also occurs on present-day Earth at mid-ocean ridges as well as within ophiolites (i.e., sections of ocean crust and mantle that have been emplaced onto land) that can act as analogues for these past and inaccessible environments.

Serpentinization, along with other associated reactions, can result in the production of methane gas (Sleep et al., 2004). Conditions at sites of serpentinization are conducive to the production of methane through abiogenic, microbial, or thermogenic pathways (Szponar et al., 2013). Abiogenic methane can be formed when hydrogen reacts with inorganic carbon present in the system (Sleep et al., 2004). Microbial methanogenesis can occur at sites of serpentinization when methanogens are able to thrive due to the reducing conditions created by the serpentinization reaction (Kelley et al., 2005; Brazelton et al., 2006; Schulte et al., 2006; Morrill et al., 2013). For example, methane can be produced microbially through either autotrophic CO₂ reduction, heterotrophic organic acid fermentation, or a combination thereof (Kohl et al., 2016

and references therein). Finally, thermogenic methane can be produced at sites of serpentinization by the thermal degradation of buried organic matter that is adjacent to, or beneath, the ultramafic rocks. Extensive fracturing caused by the serpentinization reaction can create conduits that allow thermogenic gases to travel from the subsurface by groundwater flow (Morrill et al., 2013). Independent of its source, methane, like hydrogen, can be a source of electrons for metabolism, as well as a carbon source for microbial methane oxidation.

4.1.2 Microbiological and Geochemical Studies at Sites of Serpentinization

Although the fluids that result from serpentinization reactions are rich in electron donors such as methane and hydrogen, the fluids are depleted in electron acceptors that are required for metabolic reactions (Morrill et al., 2013). Furthermore, these fluids are also typically depleted in inorganic carbon, and due to their high pH, any inorganic carbon present is in the form of the carbonate ion which is not known to be biologically available (Sorokin & Kuenen, 2005).

Although these conditions are challenging for life, evidence of microbial life has been observed at many sites of serpentinization. For example, 16S rRNA analyses on fluids and carbonates from the Lost City Hydrothermal Field (LCHF), a marine site of serpentinization located near the Mid-Atlantic Ridge, indicates the presence of chemolithoautotrophic sulfur and sulfide oxidizing, sulfate reducing, and methane-oxidizing bacteria as well as methanogenic and anaerobic methane-oxidizing archaea (Brazelton et al., 2006). Further, different microbial community compositions were detected in the deep subsurface fluids versus the shallow fluids of the LCHF (Moser et al., 2005). The deeper fluids were comprised almost exclusively of *Clostridia* affiliated with the genus *Desulfotomaculum* while shallow fluids were dominated by *Betaproteobacteria* belonging to the *Comamonadaceae* family (Brazelton et al., 2012; Moser et al., 2005). Although methanogenic archaea have been detected at LCHF, isotopic analyses on the

methane from the LCHF suggests it is mostly from abiotic sources (Bradley & Summons, 2010; Brazelton et al., 2006).

Similarly, studies of fluids from the Samail Ophiolite in Oman have shown there are different microbial communities in the deep subsurface fluids than in the surficial hyperalkaline fluids of other ophiolites studied (Rempfert et al., 2017). Deep hyperalkaline fluids from the Samail Ophiolite are largely composed of the families *Thermodesulfovibrionaceae*, chemoorganotrophic or chemolithoautotrophic bacteria capable of reducing sulfate coupled to the oxidation of H₂ or C₁-C₃ acids, and *Meiothermus*, an aerobic heterotroph (Rempfert et al., 2017). *Methanobacterium*, a methanogen that generates methane using H₂ with formate, CO, or CO₂, was also detected at the Samail Ophiolite (Rempfert et al., 2017). Although methanogens have been detected in genomic analyses of fluids from the Samail Ophiolite, isotopic analyses of methane have shown that the stable carbon isotope value ($\delta^{13}\text{C}$) of the methane is between 2.4 to 3.0 ‰ (Miller et al., 2016). These $\delta^{13}\text{C}$ values are more positive than any previously defined isotopic fields for microbial methane (Etiope & Whiticar, 2019). It is possible this methane could have been formed through abiotic reduction of dissolved CO₂ or through biogenic pathways under extreme carbon limitation (Miller et al., 2016), however, the isotopic signature of the reactants is required to confirm this.

Fluid and carbonate samples analyzed from the Chimaera Ophiolite, located in Turkey, contained both Archaea and Bacteria (Neubeck et al., 2017). At all points sampled, four distinct bacterial phyla accounted for the majority of taxa: *Proteobacteria*, *Actinobacteria*, *Chloroflexi*, and *Acidobacteria* (Neubeck et al., 2017). While members of *Chloroflexi* dominated areas of low-diversity, *Proteobacteria* were found to dominate higher-diversity areas (Neubeck et al., 2017). Methane, nitrogen, iron, and hydrogen oxidizers were all detected along with Archaea and

metal-resistant bacteria (Neubeck et al., 2017). Geochemical analyses on the methane from this seep have suggested that it is primarily abiotic in origin (Etiope et al., 2011).

At The Cedars, a site of terrestrial serpentinization located in Northern California, microbiological investigations have suggested that the fluids (both deep subsurface and more surficial) are largely dominated by Bacteria with some Archaea present (Suzuki et al., 2013). Like LCHF and the Samail Ophiolite, studies have confirmed distinct microbial communities in the ultra-basic springs (Suzuki et al., 2013). During their geomicrobiological study, Suzuki et al. (2013) identified one archaeal sequence that placed closely to *Methanosarcinales*, a methanogen, in the phylogenetic tree but did not fit with any known methanogen. Unlike the Samail Ophiolite, isotopic analysis of the methane from springs at The Cedars suggested that the methane was at least partially microbial in source (Morrill et al., 2013; Wang et al., 2015).

Microbial methanogenesis was later observed in ^{13}C labelled laboratory-based microcosm experiments using fluid and carbonates from The Cedars (Kohl et al., 2016). An increase in methane concentrations coupled with the incorporation of ^{13}C into methane in the live microcosm experiments, but not in the killed microcosm controls, demonstrated that methanol, formate, acetate, and bicarbonate were being converted microbially into methane (Kohl et al., 2016). Methanogenesis was further confirmed through microcosm experiments by Cook et al. (2021b, Chapter 3) who also observed microbial methanogenesis in microcosm experiments despite an oxic environment. These experiments demonstrate that despite the sensitivity of methanogens to oxygen, the methanogenesis occurred under oxic conditions (i.e., $E_h > 0$ mV) using material from The Cedars (Cook et al., 2021b, Chapter 3). Putative microbial methanogenesis at sites of terrestrial serpentinization is rare making The Cedars a unique site of serpentinization. It is currently not understood why The Cedars is one of the few sites of

serpentinization where there is evidence of putative microbial methanogenesis and how methanogens are able to survive under the oxic conditions created in the laboratory-based experiments.

4.1.3 Lipid Biomarkers at Sites of Serpentinization

Lipids make up the cellular membranes of Archaea, Bacteria, and Eukarya and can be useful tools to aid in understanding microbial communities at sites of serpentinization. Although lipidomics is a relatively new field with limited studies existing, microbial communities at sites of serpentinization inferred from lipid biomarkers have shown good agreement with those inferred from genomic data. For example, Bradley et al. (2009) extracted marine carbonate chimneys from the LCHF and detected the presence of isoprenoidal diethers, including *sn*-2 hydroxyarchaeol, *sn*-3 hydroxyarchaeol, and putative dihydroxyarchaeol, which were likely derived from methanogens. Additionally, glycerol mono- and diethers were detected in samples suggesting the presence of sulfate-reducing bacteria (Bradley et al., 2009). The coexistence of methanogens and sulfate-reducing bacteria is consistent with genomic data from Brazelton et al. (2006).

There have also been some studies investigating lipid biomarkers at sites of terrestrial serpentinization that have shown good agreement with previous genomic studies. Zwicker et al. (2018) extracted carbonate and ultramafic rocks from the Chimaera Ophiolite and found lipid biomarkers indicative of Archaea including pentamethylcosane (PMI), squalene, archaeol, *sn*-2 hydroxyarchaeol and *sn*-3 hydroxyarchaeol. They also identified dialkyl glycerol diethers (DAGEs) as well as monoalkyl glycerol monoethers (MAGEs) likely indicative of bacterial sulfate reducers (Zwicker et al., 2018). More recently, Newman et al. (2020) extracted carbonate, travertine, and host rock samples from the Samail Ophiolite in Oman and detected both archaeal

and bacterial lipids. Specifically, they found archaeol and isoprenoidal GDGTs, both indicative of Archaea, as well as branched GDGTs which were likely indicative of Bacteria. Newman et al. (2020) also found monoether non-isoprenoidal lipids and fatty acids that are likely indicative of sulfate-reducing bacteria.

Although genomic-based techniques can provide valuable detailed taxonomic analyses of the microbial community composition in an environment, they rely on amplified signals. Lipid biomarkers, however, do not rely on amplified signals. Furthermore, due to the fact that certain lipids have such a high preservation potential in carbonates (on the order of hundreds of millions years or longer (Love et al., 2009; Saito et al., 2015; Saito et al., 2017)), relative to that of bacterial DNA (which can only be preserved for a few millions years at most (Willerslev et al., 2004)), they provide more data about past microbial communities in extreme geochemical environments (Simoneit et al., 1998; Willerslev et al., 2004). Therefore, lipid biomarkers allow us to understand both extant microbial communities as well as extinct microbial communities that could be preserved in the rock record.

Despite the progress in understanding microbial communities at sites of serpentinization, there has been no previously published data on lipid biomarkers at The Cedars, one of the few serpentinization sites where putative microbial methane has been identified. Therefore, the overall objective of this study was to provide a better understanding of the microbial communities, extant and extinct, that inhabit The Cedars using lipid biomarkers. Specifically:

1. Provide an overall description of the archaeal and bacterial microbial community at The Cedars through investigation of lipid biomarkers.
2. Compare and contrast the lipid biomarker results with genomic results to determine if they are consistent.

3. To identify lipids indicative of methane cycling in fluids and carbonate.
4. To determine if microbial communities differ between springs with different proportions of ultra-basic fluids and the carbonate at The Cedars.

4.2 Methods

4.2.1 Site Description

The Cedars is an active site of serpentinization located in Sonoma County, CA, USA. It is a part of Northern California's Coast Range Ophiolite that was emplaced between 170-164 Ma as a part of the Franciscan Subduction Complex (Coleman, 2000; Shervais et al., 2004). At The Cedars, ultra-basic springs occur primarily along the creek bed and can be found in clusters with as many as 15-point sources of ultra-basic fluid (Morrill et al., 2013). When these ultra-basic springs exit the subsurface and come into contact with the oxic atmosphere, carbonate precipitates forming characteristic travertine deposits around the spring. Previous work has suggested that these springs can be comprised of deep subsurface groundwater, more shallow near-surface water, or a combination thereof depending on the spring (Morrill et al., 2013), and that the microbial community, based on genomic data, varies with groundwater type (Suzuki et al., 2013).

Three ultra-basic springs from The Cedars with varying mixing ratios of shallow and deep groundwater were sampled for this study (Figure 4.1). The mixing ratios of the springs, as well as the aqueous and gaseous geochemistry, have been previously determined by Morrill et al. (2013) and Cook et al. (2021, Chapter 2). The first spring, Grotto Pool Spring (GPS1) is located along Austin Creek (elevation 273 m, N38°37'16.3" W123°08'1.1"), approximately 100 m below the junction of two canyons and, based on the aqueous geochemistry, is thought to be the spring with the greatest proportion of deep subsurface groundwater (Morrill et al., 2013). Samples from GPS1 were taken directly at the discharge point such that there is little chance of exposure to the atmosphere. The second spring, Barnes Spring Complex (BSC) is located in a separate tributary of Austin Creek in the Main Canyon (elevation 282 m, N38°37'17.8"

W123°07'53.5"). BSC contains many ultra-basic spring discharge points all close together (numbered BS1 through BS7). BSC is thought to be largely composed (~86%) of more shallow near-surface water (Morrill et al., 2013). Samples from BSC were taken from the pools that form when the ultra-basic fluids discharge at the surface. These pools are exposed to the atmosphere and therefore subject to surface contributions. The third spring, NS1 is adjacent to a tributary of Austin Creek in Mineral Spring Canyon (Figure 4.1). At NS1 (elevation 321 m, N38°37'22.2" W123°08'02.8"), ultra-basic fluid discharges from a small, round opening located at the top of a travertine deposit that is approximately 0.5 m above the stream. Like BSC, NS1 is largely composed (~92%) of more shallow near-surface water (Morrill et al., 2013). Samples from NS1 were taken directly from this discharge point.

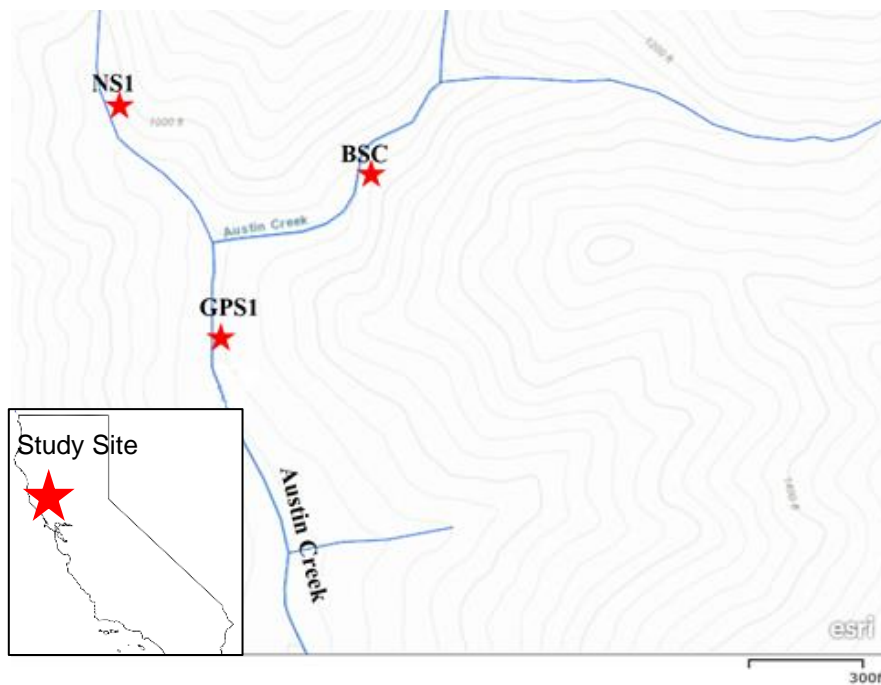


Figure 4.1. Topographic map of The Cedars, California, U.S.A (modified from the U.S. Geological Survey, Cazadera, CA, 2011). Springs discussed in this study are indicated by red stars.

4.2.2 Sample collection and preservation

Fluid samples for lipid analysis were collected on sterile polyethersulfone Sterivex cartridge filters (0.22 μm pore size) from NS1, GPS, and BS5. A Tygon® tube was inserted as close to the ultra-basic discharge point as possible to minimize contact with the atmosphere and fluid was pumped using a Masterflex® E/S™ portable peristaltic pump. The Sterivex filter was connected to the other end of the tubing and the fluid was pumped until the filter clogged. The total volume of fluid filtered was recorded (Table S1) and filters were wrapped in pre-combusted aluminum foil and frozen until analysis. Since lipids have also been detected in carbonate samples from other sites of serpentinization (e.g., the Samail Ophiolite (Newman et al., 2020) and the Chimaera Ophiolite (Zwicker et al., 2018), a carbonate sample was also collected from BS7. Carbonate was sampled from the bottom of the spring and stored in 50 mL falcon tubes. Samples were stored at $-80\text{ }^{\circ}\text{C}$ until analysis.

4.2.3 Sample extraction

Sample extraction and analysis were done in the Organic Geochemistry laboratory at Saint Mary's University in Halifax, Nova Scotia. Immediately before sample extraction, Sterivex™ filters were removed from the tinfoil and the sterile cartridge casing. Filters were added to Teflon tubes with 2.5 g of sterilized sand. In the case of the carbonate samples, samples were homogenized, and 25 g of powdered sample was added to clean Teflon tubes. Samples were then spiked with a recovery standard (1-alkyl-2-acetoxy-sn-glycero-3-phosphocholine (PAF)) and extracted using a modified Bligh and Dyer (MBD) extraction method as outlined in Sturt et al. (2004). Briefly, lipids were extracted in 6 steps using 3 solvent mixtures. The first four steps used ~6 mL (50 mL for bulk samples) of methanol/dichloromethane/buffer [2:1:0.8,

v/v] with steps one and two using a phosphate buffer (5.5 g/L Na₂HPO₄ adjusted to a pH of 7.4) and steps 3 and 4 using a trichloroacetic acid buffer (50 g/L C₂HCl₃O₂ with a pH of 2). The final 2 steps for the filters and the sediment used 6 mL (and 80 mL for bulk samples) of methanol/DCM [5:1; v/v] respectively.

Each extraction step involved sonication for 10 min followed by 5 min of centrifugation at 1250 rpm. After each extraction step, the solvent was decanted and combined in a separatory funnel to form a total lipid extract (TLE). The resulting TLE was then purified with Milli-Q water and evaporated to dryness under a continuous stream of nitrogen at 60 °C. The TLE was then spiked with 1,2-diheneicosanoyl-sn-glycero-3-phosphocholine (C₂₁-PC) and GDGT C₄₇ and stored at -20 °C until analysis.

4.2.4 Analytical methods

For mass spectral analysis, the TLE was reconstituted with methanol/DCM [9:1, v/v] and a 5 % aliquot was injected into an Agilent 1260 ultra-high-performance liquid chromatography-quadrupole time of flight mass spectrometer (uHPLC-qToF-MS) via a reverse phase electrospray spray ionization (ESI). Separation of lipids was achieved using a Zorbax RRHD Eclipse Plus C18 (2.1 mm x 150 mm x 1.8 µm) reverse phase column fitted with a guard column. The method was modified from Zhu et al. (2013) and the sample injection was 10 µL. Using a constant flow rate of 0.3 mL/min and a temperature of 45 °C, samples were eluted with a solvent gradient program using mobile phase A (methanol/formic acid/ammonium hydroxide [100:0.04:0.10, v/v]) and mobile phase B (propan-2-ol/formic acid/ammonium hydroxide [100:0.04:0.10, v/v]). Mobile phase A was held at 100 % for 10 min, followed by a linear gradient to 24 % mixing with mobile phase B extending for 5 min, then a linear gradient to 65 % B for 60 min, followed by 90

% B for 15 min, and finally 100 % A for 10 min to re-equilibrate. The injection solvent used was methanol.

4.2.5 Quantification of Lipids

The percent recoveries of the total lipid extracts were calculated based on the peak area of PAF (the recovery standard) which eluted at 2.7 min and had characteristic fragments of 523.4, and 542.4 *m/z*. The area of PAF in each sample was compared to that of the area in a blank sample containing the same amount of PAF to determine the percent recovery.

All lipids were tentatively identified by matching their mass spectral characteristics as well as their elution pattern to previously published literature (i.e., Theil et al., 2013; Chen et al., 2015; Nagai et al., 2020) (Table 4.2 and 4.3) using Agilent Technology's MassHunter software. Quantification of lipids was achieved by integrating the peak areas of each analyte and comparing it to the recovery standard (PAF). The concentration of each analyte was calculated using the following equation:

$$C_{\text{comp}} = M_{\text{std}} \times A_{\text{comp}} / A_{\text{std}} \times M_{\text{sed}} \quad [\text{Eq. 4.1}]$$

where: C_{comp} is the concentration of the compound ($\mu\text{g/g}$ sed. dw), M_{std} is the mass of standard (μg), A_{comp} is the area of the compound peak, and M_{sed} is the dry weight (dw) of sediment (g) (Bentley et al., 2022). Concentrations of lipids are reported in ng/mL of filtered water or ng/g of dry sediment weight

4.3 Results

4.3.1 Total Lipid Extracts

The TLE from the filters (reported in $\mu\text{g/L}$ fluid) and carbonate samples (reported in $\mu\text{g/g}$ sediment) from springs at The Cedars have been summarized (Table 4.1). The TLE from filters ranged from 5.71×10^{-1} to 1.06×10^1 mg/L fluid and the TLE from the carbonate sample was lean at $305 \mu\text{g/g}$ sediment. The highest TLE on the filters was from GPS while the lowest TLE was on the filter from NS1. Analysis of the peak area of the recovery standard in this study (PAF), however, revealed that the recoveries of the TLE in the samples ranged from 49 to 191 % (Table 4.S2). This is likely due to the presence of other peaks that eluted around the same time as the recovery standard. Due to the lack of confidence in the resolvability of the recovery standard, TLE was not adjusted for recovery and the values cannot be quantitatively compared.

Table 4.1. Total Lipid Extracts (TLE) from filters and carbonate samples from four springs at The Cedars.

Spring	Filter/carbonate	TLE (mg/g sed.)	TLE (mg/L fluid)
BSC*	Filter	N/A	4.02 ± 5.65
NS	Filter	N/A	5.71×10^{-1}
GPS	Filter	N/A	1.06×10^1
BSC	Filter	N/A	4.24×10^0
BSC	Carbonate	3.05×10^{-1}	N/A

*Four different BSC filters were extracted. The reported concentration is the average of the four extractions \pm one standard deviations (1σ).

4.3.2 Lipids Detected in TLE from Filters

Lipids found in TLE The Cedars filtrates (summarized in Table 4.2) were tentatively identified by their mass spectral characteristics and elution patterns through a literature review of previously published findings. The base peak chromatogram of the lipids found on the filters can be found in section 4.8 Supplemental Information (Figure 4.S1). The concentration of lipids extracted from filtered fluid from BSC ranged from 0.30 to 3.23 ng/mL, from GPS ranged from 0.02 to 1.11 ng/mL, and from NS1 ranged from 0.37 to 1.13 ng/mL. The lipids that were common at all three springs (BSC, GPS, and NS1) appeared to be bacterial/eukaryotic in origin. The majority of identified lipids were diacylglycerols (DAG) core lipids with various headgroups and one triacylglycerol (TAG). There were no archaeal lipids identified in the TLE from the filtered fluid at any springs sampled at The Cedars, however, a number of lipids could not be identified so it is not possible to determine whether these lipids were archaeal in origin.

Table 4.2. Summary of lipids present within filter samples from BSC, GPS, and NS1 at The Cedars.

Peak #	Domain	Chemical Name	Rt (min)	Molecular ion [M] ⁺	Diagnostic fragment ion	Spring: Concentration (ng/mL)	References
1	?	Unknown	1.2	820.3720	645.3, 573.3, 519.5	BSC: 3.23	-
2	?	Unknown	2.1	1045.5709	780.3, 295.1, 255.1	NS1: 1.13 GPS: 1.11	-
3	?	Unknown	2.8	1033.4067	973.4, 763.3, 549.2	NS1: 0.37 GPS: 0.36	-
4	?	U-DAG 35:2	5.9	722.5674	589.5, 406.3	BSC: 2.87	Thiel et al., 2013
6	B?	U-TAG 46:0	25.9	800.6873	523.5	BSC: 0.59	Thiel et al., 2013
7	B?	U-DAG 32:0	28.9	828.7194	551.5	BSC: 1.22	-
8	B?	U-DAG 34:1	29.5	974.8884	855.7, 577.5	BSC: 0.75	Nagai et al., 2020
9	?	U-DAG 36:2	30.6	907.7675	603.5	BSC: 1.13 NS1: <LOQ GPS: <LOQ	Thiel et al., 2013
10	B?	U-DAG 34:0	32.2	920.9989	857.8, 579.5	BSC: 0.40 NS1: <LOQ GPS: <LOQ	-
11	B?	U-DAG 34:0	35.4	884.7815	607.6, 579.5	BSC: 0.39 GPS: 0.02 NS1: <LOQ	-

*All reported mass fragment ions are of structures that contain no cyclization. Domains are reported as letters where B represents Bacteria and ? unknown lipid. Lipids that were present in a sample but below the limits of quantification are indicated by <LOQ.

There was a total of five lipids from the TLE of the filtered fluid that were unique to BSC. Of these lipids, only four could be tentatively identified as DAG 35:2, DAG 32:0, DAG 34:1, and TAG 46:0 with concentrations of 2.87, 1.22, 0.75, and 0.59 ng/mL fluid, respectively. The first unidentified lipid eluted at 1.2 with a molecular ion $[M]^+$ of 821.3998 m/z with fragments at 645.3, 573.4, and 519.2 m/z . This was also the lipid with the highest concentration in samples from BSC at 3.23 ng/mL fluid. The final unidentified lipid from BSC eluted at 5.9 min with a $[M]^+$ of 723.5752 m/z and fragments at 500.4, 589.5, and 406.3 m/z with a concentration of 2.87 ng/mL fluid.

There were no lipids that were unique to only NS1 or GPS, however, they did share two lipids that were not found in samples from BSC. The first lipid eluted at 2.1 min with a $[M]^+$ of 1045.5709 m/z with fragments at 780.3, 295.1, and 255.1 m/z and could not be identified. The concentration of this unknown lipid was 1.13 and 1.11 ng/mL fluid in GPS and NS1, respectively. The second lipid eluted at 2.8 min with a $[M]^+$ of 1033.4067 m/z and fragments at 973.4, 763.3, and 549.2 m/z but could not be identified. The concentration of this lipid in NS1 was 0.37 ng/mL fluid and 0.36 ng/mL fluid in GPS.

4.3.3 Lipids Detected in TLE from Carbonates

The lipids found in the sample carbonate are summarized in Table 4.3. The concentration of lipids in the TLE from the BSC carbonate sample ranged from 1.86 to 175.56 ng/g of sediment (dw). There were more than two times the number of peaks in the carbonate sample from BSC compared to the filters from BSC, NS1, and GPS. The base peak chromatogram of the lipids found in the carbonate sample can be found in section 4.8 Supplemental Information (Figure 4.S2). Identified lipids were likely from bacterial or eukaryotic sources mostly in the form of DAGs. A total of 14 DAGs were tentatively identified in these samples based on

comparison of their characteristic fragments with available literature (Table 4.3). The DAGs identified in the carbonate sample from BSC ranged in concentration from 2.80 to 134.77 ng/g of carbonate. At 26.2 min, DEG 34:1 (dietherglycerol) was tentatively identified based on its $[M]^+$ of 826.7031 m/z with a characteristic fragment of 577.5 m/z at a concentration of 22.63 ng/g of carbonate. Chlorophyll *a* was tentatively identified at 17.7 min based on $[M]^+$ of 892.5512 m/z with diagnostic fragments of 871.6 and 593.3 m/z . Pheophytin *a*, a breakdown product of chlorophyll *a*, was also tentatively identified at 18.6 min based on $[M]^+$ of 954.8398 m/z and diagnostic fragments of 871.6 and 593.3 m/z . The concentrations of chlorophyll *a* and pheophytin *a* were 25.94 and 1.86 ng/g carbonate, respectively.

Table 4.3. Summary of lipids detected in TLE from carbonate sample from BSC.

Peak #	Domain	Chemical Name	Rt (min)	Molecular ion [M] ⁺	Diagnostic fragment ion	Concentration (ng/g carbonate)	References
1	?	Unknown	2.4	724.5982	*613.4	67.83	-
2	?	Unknown	2.5	776.6643	627.4, 313.2	11.30	-
3	?	Unknown	2.8	668.5607	631.4	74.86	-
4	?	Unknown	3.0	754.6101	627.4	12.08	-
5	?	Unknown	3.1	754.6108	625.6, 367.3	6.91	-
6	?	Unknown	3.2	788.6542	647.5, 625.5	19.82	-
7	?	Unknown	3.4	734.4921	627.4	175.56	-
8	?	Unknown	3.7	808.6565	653.6	31.28	-
9	?	Unknown	3.9	796.6803	379.3	9.36	-
10	?	Unknown	4.0	880.9190	627.4	5.81	-
11	?	Unknown	4.4	848.6764	735.7, 394.3	44.97	-
12	?	Unknown	4.5	888.7054	761.7, 420.4	81.05	-
13	?	Unknown	5.9	785.6160	764.6, 500.4	12.33	-
14	?	U-DAG 34:2	6.4	681.6284	575.5	6.97	-
15	?	Unknown	6.8	665.6336	613.4, 543.4	11.55	-
16	?	U-DAG 36:6	7.5	944.7677	595.5, 465.5	2.80	-

18	E	Chlorophyl a	17.7	892.5512	871.6, 593.3	25.94	Chen et al. (2015)
20	E	Pheophytin a	18.6	954.8398	871.6, 673.6, 593.3	1.86	Chen et al. (2015)
22	?	U-DAG 36:5	20.4	982.8703	701.6, 597.5	6.87	Thiel et al., 2013
23	?	U-DAG 36:5	23.0	924.7189	597.5	5.25	Thiel et al., 2013
24	?	U-DAG 34:2	23.6	869.7487	575.5	20.37	Thiel et al., 2013
25	?	U-DAG 36:4	23.8	895.7625	820.7, 599.5	20.06	Thiel et al., 2013
26	?	U-DAG 36:4	24.8	921.7779	599.5	3.71	Thiel et al., 2013
27	?	U-DAG 34:2	25.4	871.7655	575.5	31.38	Thiel et al., 2013
28	?	U-DAG 36:3	25.9	897.7807	729.6, 601.5	33.13	Thiel et al., 2013
29	B?	U-DEG 34:1	26.2	826.7031	549.5	22.63	-
30	?	U-DAG 32:0	27.0	923.7942	575.5, 551.5	25.11	Thiel et al., 2013
31	?	U-DAG 36:3	28.1	899.7954	627.5, 601.5	69.59	Thiel et al., 2013
32	?	U-DAG 32:0	29.3	849.7792	603.5, 577.5, 551.5	50.13	Thiel et al., 2013
33	?	U-DAG 36:2	30.4	901.8116	603.5	134.77	Thiel et al., 2013
34	?	Unknown	31.3	1371.2613	1074.0, *694.7, *397.4	137.73	-
35	?	U-DAG 36:1	32.5	877.8117	725.6, 605.6, 577.5	11.23	Thiel et al., 2013
36	?	Unknown	33.1	1062.9641	904.8, 605.6	35.16	-

37	?	Unknown	34.3	959.8826	701.6, *397.4	4.55	-
38	?	Unknown	35.9	1282.1160	911.8, 605.6	5.41	-
39	?	Unknown	41.6	1124.0392	1107.0, 1090.0	11.21	-
40	?	Unknown	46.2	1192.1020	1175.1, 1158.1	20.94	-
41	?	Unknown	50.6	1261.1672	1243.2, 1226.1	8.25	-
42	?	Unknown	54.7	1329.2306	1295.2, 1236.1	4.71	-
43	?	Unknown	62.4	1465.3539	1448.4, 1431.3	7.19	-

*All reported mass fragment ions are of structures that contain no cyclization. Domains are reported as letters where B represents Bacteria, E represents Eukarya, and ? signifies an unknown lipid.

4.4 Discussion

4.4.1 TLE

Although it is not possible to adjust for recovery, the TLE from the carbonate sample at The Cedars was low (305 $\mu\text{g/g}$ sediment) relative to non-serpentinized sites. For example, Bentley (2021) analyzed sediment core samples from Cathedral Hill hydrothermal vent system at Guaymas Basin, Gulf of California and found that TLE extracts ranged from ~ 1700 to $11550 \mu\text{g/g}$ sediment. Although there are not many published studies that report TLE from other serpentinizing systems, Méhay et al. (2013), found that TLE concentrations in carbonate mounds from the LCHF ranged from 1 to $423 \mu\text{g/g}$. This suggests that while the TLE from The Cedars is low relative to other non-serpentinized sites, it is not uncommon for TLE from serpentinizing systems to be low and The Cedars falls within available ranges.

The TLE from filtered from at The Cedars ranged from 5.71×10^{-1} to $1.06 \times 10^1 \text{ mg/L}$ fluid. The majority of studies on TLE are from carbonates, sediment, or rocks, so it is not possible to compare these values to previously reported values. Furthermore, due to the lack of recovery standard and different units, it is not possible to make a direct comparison between the TLE from The Cedars filters and The Cedars carbonate sample. However, based solely on the number of peaks identified in each, there is a larger diversity of lipids in the carbonate sample (Tables 4.2 and 4.3). This difference in the number of peaks in the fluids and the carbonate could be due to the lack of free-floating lipids in the fluids and the presence of carbonate-hosted biofilms like those that form at LCHF (i.e., Brazelton et al., 2006) in the carbonate sample from BSC. Since the BSC carbonate is sampled from the bottom of a pool that is exposed to the atmosphere, it is likely that the sample includes surface contamination that could enter the pool and accumulate.

4.4.2 Archaeal lipids

No archaeal lipids were identified in this study in either the carbonate sample or from the fluid samples. Isoprenoidal glycerol dialkyl glycerol ether (iGDGTs) 0-4, archaeal lipids, were not detected in any samples from this study. Although the presence of iGDGTs alone is not diagnostic because they are found in most Archaea, they can be associated with anaerobic methanotrophic archaea (Koga et al., 1993; Pancost et al., 2001; Blumenburg et al., 2004). The lack of iGDGTs in the samples suggests that anaerobic methanotrophic archaea are absent in all four springs at The Cedars. Although it is possible that iGDGTs were present in the samples from The Cedars and were not detectable by the methods used in this study, other studies reporting on lipid biomarkers at sites of serpentinization have been successful in identifying iGDGTs at concentrations higher than those reported in Table 4.3. For example, studies on carbonates from the LCHF revealed the presence of iGDGTs (Méhay et al., 2013; Lincoln et al., 2013) at concentrations as high as 800,000 ng/g of carbonate. 16S rRNA gene sequences also indicated the presence of methane-oxidizing bacteria and anaerobic methane-oxidizing archaea in carbonate-hosted springs from the LCHF (Brazelton et al., 2006). 16S rRNA work published by Kraus et al. (2021) identified both aerobic methanotrophs and anaerobic methane oxidizing taxa in well water communities from the Samail Ophiolite and lipid analyses of samples from the Samail Ophiolite revealed the presence of iGDGTs. iGDGTs were largely dominated by GDGT-0 which was proposed to be indicative of anaerobic methanotrophy (Newman et al., 2020). The concentrations of iGDGTs found in the samples from the Samail Ophiolite were as high as 2 ng/g of rock. Since the lowest concentration of lipids detected in this study was 1.86 ng/g sediment, it is possible that there were iGDGTs present in the carbonate samples that could not be detected. However, experiments by Cook et al. (2021b, Chapter 3) demonstrated that while methanotrophy was

thermodynamically favourable in fluids from The Cedars, no evidence of methane oxidation could be detected in microcosm experiments created using fluid and carbonate from BSC. Additionally, genomic studies on fluids from The Cedars have demonstrated the absence of genes related to methane oxidation (Suzuki et al., 2014) further supporting the lack of lipids associated with anaerobic methanotrophic archaea.

Another noteworthy archaeal lipid that was not identified in samples from The Cedars was archaeol. Although the detection of archaeol does not necessarily indicate the presence of methanogens because this lipid is also synthesized by a variety of non-methanogenic archaea (Kates et al., 1993; Koga et al., 1998), the lack of detection of archaeol is surprising because putative microbial methanogenesis has been detected at The Cedars in previous studies. Isotopic geochemical evidence (Morrill et al., 2013; Wang et al., 2015) has suggested that the methane from BSC was, at least in part, microbial in source. This was confirmed through microcosm experiments constructed by Kohl et al. (2014) and Cook et al. (2021b, Chapter 3) using fluid and carbonate from BSC. Both studies compared live microcosm experiments with killed microcosm experiments that received mercuric chloride to eliminate any biotic changes in headspace concentrations. It is worth noting that both studies observed microbial methanogenesis even in the initial presence of oxygen (Kohl et al., 2014; Cook et al., 2021b (Chapter 3)). Interestingly, genomic studies by Suzuki et al. (2013) on microbial communities from springs at The Cedars were only able to detect the presence of a single archaeal phylotype in BSC and although the phylotype placed closely to *Methanosarcinales* in the phylogenetic tree, its sequence does not fit with any known methanogen or anaerobic methanotroph clades (Suzuki et al., 2013). Since archaeol and hydroxyarchaeol are commonly associated with *Methanosarcinales* (Koga et al.,

1998), their absence in samples from BSC, NS1, and GPS may suggest that either *Methanosarcinales* were not present in the springs or that they were below our limits of detection.

The inability to detect archaeol in samples from The Cedars is important because it has been detected at other sites of serpentinization in higher concentrations than those reported for other lipids in this study. For example, Zwicker et al. (2018) detected archaeol, *sn*2-hydroxyarchaeol, and *sn*3-hydroxyarchaeol in carbonates from the Chimaera Ophiolite (at concentrations as high as 1582, 3208, and 404 ng/g of rock, respectively) suggesting archaeal methanogenesis (Zwicker et al., 2018). 16S rRNA analyses on fluids samples from the Chimaera Ophiolite also revealed the presence of *Methanobacterium* (Neubeck et al., 2017). Archaeol was also detected in carbonate samples from the Oman Ophiolite at concentrations up to ~40 ng/g of rock (Newman et al., 2020). Furthermore, the presence of *Methanobacterium* has also been reported in subsurface fluids from this ophiolite (Howells et al., 2022; Miller et al., 2016; Rempfert et al., 2017). Lipidomic studies on carbonate mounds from the LCHF also identified *sn*2-hydroxyarchaeol (up to 6660 ng/g of rock) as the dominant lipid accompanied by the presence of archaeol, and dihydroxyarchaeol (up to 610 and 3470 ng/g of rock, respectively) (Bradley et al., 2009). Genomic studies have suggested that, like The Cedars, archaeal abundance and diversity is low at LCHF and is dominated by a single phylotype related to *Methanosarcinales* (Schrenk et al., 2004). The lack of detection of archaeol in this study suggests the archaeal community in the ultra-basic fluids and carbonates at The Cedars is small relative to other sites of serpentinization.

4.4.3 Bacterial lipids

The lipid biomarker results from this study suggest that the microbial community at The Cedars is primarily bacterial or eukaryotic in composition. While it is possible that archaeal lipids were present in springs at The Cedars in small quantities and they were therefore not detected by

our methods, this lack of Archaea is supported by genomic evidence from Suzuki et al. (2013). Suzuki et al. (2013) found that the ultra-basic springs at The Cedars were dominated by Bacteria. Although both Bacteria and Archaea were detected, only one archaeal phylotype was found (*Euryarchaeota*) and it was present in all springs analyzed (Suzuki et al., 2013). This is not the first site of serpentinization to report a predominantly bacterial microbial population. For example, while studies on the microbial communities at the Chimaera Ophiolite have detected both bacterial and archaeal lipids in rock and carbonate samples (Zwicker et al., 2018), microbial populations at the Chimaera Ophiolite appeared to be largely dominated by Bacteria (Neubeck et al., 2017). Lipid biomarkers from LCHF, have also revealed the presence of both bacterial and archaeal lipids in carbonate samples (Méhay et al., 2013). Approximately half of the samples analyzed by Méhay et al. (2013) were dominated by Bacteria while the other half were dominated by Archaea.

Although not all the individual lipids present on the filters could be identified (Table 4.1), those that could be identified were determined to be bacterial/eukaryotic in origin. Most of the lipids that were tentatively identified on the filters were diacylglycerols (DAGs). DAGs are ubiquitous, and they are involved in many eukaryotic and bacterial metabolic pathways. Therefore, they are not particularly diagnostic and do not provide a lot of information on metabolisms occurring in the subsurface.

While there were many lipids on the filters that were common among all three springs, there were also some lipids that were unique to BSC and some that were unique to NS1 and GPS. It is interesting that NS1 and GPS shared common lipids that were not identified in samples from BSC because studies have suggested that NS1 and BSC are more similar geochemically since they are both composed of a combination of surface water and subsurface ultra-basic water (Morrill et al., 2013; Cook et al., 2021 (Chapter 2)). It is possible that these lipids were found in GPS and

NS1 because, unlike BSC, the samples are taken directly from the discharge point. Carbonate and fluid from BSC are instead sampled from a large pool that is exposed to the atmosphere as well as sunlight and surface contributions (Suzuki et al., 2013) which likely influences the lipid composition at this spring.

In the carbonate sample from BSC chlorophyll *a* and pheophytin *a* were tentatively identified. Chlorophyll *a* is a pigment associated with photosynthetic organisms (i.e., plants and algae) and pheophytin *a* is a breakdown product of chlorophyll *a*. Chlorophyll *a* and pheophytin *a* could indicate the presence of cyanobacteria in BSC pool associated with the carbonate. This is supported by 16S rRNA analyses published by Suzuki et al. (2013) who detected cyanobacteria in fluid samples taken from the top portion of BS5 that is exposed to sunlight. It is not surprising that cyanobacteria are able to survive in the ultra-basic fluids at The Cedars because cyanobacteria tend to be the best adapted to extreme conditions and have been known to tolerate low availabilities of water and to develop in alkaline lakes (Rampelotto, 2016).

It is interesting that there were lipids indicative of cyanobacteria detected in carbonate samples from The Cedars but not in fluids from the sunlight portion of the spring. It is possible that this is because cyanobacteria are not present in significant enough quantities in the fluids to be detected on the filters. Recently, evidence has been published that suggests unicellular and filamentous, freshwater, marine, and terrestrial members of the phylum Cyanobacteria are capable of producing methane (Bizic et al., 2020). Specifically, the study found that although biogenic methanogenesis was once considered a strictly anaerobic process that was exclusive to Archaea, cyanobacteria appear to be capable of methane production under light, dark, oxic, and anoxic conditions (Bizic et al., 2020). It is possible that the cyanobacteria present in BSC could be contributing to the overall methane budget from The Cedars. This hypothesis is supported by data

from Cook et al. (2021b, Chapter 3) and Kohl et al. (2016) who observed spontaneous methane production in microcosms despite an oxic and light environment which methanogens are not known to thrive in (Jarrell, 1985). Further study into the possibility of cyanobacteria and their contribution to the methane budget at The Cedars is required.

4.6 Acknowledgments

The authors would like to thank David McCrory and Roger Raiche for allowing access to The Cedars. The authors would also like to thank Emily Cumming for her help in the field. This research was funded by Natural Science and Engineering Research Council (NSERC) Discovery Grant and Canada Space Agency's Flights and Fieldwork for the Advancement of Science and Technology (FAST) grant awarded to Dr. Penny Morrill and NSERC's Alexander Graham Bell Canada Graduate Scholarship-Doctoral (CGS D) awarded to Melissa Cook.

4.7 References

- Abrajano, T. A., Sturchio, N. C., Bohlke, J. K., Lyon, G. L., Poreda, R. J., & Stevens, C. M. (1988). Methane-hydrogen gas seeps, Zambales Ophiolite, Philippines: Deep or shallow origin? *Chemical geology*, *71*(1), 211-222. [https://doi.org/10.1016/0009-2541\(88\)90116-7](https://doi.org/10.1016/0009-2541(88)90116-7)
- Barnes, I., LaMarche, V. C., & Himmelberg, G. (1967). Geochemical Evidence of Present-Day Serpentinization. *Science (American Association for the Advancement of Science)*, *156*(3776), 830-832. <https://doi.org/10.1126/science.156.3776.830>
- Baumann, L. M. F., Taubner, R.-S., Bauersachs, T., Steiner, M., Schleper, C., Peckmann, J., Rittmann, S. K. M. R., & Birgel, D. (2018). Intact polar lipid and core lipid inventory of the hydrothermal vent methanogens *Methanocaldococcus villosus* and *Methanothermococcus okinawensis*. *Organic geochemistry*, *126*, 33-42. <https://doi.org/10.1016/j.orggeochem.2018.10.006>
- Bentley, J. N. (2019). *The Origins and Fate of Archaeal Intact Polar Lipids in Hydrothermally Altered Sediments of Cathedral Hill, Guaymas Basin, Gulf of California* [Saint Mary's University].
- Bizic, M., Klintzsch, T., Ionescu, D., Hindiyeh, M. Y., Gunthel, M., Muro-Pastor, A. M., Eckert, W., Urich, T., Keppler, F., & Grossart, H. P. (2020). Aquatic and terrestrial cyanobacteria produce methane. *Science advances*, *6*(3), eaax5343-eaax5343. <https://doi.org/10.1126/sciadv.aax5343>
- Blumenberg, M., Seifert, R., Reitner, J., Pape, T., & Michaelis, W. (2004). Membrane Lipid Patterns Typify Distinct Anaerobic Methanotrophic Consortia. *Proceedings of the National Academy of Sciences - PNAS*, *101*(30), 11111-11116. <https://doi.org/10.1073/pnas.0401188101>

- Bradley, A. S., Fredricks, H., Hinrichs, K.-U., & Summons, R. E. (2009). Structural diversity of diether lipids in carbonate chimneys at the Lost City Hydrothermal Field. *Organic geochemistry*, 40(12), 1169-1178. <https://doi.org/10.1016/j.orggeochem.2009.09.004>
- Bradley, A. S., & Summons, R. E. (2010). Multiple origins of methane at the Lost City Hydrothermal Field. *Earth and planetary science letters*, 297(1), 34-41. <https://doi.org/10.1016/j.epsl.2010.05.034>
- Brazelton, W. J., Nelson, B., & Schrenk, M. O. (2012). Metagenomic Evidence for H₂ Oxidation and H₂ Production by Serpentinite-Hosted Subsurface Microbial Communities. *Frontiers in Microbiology*, 2. <https://doi.org/10.3389/fmicb.2011.00268>
- Brazelton, W. J., Schrenk, M. O., Kelley, D. S., & Baross, J. A. (2006). Methane- and Sulfur-Metabolizing Microbial Communities Dominate the Lost City Hydrothermal Field Ecosystem. *Applied and Environmental Microbiology*, 72(9), 6257-6270. <https://doi.org/10.1128/AEM.00574-06>
- Chen, K., Ríos, J. J., Pérez-Gálvez, A., & Roca, M. (2015). Development of an accurate and high-throughput methodology for structural comprehension of chlorophylls derivatives. (I) Phytylated derivatives. *Journal of Chromatography A*, 1406, 99-108. <https://doi.org/10.1016/j.chroma.2015.05.072>
- Coleman, R., G. (2000). Prospecting for ophiolites along the California continental margin. *Special papers (Geological Society of America)*, 349, 351. <https://doi.org/10.1130/0-8137-2349-3.351>
- Cook, M. C., Blank, J. G., Rietze, A., Suzuki, S., Nealson, K. H., & Morrill, P. L. (2021). A Geochemical Comparison of Three Terrestrial Sites of Serpentinization: The Tablelands,

The Cedars, and Aqua de Ney. *Journal of geophysical research. Biogeosciences*.

<https://doi.org/10.1029/2021JG006316>

Cook, M. C., Blank, J. G., Suzuki, S., Neelson, K. H., & Morrill, P. L. (2021b). Assessing Geochemical Bioenergetics and Microbial Metabolisms at Three Terrestrial Sites of Serpentinization: The Tablelands (NL, CAN), The Cedars (CA, USA), and Aqua de Ney (CA, USA). *Journal of geophysical research. Biogeosciences*, 126(6), n/a.

<https://doi.org/10.1029/2019JG005542>

Ehlmann, B. L., Mustard, J. F., & Murchie, S. L. (2010). Geologic setting of serpentine deposits on Mars. *Geophysical research letters*, 37(6), n/a. <https://doi.org/10.1029/2010GL042596>

Etioppe, G., Schoell, M., & Hosgörmez, H. (2011). Abiotic methane flux from the Chimaera seep and Tekirova ophiolites (Turkey): Understanding gas exhalation from low temperature serpentinization and implications for Mars. *Earth and planetary science letters*, 310(1), 96-104. <https://doi.org/10.1016/j.epsl.2011.08.001>

Etioppe, G., & Whiticar, M. J. (2019). Abiotic methane in continental ultramafic rock systems: Towards a genetic model. *Applied geochemistry*, 102, 139-152.

<https://doi.org/10.1016/j.apgeochem.2019.01.012>

Howells, A. E. G., Leong, J. A. M., Ely, T., Santana, M., Robinson, K., Esquivel-Elizondo, S., Cox, A., Poret-Peterson, A., Krajmalnik-Brown, R., & Shock, E. L. (2022). Energetically Informed Niche Models of Hydrogenotrophs Detected in Sediments of Serpentinized Fluids of the Samail Ophiolite of Oman. *Journal of geophysical research. Biogeosciences*, 127(3), n/a. <https://doi.org/10.1029/2021JG006317>

<https://doi.org/10.1029/2021JG006317>

Koga, Y., Morii, H., Akagawa Matsushita, M., & Ohga, M. (1998). Correlation of polar lipid composition with 16S rRNA phylogeny in methanogens: Further analysis of lipid

component parts. *Bioscience, biotechnology, and biochemistry*, 62(2), 230-236.

<https://doi.org/10.1271/bbb.62.230>

Koga, Y., Nishihara, M., Morii, H., & Akagawa-Matsushita, M. (1993). Ether polar lipids of methanogenic bacteria: structures, comparative aspects, and biosyntheses.

Microbiological reviews, 57(1), 164-182. <https://doi.org/10.1128/mr.57.1.164-182.1993>

Kohl, L., Cumming, E., Cox, A., Rietze, A., Morrissey, L., Lang, S. Q., Richter, A., Suzuki, S., Nealson, K. H., & Morrill, P. L. (2016). Exploring the metabolic potential of microbial communities in ultra-basic, reducing springs at The Cedars, CA, USA: Experimental evidence of microbial methanogenesis and heterotrophic acetogenesis. *Journal of Geophysical Research: Biogeosciences*, 121(4), 1203-1220.

<https://doi.org/10.1002/2015jg003233>

Kraus, E. A., Nothaft, D., Stamps, B. W., Rempfert, K. R., Ellison, E. T., Matter, J. M., Templeton, A. S., Boyd, E. S., & Spear, J. R. (2021). Molecular Evidence for an Active Microbial Methane Cycle in Subsurface Serpentinite-Hosted Groundwaters in the Samail Ophiolite, Oman. *Applied and Environmental Microbiology*, 87(2).

<https://doi.org/10.1128/AEM.02068-20>

Méhay, S., Früh-Green, G. L., Lang, S. Q., Bernasconi, S. M., Brazelton, W. J., Schrenk, M. O., Schaeffer, P., & Adam, P. (2013). Record of archaeal activity at the serpentinite-hosted Lost City Hydrothermal Field. *Geobiology*, 11(6), 570-592.

<https://doi.org/10.1111/gbi.12062>

Miller, H. M., Matter, J. M., Kelemen, P., Ellison, E. T., Conrad, M. E., Fierer, N., Ruchala, T., Tominaga, M., & Templeton, A. S. (2016). Modern water/rock reactions in Oman

- hyperalkaline peridotite aquifers and implications for microbial habitability. *Geochimica et cosmochimica acta*, 179(C), 217-241. <https://doi.org/10.1016/j.gca.2016.01.033>
- Morrill, P. L., Kuenen, J. G., Johnson, O. J., Suzuki, S., Rietze, A., Sessions, A. L., Fogel, M. L., & Nealson, K. H. (2013). Geochemistry and geobiology of a present-day serpentinization site in California: The Cedars. *Geochimica et cosmochimica acta*, 109, 222-240. <https://doi.org/10.1016/j.gca.2013.01.043>
- Moser, D. P., Gihring, T. M., Wanger, G., Baker, B. J., Pfiffner, S. M., Lin, L.-H., Onstott, T. C., Brockman, F. J., Fredrickson, J. K., Balkwill, D. L., Dollhopf, M. E., Lollar, B. S., Pratt, L. M., Boice, E., & Southam, G. (2005). Desulfotomaculum and Methanobacterium spp. Dominate a 4- to 5-Kilometer-Deep Fault. *Applied and Environmental Microbiology*, 71(12), 8773-8783. <https://doi.org/10.1128/AEM.71.12.8773-8783.2005>
- Neubeck, A., Sun, L., Müller, B., Ivarsson, M., Hosgörmez, H., Özcan, D., Broman, C., & Schnürer, A. (2017). Microbial Community Structure in a Serpentine-Hosted Abiotic Gas Seepage at the Chimaera Ophiolite, Turkey. *Applied and Environmental Microbiology*, 83(12). <https://doi.org/10.1128/AEM.03430-16>
- Newman, S. A., Lincoln, S. A., O'Reilly, S., Liu, X., Shock, E. L., Kelemen, P. B., & Summons, R. E. (2020). Lipid Biomarker Record of the Serpentinite-Hosted Ecosystem of the Samail Ophiolite, Oman and Implications for the Search for Biosignatures on Mars. *Astrobiology*, 20(7), 830-845. <https://doi.org/10.1089/ast.2019.2066>
- Pancost, R. D., Hopmans, E. C., & Sinninghe Damsté, J. S. (2001). Archaeal lipids in Mediterranean cold seeps: molecular proxies for anaerobic methane oxidation. *Geochimica et cosmochimica acta*, 65(10), 1611-1627. [https://doi.org/10.1016/S0016-7037\(00\)00562-7](https://doi.org/10.1016/S0016-7037(00)00562-7)

- Rampelotto, P. H. (2016). *Extremophiles and extreme environments*. MDPI - Multidisciplinary Digital Publishing Institute.
- Rempfert, K. R., Miller, H. M., Bompard, N., Nothaft, D., Matter, J. M., Kelemen, P., Fierer, N., & Templeton, A. S. (2017). Geological and Geochemical Controls on Subsurface Microbial Life in the Samail Ophiolite, Oman. *Frontiers in Microbiology*, 8, 56-56. <https://doi.org/10.3389/fmicb.2017.00056>
- Schrenk, M. O., Kelley, D. S., Bolton, S. A., & Baross, J. A. (2004). Low archaeal diversity linked to seafloor geochemical processes at the Lost City Hydrothermal Field, Mid-Atlantic Ridge. *Environmental microbiology*, 6(10), 1086-1095. <https://doi.org/10.1111/j.1462-2920.2004.00650.x>
- Schulte, M., Blake, D., Hoehler, T., & McCollom, T. (2006). Serpentinization and its implications for life on the early Earth and Mars. *Astrobiology*, 6(2), 364-376. <https://doi.org/10.1089/ast.2006.6.364>
- Shervais, J. W., Kimbrough, D. L., Renne, P., Hanan, B. B., Murchey, B., Snow, C. A., Zoglman Schuman, M. M., & Beaman, J. (2004). Multi-Stage Origin of the Coast Range Ophiolite, California: Implications for the Life Cycle of Supra-Subduction Zone Ophiolites. *International Geology Review*, 46(4), 289-315. <https://doi.org/10.2747/0020-6814.46.4.289>
- Simoneit, B. R. T., Lein, A. Y., Peresykin, V. I., & Osipov, G. A. (2004). Composition and origin of hydrothermal petroleum and associated lipids in the sulfide deposits of the Rainbow field (Mid-Atlantic Ridge at 36°N). *Geochimica et cosmochimica acta*, 68(10), 2275-2294. <https://doi.org/10.1016/j.gca.2003.11.025>

- Simoneit, B. R. T., Summons, R. E., & Jahnke, L. L. (1998). Biomarkers as Tracers for Life on Early Earth and Mars. *Origins of life and evolution of biospheres*, 28(4), 475-483.
<https://doi.org/10.1023/A:1006508012904>
- Sleep, N. H., Bird, D. K., & Pope, E. C. (2011). Serpentinite and the dawn of life. *Philosophical transactions. Biological sciences*, 366(1580), 2857-2869.
<https://doi.org/10.1098/rstb.2011.0129>
- Sleep, N. H., Meibom, A., Th, F., Coleman, R. G., & Bird, D. K. (2004). H₂-Rich Fluids from Serpentinization: Geochemical and Biotic Implications. *Proceedings of the National Academy of Sciences - PNAS*, 101(35), 12818-12823.
<https://doi.org/10.1073/pnas.0405289101>
- Sorokin, D. Y., & Kuenen, J. G. (2005). Haloalkaliphilic sulfur-oxidizing bacteria in soda lakes. *FEMS Microbiology Reviews*, 29(4), 685-702.
<https://doi.org/10.1016/j.femsre.2004.10.005>
- Sturt, H. F., Summons, R. E., Smith, K., Elvert, M., & Hinrichs, K. U. (2004). Intact polar membrane lipids in prokaryotes and sediments deciphered by high-performance liquid chromatography/electrospray ionization multistage mass spectrometry--new biomarkers for biogeochemistry and microbial ecology. *Rapid Commun Mass Spectrom*, 18(6), 617-628. <https://doi.org/10.1002/rcm.1378>
- Suzuki, S., Ishii, S. i., Wu, A., Cheung, A., Tenney, A., Wanger, G., Kuenen, J. G., & Nealson, K. H. (2013). Microbial diversity in The Cedars, an ultrabasic, ultrareducing, and low salinity serpentinizing ecosystem. *Proceedings of the National Academy of Sciences - PNAS*, 110(38), 15336-15341. <https://doi.org/10.1073/pnas.1302426110>

- Suzuki, S., Kuenen, J. G., Schipper, K., Van der Velde, S., Ishii, S., Wu, A., Sorokin, D. Y., Tenney, A., Meng, X. Y., Morrill, P. L., Kamagata, Y., Muyzer, G., & Nealson, K. H. (2014). Physiological and genomic features of highly alkaliphilic hydrogen-utilizing Betaproteobacteria from a continental serpentinizing site. *Nature communications*, 5(1), 3900-3900. <https://doi.org/10.1038/ncomms4900>
- Szponar, N., Brazelton, W. J., Schrenk, M. O., Bower, D. M., Steele, A., & Morrill, P. L. (2013). Geochemistry of a continental site of serpentinization, the Tablelands Ophiolite, Gros Morne National Park: A Mars analogue. *Icarus (New York, N.Y. 1962)*, 224(2), 286-296. <https://doi.org/10.1016/j.icarus.2012.07.004>
- Vance, S., Harnmeijer, J., Kimura, J., Hussmann, H., Demartin, B., & Brown, J. M. (2007). Hydrothermal systems in small ocean planets. *Astrobiology*, 7(6), 987-1005. <https://doi.org/10.1089/ast.2007.0075>
- Wang, D., T. , Gruen, D. S., Sherwood Lollar, B., Kai-Uwe, H., Lucy, C. S., James, F. H., Alexander, N. H., John, W. P., Penny, L. M., Martin, K., Kyle, B. D., Eoghan, P. R., Chelsea, N. S., Daniel, J. R., Jeffrey, S. S., Jennifer, C. M., Harold, F. H., Michael, D. K., Dawn, C., Tori, M. H., & Shuhei, O. (2015). Nonequilibrium clumped isotope signals in microbial methane. *Science (American Association for the Advancement of Science)*, 348(6233), 428-431. <https://doi.org/10.1126/science.aaa4326>
- Willerslev, E., Hansen, A. J., Rønn, R., Brand, T. B., Barnes, I., Wiuf, C., Gilichinsky, D., Mitchell, D., & Cooper, A. (2004). Long-term persistence of bacterial DNA. *Current biology*, 14(1), R9-R10. <https://doi.org/10.1016/j.cub.2003.12.012>
- Zhu, C., Lipp, J. S., Wörmer, L., Becker, K. W., Schröder, J., & Hinrichs, K.-U. (2013). Comprehensive glycerol ether lipid fingerprints through a novel reversed phase liquid

chromatography–mass spectrometry protocol. *Organic geochemistry*, 65, 53-62.

<https://doi.org/10.1016/j.orggeochem.2013.09.012>

Zwicker, J., Birgel, D., Bach, W., Richoz, S., Smrzka, D., Grasmann, B., Gier, S., Schleper, C.,

Rittmann, S. K. M. R., Koşun, E., & Peckmann, J. (2018). Evidence for archaeal

methanogenesis within veins at the onshore serpentinite-hosted Chimaera seeps, Turkey.

Chemical geology, 483, 567-580. <https://doi.org/10.1016/j.chemgeo.2018.03.027>

4.8 Supplemental Information

Table 4.S1. Spring where samples were taken from and volume of fluid filtered (L) through Sterivex for lipid extracts.

Sample ID	Spring	Volume of Fluid Filtered (L)
4-BS5	BSC	0.90
4-BS7	BSC	0.22
2-BS7	BSC	0.06
1-BS7	BSC	0.1
NS1-CEDARS-OCT2011	NS1	1.19
GPS1-CEDARS-OCT2011	GPS1	1.19
BS5-CEDARS-OCT2011	BSC	0.81

Table 4.S2. Recoveries (%) of filters and spring where the samples were taken from.

Sample ID	Spring	% Recovery
4-BS5	BSC	66%
4-BS7	BSC	115%
2-BS7	BSC	49%
1-BS7	BSC	
NS1-CEDARS-OCT2011	NS1	143%
GPS1-CEDARS-OCT2011	GPS1	191%
BS5-CEDARS-OCT2011	BSC	175%

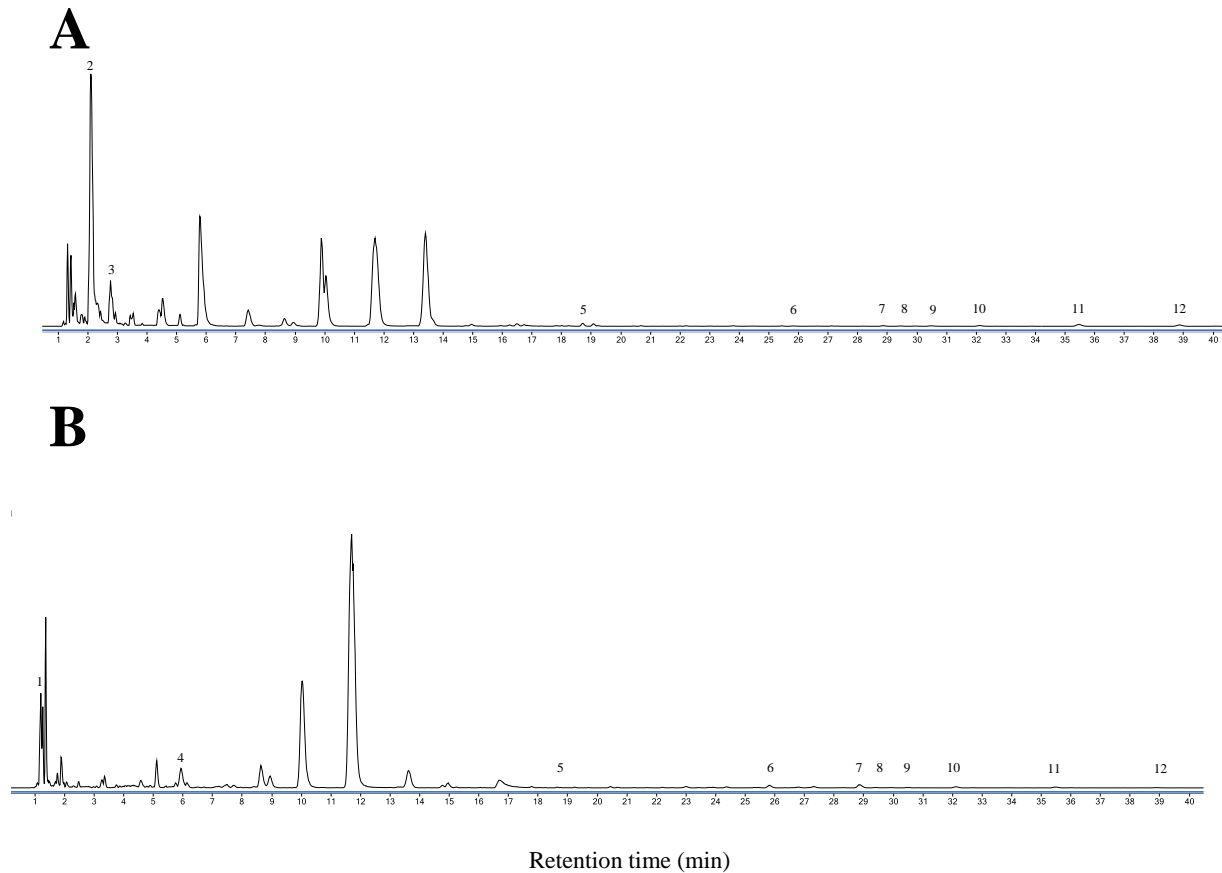


Figure 4.S1. Base peak chromatogram (BPC) showing detectable lipids extracted from (A) the filters from GPS1 and NS1 and (B) the filter from BSC. The numbers correspond to the numbered lipids in Table 4.2.

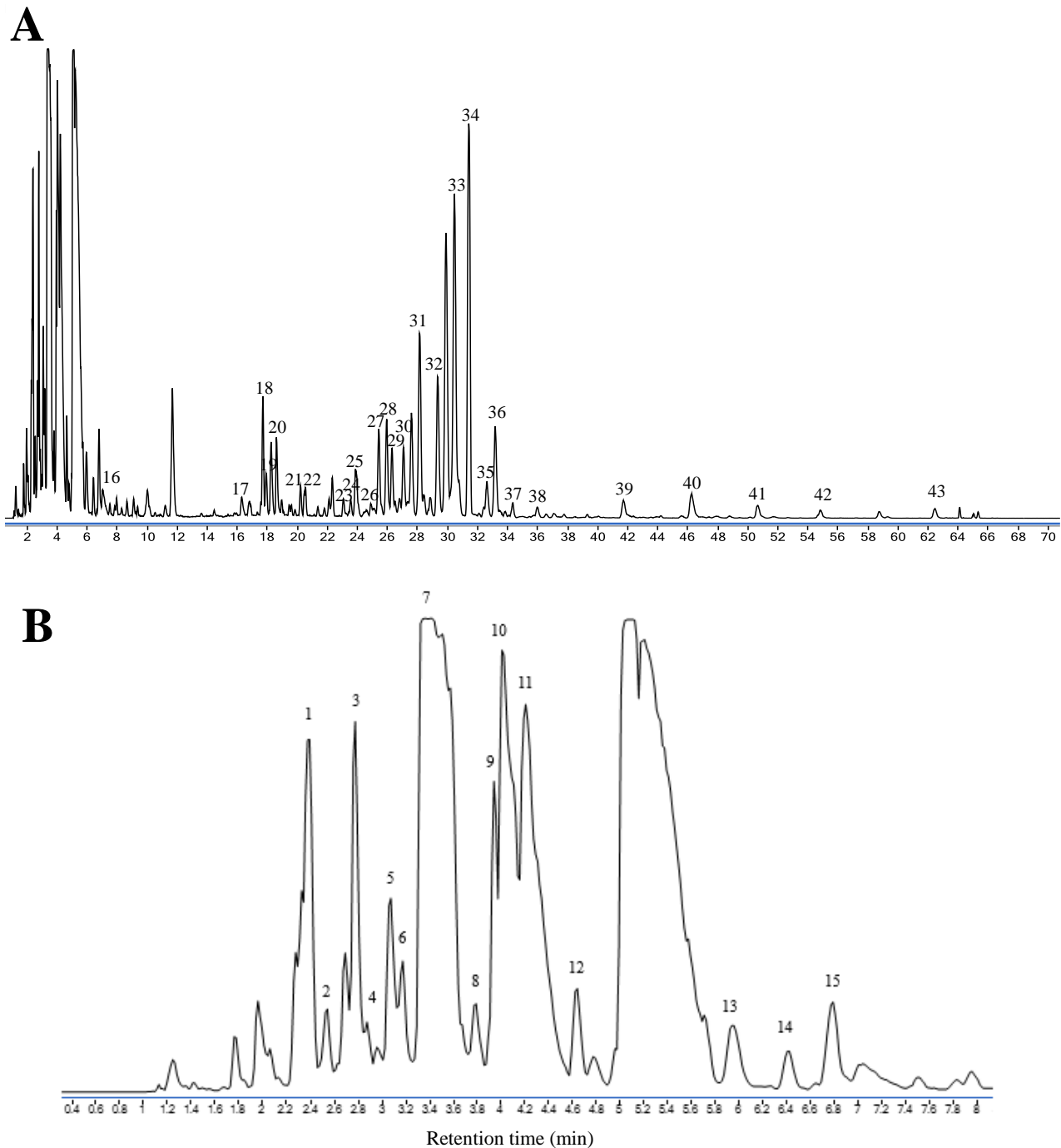


Figure 4.S2. (A) Base peak chromatogram (BPC) showing detectable lipids extracted from the carbonates from BSC and Camp1 and (B) enlarged BPC from 0 to 8 min. The numbers correspond to the numbered lipids in Table 4.3.

Chapter 5. The Microbial Community Composition Within Ultra-basic Springs at an Active Site of Serpentinization: the Tablelands, NL, CAN

Abstract

In this ultramafic Mars analogue study, two serpentinite-hosted ultra-basic springs at the Tablelands (Newfoundland, Canada) were analyzed for geochemical and phospholipid fatty acid (PLFA) biomarkers. The first site, WHC2, was a pool filled with ultra-basic water with two distinct discharge points (WHC2a and WHC2b) at the bottom of the pool and a third sampling point (WHC2c) closer to the top of the pool where it is exposed to the atmosphere. The second site, WHCMO, was created by drilling three boreholes (WHCMO1, WHCMO2, and WHCMO3) in an actively discharging spring. WHCMO housed flow-through incubators containing crushed ultramafic rock and was intended to be representative of subsurface ultra-basic fluids with little surface contributions.

Total biomass extract from PLFA analyses on WHC2 and WHCMO suggested that more reducing fluids had higher biomass than sites with larger surface contributions. Furthermore, sites with more reducing fluids showed more bacterial-dominated microbial communities while those with less reducing fluids contained more diverse microbial communities. The results from this study suggest that ultra-basic fluids support unique microbial communities adapted to survive in extreme conditions created by serpentinization reactions and serve as good candidates when searching for life on other planetary bodies.

5.1 Introduction

Serpentinization reactions are a series of exothermic reactions through which ultramafic or mafic rocks are hydrated. These reactions produce serpentine group minerals (e.g., chrysotile, antigorite, and lizardite) as well as a suite of secondary minerals including brucite, talc, and magnetite. Serpentinization is common on Earth in settings such as mid-ocean ridges, forearc systems, and in ophiolites (sections of obducted oceanic crust and upper mantle) (Schrenk et al., 2013). Extraterrestrially, there is evidence to suggest that serpentinization is also occurring or has occurred on many planetary bodies including on Jupiter's moon Europa, on Saturn's moons Enceladus and Titan, and on Mars (Ehlmann et al., 2010; Vance et al., 2007). On Mars, serpentine-bearing rocks have been identified in several locations (Ehlmann et al., 2010). For example, serpentine is found in outcrops associated with olivine and carbonate in the Nili Fossae region of Mars (the Mars 2020 landing site) and in the tectonically deformed Thaumasia Highlands (Viviano-Beck et al., 2017). There is also strong evidence for past serpentinization on Mars in the nakhlite group of meteorites (Vance & Daswani, 2020).

Serpentinization reactions produce fluids that are ultra-basic and depleted in electron acceptors (e.g., O_2 , SO_4^{2-} , NO_3^-) (Morrill et al., 2013). Furthermore, due to the high pH of the fluids, any inorganic carbon present in the system is predominately in the form of the carbonate ion which, unlike the bicarbonate ion, is not known to be biologically available (Sorokin & Kuenen, 2005). Although these fluids are considered extreme for life, serpentinization and associated reactions also result in the production of H_2 gas, CH_4 , hydrocarbons, and organic acids which provide electron donors and carbon sources to the system that could be exploited by potential microbial communities (Lang et al., 2012; Schulte et al., 2006). Furthermore, when these ultra-basic, reducing fluids rich in electron donors mix with oxic water rich in electron acceptors, a disequilibrium is created. This disequilibrium can supply potential energy to the

system that could help support microbial metabolisms. The potential energy has been quantified for many sites of serpentinization (e.g., Canovas et al. (2017); Cook, et al. (2021b; Chapter 3)) and results suggest that many metabolisms including carbon monoxide utilization, hydrogen utilization, methanotrophy, and methanogenesis could be supported at terrestrial sites of serpentinization (Cook et al., 2021; Chapter 2).

Microbiological studies on sediments and fluids from serpentinized fluids at ophiolites have confirmed that life does exist at many sites of serpentinization. 16S rRNA sequence data from different sites within the Chimaera ophiolite, Turkey, revealed the presence of a bacterial-dominated microbial community including bacteria capable of oxidizing hydrogen, methane, nitrogen, and iron (Neubeck et al., 2017). *Methanobacterium*, a methanogen capable of generating CH₄ using H₂ with formate, CO, or CO₂, was also detected in fluids from the Samail ophiolite, Oman (Rempfert et al., 2017). Similarly, 16S rRNA analyses on the microbial communities at The Cedars, USA revealed the presence of an archaeal sequence that placed closely to the order *Methanosarcinales* in the phylogenetic tree (Suzuki et al., 2013). Later isotopic and geochemical analyses further confirmed that the methane from The Cedars was, at least in part, microbially produced (Cook, et al., 2021 (Chapter 2); Cook, et al., 2021b (Chapter 3); Kohl et al., 2016; Morrill et al., 2013; Wang et al., 2015). *Serpentinomonas*, a *Betaproteobacteria* that is closely related to the genus *Hydrogenophaga*, has also been identified in ultra-basic serpentinized springs at almost every terrestrial site of serpentinization (e.g., Brazelton et al. (2013); Brazelton et al. (2012); Quéméneur et al. (2015); Suzuki et al. (2014); Twing et al. (2017)). *Serpentinomonas* are autotrophic bacteria that are well adapted to the extreme conditions created by serpentinization reactions through using the abundant hydrogen in the system as an electron donor and calcium carbonate as a carbon source (Suzuki et al., 2014).

The identification of *Serpentimonas*, and their unique adaptations to survive in the extreme environments (e.g., bicarbonate-limited, ultra-basic, reducing fluids) created by serpentinization reactions, highlights the importance of understanding microbial communities at sites of serpentinization when considering life on other planets. Although it is not necessarily anticipated that the same microbial communities that exist on Earth would be found on extraterrestrial bodies, the presence of abiotic carbon sources and life at sites of serpentinization suggests that serpentinite-hosted spring water is habitable and that microbial life with similar adaptations could be present in analogous environments on other planetary bodies. Although the surface of Mars is inhabitable due to the harmful solar wind particles that result from the lack of a significant intrinsic magnetic field, there is evidence to suggest the presence of subsurface groundwaters (Ehlmann et al., 2011) that could provide habitable environments for chemolithoautotrophs (Boston et al., 1992; Michalski et al., 2013; Nealson et al., 2005). The challenge in search for this life lies in biomarker detection.

One example of a potential biomarker that has been previously used is methane. Methane has been detected in the Martian atmosphere by some instruments (e.g., the Planetary Fourier Spectrometer onboard the Mars Express spacecraft (Formisano et al., 2004) and high-dispersion infrared spectrometers at ground-based telescopes (Mumma et al., 2009)). While this methane could be indicative of microbial methanogenesis in the subsurface, it is also possible that it could be abiotically produced by geologic process such as serpentinization.

Because methane can be produced both biotically and non-biotically, the detection of methane alone is not necessarily indicative of life. This further complicates the search for life in the subsurface of Mars. Therefore, the detection of extraterrestrial life often requires a combination of multiple lines of evidence, which could include isotopic (e.g., $\delta^{13}\text{C}_{\text{CH}_4}$ and

$\delta^2\text{H}_{\text{CH}_4}$) and molecular biomarkers. Potential molecular biomarkers that could be used for life detection are lipids, and their derivatives, due to their odd/even biogenic patterns and their preservation potential (Georgiou & Deamer, 2014). Phospholipid fatty acids (PLFAs) self-assemble to form double layered membranes of Bacteria and Eukarya on Earth. Different groups of bacteria and eukaryotes synthesize different PLFA compounds within their cell membranes so PLFAs can be used to gain insight into the microbial communities present in an environment. For example, the presence of PLFAs 16:1 ω 7t and 16:1 ω 7c are typically associated with gram negative bacteria (e.g., *Hydrogenophaga*) (O'Leary & Wilkinson, 1988). PLFAs tend to degrade rapidly after the cell dies which means they can be used to provide an overall understanding of the viable (extant) microbial community at the time of sampling (White et al., 1979). Therefore, when combined with other techniques (e.g., geochemical analyses), the combined results produce a more comprehensive understanding of the extant microbial community within in environment.

This biomarker study was part of a larger overall project known as SERP (Study of Electrical Potential, Remote sensing, and Preservation of biosignatures). The goals of the SERP project were to develop methods to detect serpentinized springs and identify biosignatures of current life at a Mars analogue site of serpentinization - Bay of Island Ophiolite Complex (BIOC), NL, Canada. The main objectives of SERP were to discover and organic indicators of microbial life to develop, deploy, and validate spectral and remote sensing (RS) methods to detect surface expressions of serpentinization; and to simulate an end-to-end mission to Mars to look for serpentinized springs, map subsurface serpentinized groundwater flow through electrical potential and magnetic measurements, and search for signs of microbial life in serpentinite-hosted springs. Within this context the first goal of this particular study was to characterize the

microbial community composition associated with active serpentinite-hosted springs at a site of known serpentinization, the Tablelands, NL, CAN. To achieve this goal, lipid biomarkers were used to create a profile of the microbial community composition and total biomass within serpentinite-hosted ultra-basic springs at the Tablelands. The second goal of this study was to understand how the microbial community structure and total biomass were influenced by the spring geochemistry. To achieve this goal, the geochemistry of the springs was determined and used to create thermodynamic predictions of potential available energy. These thermodynamic predictions were then compared to determine the impact of spring geochemistry on the microbial community composition and total biomass.

5.2 Methods

5.2.1 Site Description

The Tablelands is located on the west coast of Newfoundland, Canada and is one of four peridotite-dominated massifs that makes up the BOIC (Williams, 1979). The Tablelands ophiolite was emplaced during the Middle Ordovician between 500-485 Ma (Dunning & Krogh, 1985). Ultra-basic pools have been identified within the Tablelands including one that is approximately 40 cm deep and 126 cm wide, referred to as Winterhouse Canyon 2 (WHC2). WHC2 was fed by at least 2 groundwater water springs discharging at its base (WHC2a and b). However, this pool also receives surface contributions through overland flow, predominantly at a location labelled WHC2c. The WHC2 pool is also exposed to the atmosphere and is surrounded by calcium carbonates. This WHC2 pool has been geochemically characterized by previous studies (e.g., Cook et al., 2021 (Chapter 2); Cook et al., 2021b (Chapter 3); Cumming et al., 2019; Morrill et al., 2014; Szponar et al., 2013). Geochemical analyses on WHC2 have determined that methane and hydrogen, two known products of the serpentinization reaction, are the major components of the dissolved gases in the pool (Morrill et al., 2014; Cook et al., 2021 (Chapter 2); Szponar et al., 2013). Further geochemical analyses have discerned that the methane in the fluids sampled from WHC2 is likely formed non-microbially (i.e., thermogenically or abiotically) (Cumming et al., 2019; Cook et al., 2021 (Chapter 2)).

WHC2 has also been microbiologically characterized: life was detected in the ultra-basic fluids and carbonate surfaces using an ATP illuminometer and LAL assay (Szponar, 2012). Subsequently, metagenomic studies of fluids from WHC2 revealed that the microbial community was dominated by Bacteria with very few archaeal sequences identified (Brazelton et al., 2013; Brazelton et al., 2012). Furthermore, the Bacterial community composition changed with water

chemistry such that the *Firmicutes* genus *Erysipelothrix* inhabit the subsurface ultra-basic fluids WHC2a and b (Brazelton et al., 2013; Morrill et al., 2014) while *Hydrogenophaga*, was found to dominate the area where overland flow mixed with ultra-basic water, WHC2c (Brazelton et al., 2013; Morrill et al., 2014).

5.2.2 Sampling Sites

Two discharge points have been identified at the bottom of WHC2 (referred to as WHC2a and WHC2b) that supply ultra-basic, reducing fluids to the pool. A third location (WHC2c) was also sampled closer to the surface of the pool where more mixing can occur (Figure 5.1 A, Figure 5.2). Fluids for geochemical analysis and sediments for PLFA analyses were sampled from WHC2a, WHC2b, and WHC2c to represent different geochemical environments from a more ultra-basic environment to an environment that is a combination of ultra-basic spring water and surface contributions. To discern potential surface contributions to the pool, samples were also taken from the adjacent river, Winter House Brook (WHB) (Figure 5.1B, Figure 5.2).

While serpentinite-hosted springs like WHC2 can provide one of the best natural windows into the subsurface geochemistry and microbial communities, it is often difficult to isolate these subsurface fluids from surface contributions. Currently, all of the information about the microbial communities (i.e., genomic, isotopic, and microcosms) at the Tablelands rely on fluids sampled from WHC2 which is not completely isolated from surface contributions. To study the subsurface geochemistry and microbial communities without the influence of surface fluids, a microbial observatory (WHCMO) was created in July 2018. The site was chosen after testing the pH of various spring outflows and determining the spot that had the highest pH water and was surrounded by a characteristic carbonate travertine deposit. Three holes were drilled

approximately 30 cm apart in the area where the high pH water was identified. The holes were approximately 30 cm in depth and were lined with polyvinyl chloride tubing to ensure they remained open and did not fill in with carbonate precipitation over the years. These boreholes were labelled WHCMO1, WHCMO2, and WHCMO3 (Figure 5.1C, Figure 5.2) and were intended to represent replicates of the same subsurface environment. However, fluid was sampled from only one borehole (WHCMO1) to provide a better understanding of subsurface geochemistry.

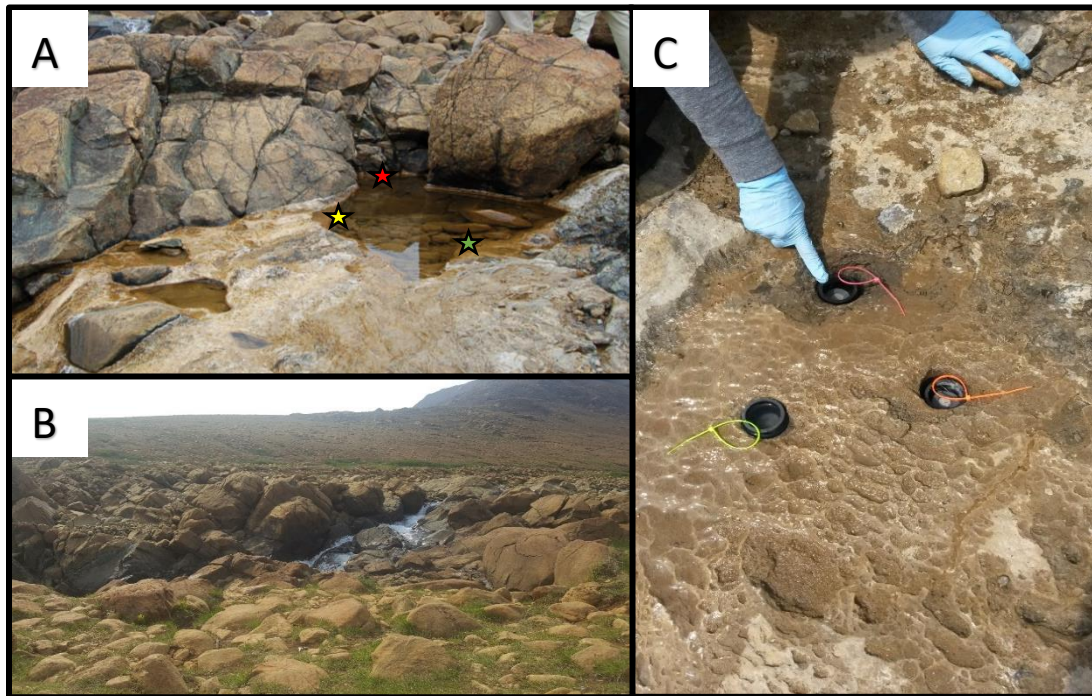


Figure 5.1. Images of sampling locations at the Tablelands (A) Winterhouse Canyon 2 (WHC2) where the green star represents WHC2a, the yellow star WHC2b, and the red star WHC2c (B) Winter House Brook (WHB) and (C) Winterhouse Canyon Microbial Observatory 1 (WHCMO1) (pink), WHCMO2 (orange), and WHCMO3 (yellow).

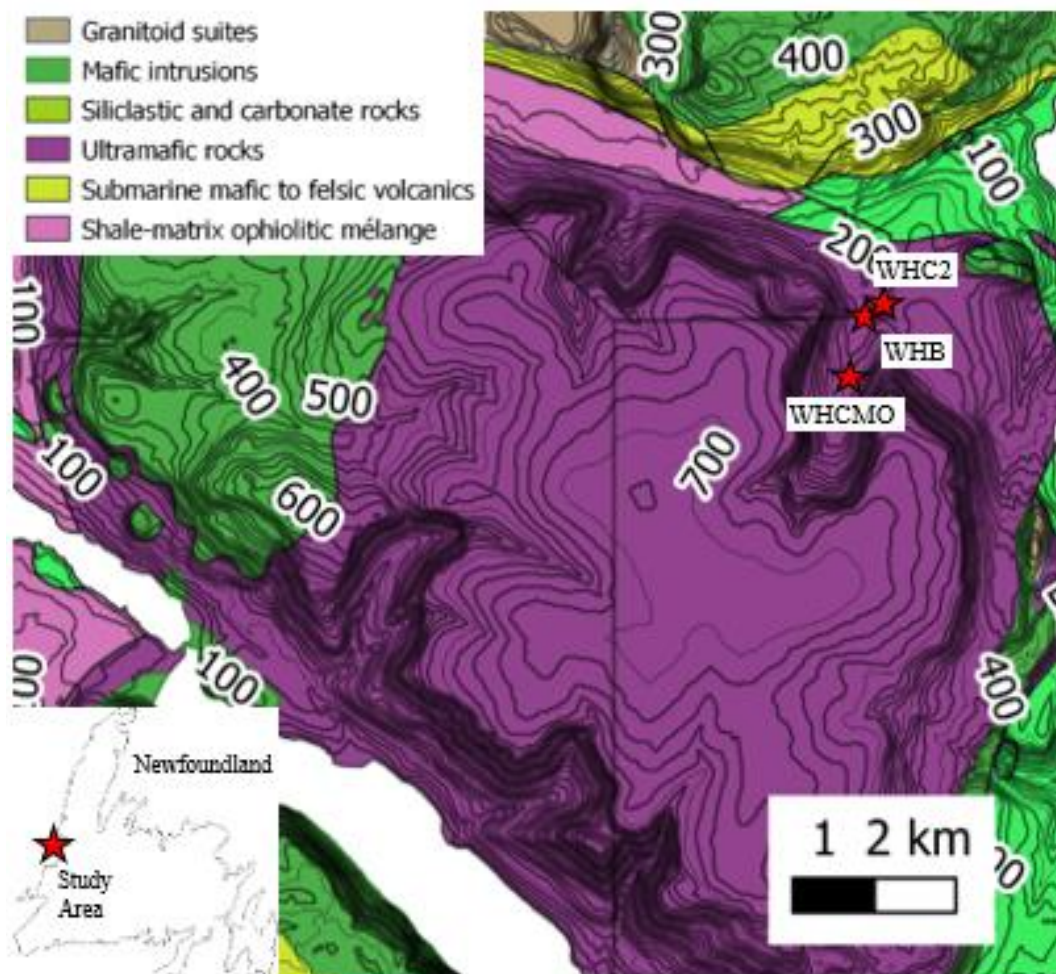


Figure 5.2. Geologic map (modified from Berger et al., 1992) demonstrating the sampling locations (red stars) within the Tablelands massif. Map modified from Cook et al. (2021, Chapter 2).

5.2.3 Aqueous Geochemistry and Dissolved Gases

Samples for aqueous geochemical analyses were collected from WHC2a, WHC2b, and WHC2c in October 2012, from WHB in July 2018, and from WHCMO in June 2019. Prior to sample collection, the pH and temperature of the fluid from the sampling site were measured in the field using an Oakton handheld waterproof field probe meter. The meter was calibrated daily

before use with 4, 7, and 10 pH buffers. The oxidation-reduction potential (ORP) of the fluid was also measured daily using an ORPTestr 10 m (Eutech Instruments). The accuracy of the ORP meter was confirmed using 4 and 7 pH buffers that had been saturated with quinhydrone solutions with ORP values of +93 mV and +267 mV respectively. To create these solutions, 0.1 g of quinhydrone was added to 50 mL of each pH buffer. The ORP meter had a double junction platinum electrode such that a correction was required to convert ORP to Eh. Field measurements were therefore converted from ORP to Eh by adding 241.0 to the field values (YSI, 2005).

Fluid samples for geochemical analysis were collected directly using a Masterflex® E/STM portable peristaltic pump with Tygon® tubing to minimize interaction with the atmosphere. The Tygon® tubing was sterilized by autoclaving before use. At the time of sampling, fluids for dissolved trace element analyses were filtered through 0.22 µm mixed cellulose ester (MCE) filters and collected in sterile 15 mL Falcon® tubes and immediately frozen. Immediately prior to analysis, samples were thawed and acidified (pH < 2) with nitric acid for trace element analysis. Samples for total inorganic carbon (TIC) analysis were collected in pre-combusted 40 mL amber glass vials with no headspace. A drop of concentrated mercuric chloride (HgCl₂) was added to samples to eliminate microbial activity and sample vials were sealed with a black butyl septum following the method described in (Wilson et al., 2020). Samples for dissolved organic carbon (DOC) analysis were filtered through pre-combusted Cytiva Whatman® glass fiber filters (GFF) and 30 mL of fluid was collected in pre-combusted glass vials. Samples were preserved with phosphoric acid (H₃PO₄) and sealed with Teflon septum following the method described in Wilson, Munizzi, and Erhardt (2020). Samples for TIC and DOC were both stored dark and cold until analysis. Samples for δ²H and δ¹⁸O analysis

were collected in 4 mL pre-combusted amber vials with no headspace and were stored dark and cold until analysis (Szponar et al., 2013).

Dissolved gases were collected following the methods outlined in Cumming et al. (2019) that were adapted from Rudd, Hamilton, and Campbell (1974). In short, 30 mL of fluid was collected in a 60 mL syringe that contained an equivalent volume of either helium or nitrogen gas. The syringe was then sealed and shaken for 5 minutes to partition the dissolved gases into the gaseous phase. The gas phase was injected into a pre-combusted 30 mL serum vial displacing the degassed Nanopure water. These vials were pre-sealed with blue butyl septum (Chemglass Life Sciences) that were conditioned as described by Oremland, Miller, and Whiticar (1987). Mercuric chloride was added to the samples after collection to inhibit microbial activity and the samples were stored dark and cold until analysis.

5.2.3 Phospholipid Fatty Acids

Sediment samples for PLFA analysis were collected from the bottom of WHC2 in June 2010, July 2018, and August 2019 in pre-combusted amber glass vials and frozen until extraction. Before extraction, samples were freeze-dried. Therefore, PLFA from these samples are reported in μg of C/g of dried sediment weight. Since no sediment sample was available at WHB, water was filtered through sterile Sterivex™ cartridge filters in July 2018. The total volume of water filtered was recorded and filters were wrapped in pre-combusted aluminum foil and frozen until extraction.

Incubators from WHCMO were created using sterilized tubes that were enclosed on either end with mesh (Figure 5.3A). Crushed peridotite (to maximize surface area) was sterilized at 120°C in an oven for 24 h and added to the incubators. Incubators were then inserted into the

boreholes and remained for either one year (samples from June 2019) or two years (samples from August 2019) before being retrieved. Once the incubators were retrieved, they were replaced with new, sterile incubators to repeat the experiment. The collected incubators were stored in pre-combusted amber vials and frozen (Figure 5.3B). Subsequently, these samples were freeze dried in preparation for PLFA extraction. Two incubators were collected from separate boreholes in June 2019 (WHCMO2 and WHCMO3) and three incubators were collected in August 2021 (WHCMO1, WHCMO2, and WHCMO3). Incubators were analyzed for PLFA identification and results are reported in μg of C/g of dried sample weight.



Figure 5.3. (A) The sterilized incubators and (B) the incubators after a year of exposure to the ultra-basic fluids at WHCMO.

5.2.4 Analytical Methods

5.2.4.1 Geochemical Analytical Methods

Dissolved (after 0.22 μm filtration) trace element abundances (Cl, Br, Ca, Mg, Mn, and Fe) were measured using an inductively coupled plasma mass spectrometer (ELAN DRC II ICP-MS) in Memorial University's Core Research Equipment & Instrument Training (CREAIT)

Network. ICP-MS laboratory standards (river water and dissolved powder geological reference materials) were used for quality control. The RSD (1σ) was less than 10 % between duplicate measurements of reference materials. The detection limits on conservative ions Cl and Br were $<1.47 \times 10^{-5}$ M and $<4.94 \times 10^{-8}$ M, respectively. The detection limits on Ca, Mg, Mn, and Fe were $<9.17 \times 10^{-7}$ M, $<3.43 \times 10^{-8}$ M, $<3.11 \times 10^{-10}$ M, and $<1.83 \times 10^{-7}$ M, respectively.

Sodium and potassium concentrations were measured on an inductively coupled plasma optical emissions spectrometer (Thermo Scientific iCAP 6500 Series) Geochemical Laboratory, Government of Newfoundland. Certified reference materials were used for quality control and the RSD (1σ) was less than 10% between duplicate measurements. The detection limits on Na and K were $<4.35 \times 10^{-7}$ M and $<1.00 \times 10^{-6}$ M, respectively.

Nitrate and sulfate concentrations were measured using ion chromatography (Thermo Fisher ICS 5000) in Memorial University's Boreal Ecosystem Research Facility. Ions were separated using an AS23 column with an ASG23 guard column and a carbonate eluent with a 1.0 mL/min flow rate. Standards purchased from Sigma Aldrich were used to create calibration curves to quantify nitrate and sulfate concentrations. Additionally, a standard containing 61 μ M nitrate and 52 μ M sulfate was injected during the analysis to check for instrument drift. The detection limits for nitrate and sulfate were <1.6 and <2.60 μ M, respectively.

Samples for TIC and DOC were analyzed for their concentrations and stable carbon isotope values at the Ján Veizer Stable Isotope Laboratory at the University of Ottawa using methods outlined in Murseli et al. (2019) and St-Jean (2003). Samples were analyzed using a modified OI Analytical Aurora Model 1030 Wet TOC Analyser with a model 1051 autosampler and a combustion unit. TIC concentrations were determined using non-destructive infrared (NDIR) detector coupled to a Thermo Finnigan Mat DeltaPlusXP isotope ratio mass

spectrometer (IRMS). DOC concentrations and stable carbon isotope values were also determined on the same system using the non-purgeable organic carbon (N-POC) method. The detection limit for the concentrations and carbon isotope values were $<3.33 \times 10^{-5}$ M of C. The analytical precision for concentration analysis was 0.5 ppm C (2σ) and 0.2 ‰ (2σ) for the $\delta^{13}\text{C}$ analysis. These precision values were based on long-term measurements of laboratory standards.

Water samples were sent for $\delta^2\text{H}$ and $\delta^{18}\text{O}$ analysis at Isotope Tracer Technologies, Inc., in Waterloo, Ontario. They were analyzed using Picarro Cavity Ring Down Spectroscopy Analyzer (Model L2130-i). Three standards were used to normalize the results (V-SMOW, SLAP, and GISP) and the results have been reported relative to the VSMOW reference standard. The precision on $\delta^2\text{H}$ and $\delta^{18}\text{O}$ measurements was ± 1 ‰ (1σ) and ± 0.1 ‰ (1σ) respectively.

Hydrogen and oxygen gas concentrations were measured on an Agilent 6890A GC in Memorial University's CREAT Network. The GC was equipped with a micro thermal conductivity detector (TCD) using a Carbon 1010 capillary column (30 m x 0.32 mm inside diameter, 15 μm film thickness) with nitrogen as a carrier gas. The oven temperature was 50 °C isothermal for 13 minutes. A mixed gas standard (Scott™) was used to create the calibration curves for hydrogen and oxygen. The gas standard contained 0.5 % oxygen, 0.5 % carbon monoxide, 0.5 % carbon dioxide and 0.5 % hydrogen in a balance of helium. The detection limits for hydrogen and oxygen in the gas phase were 10 and 15 μM respectively. The precision on triplicate injections of the standard was always less than 5 % relative standard deviation (RSD) (2σ).

The methane concentration was analyzed in Memorial University's DELTAS laboratory using an SRI 8610 gas chromatograph (GC) equipped with a Flame Ionization Detector (FID) and a methanizer. A Carboxen 1010 capillary column (30 m x 0.32 mm inside diameter, 15 μm

film thickness) was used with helium as the carrier gas following procedures outlined in Morrill et al. (2014). In short, the oven temperature was held constant at 40 °C for 16 min then increased by 15 °C/min to a final temperature of 125 °C, which was held constant for 3 min. A methane gas standard (Scott™) of 1 % methane in a balance of helium was used to create the calibration curves for methane. The detection limits for methane in the gas phase was 5 µM (Morrill et al., 2014). The precision on triplicate injections of the standard was always less than 5 % (RSD) (2σ).

5.2.4.2 PLFA Analytical Methods

Samples were extracted for PLFAs following a modified Bligh Dyer process that is outlined in Morrill et al. (2014) and Ziegler et al. (2013). Samples were freeze-dried prior to extraction. For every gram of sample 1 mL of DCM and 2 mL of MeOH were used such that there was always a DCM:MeOH ratio of 1:2. Samples were then sonicated for 5 min before leaving overnight in a 5°C fridge. Samples were then filtered and rinsed with DCM followed by MeOH. The resulting total lipid extract (TLE) was transferred to a separatory funnel with 20 mL of Nanopure water. The TLE was shaken and then left to separate overnight. The organic layer was collected and evaporated to 1 mL under a gentle stream of nitrogen at 35°C. The TLE was then separated into three fractions (F1, F2, and F3) using fully activated silica gel chromatography and 10 mL of DCM followed by 10 mL of acetone and finally 10 mL of MeOH. The polar fraction (F3) contained the PLFAs and was evaporated to dryness under a gentle stream of nitrogen and stored in the freezer.

The PLFAs were transesterified into fatty acid methyl esters (FAMES) by mild alkanolysis (Guckert et al., 1985) and spiked with an internal standard (10 µg methyl nonadecanoate (C19:0)). FAMES were separated by an Agilent 6890 Gas Chromatography (30 m

x 0.25 mm BPX-70 column, 30 m x 0.32 mm, 0.25 μm film thickness) interfaced with an Agilent 5973 mass spectrometer and quantified using an Agilent 6890 equipped with a flame ionization detector. The GC oven temperature was initially 70°C, ramped at 10°C/min to 160°C, hold for 5 min, ramp at 4°C/min to 280°C, hold for 20 min.

Calibration curves for samples collected in 2010 were created using a bacterial reference standard (Bacterial Acid Methyl Esters (BAME) CP mix, Matreya Inc.) while calibration curves for samples collected in 2018 and 2019 were created using a GRAIN FAME mix and C4-C24 Even Carbon Saturated FAMES standards (Sigma Aldrich). In addition to the standards, a National Institute of Standards and Technology (NIST 02) library was used to identify PLFAs. FAMES generated from PLFAs were named according to a standard C:M ω X nomenclature where C represents the number of carbon atoms in the chain, M the number of the double bonds in the chain and X the position of the double bond relative to the aliphatic end of the compound. The PLFA molecules can also be divided into *cis* and *trans* isomers which are denoted by the suffix c and t, respectively. PLFAs are reported as mol% relative to the total PLFA in the sample.

5.2.5 Thermodynamic Calculations

Chemical affinities (A_r) of eight reactions (Table 5.1) likely to occur at sites of terrestrial serpentinization were calculated using the following equation:

$$A_r = RT \ln \left(\frac{K_r}{Q_r} \right) \quad [\text{Eq. 5.1}]$$

where R is the ideal gas constant, T is the temperature (in Kelvin), K_r is the equilibrium constant and Q_r is the activity product. The equilibrium constant (K_r) is calculated using the Gibbs free energy ($\Delta_r G^\circ$) of the reaction:

$$K_r = e^{-\Delta G^\circ/RT} \quad [\text{Eq. 5.2}]$$

The Gibbs free energy for each reaction was calculated using Gibbs free energies of formation (ΔG°) values from Amend and Shock (2001). The activity product (Q_r) was calculated using the activities of each chemical species. The activity product calculations were based on data from field samples collected at WHCMO, WHC2a, WHC2b, and WHC2c (Table 5.2). Activities were calculated using the Debye-Hückel equation (cf. Table 5.S1). A temperature of 18 °C was used in all affinity calculations, a value within 10 °C of the temperature of the spring water at each site. A sensitivity test was also performed to determine the affect using a temperature of 18 °C had on the A_r value and it was determined to be insignificant.

Table 5.1. Reactions Used for Chemical Affinity and Energy Density Calculations and Corresponding Number of Electrons (e-) Transferred for Each Reaction.

Eq #	Reaction Name	Stoichiometric Equation	e ⁻
3	Hydrogen oxidation	$\text{H}_{2(\text{aq})} + 0.5\text{O}_{2(\text{aq})} \leftrightarrow \text{H}_2\text{O}$	2
4	Water-gas shift	$\text{CO}_{(\text{aq})} + \text{H}_2\text{O}_{(\text{aq})} \leftrightarrow \text{CO}_{2(\text{aq})} + \text{H}_2$	2
5	Carbon monoxide oxidation	$\text{CO}_{(\text{aq})} + 0.5\text{O}_{2(\text{aq})} \leftrightarrow \text{CO}_{2(\text{aq})}$	2
6	Carbon monoxide reduction	$3\text{H}_{2(\text{aq})} + \text{CO}_{(\text{aq})} \leftrightarrow \text{CH}_{4(\text{aq})} + \text{H}_2\text{O}$	6
7	Methanogenesis (CO ₂)	$\text{CO}_{2(\text{aq})} + 4\text{H}_{2(\text{aq})} \leftrightarrow \text{CH}_{4(\text{aq})} + 2\text{H}_2\text{O}$	8
8	Methanotrophy (nitrate)	$8\text{NO}_3^- + 8\text{H}^+ + 5\text{CH}_{4(\text{aq})} \leftrightarrow 4\text{N}_{2(\text{aq})} + 5\text{CO}_{2(\text{aq})} + 14\text{H}_2\text{O}$	40
9	Methanotrophy (sulfate)	$\text{CH}_{4(\text{aq})} + \text{SO}_4^{2-}{}_{(\text{aq})} \leftrightarrow \text{HCO}_3^-{}_{(\text{aq})} + \text{HS}^- + 2\text{H}_2\text{O}$	8
10	Aerobic methanotrophy	$\text{CH}_{4(\text{aq})} + 2\text{O}_{2(\text{aq})} \leftrightarrow \text{CO}_{2(\text{aq})} + 2\text{H}_2\text{O}$	8

Chemical affinities of ten possible reactions in ultra-basic reducing pools were calculated using field data from WHCMO, WHC2a, WHC2b, and WHC2c. These values were calculated in kcal per mole of electrons transferred in each reaction so that a comparison between reactions was possible.

To understand available energy with respect to the limiting electron reactant, energy densities were then calculated using the following equation (LaRowe & Amend, 2014):

$$E_r = \left| \frac{\Delta G_r}{\nu_i} \right| [i] \quad [\text{Eq. 5.11}]$$

Where $[i]$ represents the concentration of the limiting reactant and v_i represents the stoichiometric coefficient.

5.3 Results

5.3.1 Geochemical Description of the Site

Table 5.2 summarizes the geochemistry of the spring water and surface waters sampled between 2012 and 2019 at the Tablelands. This data shows that the spring waters (WHCMO, WHC2a, WHC2b, and WHC2c) are geochemically distinct from the surface water (WHB). The sampling location most geochemically similar to the surface water is WHC2c, which was expected since this location is where overland flow contributes to the WHC2 pool. Despite this addition, all of the spring waters sampled were ultra-basic, ranging from 11.7 to 12.3, demonstrating the buffering capacity of the system. WHC2b had the most distinct aqueous chemistry of all of the springs. For example, WHC2b had the lowest nutrients (sulfate, nitrate), dissolved carbon (TIC and DOC), and Mg, as well as the highest Na, K, Ca, Cl, and Br of all of the samples. These observations (low nutrients and carbon, as well as high ion concentrations, with the exception of Mg) are characteristic of serpentinite-hosted springs (Cook et al., 2021 (Chapter 2)). In comparison, the surface water (WHB) had the highest nutrients, and the lowest Na, K, Ca, and Cl. The surface water also had the most ^{13}C enriched TIC (with a $\delta^{13}\text{C}$ of -2.4 ‰), and the most ^{13}C depleted DOC (with a $\delta^{13}\text{C}$ of -29.9 ‰) with an isotopic separation of 27.4 ‰. The isotopic separation between TIC and DOC was much less for the ultra-basic spring waters, ranging from 0.6 to 9.5 ‰.

Table 5.2. Summary of geochemical parameters of WHCMO, WHC2a, WHC2b, WHC2c, and WHB at the Tablelands.

	WHCMO 2019	WHC2a 2012	WHC2b 2012	WHC2c 2012	WHB* 2018
pH	12.3	12.2	12.2	11.7	8.1
E_h (mV)	+102	-406	-401	-227	+127
Na (μM)	1.10 x 10 ³	5.61 x 10 ³	4.06 x 10 ⁴	4.16 x 10 ³	1.21 x 10 ²
K (μM)	4.07 x 10 ¹	9.26 x 10 ¹	3.20 x 10 ²	6.98 x 10 ¹	1.04 X 10 ¹
Ca (μM)	1.14 x 10 ³	4.74 x 10 ²	1.50 x 10 ³	8.66 x 10 ¹	1.43 x 10 ¹
Mg (μM)	1.82 x 10 ¹ (± 6.63)	2.48 x 10 ²	2.99	4.98 x 10 ²	2.37 x 10 ² (± 4.27 x 10 ¹)
Fe (μM)	< d.l.	<d.l.	<d.l.	<d.l.	< d.l.
Mn (μM)	2.05 x10 ⁻³ (± 5.23 x 10 ⁻⁴)	<d.l.	3.69 x 10 ⁻¹	3.54 x 10 ⁻¹	< d.l.
Cl (μM)	1.06 x 10 ³	3.89 x 10 ³	1.17 x 10 ⁴	6.54 x 10 ²	1.68 x 10 ² (±3.09 x 10 ¹)
Br (μM)	9.74 x 10 ⁻²	4.26	1.23 x 10 ¹	7.97 x 10 ⁻¹	3.35 x 10 ^{-1*}
SO₄ (μM)	5.54 x 10 ⁻³	1.35 x 10 ⁻²	4.56 x 10 ⁻³	1.30 x 10 ⁻²	7.09
NO₃ (μM)	9.22 x 10 ⁻³	2.29 x 10 ⁻³	1.15 x 10 ⁻³	2.77 x 10 ⁻³	7.42
Ca/Mg	6.26 x 10 ¹	3	8.27 x 10 ²	3.00 x 10 ⁻¹	6.03 x 10 ⁻²
TIC (moles of C·L⁻¹)	5.69 x 10 ⁻⁵ (± 1.90 x 10 ⁻⁵)	2.29 x 10 ⁻⁴	1.83 x 10 ⁻⁵	1.40 x 10 ⁻³	7.35 x 10 ⁻⁴
δ¹³C TIC (‰)	-17.5	-17.1	-13.9	-14.2	-2.4
DOC (moles of C·L⁻¹)	7.60 x 10 ⁻⁵	2.91 x 10 ⁻⁵ (± 1.66 x 10 ⁻⁵) ^b	2.41 x 10 ^{-5b}	6.99 x 10 ^{-5b}	3.13 x 10 ⁻⁵
δ¹³C DOC (‰)	-24.7	-17.7 ^b	-22.1 (± 6.0) ^b	-23.7 ^b	-29.8
δ¹⁸O H₂O (‰)	-10.9	-7.7	-8.4	-8.8	-9.0
δ²H H₂O (‰)	-70	-55	-54	-56	-56

Standard deviations of measurements were less than 10 % unless otherwise indicated. Parameters below limits of detection are indicated by “< d.l.”. Data reported in this table were collected for this study except where noted: ^aCook et al. (2021), ^bSzponar et al. (2012).

To better understand the aqueous geochemistry of WHC2a, WHC2b, WHC2c, and WHCMO, the major ions from each site were plotted on a Piper diagram (Piper, 1953) (Figure 5.4). Figure 5.4 further demonstrates that, despite their similar geographic location and ultra-basic pH (i.e., > 11), each sampling site was distinct (with the exception of WHC2a and WHCb which plotted closely together) and did not plot near the surface contributions (i.e., WHB) on the Piper diagram. When the geochemistry of the fluids sampled in this study are broken down by water types on the Piper diagram, the fluid from WHB plots in the Mg-HCO₃-type water, WHCMO in the Ca-Cl-type water, WHC2a and WHC2b in the Na-Cl-type water, and WHC2c plots in the mixed-type waters.

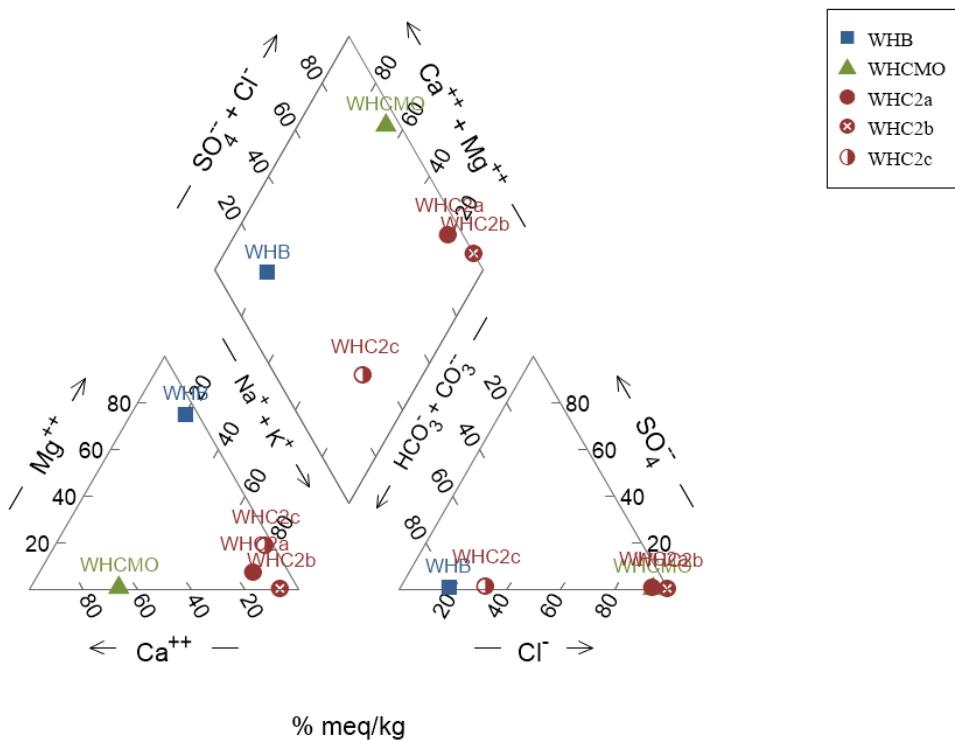


Figure 5.4. Piper diagram illustrating the relationships in fluid composition between WHC2a, WHC2b, WHC2c, WHCMO, and WHB.

Hydrogen and oxygen isotope values ($\delta^2\text{H}$ and $\delta^{18}\text{O}$) of the water from WHCMO, WHC2a, WHC2b, WHC2c, and WHB ranged from -70 to -54 ‰ and -10.9 to -7.7 ‰, respectively. These values were plotted against the Global Meteoric Water Line (GMWL) and the Local Meteoric Water Line (LMWL) for Corner Brook, Newfoundland (Marche, 2016) (Figure 5.5). All samples were well described by the GMWL and the LMWL, indicating that the waters from the Tablelands are meteoric in origin.

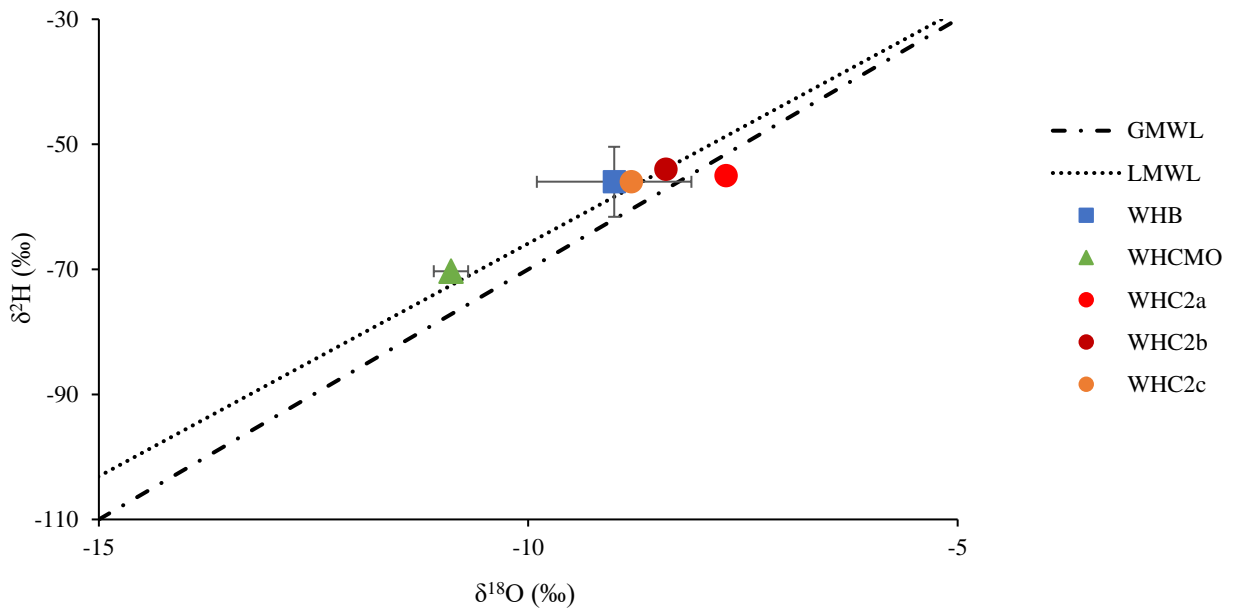


Figure 5.5. Hydrogen and oxygen isotope values of water samples from WHC2, WHB, and WHCMO compared to the Global Meteoric Water Line (GMWL), $\delta^2\text{H} = 8 \delta^{18}\text{O} + 10$ (Harmon, 1961) and Newfoundland Local Meteoric Water Line (LMWL) (Marche, 2016). The error bars are the standard deviations (1σ) of the duplicate samples. The error bar for the $\delta^2\text{H}_{\text{H}_2\text{O}}$ of water sampled from WHCMO is smaller than the plotted symbol.

The composition of the dissolved gases measured in WHC2a, WHC2b, WHC2c, and the WHCMO have been summarized in Table 5.3. Hydrogen was detected in the dissolved phase in WHC2a, WHC2b, and WHCMO (4.72×10^2 , 5.29×10^2 and 4.64×10^2 μM , respectively). Methane was also detected in the dissolved phase in samples from WHC2a, WHC2b, and WHC2c (26, 37, and 13 μM , respectively).

Table 5.3. Composition of dissolved gases measured in WHC2 and WHCMO.

	WHC2a 2012	WHC2b 2012	WHC2c 2012	WHCMO 2019
H₂ [μM]	4.72×10^2	5.29×10^2	<d.l.	$4.64 \times 10^2 \pm 0.07 \times 10^2$
CH₄ [μM]	26	37	13	<d.l.

Parameters below limits of detection are indicated by the letters d.l.

5.3.2 PLFA Results

Total PLFA extraction yields were calculated for samples where a recovery standard was added at the beginning of the extraction (i.e., all samples except for those from 2010) (Figure 5.6). The highest overall total PLFA extraction yield was in the sample from WHC2b collected in 2021 (1.53×10^3 μg of C/g). The extraction yields from WHCMO showed the greatest amount of variability between sampling years while the extraction yields from WHC2 were more consistent. PLFA extraction yields were lowest in incubator samples from WHCMO2 and WHCMO3 from 2019 with 2.3×10^{-1} and 1.5×10^{-1} μg of C/g of ultramafic substrate, respectively.

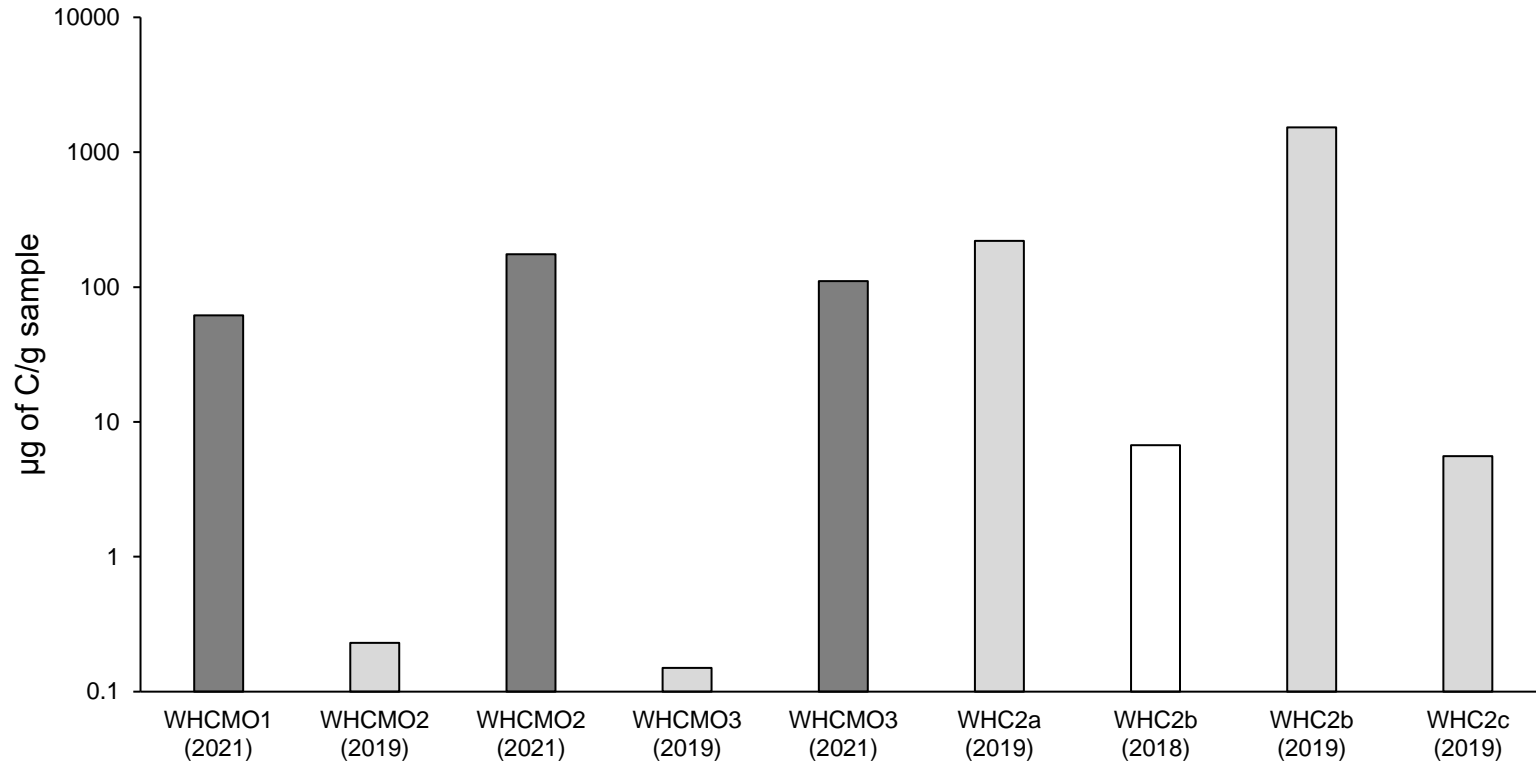


Figure 5.6. Total concentrations of PLFAs extracted from samples from WHC2 (μg of C/g of carbonate) and WHCMO (μg of C/g of ultramafic substrate) presented on a logarithmic scale. The total PLFA extract from WHB (2018) was $4.7 \mu\text{g}$ of C/mL of water.

The individual PLFA distributions, calculated as mol% of the total PLFA, from carbonate sediment collected from WHC2a, WHC2b, and WHC2c, as well as from the Sterivex™ filter collected from WHB are summarized in Table 5.4 and from the ultramafic substrate in the incubators at WHCMO1, WHCMO2, and WHCMO3 in Table 5.5. Overall, samples collected from WHCMO and WHB were more homogeneous and contained a lower diversity of PLFAs relative to samples collected from WHC2. For example, the PLFA composition in WHB and samples collected from WHCMO2 and WHCMO3 in June 2019 were all dominated by Heptacosane which made up 84.8, 88.6, and 51.9 mol %, respectively. Samples collected from WHCMO2 and WHCMO3 in August 2021 showed very similar community structure and were dominated by the PLFAs 16:0 and 18:0. The sample collected from WHCMO1 in 2021 was also dominated by 16:0 and 18:0, however, it also contained smaller percentages of 16:1 ω 9, 18:1 ω 9c, and 18:3 ω 6.

The PLFA composition in samples collected from WHC2 showed more variation in PLFAs between samples with the exception of the sample collected from WHC2c in July 2018 which was dominated (> 97 mol%) by 16:1 ω 9. The PLFA composition in the sample from WHC2a was dominated by PLFA 16:0 followed by 16:1 ω 7 in June 2010 and by PLFA 16:0 and 16:1 ω 9c in August 2019. Similarly, the PLFA composition in the sample from WHC2b was dominated by PLFA 16:1 ω 7 followed by 16:0 in June 2010 and by PLFA 16:1 ω 9 followed by 16:0 in August 2019. Unlike WHC2a and WHC2b, WHC2c was dominated by PLFA 18:1 ω 9c followed by 16:1 ω 7 in June 2010, however in August 2019 it was also dominated by PLFAs 16:1 ω 9 and 16:0.

Table 5.4. Distribution of mol% of PLFAs detected in WHC2a, WHC2b, WHC2c, and WHB.

	WHC2a 2010	WHC2a 2019	WHC2b 2010	WHC2b 2018	WHC2b 2019	WHC2c 2010	WHC2c 2019	WHB 2018
PLFA ID	Mol %	Mol %	Mol%	Mol %	Mol %	Mol %	Mol %	Mol %
14:0	5.7	6.8	4.7	<d.l.	7.8	3.0	12.4	<d.l.
a-15:0	<d.l.	-	4.1	<d.l.	-	2.1	-	<d.l.
i-15:0	4.1	-	3.8	<d.l.	-	2.1	-	<d.l.
15:0	<d.l.	<d.l.	<d.l.	<d.l.	<d.l.	0.9	2.4	<d.l.
i-16:0	<d.l.	-	<d.l.	<d.l.	-	1.1	-	<d.l.
16:0	19.9	25.2	17.0	2.7	29.7	14.3	28.2	<d.l.
16:1ω7	12.4	<d.l.	17.7	<d.l.	<d.l.	14.7	<d.l.	<d.l.
16:1ω9	<d.l.	25.8	<d.l.	97.3	37.1	<d.l.	27.2	<d.l.
16:1ω?^a	<d.l.	-	<d.l.	<d.l.	-	2.8	-	<d.l.
16:2ω6	<d.l.	-	<d.l.	<d.l.	-	1.3	-	<d.l.
i-17:0	<d.l.	-	<d.l.	<d.l.	-	0.9	-	<d.l.
Δ 17:0	<d.l.	-	<d.l.	<d.l.	-	1.0	-	<d.l.
17:0	<d.l.	<d.l.	<d.l.	<d.l.	<d.l.	0.7	<d.l.	<d.l.
18:0	10.8	5.5	7.6	<d.l.	4.1	3.9	1.5	<d.l.
18:1ω4t	<d.l.	-	<d.l.	<d.l.	-	1.5	-	<d.l.
18:1ω9c	10.8	17.6	13.5	<d.l.	13.0	20.1	10.2	<d.l.
18:1ω9t	8.6	<d.l.	6.3	<d.l.	<d.l.	5.5	3.7	<d.l.

18:1ω10	<d.l.	-	<d.l.	<d.l.	-	<d.l.	-	<d.l.
18:2ω5	<d.l.	-	<d.l.	<d.l.	-	1.7	-	<d.l.
18:2ω6	4.0	7.1	3.8	<d.l.	<d.l.	4.5	<d.l.	<d.l.
18:3ω3	<d.l.	1.0	<d.l.	<d.l.	3.7	2.3	6.5	<d.l.
18:3ω6	5.4	7.3	4.4	<d.l.	<d.l.	3.2	<d.l.	<d.l.
18:3 ω9, 12, 15	<d.l.	-	<d.l.	<d.l.	-	<d.l.	-	<d.l.
18:4ω3	<d.l.	-	<d.l.	<d.l.	-	1.0	-	<d.l.
20:0	5.9	1.6	4.1	<d.l.	<d.l.	1.3	<d.l.	<d.l.
20:4ω6	<d.l.	<d.l.	2.4	<d.l.	<d.l.	1.7	2.1	<d.l.
20:5ω3	<d.l.	<d.l.	3.6	<d.l.	4.6	4.9	5.9	<d.l.
22:0	4.7	1.2	3.4	<d.l.	<d.l.	1.0	<d.l.	<d.l.
22:5ω6	3.7	-	<d.l.	-	-	0.8	-	-
22:6ω6	<d.l.	-	<d.l.	<d.l.	-	0.7	-	<d.l.
24:0	4.1	1.0	3.6	<d.l.	<d.l.	0.9	<d.l.	<d.l.
E-8-methyl-9-tetradecen-1-ol acetate	<d.l.	-	<d.l.	<d.l.	-	<d.l.	-	15.2
Heptacosane	<d.l.	-	<d.l.	<d.l.	-	<d.l.	-	84.8
Total	100.1	100.1	100.0	100.0	100.0	99.9	100.1	100.0

^a The position of the double bond for PLFA 16:1 ω ? is unknown. Parameters below limits of detection are indicated by the letters d.l and parameters not measured are indicated by “-”.

Table 5.5. Distribution of mol% of PLFAs detected in WHCMO1, WHCMO2, and WHCMO3.

	WHCMO1 2021	WHCMO2 2019	WHC2MO2 2021	WHCMO3 2019	WHC2MO3 2021
PLFA ID	Mol %	Mol %	Mol %	Mol%	Mol %
14:0	<d.l.	0.1	<d.l.	<d.l.	<d.l.
a-15:0	-	<d.l.	-	<d.l.	-
i-15:0	-	<d.l.	-	<d.l.	-
15:0	<d.l.	<d.l.	<d.l.	<d.l.	<d.l.
i-16:0	-	<d.l.	-	<d.l.	-
16:0	30.9	4.5	52.0	<d.l.	56.6
16:1ω7	<d.l.	<d.l.	<d.l.	<d.l.	<d.l.
16:1ω9	15.4	<d.l.	<d.l.	<d.l.	<d.l.
16:1ω?^a	-	<d.l.	-	<d.l.	-
16:2ω6	-	<d.l.	-	<d.l.	-
i-17:0	-	<d.l.	-	<d.l.	-
Δ 17:0	-	<d.l.	-	<d.l.	-
17:0	<d.l.	<d.l.	<d.l.	<d.l.	<d.l.
18:0	28.0	6.2	48.0	<d.l.	43.4
18:1ω4t	-	<d.l.	-	<d.l.	-
18:1ω9c	13.3	<d.l.	<d.l.	<d.l.	<d.l.
18:1ω9t	<d.l.	<d.l.	<d.l.	<d.l.	<d.l.

18:1ω10	-	0.1	-	<d.l.	-
18:2ω5	-	<d.l.	-	<d.l.	-
18:2ω6	<d.l.	<d.l.	<d.l.	<d.l.	<d.l.
18:3ω3	<d.l.	<d.l.	<d.l.	<d.l.	<d.l.
18:3ω6	12.4	<d.l.	<d.l.	<d.l.	<d.l.
18:3 ω9, 12, 15	-	<d.l.	-	48.1	-
18:4ω3	-	<d.l.	-	<d.l.	-
20:0	<d.l.	<d.l.	<d.l.	<d.l.	<d.l.
20:4ω6	<d.l.	<d.l.	<d.l.	<d.l.	<d.l.
20:5ω3	<d.l.	<d.l.	<d.l.	<d.l.	<d.l.
22:0	<d.l.	<d.l.	<d.l.	<d.l.	<d.l.
22:5ω6	-	-	-	-	-
22:6ω6	-	<d.l.	-	<d.l.	-
24:0	<d.l.	<d.l.	<d.l.	<d.l.	<d.l.
E-8-methyl-9-tetradecen-1-ol acetate	-	<d.l.	-	<d.l.	-
Heptacosane	-	88.6	-	51.9	-
Total	100.0	100.0	100.0	100.0	100.0

^a The position of the double bond for PLFA 16:1 ω ? is unknown. Parameters below limits of detection are indicated by the letters d.l and parameters not measured are indicated by “-”.

5.4 Discussion

5.4.1 Characterizing the Microbial Community Composition at the Tablelands

PLFAs can be used as biomarkers to identify microorganisms on the phylum taxonomic level (e.g., Frostegård and Bååth (1996); Willers et al. (2015)). Therefore, based on literature reviews, PLFA biomarkers were divided into six key groups as outlined in Table 5.6. Based on the groupings outlined in Table 5.6, key phylogenetic groupings were then interpreted from each site to understand the microbial community composition at each site within the Tablelands (Figure 5.7).

Table 5.6. Summary of PLFA detected in this study and their interpretation for WHC2, WHB, and WHCMO.

PLFA Biomarker	Type	Group	Reference	Spring
i15:0, a15:0, i16:0, i17:0	Methyl Branched	Bacteria, gram positive	O'Leary and Wilkinson (1988); White et al. (1996); Wilkinson (1988)	WHC2a, WHC2b, WHC2c
16:1w7, Δ17:0, 18:1w9t, 18:1w4t, 16:1ω9, 18:1ω10	Monounsaturated and cyclopropane unsaturated	Bacteria, gram negative	O'Leary and Wilkinson (1988); White et al. (1996); Wilkinson (1988); Yang et al. (2018)	WHC2a, WHC2b, WHC2c, WHCMO2
14:0, 15:0, 16:0, 17:0, 18:0	Saturated straight chained (<20C)	Bacteria (non- specific)	Boschker and Middelburg (2002); Lechevalier and Moss (1977); Yang et al. (2018)	WHC2a, WHC2b, WHC2c, WHCMO1, WHCMO2, WHCMO3
18:2w6, 18:3w6c, 24:0	Monounsaturated and polyunsaturated	Fungi	Frostegård and Bååth (1996); Frostegård et al. (1993)	WHC2a, WHC2b, WHC2c, WHCMO1
18:1w9c ,18:3w3, 18:4w3, 20:4w6, 20:5w3, 22:5w6	Monosaturated and polyunsaturated	Cyanobacteria, green algae, diatoms	Ahlgren et al. (1992); Boschker and Middelburg (2002); Volkman et al. (1989)	WHC2a, WHC2b, WHC2c, WHCMO1
16:2w6, 18:2w5, 20:0, 22:0, 22:6w6, 18:3ω9,12,15, Heptacosane, E-8- methyl-9-tetradecen- 1-ol acetate	Saturated straight chained (>20C), Polyunsaturated, Straight-chain alkane, monounsaturated	Eukaryotes, microeukaryotes, higher plants, mosses	Khatua et al. (2016); Rency et al. (2015); Routaboul et al. (2000); Volkman et al. (1989); Zelles (1999)	WHC2a, WHC2b, WHC2c, WHB, WHCMO2, WHCMO3

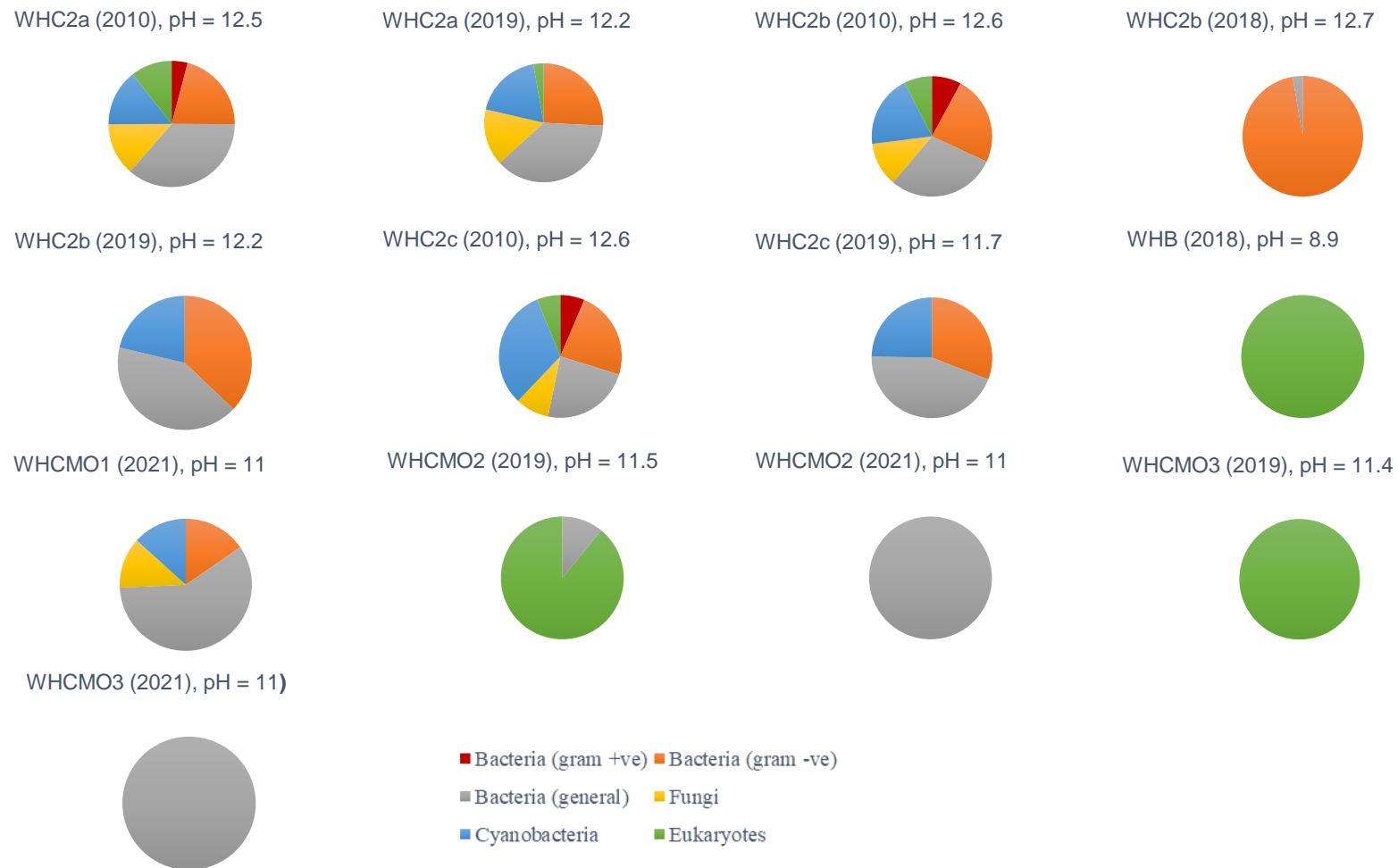


Figure 5.7. Microbial community composition at the Tablelands by phylogenetic groupings as assigned according to references in Table 5.5.

In 2019, samples from WHCMO (i.e., WHMO2 and WHCMO3), were all largely composed (i.e., greater than 88%) of lipids indicative of eukaryotes (Figure 5.8). While it was expected that samples from WHCMO would be composed of similar microbial community compositions since samples from WHCMO represent three identically prepared boreholes (~10 cm apart) that housed flow-through style incubators, it was not expected that these microbial communities would be dominated by eukaryotes. Life in extreme environments (i.e., reducing, ultra-basic) are assumed to be almost exclusively inhabited by non-eukaryotes (i.e., viruses, Bacteria, and Archaea) (Danovaro et al., 2008; Hinrichs et al., 2008; Sinninghe Damsté et al., 2003). Suzuki et al. (2013) for example, detected the presence of both Bacteria and Archaea in ultra-basic fluids from The Cedars but the absence, or very low density, of Eukarya, except for on the surface of the BS5 pool where potential external contamination was unavoidable (Suzuki et al., 2013). It is therefore, assumed that the presence of PLFAs indicative of eukaryotes in samples from WHCMO was due to surface contributions rather than representative of subsurface ultra-basic fluids. The non-reducing environment measured in samples from WHCMO ($E_h = +102$ mV) and the fact that the microbial community composition at WHCMO closely resembled that of WHB further support this.

PLFAs in samples from WHCMO2 and WHCMO3 collected in 2021, by contrast, were entirely composed of bacteria and did not contain any PLFAs indicative of eukaryotes. It is possible that the shift in the microbial community composition at WHCMO between sampling years could be due to the length of time the incubators remained in the subsurface (one year versus two years). However, it is more likely that this microbial community shift is reflective of seasonal shifts in surface contributions since the samples were retrieved during different months.

Samples collected in June 2019 would likely experience more snowmelt and precipitation compared to those collected in August 2021.

Samples from WHCMO1 in August 2021 indicated that the microbial community in this borehole was much more diverse than samples from WHCMO2 and WHCMO3 and was largely composed (i.e., greater than 75%) of bacteria (non-specific and gram-negative) with smaller amounts of fungi and cyanobacteria. This was unexpected because at the time of sampling, it was noted that the water pressure in WHCMO1 was the highest so it was assumed it would receive the least amount of surface infiltration however, the presence of cyanobacteria suggests a larger surface contribution than in WHCMO2 and WHCMO3. This could have led to a microbial community more representative of a mixed spring as opposed to purely subsurface ultra-basic fluids.

The microbial community composition at WHC2 was more diverse than at WHCMO (Figure 5.7). Since WHC2 is a pool that is exposed to the atmosphere and surface contributions it was expected that the site would contain a mixture of eukaryotic lipids reflective of surface contributions and non-eukaryotic lipids reflective of ultra-basic subsurface fluids. All samples from WHC2, with the exception of the sample from WHC2b collected in July 2018, contained PLFAs indicative of cyanobacteria. These cyanobacteria are assumed to be reflective of surface contributions to the pool where it is exposed to sunlight unlike WHCMO. The microbial community in samples from WHC2a in 2010, however, was mostly (i.e., greater than 60%) composed of bacteria (gram-negative and non-specific). Similarly, samples from WHC2a in 2021 were consistent with those from 2010 and contained similar proportions of bacteria (i.e., greater than 60%). Geochemical measurements indicated that WHC2a was the most reducing of the sites sampled (i.e., $E_h = -406$ mV) so it was expected that the microbial community was

bacterial dominated and likely representative of ultra-basic fluids. Like WHC2a, the sample from WHC2b in June 2010 was mostly bacterial dominated (i.e., greater than 60%) which is consistent with its similarly reducing environment ($E_h = -401$ mV), suggesting it is also representative of ultra-basic subsurface fluids with small surface contributions. In the subsequent years, however, there was a shift towards a more bacterial dominated microbial community (i.e., greater than 79%) potentially reflecting a higher proportion of ultra-basic fluid in the pool.

Samples from WHC2c contained the largest proportions of cyanobacteria of all sites analyzed. It is likely that the high proportion of cyanobacteria at WHC2c relative WHC2a and WHC2b was due to the stratification of the WHC2 pool (Szponar et al., 2013) and little surface contributions reaching the bottom of the pool. While samples for WHC2a and WHC2b are sourced from the bottom of the pool, WHC2c is closer to the sunlight surface. This is further confirmed by the less reducing environment in WHC2c ($E_h = -227$ mV) relative to WHC2a and WHC2b ($E_h = -406$ and -401 mV, respectively). Furthermore, while the microbial community composition in WHC2c sampled in June 2010 was largely cyanobacterial (32%) followed by smaller proportions of gram-negative bacteria (23%) and bacteria (non-specific) (23%), the microbial community in August 2021 was dominated by bacteria (non-specific) (44%) followed by gram-negative bacteria (31%) with smaller amounts of cyanobacteria (25%). Cook et al. (2021; Chapter 2) plotted fluid from WHC2c (sampled in July 2018) on a Piper diagram and found that it did not plot in the mixed type-waters but rather in the Na-Cl Type water like WHC2a and WHC2b. This change in the aqueous geochemistry between sampling years likely influenced the shift in the microbial community composition observed between June 2010 and subsequent samples.

To better understand how the microbial community composition is influenced by the pH and the E_h of the fluid, the combined bacterial fraction (non-specific, gram-negative, and gram-positive bacteria) was plotted against the pH of the fluid (Figure 5.8A) and the E_h of the fluid (Figure 5.8B). The cyanobacteria fraction was not included in the combined bacterial fraction since it was assumed to be representative of surface contributions and not of ultra-basic fluids.

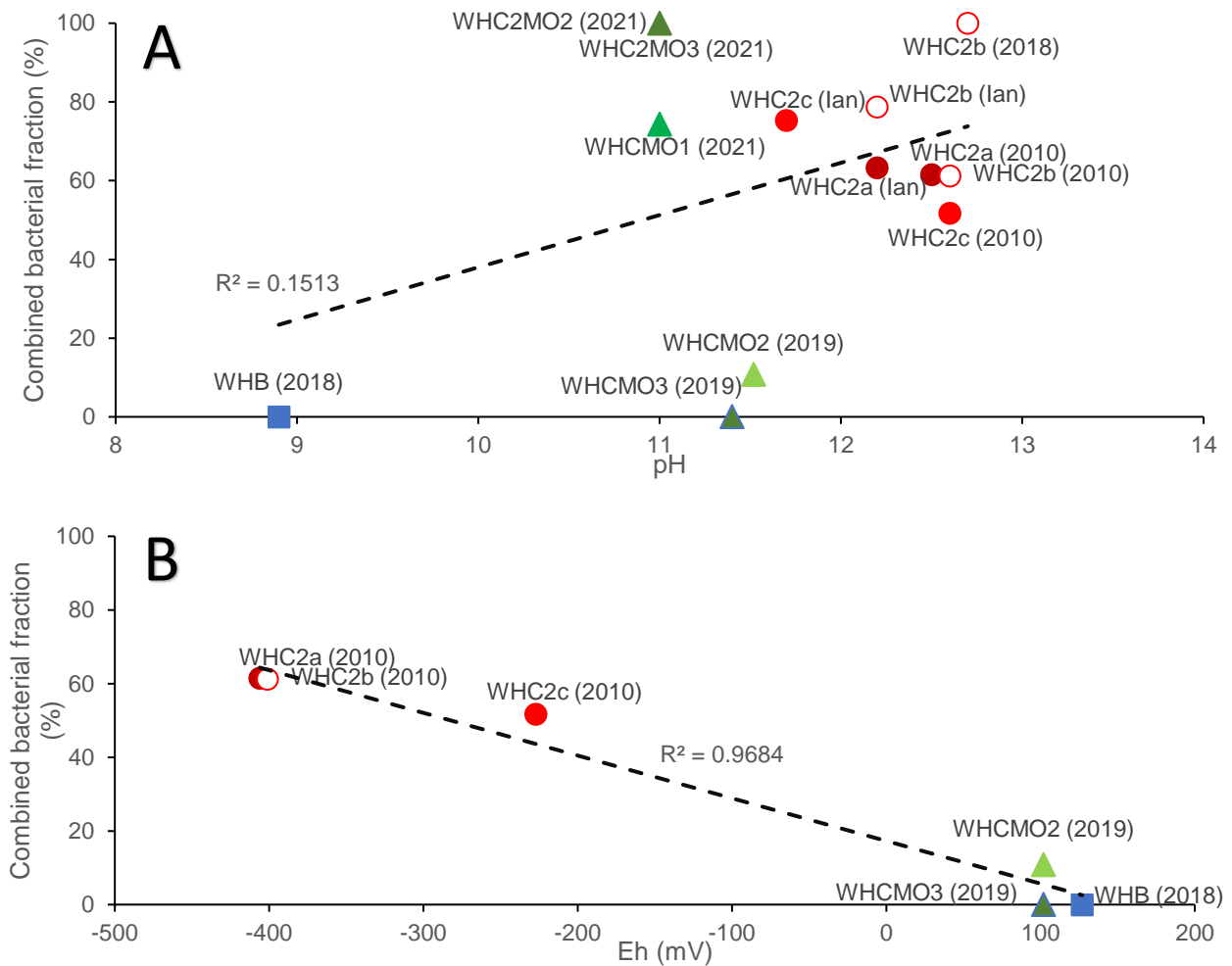


Figure 5.8. (A) Relationship between the pH of ultra-basic springs within the Tablelands and the combined bacterial fraction (%) and (B) relationship between the E_h of the ultra-basic springs within the Tablelands and the combined bacterial fraction (%). Note that the combined bacterial

fraction only includes non-specific, gram-negative, and gram-positive bacteria and only samples where data is available were plotted.

Figure 5.8A does not show any correlation ($R^2 = 0.15$) between the pH of the fluids and bacterial fraction, likely due to the buffering capacity of the ultra-basic fluids. Figure 5.8B, however, shows a negative correlation ($R^2 = 0.97$) between the bacterial fraction and the E_h of the fluid. Figure 5.8B suggests the extreme nature of the reducing ultra-basic fluids limits the diversity of the microbial community and there is a shift towards a more bacterial-dominated community. The shift in the microbial community indicates that ultra-basic reducing springs are fostering unique environments where only bacteria can thrive.

5.4.2 Biomass Variation at the Tablelands

The extreme geochemistry within the ultra-basic springs (i.e., high pH, low E_h , few electron acceptors) that results in a more bacterial dominated community also limits the growth of microorganisms which tends to result in low biomass (Schrenk et al., 2013; Schrenk et al., 2004; Tiago et al., 2004). It is therefore interesting that the highest total PLFA extracts from this study corresponded with the more subsurface sites influenced (i.e., WHC2b, WHC2b, WHMO1 (2021), WHCMO2 (2021), and WHCMO3 (2021)) relative to the more surface influenced sites (i.e., WHB and WHC2c). This is further supported by cell counts on fluids from WHB and WHC2 by Brazelton et al. (2013) who found higher numbers of cells in samples from WHC2 (ranging from 5.3 to 40.2×10^4 cells/mL) compared to those from WHB ($5.1 \pm 1.3 \times 10^4$ cells/mL). The Tablelands is not the only site of serpentinization where higher biomass has been reported associated with serpentinizing fluids relative to surface habitats. For example, higher

biomass has also been reported in surface-attached habitats where fluids that result from serpentinization reactions mix with oxic water at the Lost City carbonate chimneys (e.g., biofilms found at the Lost City carbonate chimneys) (Schrenk et al., 2013). It has been proposed that the higher biomass recorded at mixing sites is a result of the hydrogen, methane, and fermentative processes that are supplied to the microbial communities when these fluids mix (Schrenk et al., 2013). This mixing results in large quantities of available energy that could be exploited by microbial communities (Canovas et al., 2017; Cook et al., 2021b (Chapter 3)) and lead to higher biomass.

To further test hypothesize and to determine if the amount of available energy for metabolic reactions could have had an impact on the total biomass variation observed within serpentinite-hosted springs at the Tablelands, chemical affinities were calculated (Table 5.7). Table 5.7 demonstrates that although the A_r values differ among the eight metabolic reactions considered, the energy produced follows the same trend at all sites. Carbon monoxide oxidation is predicted to provide the greatest potential energy for all of the sites, followed by hydrogen oxidation and aerobic methanotrophy. The A_r values for these reactions, however, were largest in the subsurface site (i.e., WHCMO) and lowest in the mixing site (i.e., WHC2c). The only reaction that was predicted to provide more energy in the mixing site compared to the subsurface was the water-gas shift reaction where the A_r was 12 and 10 kcal/mol·e⁻, respectively.

Table 5.7. Affinities (A_r) (in kcal/mol·e⁻) of 8 possible reactions at the Tablelands organized by decreasing values of A_r .

Reaction	WHCMO	WHC2a	WHC2b	WHC2c
CO oxidation $\text{CO}_{(\text{aq})} + 0.5\text{O}_{2(\text{aq})} \leftrightarrow \text{CO}_{2(\text{aq})}$	32	31	31	30
Hydrogen oxidation $\text{H}_{2(\text{aq})} + 0.5\text{O}_{2(\text{aq})} \leftrightarrow \text{H}_2\text{O}$	28	28	28	26
Aerobic methanotrophy $\text{CH}_{4(\text{aq})} + 2\text{O}_{2(\text{aq})} \leftrightarrow \text{CO}_{2(\text{aq})} + 2\text{H}_2\text{O}$	24	24	24	24
Methanotrophy (nitrate) $8\text{NO}_3^- + 8\text{H}^+ + 5\text{CH}_{4(\text{aq})} \leftrightarrow 4\text{N}_{2(\text{aq})} + 5\text{CO}_{2(\text{aq})} + 14\text{H}_2\text{O}$	20	20	20	19
CO reduction $3\text{H}_{2(\text{aq})} + \text{CO}_{(\text{aq})} \leftrightarrow \text{CH}_{4(\text{aq})} + \text{H}_2\text{O}$	6	6	6	4
Water-gas shift $\text{CO}_{(\text{aq})} + \text{H}_2\text{O}_{(\text{aq})} \leftrightarrow \text{CO}_{2(\text{aq})} + \text{H}_2$	10	12	12	12
Methanogenesis (CO ₂) $\text{CO}_{2(\text{aq})} + 4\text{H}_{2(\text{aq})} \leftrightarrow \text{CH}_{4(\text{aq})} + 2\text{H}_2\text{O}$	4	3	3	2
Methanotrophy (sulfate) $\text{CH}_{4(\text{aq})} + \text{SO}_4^{2-}{}_{(\text{aq})} \leftrightarrow \text{HCO}_3^-{}_{(\text{aq})} + \text{HS}^- + 2\text{H}_2\text{O}$	0	1	1	0

To further understand the available energy at each site and how it would be impacted by the limiting reactant (i.e., the electron acceptor or electron donor), the energy densities (E_r) were calculated (Table 5.8). The energy density calculations shifted the likely reactions compared to the A_r calculations. WHCMO, WHC2a and WHC2b all followed the same trend whereby hydrogen oxidation, aerobic methanotrophy, and carbon monoxide oxidation were most favoured and anaerobic methanotrophy was least. At WHC2c, however, aerobic methanotrophy was the most favoured followed by carbon monoxide oxidation and hydrogen oxidation. The least favoured was carbon monoxide reduction. In addition to having different likely reactions, the highest E_r values at WHC2c were 2 orders of magnitude lower than the highest E_r values at WHCMO. Unfortunately, geochemical data is not available for all years, so it is not possible to comment on fluctuations in total biomass between years at the sites. However, it is worth noting that the sites where the highest total biomass was detected (i.e., WHCMO, WHC2a, and

WHC2b) correspond to the sites where the thermodynamic predictions suggest there would be more available energy.

Table 5.8. Energy densities (E_r) (in kcal/L H_2O) of 8 possible reactions at the Tablelands organized by decreasing values of A_r .

Reaction	WHCMO	WHC2a	WHC2b	WHC2c
CO oxidation $CO_{(aq)} + 0.5O_{2(aq)} \leftrightarrow CO_{2(aq)}$	2.88×10^{-3}	6.20×10^{-5}	6.20×10^{-5}	5.90×10^{-5}
Hydrogen oxidation $H_{2(aq)} + 0.5O_{2(aq)} \leftrightarrow H_2O$	1.12×10^{-2}	1.10×10^{-4}	1.10×10^{-4}	5.10×10^{-5}
Aerobic methanotrophy $CH_{4(aq)} + 2O_{2(aq)} \leftrightarrow CO_{2(aq)} + 2H_2O$	9.75×10^{-4}	9.55×10^{-5}	9.55×10^{-5}	3.88×10^{-4}
Methanotrophy (nitrate) $8NO_3^- + 8H^+ + 5CH_{4(aq)} \leftrightarrow 4N_{2(aq)} + 5CO_{2(aq)} + 14H_2O$	4.42×10^{-11}	5.63×10^{-11}	5.35×10^{-11}	4.31×10^{-11}
CO reduction $3H_{2(aq)} + CO_{(aq)} \leftrightarrow CH_{4(aq)} + H_2O$	1.67×10^{-3}	3.40×10^{-5}	3.40×10^{-5}	3.28×10^{-13}
Water-gas shift $CO_{(aq)} + H_2O_{(aq)} \leftrightarrow CO_{2(aq)} + H_2$	8.96×10^{-4}	2.30×10^{-5}	2.30×10^{-5}	2.39×10^{-5}
Methanogenesis (CO_2) $CO_{2(aq)} + 4H_{2(aq)} \leftrightarrow CH_{4(aq)} + 2H_2O$	1.45×10^{-4}	2.70×10^{-5}	2.70×10^{-5}	4.00×10^{-6}
Methanotrophy (sulfate) $CH_{4(aq)} + SO_4^{2-}{}_{(aq)} \leftrightarrow HCO_3^-{}_{(aq)} + HS^- + 2H_2O$	1.05×10^{-8}	3.35×10^{-8}	1.13×10^{-8}	2.65×10^{-8}

To determine the relationship between the total biomass and the geochemistry of the fluids, the sum of all E_r values and total biomass were plotted against the E_h of the fluids from each site (Fig 5.9).

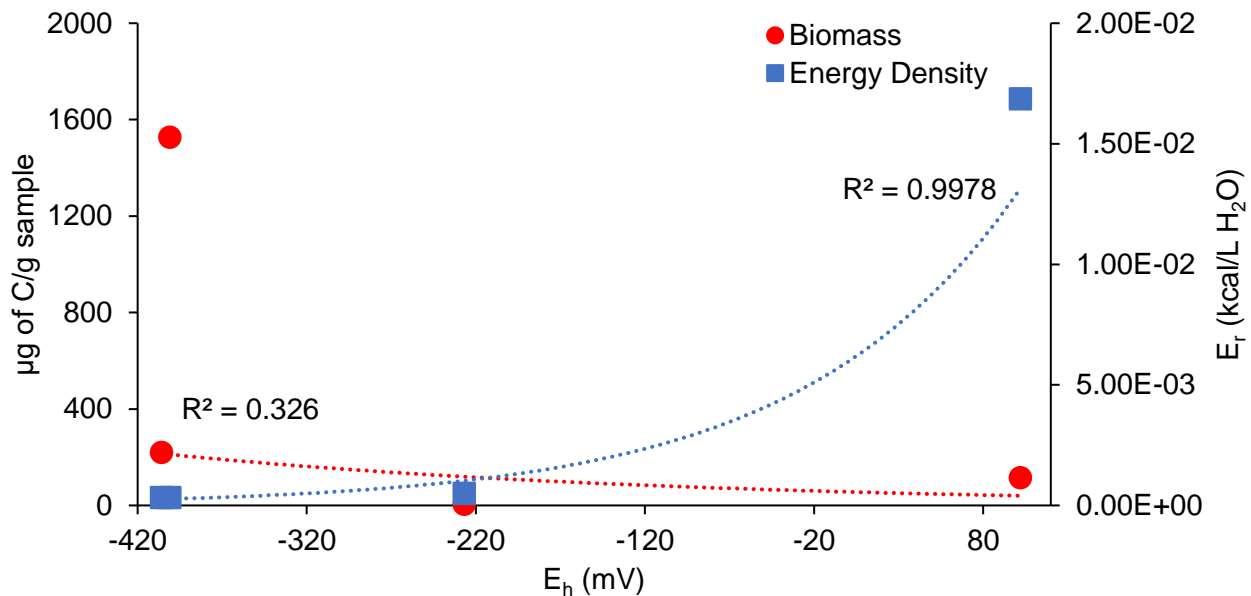


Fig 5.9. Relationship between the total PLFA biomass extracted from WHC2a, WHC2b, WHC2c, and WHCMO ($\mu\text{g of C/g sample}$), the sum of energy densities ($\text{kcal/L H}_2\text{O}$) and E_h (mV).

Although there was a correlation between the E_r values and the E_h of the fluids ($R^2 = 0.99$), there was no correlation between the total biomass and E_h of the fluids ($R^2 = 0.33$).

Although the E_r calculations suggested that the more reducing fluids would have lower available energy for microbial metabolisms, it was not reflected in the total biomass. By contrast, the highest total biomass was found in the more reducing fluids suggesting that more serpentinized fluids had higher biomass.

5.4.3 Relevance to Mars Missions

While the surface of Mars is likely inhabitable due to the lack of a magnetic field and resulting solar wind particles that reach the surface, it is possible that the subsurface of Mars could provide a habitable environment for chemolithoautotrophs. These microorganisms would require chemical (i.e., non-photosynthetic) sources of energy and the serpentinization reaction

could provide this through production of H_2 . The results of this study demonstrate suggest that sites of terrestrial serpentinization harbour uniquely adapted microbial communities that are distinct from surface communities. These microbial communities appear to be directly influenced by the geochemical parameters resulting from serpentinization reactions (i.e., the reducing fluids). While microbial communities in mixing zones are more diverse and composed of eukaryotes, fungi, cyanobacteria as well as bacteria, as the fluids become more dominated by subsurface ultra-basic inputs (i.e., become more reducing), the microbial community appears to shift towards more bacterial dominated. Furthermore, based on total PLFA extracts, it appears that sites that are mostly composed of ultra-basic fluids contain more biomass than those that are more representative of oxic surface waters.

Although thermodynamic calculations (A_r and E_r) suggest that sites of serpentinization (i.e., reducing fluids) have less potential energy available to support microbial metabolisms, this was not reflected in the total biomass extracted from sediments in this study. This high biomass in subsurface samples is important when considering potential habitable environments extraterrestrially specifically sites of serpentinization in the subsurface of Mars where solar radiation cannot penetrate. The results of this study suggest that despite thermodynamic predictions suggesting lower available energy, the subsurface reducing fluids harbour more biomass than mixing pools with more surface contributions.

It is important to understand how fluid geochemistry influences the microbial community composition and total biomass when identifying locations to search for potential life outside of Earth. This study suggests that subsurface serpentinite-hosted springs are good proxies for Mars and that they harbour microbial communities with high biomass. Furthermore, the geochemistry of these fluids can be used as a good indicator of the microbial community composition. While

previous missions have been unsuccessful in identifying extinct or extant life on Mars (Biemann et al., 1977; Biemann et al., 1976), the strategy in the search for life extra-terrestrially remains one based on water availability and the possibility of thermodynamically favorable reactions that could be exploited by life. Although no site of serpentinization has been chosen for any past mission to Mars, the results of this study suggest that there is a strong potential to find bacterial-dominated microbial communities at these sites.

5.6 Acknowledgments

The authors would like to thank Parks Canada for providing access to the Tablelands. The authors would also like to thank Matthew Schrenk, Ben Taylor, and Michael Babechuk for their help in the field, and Geert van Biesen (CREAIT – Stable Isotope Laboratory) and Inês Nobre Silva (CREAIT – ICPMS) for their expertise. This research was funded by Natural Science and Engineering Research Council (NSERC) Discovery Grant and Canada Space Agency’s Flights and Fieldwork for the Advancement of Science and Technology (FAST) grant awarded to Dr. Penny Morrill and NSERC’s Alexander Graham Bell Canada Graduate Scholarship-Doctoral (CGS D) awarded to Melissa Cook.

5.7 References

- Amend, J. P., & Shock, E. L. (2001). Energetics of overall metabolic reactions of thermophilic and hyperthermophilic Archaea and Bacteria. *FEMS Microbiology Reviews*, 25(2), 175-243. <https://doi.org/10.1111/j.1574-6976.2001.tb00576.x>
- Biemann, K., Oro, J., Toulmin III, P., Orgel, L. E., Nier, A. O., Anderson, D. M., Simmonds, P. G., Flory, D., Diaz, A. V., Rushneck, D. R., Biller, J. E., & Lafleur, A. L. (1977). The search for organic substances and inorganic volatile compounds in the surface of Mars. *Journal of Geophysical Research (1896-1977)*, 82(28), 4641-4658. <https://doi.org/https://doi.org/10.1029/JS082i028p04641>
- Biemann, K., Oro, J., Toulmin, P., Orgel, L. E., Nier, A. O., Anderson, D. M., Simmonds, P. G., Flory, D., Diaz, A. V., Rushneck, D. R., & Biller, J. A. (1976). Search for Organic and Volatile Inorganic Compounds in Two Surface Samples from the Chryse Planitia Region of Mars. *Science*, 194(4260), 72-76. <https://doi.org/doi:10.1126/science.194.4260.72>
- Boschker, H. T. S., Nold, s. c., Wellsbury, P., Bos, D., De Graaf, W., Pel, R., Parkes, R. J., & Cappenberg, T. E. (1998). Direct linking of microbial populations to specific biogeochemical processes by ¹³C-labelling of biomarkers. *Nature (London)*, 392(6678), 801-805. <https://doi.org/10.1038/33900>
- Boston, P. J., Ivanov, M. V., & P. McKay, C. (1992). On the possibility of chemosynthetic ecosystems in subsurface habitats on Mars. *Icarus (New York, N.Y. 1962)*, 95(2), 300-308. [https://doi.org/10.1016/0019-1035\(92\)90045-9](https://doi.org/10.1016/0019-1035(92)90045-9)
- Brazelton, W. J., Morrill, P. L., Szponar, N., & Schrenk, M. O. (2013). Bacterial Communities Associated with Subsurface Geochemical Processes in Continental Serpentinite Springs.

- Applied and Environmental Microbiology*, 79(13), 3906-3916.
<https://doi.org/10.1128/AEM.00330-13>
- Brazelton, W. J., Nelson, B., & Schrenk, M. O. (2012). Metagenomic Evidence for H₂ Oxidation and H₂ Production by Serpentinite-Hosted Subsurface Microbial Communities. *Frontiers in Microbiology*, 2. <https://doi.org/10.3389/fmicb.2011.00268>
- Canovas, P. A., Hoehler, T., & Shock, E. L. (2017). Geochemical bioenergetics during low-temperature serpentinization: An example from the Samail ophiolite, Sultanate of Oman. *Journal of Geophysical Research: Biogeosciences*, 122(7), 1821-1847.
<https://doi.org/https://doi.org/10.1002/2017JG003825>
- Cook, M. C., Blank, J. G., Rietze, A., Suzuki, S., Nealson, K. H., & Morrill, P. L. (2021). A Geochemical Comparison of Three Terrestrial Sites of Serpentinization: The Tablelands, The Cedars, and Aqua de Ney. *Journal of geophysical research. Biogeosciences*.
<https://doi.org/10.1029/2021JG006316>
- Cook, M. C., Blank, J. G., Suzuki, S., Nealson, K. H., & Morrill, P. L. (2021b). Assessing Geochemical Bioenergetics and Microbial Metabolisms at Three Terrestrial Sites of Serpentinization: The Tablelands (NL, CAN), The Cedars (CA, USA), and Aqua de Ney (CA, USA). *Journal of geophysical research. Biogeosciences*, 126(6).
<https://doi.org/10.1029/2019JG005542>
- Coplen, T. B. (2011). Guidelines and recommended terms for expression of stable-isotope-ratio and gas-ratio measurement results: Guidelines and recommended terms for expressing stable isotope results. *Rapid communications in mass spectrometry*, 25(17), 2538-2560.
<https://doi.org/10.1002/rcm.5129>

- Cowie, B. R., Greenberg, B. M., & Slater, G. F. (2010). Determination of Microbial Carbon Sources and Cycling during Remediation of Petroleum Hydrocarbon Impacted Soil Using Natural Abundance ^{14}C Analysis of PLFA. *Environmental science & technology*, *44*(7), 2322-2327. <https://doi.org/10.1021/es9029717>
- Cumming, E. A., Rietze, A., Morrissey, L. S., Cook, M. C., Rhim, J. H., Ono, S., & Morrill, P. L. (2019). Potential sources of dissolved methane at the Tablelands, Gros Morne National Park, NL, CAN: A terrestrial site of serpentinization. *Chemical geology*, *514*, 42-53. <https://doi.org/10.1016/j.chemgeo.2019.03.019>
- Danovaro, R., Dell'Anno, A., Corinaldesi, C., Magagnini, M., Noble, R., Tamburini, C., & Weinbauer, M. (2008). Major viral impact on the functioning of benthic deep-sea ecosystems. *Nature*, *454*, 1084-1109. <https://doi.org/10.1038/nature07268>
- Ehlmann, B. L., Mustard, J. F., & Murchie, S. L. (2010). Geologic setting of serpentine deposits on Mars. *Geophysical research letters*, *37*(6), n/a. <https://doi.org/10.1029/2010GL042596>
- Ehlmann, B. L., Mustard, J. F., Murchie, S. L., Bibring, J.-P., Meunier, A., Fraeman, A. A., & Langevin, Y. (2011). Subsurface water and clay mineral formation during the early history of Mars. *Nature (London)*, *479*(7371), 53-60. <https://doi.org/10.1038/nature10582>
- Etioppe, G., Schoell, M., & Hosgörmez, H. (2011). Abiotic methane flux from the Chimaera seep and Tekirova ophiolites (Turkey): Understanding gas exhalation from low temperature serpentinization and implications for Mars. *Earth and planetary science letters*, *310*(1), 96-104. <https://doi.org/10.1016/j.epsl.2011.08.001>
- Formisano, V., Atreya, S., Encrenaz, T., Ignatiev, N., & Giuranna, M. (2004). Detection of Methane in the Atmosphere of Mars. *Science (American Association for the Advancement of Science)*, *306*(5702), 1758-1761. <https://doi.org/10.1126/science.1101732>

- Frostegård, Å., & Bååth, E. (1996). The use of phospholipid fatty acid analysis to estimate bacterial and fungal biomass in soil. *Biology and fertility of soils*, 22(1-2), 59-65.
<https://doi.org/10.1007/BF00384433>
- Frostegård, Å., Bååth, E., & Tunlio, A. (1993). Shifts in the structure of soil microbial communities in limed forests as revealed by phospholipid fatty acid analysis. *Soil biology & biochemistry*, 25(6), 723-730. [https://doi.org/10.1016/0038-0717\(93\)90113-P](https://doi.org/10.1016/0038-0717(93)90113-P)
- Harmon, C. (1961). Isotopic Variations in Meteoric Waters. *Science (American Association for the Advancement of Science)*, 133(3465), 1702-1703.
<https://doi.org/10.1126/science.133.3465.1702>
- Hinrichs, K.-U., Lipp, J. S., Morono, Y., & Inagaki, F. (2008). Significant contribution of Archaea to extant biomass in marine subsurface sediments. *Nature (London)*, 454(7207), 991-994. <https://doi.org/10.1038/nature07174>
- Khatua, S., Pandey, A., & Bisway, S. J. (2016). Phytochemical evaluation and antimicrobial properties of *Trichosanthes dioica* root extract. *Journal of Pharmacognosy and Phytochemistry*, 5(5), 410-413.
- LaRowe, D., & Amend, J. (2014). Energetic constraints on life in marine deep sediments. In (Vol. 1, pp. 279-302). DE GRUYTER. <https://doi.org/10.1515/9783110300130.279>
- Marche, B. (2016). *A Climate Study in Western Newfoundland: Precipitation d18O and d2H Examination Using Picarro L2130-I Liquid Water Isotope Analyzer* Memorial University of Newfoundland]. Corner Brook, Newfoundland.
- Michalski, J. R., Cuadros, J., Niles, P. B., Parnell, J., Deanne Rogers, A., & Wright, S. P. (2013). Groundwater activity on Mars and implications for a deep biosphere. *Nature geoscience*, 6(2), 133-138. <https://doi.org/10.1038/ngeo1706>

- Miller, H. M., Matter, J. M., Kelemen, P., Ellison, E. T., Conrad, M. E., Fierer, N., Ruchala, T., Tominaga, M., & Templeton, A. S. (2016). Modern water/rock reactions in Oman hyperalkaline peridotite aquifers and implications for microbial habitability. *Geochimica et cosmochimica acta*, 179(C), 217-241. <https://doi.org/10.1016/j.gca.2016.01.033>
- Morrill, P. L., Brazelton, W. J., Kohl, L., Rietze, A., Miles, S. M., Kavanagh, H., Schrenk, M. O., Ziegler, S. E., & Lang, S. Q. (2014). Investigations of potential microbial methanogenic and carbon monoxide utilization pathways in ultra-basic reducing springs associated with present-day continental serpentinization: the Tablelands, NL, CAN. *Frontiers in Microbiology*, 5. <https://doi.org/10.3389/fmicb.2014.00613>
- Morrill, P. L., Kuenen, J. G., Johnson, O. J., Suzuki, S., Rietze, A., Sessions, A. L., Fogel, M. L., & Nealson, K. H. (2013). Geochemistry and geobiology of a present-day serpentinization site in California: The Cedars. *Geochimica et cosmochimica acta*, 109, 222-240. <https://doi.org/10.1016/j.gca.2013.01.043>
- Mumma, M. J., Villanueva, G. L., Novak, R. E., Hewagama, T., Bonev, B. P., Disanti, M. A., Mandell, A. M., & Smith, M. D. (2009). Strong Release of Methane on Mars in Northern Summer 2003. *Science (American Association for the Advancement of Science)*, 323(5917), 1041-1045. <https://doi.org/10.1126/science.1165243>
- Murseli, S., Middlestead, P., St-Jean, G., Zhao, X., Jean, C., Crann, C. A., Kieser, W. E., & Clark, I. D. (2019). The Preparation of Water (DIC, DOC) and Gas (CO₂, CH₄) Samples for Radiocarbon Analysis at AEL-AMS, Ottawa, Canada. *Radiocarbon*, 61(5), 1563-1571. <https://doi.org/10.1017/RDC.2019.14>

- Nealson, K. H., Inagaki, F., & Takai, K. (2005). Hydrogen-driven subsurface lithoautotrophic microbial ecosystems (SLiMEs): do they exist and why should we care? *Trends in microbiology (Regular ed.)*, *13*(9), 405-410. <https://doi.org/10.1016/j.tim.2005.07.010>
- Neubeck, A., Sun, L., Müller, B., Ivarsson, M., Hosgörmez, H., Özcan, D., Broman, C., & Schnürer, A. (2017). Microbial Community Structure in a Serpentine-Hosted Abiotic Gas Seepage at the Chimaera Ophiolite, Turkey. *Applied and Environmental Microbiology*, *83*(12). <https://doi.org/10.1128/AEM.03430-16>
- O'Leary, W. M., & Wilkinson, S. G. (1988). *Gram-positive bacteria* (Vol. 1). London Academic Press.
- Oremland, R. S., Miller, L. G., & Whiticar, M. J. (1987). Sources and flux of natural gases from Mono Lake, California. *Geochimica et cosmochimica acta*, *51*(11), 2915-2929. [https://doi.org/10.1016/0016-7037\(87\)90367-X](https://doi.org/10.1016/0016-7037(87)90367-X)
- Piper, A. M. (1953). *A graphic procedure in the geochemical interpretation of water analysis / by Arthur M. Piper*. District of Columbia: U.S. Dept. of the Interior, Geological Survey, Water Resources Division, Ground Water Branch, 1953.
- Rempfert, K. R., Miller, H. M., Bompard, N., Nothaft, D., Matter, J. M., Kelemen, P., Fierer, N., & Templeton, A. S. (2017). Geological and Geochemical Controls on Subsurface Microbial Life in the Samail Ophiolite, Oman. *Frontiers in Microbiology*, *8*, 56-56. <https://doi.org/10.3389/fmicb.2017.00056>
- Rency, R., Vasantha, K., & Maruthasalam, A. (2015). Identification of bioactive compounds from ethanolic leaf extracts of *Premnaser ratifolia* L. using GC-MS. *Bioscience Discovery*, *6*(2), 96-101.

- Rietze, A. (2015). *Investigating geochemistry and habitability of continental sites of serpentinization: the Cedars, California, USA and the Tablelands, Newfoundland, CAN* Memorial University of Newfoundland].
- Routaboul, J. M., Fischer, S. F., & Browse, J. (2000). Trienoic Fatty Acids Are Required to Maintain Chloroplast Function at Low Temperatures. *Plant physiology (Bethesda)*, 124(4), 1697-1705. <https://doi.org/10.1104/pp.124.4.1697>
- Rudd, J. W. M., Hamilton, R. D., & Campbell, N. E. R. (1974). Measurement of Microbial Oxidation of Methane in Lake Water. *Limnology and oceanography*, 19(3), 519-524. <https://doi.org/10.4319/lo.1974.19.3.0519>
- Schrenk, M. O., Brazelton, W. J., & Lang, S. Q. (2013). Serpentinization, carbon, and deep life. *Reviews in mineralogy and geochemistry*, 75(1), 575-606. <https://doi.org/10.2138/rmg.2013.75.18>
- Sinninghe Damsté, J. S., Kuypers, M. M. M., Sliemers, O., Lavik, G., Schmid, M., Jørgensen, B. B., Kuenen, J. G., Strous, M., & Jetten, M. S. M. (2003). Anaerobic ammonium oxidation by Anammox bacteria in the Black Sea. *Nature (London)*, 422(6932), 608-611. <https://doi.org/10.1038/nature01472>
- Sleep, N. H., Meibom, A., Th, F., Coleman, R. G., & Bird, D. K. (2004). H₂-Rich Fluids from Serpentinization: Geochemical and Biotic Implications. *Proceedings of the National Academy of Sciences - PNAS*, 101(35), 12818-12823. <https://doi.org/10.1073/pnas.0405289101>
- St-Jean, G. (2003). Automated quantitative and isotopic (¹³C) analysis of dissolved inorganic carbon and dissolved organic carbon in continuous-flow using a total organic carbon

- analyser. *Rapid communications in mass spectrometry*, 17(5), 419-428.
<https://doi.org/10.1002/rcm.926>
- Szponar, N. (2012). *Carbon Cycling at a Site of Present-Day Serpentinization: The Tablelands, Gros Morne National Park* Memorial University of Newfoundland].
- Szponar, N., Brazelton, W. J., Schrenk, M. O., Bower, D. M., Steele, A., & Morrill, P. L. (2013). Geochemistry of a continental site of serpentinization, the Tablelands Ophiolite, Gros Morne National Park: A Mars analogue. *Icarus (New York, N.Y. 1962)*, 224(2), 286-296.
<https://doi.org/10.1016/j.icarus.2012.07.004>
- Vance, S., Harnmeijer, J., Kimura, J., Hussmann, H., Demartin, B., & Brown, J. M. (2007). Hydrothermal systems in small ocean planets. *Astrobiology*, 7(6), 987-1005.
<https://doi.org/10.1089/ast.2007.0075>
- Vance, S. D., & Daswani, M. M. (2020). Serpentinite and the search for life beyond Earth. *Philosophical transactions of the Royal Society of London. Series A: Mathematical, physical, and engineering sciences*, 378(2165), 20180421-20180421.
<https://doi.org/10.1098/rsta.2018.0421>
- Viviano-Beck, C. E., Murchie, S. L., Beck, A. W., & Dohm, J. M. (2017). Compositional and structural constraints on the geologic history of eastern Tharsis Rise, Mars. *Icarus (New York, N.Y. 1962)*, 284, 43-58. <https://doi.org/10.1016/j.icarus.2016.09.005>
- Volkman, J. K., Jeffrey, S. W., Nichols, P. D., Rogers, G. I., & Garland, C. D. (1989). Fatty acid and lipid composition of 10 species of microalgae used in mariculture. *Journal of experimental marine biology and ecology*, 128(3), 219-240. [https://doi.org/10.1016/0022-0981\(89\)90029-4](https://doi.org/10.1016/0022-0981(89)90029-4)

- Wang, D., T. , Gruen, D. S., Sherwood Lollar, B., Kai-Uwe, H., Lucy, C. S., James, F. H., Alexander, N. H., John, W. P., Penny, L. M., Martin, K., Kyle, B. D., Eoghan, P. R., Chelsea, N. S., Daniel, J. R., Jeffrey, S. S., Jennifer, C. M., Harold, F. H., Michael, D. K., Dawn, C., Tori, M. H., & Shuhei, O. (2015). Nonequilibrium clumped isotope signals in microbial methane. *Science (American Association for the Advancement of Science)*, 348(6233), 428-431. <https://doi.org/10.1126/science.aaa4326>
- White, D. C., Stair, J. O., & Ringelberg, D. B. (1996). Quantitative comparisons of in situ microbial biodiversity by signature biomarker analysis: Microbial diversity. I. *Journal of industrial microbiology*, 17(3-4), 185-196.
- Wilson, J., Munizzi, J., & Erhardt, A. M. (2020). Preservation methods for the isotopic composition of dissolved carbon species in non-ideal conditions. *Rapid communications in mass spectrometry*, 34(21), e8903-n/a. <https://doi.org/10.1002/rcm.8903>
- Yang, M., Yang, D., & Yu, X. (2018). Soil microbial communities and enzyme activities in seabuckthorn (*Hippophae rhamnoides*) plantation at different ages. *PloS one*, 13(1), e0190959-e0190959. <https://doi.org/10.1371/journal.pone.0190959>
- YSI. (2005). *Measuring ORP on YSI 6-Series Sondes: Tips, Cautions and Limitations*. <https://www.yei.com/File%20Library/Documents/Technical%20Notes/T608-Measuring-ORP-on-YSI-6-Series-Sondes-Tips-Cautions-and-Limitations.pdf>
- Zelles, L. (1999). Fatty acid patterns of phospholipids and lipopolysaccharides in the characterisation of microbial communities in soil: a review. *Biology and fertility of soils*, 29(2), 111-129. <https://doi.org/10.1007/s003740050533>

5.8 Supplemental Information

Table 5.S1. Activity coefficients (γ) and activities calculated using the Debye-Hückel equation.

Analyte	WHCMO		WHC2a		WHC2b		WHC2c	
	γ	Activity	γ	Activity	γ	Activity	γ	Activity
H ₂	1	4.64 x 10 ⁻⁴	1	4.72 x 10 ⁻⁴	1	5.29 x 10 ⁻⁴	1	1.00 x 10 ⁻⁶
O ₂	1	1.00 x 10 ⁻⁶	1	1.00 x 10 ⁻⁶	1	1.00 x 10 ⁻⁶	1	1.00 x 10 ⁻⁶
CO	1	1.00 x 10 ⁻⁶	1	1.00 x 10 ⁻⁶	1	1.00 x 10 ⁻⁶	1	1.00 x 10 ⁻⁶
CO ₂	1	1.00 x 10 ⁻⁶	1	1.00 x 10 ⁻⁶	1	1.00 x 10 ⁻⁶	1	1.08 x 10 ⁻⁴
CH ₄	1	5.00 x 10 ⁻⁶	1	2.60 x 10 ⁻⁵	1	3.70 x 10 ⁻⁵	1	1.30 x 10 ⁻⁵
SO ₄ ²⁻	0.63	3.49 x 10 ⁻⁹	0.62	8.38 x 10 ⁻⁹	0.50	2.26 x 10 ⁻⁹	0.68	8.85 x 10 ⁻⁹
HCO ₃ ⁻	0.63	3.59 x 10 ⁻⁵	0.62	1.42 x 10 ⁻⁴	0.50	9.07 x 10 ⁻⁶	0.68	9.53 x 10 ⁻⁴
HS ⁻	0.89	8.90 x 10 ⁻⁷	0.89	8.90 x 10 ⁻⁷	0.84	8.40 x 10 ⁻⁷	0.91	9.10 x 10 ⁻⁷
NO ₃ ⁻	0.89	8.18 x 10 ⁻⁹	0.89	8.14 x 10 ⁻⁹	0.83	9.54 x 10 ⁻¹⁰	0.91	2.51 x 10 ⁻⁹

Chapter 6. Summary

6.1 Conclusions

Serpentinization reactions produce fluids that are ultra-basic ($\text{pH} > 11$), reducing, and depleted in electron acceptors. Although these conditions are considered challenging for life, microbial communities have been identified at sites of terrestrial serpentinization. The range of geochemistry that can exist at these sites and how it influences the microbial communities that inhabit these serpentinized fluids were not well constrained. Therefore, the second chapter of this thesis characterized the range of geochemistry at three distinct sites of serpentinization: The Cedars (CA, USA), Aqua de Ney (CA, USA), and the Tablelands (NL, CAN). The Tablelands ophiolite had the oldest date of emplacement of the sites studied, The Cedars was the only site where microbial methanogenesis had previously been identified (Morrill et al., 2013; Kohl et al., 2016), and Aqua de Ney was the only site known to have high sulfur concentrations (Feth et al., 1961). Isotopic and compositional analyses on the methane from these sites revealed the methane was non-microbial in origin at the Tablelands and abiogenic at Aqua de Ney. Furthermore, despite being a product of the serpentinization reaction, no hydrogen was identified at Aqua de Ney. This was likely due to the formation of abiogenic methane as well as the reaction of the hydrogen with sulfate in the system to produce hydrogen sulfide. Despite the geochemical differences between the sites, many commonalities were identified between the sites including their ultra-basic reducing fluids that are rich in Cl, Na, K and Br as well as depleted concentrations of Mg.

The third chapter of this thesis applied the geochemical results from Chapter 2, to create thermodynamic predictions (A_r) for possible metabolic reactions associated with sites of terrestrial serpentinization. The A_r results were then ranked and compared between sites and reactions to determine which microbial metabolisms were likely at sites of terrestrial

serpentinization. Although the chemical affinities were similar between The Cedars, Aqua de Ney, and the Tablelands, there was variation among the reactions calculated. For example, the results suggested that carbon monoxide oxidation was the reaction that would provide the most energy at The Cedars, the Tablelands, and Aqua de Ney, followed by hydrogen oxidation and methanotrophy. The results also suggested that methanogenesis via carbon dioxide reduction and methanogenesis with formate acting as the electron donor, would yield little to no energy at the sites and was therefore unlikely to be observed. These possible metabolisms were then tested through construction of microcosm experiments using material from The Cedars, the Tablelands, or Aqua de Ney. Despite having the highest calculated chemical affinity, carbon monoxide oxidation, hydrogen oxidation, and methanotrophy were not observed. Evidence of methanogenesis was observed in microcosms using material from The Cedars despite the A_r predictions and the oxic environment created in the microcosms. These results demonstrate the resilience of methanogens at The Cedars.

The fourth chapter of this thesis used lipid biomarkers to create a profile of the microbial communities present at The Cedars. Because lipids can be preserved in the rock record for long periods of time, they allow a better understanding of both extinct and extant microbial communities than other techniques. Therefore, this chapter also compares the results of the lipid biomarkers to previously published genomic studies to create a better overview of microbial communities at The Cedars. Although not all lipids present in the samples from The Cedars could be identified, those that were identified were mostly diacylglycerols (DAGs), lipids that can be involved in many eukaryotic and bacterial metabolic pathways. No archaeal lipid biomarkers were detected in this study which is consistent with previously published genomic studies on The Cedars that also identified a mostly bacterial community composition at The

Cedars (Suzuki et al., 2013). Furthermore, despite isotopic geochemical evidence that the methane from The Cedars is microbial in source and the presence of a single archaeal phylotype that places closely to *Methanosarcinales* in the phylogenetic tree, no lipids indicative of methanogens could be detected. Chlorophyll *a* and pheophytin *a*, pigments associated with photosynthetic organisms, were detected in carbonate samples from BSC. This is consistent with results from Suzuki et al. (2013) where cyanobacteria were detected in the carbonate from BSC. Since recent studies have suggested that cyanobacteria are capable of methane production (Bizic et al., 2021), it is possible that cyanobacteria could be contributing to the overall methane budget at The Cedars. This could help explain the results from Chapter 3, where methanogenesis was observed despite an oxic environment.

In the fifth chapter of this thesis, three different locations at an active site of serpentinization, Winterhouse Canyon (WHC) at the Tablelands, NL, were geochemically analyzed and their microbial community composition was determined using phospholipid fatty acid (PLFA) biomarkers. First a nearby brook (WHB) which represented the oxic surface water at the Tablelands was analyzed. Next, a pool (WHC2) where ultra-basic fluids mix with oxic surface waters was analyzed. Finally, in order to isolate the subsurface fluids and understand the differences in geochemistry and microbial community composition between the mixed pools and subsurface waters, a microbial observatory (WHCMO) was established. This was done by drilling a series of three boreholes and inserting flow-through incubators that contained sterilized crushed ultramafic rock. The PLFA biomarkers revealed while the mixing sites had a diverse microbial community, as fluids became more reducing, there was a shift to a microbial community dominated by bacteria. Furthermore, although energy density calculations suggested that subsurface sites would have lower biomass than mixing sites, the sites with the highest

biomass were the more reducing sites. The results of this chapter suggest that when searching for life on other planetary bodies, there is a strong potential to find bacteria dominated microbial communities with high biomass at sites of serpentinization in the subsurface where solar radiation cannot penetrate.

6.2 Outlook

Although the results of this thesis help further the understanding of the fluid geochemistry and its influence on native microbial communities at sites of terrestrial serpentinization, the results also generate important questions that should be the focus of future research. For example, why there is variation between the microbial communities at sites of terrestrial serpentinization despite consistent thermodynamic predictions of available energy between sites is still not understood. Although chemical affinities were calculated for the mixing sites and ultra-basic endmembers, these could be expanded by calculating energy densities which take into account the limiting electron acceptor or donor. Energy densities could help explain the observed variation in microbial metabolisms between The Cedars, the Tablelands, and Aqua de Ney (Ch. 3).

Furthermore, despite thermodynamic predictions that methanogenesis should not be supported at sites of terrestrial serpentinization, methanogenesis continues to be observed in ultra-basic pools at The Cedars. Further research is required to determine why microbial methanogenesis occurs at The Cedars but not at Aqua de Ney or the Tablelands. Despite evidence of microbial methanogenesis at The Cedars (e.g., Cook et al. (2021b; Chapter 3)), no lipids indicative of methanogens were detected at The Cedars. Although the lipid data clearly suggests the microbial community at The Cedars is dominated by Bacteria and that the archaeal microbial community is small, future research into the lack of lipids indicative of methanogens is

required. It is possible that methanogens are only located deep in the subsurface and are not present in the fluids sampled at the surface. However, it is worth noting that fluid and carbonate samples for the microcosms where methanogenesis was observed were taken from the same location. Therefore, future research should include genomic analysis of the fluids and carbonate used in microcosm experiments as well as determining whether cyanobacteria could be contributing to the methane detected in the microcosm experiments (Cook et al., 2021b; Chapter 3).

While PLFA biomarkers provided a general overview of the extant microbial community at the time of sampling (Chapter 5), they cannot provide information on extinct life. Biomarkers indicative of extinct microbial life are important when considering past serpentinization on other planetary bodies. Lipid biomarkers (Chapter 4), although not as well constrained, can provide information about extant and extinct microbial communities. Furthermore, in addition to being preserved in fluids and carbonate, lipids can also be preserved in rock (e.g., serpentinite). Therefore, future research should focus on understanding extinct microbial communities at the Tablelands specifically those preserved in serpentinites.

Future research should also focus on the origin of the unique geochemistry at Aqua de Ney. Specifically, whether these fluids are a product of evaporation occurring in the cistern or the product of a dehydrating slab as suggested by Boschetti et al. (2017). Although it was not a topic of this thesis, methane can be introduced to serpentinizing fluids through fluid inclusion mining (e.g., Wang et al., 2018). Although clumped isotope thermometry of methane from the Tablelands indicates an apparent temperature of 85 ± 7 °C (Cumming et al., 2018), this concept has not been explored for Aqua de Ney. Future work should focus on analysis of clumped

isotopologues of methane from Aqua de Ney which could help provide a more thorough understanding of the methane present at this site.

Finally, although sites of terrestrial serpentinization are often used as analogues for serpentinization on Mars there are important differences that should be acknowledged. Specifically, the olivine on Mars is much more iron rich than the olivine on Earth. This could have important implications for the geochemistry and the H₂ concentrations at these sites. The impact of iron rich olivine and increased H₂ concentrations on the thermodynamic predictions for potential energy in serpentinizing fluids should be explored to better understand energy available for microbial metabolisms in the subsurface of Mars.

References

- Abrajano, T. A., Sturchio, N. C., Bohlke, J. K., Lyon, G. L., Poreda, R. J., & Stevens, C. M. (1988). Methane-hydrogen gas seeps, Zambales Ophiolite, Philippines: Deep or shallow origin? *Chemical geology*, 71(1), 211-222. [https://doi.org/10.1016/0009-2541\(88\)90116-7](https://doi.org/10.1016/0009-2541(88)90116-7)
- Ahlgren, G., Gustafsson, I.-B., & Boberg, M. (1992). FATTY ACID CONTENT AND CHEMICAL COMPOSITION OF FRESHWATER MICROALGAE. *Journal of phycology*, 28(1), 37-50. <https://doi.org/10.1111/j.0022-3646.1992.00037.x>
- Amend, J. P., & Shock, E. L. (2001). Energetics of overall metabolic reactions of thermophilic and hyperthermophilic Archaea and Bacteria. *FEMS microbiology reviews*, 25(2), 175-243. [https://doi.org/10.1016/S0168-6445\(00\)00062-0](https://doi.org/10.1016/S0168-6445(00)00062-0)
- Bach, W., Paulick, H., Garrido, C. J., Ildefonse, B., Meurer, W. P., & Humphris, S. E. (2006). Unraveling the sequence of serpentinization reactions: petrography, mineral chemistry, and petrophysics of serpentinites from MAR 15°N (ODP Leg 209, Site 1274). *Geophysical research letters*, 33(13), L13306-n/a. <https://doi.org/10.1029/2006GL025681>
- Barnes, I., LaMarche, V. C., & Himmelberg, G. (1967). Geochemical Evidence of Present-Day Serpentinization. *Science (American Association for the Advancement of Science)*, 156(3776), 830-832. <https://doi.org/10.1126/science.156.3776.830>
- Baumann, L. M. F., Taubner, R.-S., Bauersachs, T., Steiner, M., Schleper, C., Peckmann, J., Rittmann, S. K. M. R., & Birgel, D. (2018). Intact polar lipid and core lipid inventory of the hydrothermal vent methanogens *Methanocaldococcus villosus* and

- Methanothermococcus okinawensis. *Organic geochemistry*, 126, 33-42.
<https://doi.org/10.1016/j.orggeochem.2018.10.006>
- Bentley, J. N. (2019). *The Origins and Fate of Archaeal Intact Polar Lipids in Hydrothermally Altered Sediments of Cathedral Hill, Guaymas Basin, Gulf of California* [Saint Mary's University].
- Biemann, K., Oro, J., Toulmin III, P., Orgel, L. E., Nier, A. O., Anderson, D. M., Simmonds, P. G., Flory, D., Diaz, A. V., Rushneck, D. R., Biller, J. E., & Lafleur, A. L. (1977). The search for organic substances and inorganic volatile compounds in the surface of Mars. *Journal of Geophysical Research (1896-1977)*, 82(28), 4641-4658.
<https://doi.org/https://doi.org/10.1029/JS082i028p04641>
- Biemann, K., Oro, J., Toulmin, P., Orgel, L. E., Nier, A. O., Anderson, D. M., Simmonds, P. G., Flory, D., Diaz, A. V., Rushneck, D. R., & Biller, J. A. (1976). Search for Organic and Volatile Inorganic Compounds in Two Surface Samples from the Chryse Planitia Region of Mars. *Science*, 194(4260), 72-76. <https://doi.org/doi:10.1126/science.194.4260.72>
- Bizic, M., Klintzsch, T., Ionescu, D., Hindiyeh, M. Y., Gunthel, M., Muro-Pastor, A. M., Eckert, W., Urich, T., Keppler, F., & Grossart, H. P. (2020). Aquatic and terrestrial cyanobacteria produce methane. *Science advances*, 6(3). <https://doi.org/10.1126/sciadv.aax5343>
- Blank, J. G., Etiope, G., Stamenković, V., Rowe, A. R., Kohl, I., Li, S., & Young, E. D. (2017). *Methane at the Aqua de Ney hyperalkaline spring (N. California USA), a site of active serpentinization*. Paper presented at the Astrobiology Science Conference 2017, Mesa, Arizona, USA.
- Blank, J. G., Green, S. J., Blake, D., Valley, J. W., Kita, N. T., Treiman, A., & Dobson, P. F. (2009). An alkaline spring system within the Del Puerto Ophiolite (California, USA): A

- Mars analog site. *Planetary and space science*, 57(5), 533-540.
<https://doi.org/10.1016/j.pss.2008.11.018>
- Blumenberg, M., Seifert, R., Reitner, J., Pape, T., & Michaelis, W. (2004). Membrane Lipid Patterns Typify Distinct Anaerobic Methanotrophic Consortia. *Proceedings of the National Academy of Sciences - PNAS*, 101(30), 11111-11116.
<https://doi.org/10.1073/pnas.0401188101>
- Boschetti, T., Toscani, L., Iacumin, P., & Selmo, E. (2017). Oxygen, Hydrogen, Boron and Lithium Isotope Data of a Natural Spring Water with an Extreme Composition: A Fluid from the Dehydrating Slab? *Aquatic geochemistry*, 23(5), 299-313.
<https://doi.org/10.1007/s10498-017-9323-9>
- Boschker, H. T. S., & Middelburg, J. J. (2002). Stable isotopes and biomarkers in microbial ecology. *FEMS Microbiology Ecology*, 40(2), 85-95. [https://doi.org/10.1016/S0168-6496\(02\)00194-0](https://doi.org/10.1016/S0168-6496(02)00194-0)
- Boston, P. J., Ivanov, M. V., & P. McKay, C. (1992). On the possibility of chemosynthetic ecosystems in subsurface habitats on Mars. *Icarus (New York, N.Y. 1962)*, 95(2), 300-308. [https://doi.org/10.1016/0019-1035\(92\)90045-9](https://doi.org/10.1016/0019-1035(92)90045-9)
- Boudier, F., Sueur, E. L., & Nicolas, A. (1989). Structure of an atypical ophiolite: The Trinity complex, eastern Klamath Mountains, California. *Geological Society of America Bulletin*, 101(6), 820-833.
- Bradley, A. S., Fredricks, H., Hinrichs, K.-U., & Summons, R. E. (2009). Structural diversity of diether lipids in carbonate chimneys at the Lost City Hydrothermal Field. *Organic geochemistry*, 40(12), 1169-1178. <https://doi.org/10.1016/j.orggeochem.2009.09.004>

- Bradley, A. S., & Summons, R. E. (2010). Multiple origins of methane at the Lost City Hydrothermal Field. *Earth and planetary science letters*, 297(1), 34-41.
<https://doi.org/10.1016/j.epsl.2010.05.034>
- Brazelton, W. J., Morrill, P. L., Szponar, N., & Schrenk, M. O. (2013). Bacterial Communities Associated with Subsurface Geochemical Processes in Continental Serpentinite Springs. *Applied and Environmental Microbiology*, 79(13), 3906-3916.
<https://doi.org/10.1128/AEM.00330-13>
- Brazelton, W. J., Nelson, B., & Schrenk, M. O. (2012). Metagenomic Evidence for H₂ Oxidation and H₂ Production by Serpentinite-Hosted Subsurface Microbial Communities. *Frontiers in Microbiology*, 2. <https://doi.org/10.3389/fmicb.2011.00268>
- Brazelton, W. J., Schrenk, M. O., Kelley, D. S., & Baross, J. A. (2006). Methane- and Sulfur-Metabolizing Microbial Communities Dominate the Lost City Hydrothermal Field Ecosystem. *Applied and Environmental Microbiology*, 72(9), 6257-6270.
<https://doi.org/10.1128/AEM.00574-06>
- Brazelton, W. J., Thornton, C. N., Hyer, A., Twing, K. I., Longino, A. A., Lang, S. Q., Lilley, M. D., Früh-Green, G. L., & Schrenk, M. O. (2017). Metagenomic identification of active methanogens and methanotrophs in serpentinite springs of the Voltri Massif, Italy. *PeerJ (San Francisco, CA)*, 5, e2945-e2945. <https://doi.org/10.7717/peerj.2945>
- Brock, T. D. (1991). *Biology of microorganisms* (6th ed.. ed.). Englewood Cliffs, N.J. : Prentice Hall.
- Bruni, J., Canepa, M., Chiodini, G., Cioni, R., Cipolli, F., Longinelli, A., Marini, L., Ottonello, G., & Vetuschi Zuccolini, M. (2002). Irreversible water-rock mass transfer accompanying the generation of the neutral, Mg-HCO₃ and high-pH, Ca-OH spring

- waters of the Genova province, Italy. *Applied geochemistry*, 17(4), 455-474.
[https://doi.org/10.1016/S0883-2927\(01\)00113-5](https://doi.org/10.1016/S0883-2927(01)00113-5)
- Canovas, P. A., Hoehler, T., & Shock, E. L. (2017). Geochemical bioenergetics during low-temperature serpentinization: An example from the Samail ophiolite, Sultanate of Oman. *Journal of Geophysical Research: Biogeosciences*, 122(7), 1821-1847.
<https://doi.org/10.1002/2017JG003825>
- Chen, K., Ríos, J. J., Pérez-Gálvez, A., & Roca, M. (2015). Development of an accurate and high-throughput methodology for structural comprehension of chlorophylls derivatives. (I) Phytylated derivatives. *Journal of Chromatography A*, 1406, 99-108.
<https://doi.org/10.1016/j.chroma.2015.05.072>
- Clark, I. D., & Fritz, P. (1997). *Environmental isotopes in hydrogeology*. Boca Raton, FL : Lewis Publishers.
- Coleman, R., G. (2000). Prospecting for ophiolites along the California continental margin. *Special papers (Geological Society of America)*, 349, 351. <https://doi.org/10.1130/0-8137-2349-3.351>
- Coleman, R. G. (2004). Geologic nature of the Jasper Ridge Biological Preserve, San Francisco Peninsula, California. *International Geology Review*, 46(7), 629-637.
<http://pubs.er.usgs.gov/publication/70027010>
- Cook, M. C., Blank, J. G., Rietze, A., Suzuki, S., Nealson, K. H., & Morrill, P. L. (2021). A Geochemical Comparison of Three Terrestrial Sites of Serpentinization: The Tablelands, The Cedars, and Aqua de Ney. *Journal of geophysical research. Biogeosciences*.
<https://doi.org/10.1029/2021JG006316>

- Cook, M. C., Blank, J. G., Suzuki, S., Neelson, K. H., & Morrill, P. L. (2021b). Assessing Geochemical Bioenergetics and Microbial Metabolisms at Three Terrestrial Sites of Serpentinization: The Tablelands (NL, CAN), The Cedars (CA, USA), and Aqua de Ney (CA, USA). *Journal of geophysical research. Biogeosciences*, 126(6), n/a.
<https://doi.org/10.1029/2019JG005542>
- Coplen, T. B. (2011). Guidelines and recommended terms for expression of stable-isotope-ratio and gas-ratio measurement results: Guidelines and recommended terms for expressing stable isotope results. *Rapid communications in mass spectrometry*, 25(17), 2538-2560.
<https://doi.org/10.1002/rcm.5129>
- Coplen, T. B., & Kendall, C. (2000). Stable Hydrogen and Oxygen Isotope Ratios for Selected Sites of the U.S. Geological Survey's NASQAN and Benchmark Surface-Water Networks.
- Crespo-Medina, M., Twing, K. I., Kubo, M. D. Y., Hoehler, T. M., Cardace, D., McCollom, T., & Schrenk, M. O. (2014). Insights into environmental controls on microbial communities in a continental serpentinite aquifer using a microcosm-based approach. *Frontiers in Microbiology*, 5, 604-604. <https://doi.org/10.3389/fmicb.2014.00604>
- Cumming, E. A., Rietze, A., Morrissey, L. S., Cook, M. C., Rhim, J. H., Ono, S., & Morrill, P. L. (2019). Potential sources of dissolved methane at the Tablelands, Gros Morne National Park, NL, CAN: A terrestrial site of serpentinization. *Chemical geology*, 514, 42-53.
<https://doi.org/10.1016/j.chemgeo.2019.03.019>
- Daae, F. L., Økland, I., Dahle, H., Jørgensen, S. L., Thorseth, I. H., & Pedersen, R. B. (2013). Microbial life associated with low-temperature alteration of ultramafic rocks in the Leka ophiolite complex. *Geobiology*, 11(4), 318-339. <https://doi.org/10.1111/gbi.12035>

- Danovaro, R., Dell'Anno, A., Corinaldesi, C., Magagnini, M., Noble, R., Tamburini, C., & Weinbauer, M. (2008). Major viral impact on the functioning of benthic deep-sea ecosystems. *Nature*, 454, 1084-1109. <https://doi.org/10.1038/nature07268>
- Dunning, G. R., & Krogh, T. E. (1985). Geochronology of ophiolites of the Newfoundland Appalachians. *Canadian journal of earth sciences*, 22(11), 1659-1670. <https://doi.org/10.1139/e85-174>
- Dygert, N., Liang, Y., & Kelemen, P. B. (2016). Formation of Plagioclase Lherzolite and Associated Dunite–Harzburgite–Lherzolite Sequences by Multiple Episodes of Melt Percolation and Melt–Rock Reaction: an Example from the Trinity Ophiolite, California, USA. *Journal of Petrology*, 57(4), 815-838. <https://doi.org/10.1093/petrology/egw018>
- Ehlmann, B. L., Mustard, J. F., & Murchie, S. L. (2010). Geologic setting of serpentine deposits on Mars. *Geophysical research letters*, 37(6), n/a. <https://doi.org/10.1029/2010GL042596>
- Ehlmann, B. L., Mustard, J. F., Murchie, S. L., Bibring, J.-P., Meunier, A., Fraeman, A. A., & Langevin, Y. (2011). Subsurface water and clay mineral formation during the early history of Mars. *Nature (London)*, 479(7371), 53-60. <https://doi.org/10.1038/nature10582>
- Ehlmann, B. L., Mustard, J. F., & Murchie, S. L. (2010). Geologic setting of serpentine deposits on Mars. *Geophysical research letters*, 37(6), n/a. <https://doi.org/10.1029/2010GL042596>
- Ehlmann, B. L., Mustard, J. F., Murchie, S. L., Bibring, J.-P., Meunier, A., Fraeman, A. A., & Langevin, Y. (2011). Subsurface water and clay mineral formation during the early history of Mars. *Nature (London)*, 479(7371), 53-60. <https://doi.org/10.1038/nature10582>
- Elder, D., & Cashman, S. M. (1992). Tectonic control and fluid evolution in the Quartz Hill, California, lode gold deposits. *Economic geology and the bulletin of the Society of Economic Geologists*, 87(7), 1795-1812. <https://doi.org/10.2113/gsecongeo.87.7.1795>

- Etiopio, G., Schoell, M., & Hosgörmez, H. (2011). Abiotic methane flux from the Chimaera seep and Tekirova ophiolites (Turkey): Understanding gas exhalation from low temperature serpentinization and implications for Mars. *Earth and planetary science letters*, 310(1), 96-104. <https://doi.org/10.1016/j.epsl.2011.08.001>
- Etiopio, G., & Sherwood Lollar, B. (2013). ABIOTIC METHANE ON EARTH. *Reviews of geophysics* (1985), 51(2), 276-299. <https://doi.org/10.1002/rog.20011>
- Etiopio, G., & Whiticar, M. J. (2019). Abiotic methane in continental ultramafic rock systems: Towards a genetic model. *Applied geochemistry*, 102, 139-152. <https://doi.org/10.1016/j.apgeochem.2019.01.012>
- Feth, J. H., Rogers, S. M., & Roberson, C. E. (1961). Aqua de Ney, California, a spring of unique chemical character. *Geochimica et cosmochimica acta*, 22(2), 75,IN71,77-76,IN72,86. [https://doi.org/10.1016/0016-7037\(61\)90107-7](https://doi.org/10.1016/0016-7037(61)90107-7)
- Fones, E. M., Colman, D. R., Kraus, E. A., Nothaft, D. B., Poudel, S., Rempfert, K. R., Spear, J. R., Templeton, A. S., & Boyd, E. S. (2019). Physiological adaptations to serpentinization in the Samail Ophiolite, Oman. *The ISME Journal*, 13(7), 1750-1762. <https://doi.org/10.1038/s41396-019-0391-2>
- Formisano, V., Atreya, S., Encrenaz, T., Ignatiev, N., & Giuranna, M. (2004). Detection of Methane in the Atmosphere of Mars. *Science (American Association for the Advancement of Science)*, 306(5702), 1758-1761. <https://doi.org/10.1126/science.1101732>
- Frostegård, Å., & Bååth, E. (1996). The use of phospholipid fatty acid analysis to estimate bacterial and fungal biomass in soil. *Biology and fertility of soils*, 22(1-2), 59-65. <https://doi.org/10.1007/BF00384433>

- Frostegård, Å., Bååth, E., & Tunlio, A. (1993). Shifts in the structure of soil microbial communities in limed forests as revealed by phospholipid fatty acid analysis. *Soil biology & biochemistry*, 25(6), 723-730. [https://doi.org/10.1016/0038-0717\(93\)90113-P](https://doi.org/10.1016/0038-0717(93)90113-P)
- García-Ruiz, J. M., Nakouzi, E., Kotopoulou, E., Tamborrino, L., & Steinbock, O. (2017). Biomimetic mineral self-organization from silica-rich spring waters. *Science advances*, 3(3), e1602285-e1602285. <https://doi.org/10.1126/sciadv.1602285>
- Georgiou, C. D., & Deamer, D. W. (2014). Lipids as Universal Biomarkers of Extraterrestrial Life. *Astrobiology*, 14(6). [https://doi.org/DOI: 10.1089/ast.2013.1134](https://doi.org/DOI:10.1089/ast.2013.1134)
- Giampouras, M., Garrido, C. J., Zwicker, J., Vadillo, I., Smrzka, D., Bach, W., Peckmann, J., Jiménez, P., Benavente, J., & García-Ruiz, J. M. (2019). Geochemistry and mineralogy of serpentinization-driven hyperalkaline springs in the Ronda peridotites. *Lithos*, 350-351, 105215. <https://doi.org/10.1016/j.lithos.2019.105215>
- Gold, T. (1992). The deep, hot biosphere. *Proc Natl Acad Sci U S A*, 89(13), 6045-6049.
- Grassle, J. F. (1987). The Ecology of Deep-Sea Hydrothermal Vent Communities. In J. H. S. Blaxter & A. J. Southward (Eds.), *Advances in Marine Biology* (Vol. 23, pp. 301-362). Academic Press. [https://doi.org/https://doi.org/10.1016/S0065-2881\(08\)60110-8](https://doi.org/https://doi.org/10.1016/S0065-2881(08)60110-8)
- Guckert, J. B., Antworth, C. P., Nichols, P. D., & White, D. C. (1985). Phospholipid, ester-linked fatty acid profiles as reproducible assays for changes in prokaryotic community structure of estuarine sediments. *FEMS microbiology letters*, 31(3), 147-158. [https://doi.org/10.1016/0378-1097\(85\)90016-3](https://doi.org/10.1016/0378-1097(85)90016-3)
- Günthel, M., Donis, D., Kirillin, G., Ionescu, D., Bizic, M., McGinnis, D. F., Grossart, H.-P., & Tang, K. W. (2019). Contribution of oxic methane production to surface methane

- emission in lakes and its global importance. *Nature communications*, *10*(1), 5497-5410.
<https://doi.org/10.1038/s41467-019-13320-0>
- Hans-Peter, G., Katharina, F., Claudia, D., Werner, E., & Kam, W. T. (2011). Microbial methane production in oxygenated water column of an oligotrophic lake. *Proceedings of the National Academy of Sciences - PNAS*, *108*(49), 19657-19661.
<https://doi.org/10.1073/pnas.1110716108>
- Harmon, C. (1961). Isotopic Variations in Meteoric Waters. *Science (American Association for the Advancement of Science)*, *133*(3465), 1702-1703.
<https://doi.org/10.1126/science.133.3465.1702>
- Helgeson, H. C., & Murphy, W. M. (1983). Calculation of mass transfer among minerals and aqueous solutions as a function of time and surface area in geochemical processes. I. computational approach. *Journal of the International Association for Mathematical Geology*, *15*(1), 109-130. <https://doi.org/10.1007/BF01030078>
- Hinrichs, K.-U., Lipp, J. S., Morono, Y., & Inagaki, F. (2008). Significant contribution of Archaea to extant biomass in marine subsurface sediments. *Nature (London)*, *454*(7207), 991-994. <https://doi.org/10.1038/nature07174>
- Horibe, Y., & Craig, H. (1995). D/H fractionation in the system methane-hydrogen-water. *Geochimica et cosmochimica acta*, *59*(24), 5209-5217. [https://doi.org/10.1016/0016-7037\(95\)00391-6](https://doi.org/10.1016/0016-7037(95)00391-6)
- Howells, A. E. G., Leong, J. A. M., Ely, T., Santana, M., Robinson, K., Esquivel-Elizondo, S., Cox, A., Poret-Peterson, A., Krajmalnik-Brown, R., & Shock, E. L. (2022). Energetically Informed Niche Models of Hydrogenotrophs Detected in Sediments of Serpentinized

- Fluids of the Samail Ophiolite of Oman. *Journal of geophysical research. Biogeosciences*, 127(3), n/a. <https://doi.org/10.1029/2021JG006317>
- Jarrell, K. F. (1985). Extreme Oxygen Sensitivity in Methanogenic Archaeobacteria. *BioScience*, 35(5), 298-302. <https://doi.org/10.2307/1309929>
- Kelley, D. S., Karson, J. A., Jakuba, M., Bradley, A., Larson, B., Ludwig, K., Glickson, D., Buckman, K., Bradley, A. S., Brazelton, W. J., Roe, K., Elend, M. J., Fr  H-Green, G. L., Delacour, A., Bernasconi, S. M., Lilley, M. D., Baross, J. A., Summons, R. E., Sylva, S. P., . . . Proskurowski, G. (2005). A Serpentinite-Hosted Ecosystem: The Lost City Hydrothermal Field. *Science (American Association for the Advancement of Science)*, 307(5714), 1428-1434. <https://doi.org/10.1126/science.1102556>
- Kendall, C., & Coplen, T. B. (2001). Distribution of oxygen-18 and deuterium in river waters across the United States. *Hydrological processes*, 15(7), 1363-1393. <https://doi.org/10.1002/hyp.217>
- Khatua, S., Pandey, A., & Bisway, S. J. (2016). Phytochemical evaluation and antimicrobial properties of *Trichosanthes dioica* root extract. *Journal of Pharmacognosy and Phytochemistry*, 5(5), 410-413.
- Koga, Y., Morii, H., Akagawa Matsushita, M., & Ohga, M. (1998). Correlation of polar lipid composition with 16S rRNA phylogeny in methanogens: Further analysis of lipid component parts. *Bioscience, biotechnology, and biochemistry*, 62(2), 230-236. <https://doi.org/10.1271/bbb.62.230>
- Koga, Y., Nishihara, M., Morii, H., & Akagawa-Matsushita, M. (1993). Ether polar lipids of methanogenic bacteria: structures, comparative aspects, and biosyntheses. *Microbiological reviews*, 57(1), 164-182. <https://doi.org/10.1128/mr.57.1.164-182.1993>

- Kohl, L., Cumming, E., Cox, A., Rietze, A., Morrissey, L., Lang, S. Q., Richter, A., Suzuki, S., Neelson, K. H., & Morrill, P. L. (2016). Exploring the metabolic potential of microbial communities in ultra-basic, reducing springs at The Cedars, CA, USA: Experimental evidence of microbial methanogenesis and heterotrophic acetogenesis. *Journal of Geophysical Research: Biogeosciences*, 121(4), 1203-1220.
<https://doi.org/10.1002/2015jg003233>
- Kraus, E. A., Nothaft, D., Stamps, B. W., Rempfert, K. R., Ellison, E. T., Matter, J. M., Templeton, A. S., Boyd, E. S., & Spear, J. R. (2021). Molecular Evidence for an Active Microbial Methane Cycle in Subsurface Serpentinite-Hosted Groundwaters in the Samail Ophiolite, Oman. *Applied and Environmental Microbiology*, 87(2).
<https://doi.org/10.1128/AEM.02068-20>
- Krulwich, T. A., Sachs, G., & Padan, E. (2011). Molecular aspects of bacterial pH sensing and homeostasis. *Nature Reviews. Microbiology*, 9(5), 330-343.
<https://doi.org/10.1038/nrmicro2549>
- Lang, S. Q., & Brazelton, W. J. (2020). Habitability of the marine serpentinite subsurface: a case study of the Lost City hydrothermal field. *Philos Trans A Math Phys Eng Sci*, 378(2165), 20180429. <https://doi.org/10.1098/rsta.2018.0429>
- Lang, S. Q., Früh-Green, G. L., Bernasconi, S. M., Brazelton, W. J., Schrenk, M. O., & McGonigle, J. M. (2018). Deeply-sourced formate fuels sulfate reducers but not methanogens at Lost City hydrothermal field. *Scientific Reports*, 8(1), 755.
<https://doi.org/10.1038/s41598-017-19002-5>
- Lang, S. Q., Früh-Green, G. L., Bernasconi, S. M., Lilley, M. D., Proskurowski, G., Méhay, S., & Butterfield, D. A. (2012). Microbial utilization of abiogenic carbon and hydrogen in a

serpentinite-hosted system. *Geochimica et cosmochimica acta*, 92, 82-99.

<https://doi.org/10.1016/j.gca.2012.06.006>

LaRowe, D., & Amend, J. (2014). Energetic constraints on life in marine deep sediments. In (Vol. 1, pp. 279-302). DE GRUYTER. <https://doi.org/10.1515/9783110300130.279>

Lechevalier, M. P., & Moss, C. W. (1977). Lipids in Bacterial Taxonomy - A Taxonomist's View. *CRC Critical Reviews in Microbiology*, 5(2), 109-210.

<https://doi.org/doi:10.3109/10408417709102311>

Lutz, R. A., & Kennish, M. J. (1993). Ecology of deep-sea hydrothermal vent communities: A review. *Reviews of geophysics* (1985), 31(3), 211-242.

<https://doi.org/10.1029/93RG01280>

Marche, B. (2016). *A Climate Study in Western Newfoundland: Precipitation d18O and d2H Examination Using Picarro L2130-I Liquid Water Isotope Analyzer* Memorial University of Newfoundland]. Corner Brook, Newfoundland.

of Newfoundland]. Corner Brook, Newfoundland.

Mariner, R. H., Evans, W. C., Presser, T. S., & White, L. D. (2003). Excess nitrogen in selected thermal and mineral springs of the Cascade Range in northern California, Oregon, and Washington: sedimentary or volcanic in origin? *Journal of volcanology and geothermal research*, 121(1), 99-114. [https://doi.org/10.1016/S0377-0273\(02\)00414-6](https://doi.org/10.1016/S0377-0273(02)00414-6)

Mariner, R. H., Presser, T. S., Evans, W. C., & Pringle, M. K. W. (1990). Discharge rates of fluid and heat by thermal springs of the Cascade Range, Washington, Oregon, and northern California. *Journal of Geophysical Research: Solid Earth*, 95(B12), 19517-19531. <https://doi.org/10.1029/JB095iB12p19517>

- McCollom, T. M., & Seewald, J. S. (2007). Abiotic synthesis of organic compounds in deep-sea hydrothermal environments. *Chem Rev*, *107*(2), 382-401.
<https://doi.org/10.1021/cr0503660>
- McCollom, T. M., & Seewald, J. S. (2013). Serpentinites, hydrogen, and life. *Elements (Quebec)*, *9*(2), 129-134. <https://doi.org/10.2113/gselements.9.2.129>
- McCollom, T. M., & Shock, E. L. (1997). Geochemical constraints on chemolithoautotrophic metabolism by microorganisms in seafloor hydrothermal systems. *Geochimica et cosmochimica acta*, *61*(20), 4375-4391. [https://doi.org/10.1016/s0016-7037\(97\)00241-x](https://doi.org/10.1016/s0016-7037(97)00241-x)
- Méhay, S., Früh-Green, G. L., Lang, S. Q., Bernasconi, S. M., Brazelton, W. J., Schrenk, M. O., Schaeffer, P., & Adam, P. (2013). Record of archaeal activity at the serpentinite-hosted Lost City Hydrothermal Field. *Geobiology*, *11*(6), 570-592.
<https://doi.org/10.1111/gbi.12062>
- Michalski, J. R., Cuadros, J., Niles, P. B., Parnell, J., Deanne Rogers, A., & Wright, S. P. (2013). Groundwater activity on Mars and implications for a deep biosphere. *Nature geoscience*, *6*(2), 133-138. <https://doi.org/10.1038/ngeo1706>
- Miller, H. M., Matter, J. M., Kelemen, P., Ellison, E. T., Conrad, M. E., Fierer, N., Ruchala, T., Tominaga, M., & Templeton, A. S. (2016). Modern water/rock reactions in Oman hyperalkaline peridotite aquifers and implications for microbial habitability. *Geochimica et cosmochimica acta*, *179*(C), 217-241. <https://doi.org/10.1016/j.gca.2016.01.033>
- Morrill, P. L., Brazelton, W. J., Kohl, L., Rietze, A., Miles, S. M., Kavanagh, H., Schrenk, M. O., Ziegler, S. E., & Lang, S. Q. (2014). Investigations of potential microbial methanogenic and carbon monoxide utilization pathways in ultra-basic reducing springs

- associated with present-day continental serpentinization: the Tablelands, NL, CAN. *Frontiers in Microbiology*, 5. <https://doi.org/10.3389/fmicb.2014.00613>
- Morrill, P. L., Kuenen, J. G., Johnson, O. J., Suzuki, S., Rietze, A., Sessions, A. L., Fogel, M. L., & Nealson, K. H. (2013). Geochemistry and geobiology of a present-day serpentinization site in California: The Cedars. *Geochimica et cosmochimica acta*, 109, 222-240. <https://doi.org/10.1016/j.gca.2013.01.043>
- Moser, D. P., Gihring, T. M., Wanger, G., Baker, B. J., Pfiffner, S. M., Lin, L.-H., Onstott, T. C., Brockman, F. J., Fredrickson, J. K., Balkwill, D. L., Dollhopf, M. E., Lollar, B. S., Pratt, L. M., Boice, E., & Southam, G. (2005). Desulfotomaculum and Methanobacterium spp. Dominate a 4- to 5-Kilometer-Deep Fault. *Applied and Environmental Microbiology*, 71(12), 8773-8783. <https://doi.org/10.1128/AEM.71.12.8773-8783.2005>
- Mumma, M. J., Villanueva, G. L., Novak, R. E., Hewagama, T., Bonev, B. P., Disanti, M. A., Mandell, A. M., & Smith, M. D. (2009). Strong Release of Methane on Mars in Northern Summer 2003. *Science (American Association for the Advancement of Science)*, 323(5917), 1041-1045. <https://doi.org/10.1126/science.1165243>
- Murseli, S., Middlestead, P., St-Jean, G., Zhao, X., Jean, C., Crann, C. A., Kieser, W. E., & Clark, I. D. (2019). The Preparation of Water (DIC, DOC) and Gas (CO₂, CH₄) Samples for Radiocarbon Analysis at AEL-AMS, Ottawa, Canada. *Radiocarbon*, 61(5), 1563-1571. <https://doi.org/10.1017/RDC.2019.14>
- Muyzer, G., & Stams, A. J. M. (2008). The ecology and biotechnology of sulphate-reducing bacteria. *Nature Reviews. Microbiology*, 6(6), 441-454. <https://doi.org/http://dx.doi.org/10.1038/nrmicro1892>

- Nathenson, M., Thompson, J. M., & White, L. D. (2003). Slightly thermal springs and non-thermal springs at Mount Shasta, California: Chemistry and recharge elevations. *Journal of volcanology and geothermal research*, *121*(1), 137-153.
[https://doi.org/10.1016/S0377-0273\(02\)00426-2](https://doi.org/10.1016/S0377-0273(02)00426-2)
- Nealson, K. H., Inagaki, F., & Takai, K. (2005). Hydrogen-driven subsurface lithoautotrophic microbial ecosystems (SLiMEs): do they exist and why should we care? *Trends in microbiology (Regular ed.)*, *13*(9), 405-410. <https://doi.org/10.1016/j.tim.2005.07.010>
- Neubeck, A., Sun, L., Müller, B., Ivarsson, M., Hosgörmez, H., Özcan, D., Broman, C., & Schnürer, A. (2017). Microbial Community Structure in a Serpentine-Hosted Abiotic Gas Seepage at the Chimaera Ophiolite, Turkey. *Applied and Environmental Microbiology*, *83*(12). <https://doi.org/10.1128/AEM.03430-16>
- O'Leary, W. M., & Wilkinson, S. G. (1988). *Gram-positive bacteria* (Vol. 1). London Academic Press.
- Oremland, R. S., Miller, L. G., & Whiticar, M. J. (1987). Sources and flux of natural gases from Mono Lake, California. *Geochimica et cosmochimica acta*, *51*(11), 2915-2929.
[https://doi.org/10.1016/0016-7037\(87\)90367-X](https://doi.org/10.1016/0016-7037(87)90367-X)
- Pan, Y., Koopmans, G. F., Bonten, L. T. C., Song, J., Luo, Y., Temminghoff, E. J. M., & Comans, R. N. J. (2014). Influence of pH on the redox chemistry of metal (hydr)oxides and organic matter in paddy soils. *Journal of soils and sediments*, *14*(10), 1713-1726.
<https://doi.org/10.1007/s11368-014-0919-z>
- Pancost, R. D., Hopmans, E. C., & Sinninghe Damsté, J. S. (2001). Archaeal lipids in Mediterranean cold seeps: molecular proxies for anaerobic methane oxidation.

Geochimica et cosmochimica acta, 65(10), 1611-1627. [https://doi.org/10.1016/S0016-7037\(00\)00562-7](https://doi.org/10.1016/S0016-7037(00)00562-7)

Paukert, A. N., Matter, J. M., Kelemen, P. B., Shock, E. L., & Havig, J. R. (2012). Reaction path modeling of enhanced in situ CO₂ mineralization for carbon sequestration in the peridotite of the Samail Ophiolite, Sultanate of Oman. *Chemical geology*, 330-331, 86-100. <https://doi.org/10.1016/j.chemgeo.2012.08.013>

Piper, A. M. (1953). *A graphic procedure in the geochemical interpretation of water analysis / by Arthur M. Piper*. District of Columbia: U.S. Dept. of the Interior, Geological Survey, Water Resources Division, Ground Water Branch, 1953.

Quéméneur, M., Palvadeau, A., Postec, A., Monnin, C., Chavagnac, V., Ollivier, B., & Erauso, G. (2015). Endolithic microbial communities in carbonate precipitates from serpentinite-hosted hyperalkaline springs of the Voltri Massif (Ligurian Alps, Northern Italy). *Environmental science and pollution research international*, 22(18), 13613-13624. <https://doi.org/10.1007/s11356-015-4113-7>

Quick, J. E. (1981). Petrology and petrogenesis of the Trinity peridotite, An upper mantle diapir in the eastern Klamath Mountains, northern California. *Journal of Geophysical Research: Solid Earth*, 86(B12), 11837-11863. <https://doi.org/10.1029/JB086iB12p11837>

Quick, J. E. (1982). The origin and significance of large, tabular dunite bodies in the Trinity peridotite, northern California. *Contributions to mineralogy and petrology*, 78(4), 413-422. <https://doi.org/10.1007/BF00375203>

Rampelotto, P. H. (2016). *Extremophiles and extreme environments*. MDPI - Multidisciplinary Digital Publishing Institute.

- Rempfert, K. R., Miller, H. M., Bompard, N., Nothaft, D., Matter, J. M., Kelemen, P., Fierer, N., & Templeton, A. S. (2017). Geological and Geochemical Controls on Subsurface Microbial Life in the Samail Ophiolite, Oman. *Frontiers in Microbiology*, 8, 56-56.
<https://doi.org/10.3389/fmicb.2017.00056>
- Rency, R., Vasantha, K., & Maruthasalam, A. (2015). Identification of bioactive compounds from ethanolic leaf extracts of *Premnas ratifolia* L. using GC-MS. *Bioscience Discovery*, 6(2), 96-101.
- Rietze, A. (2015). *Investigating geochemistry and habitability of continental sites of serpentinization: the Cedars, California, USA and the Tablelands, Newfoundland, CAN* Memorial University of Newfoundland].
- Routaboul, J. M., Fischer, S. F., & Browse, J. (2000). Trienoic Fatty Acids Are Required to Maintain Chloroplast Function at Low Temperatures. *Plant physiology (Bethesda)*, 124(4), 1697-1705. <https://doi.org/10.1104/pp.124.4.1697>
- Rudd, J. W. M., Hamilton, R. D., & Campbell, N. E. R. (1974). Measurement of Microbial Oxidation of Methane in Lake Water. *Limnology and oceanography*, 19(3), 519-524.
<https://doi.org/10.4319/lo.1974.19.3.0519>
- Sabuda, M. C. (2017). *Biogeochemistry of Environmental Gradients in Serpentinization-Influenced Groundwater at the Coast Range Ophiolite Microbial Observatory, California*: Michigan State University.
- Sabuda, M. C., Brazelton, W. J., Putman, L. I., McCollom, T. M., Hoehler, T. M., Kubo, M. D. Y., Cardace, D., & Schrenk, M. O. (2020). A dynamic microbial sulfur cycle in a serpentinizing continental ophiolite. *Environ Microbiol*, 22(6), 2329-2345.
<https://doi.org/10.1111/1462-2920.15006>

- Sánchez-Murillo, R., Gazel, E., Schwarzenbach, E.M., Crespo-Medina, M., Schrenk, M.O., Boll, J., & Gill, B.C. (2014). Geochemical evidence for active tropical serpentinization in the Santa Elena Ophiolite, Costa Rica: An analog of a humid early Earth? *Geochemistry, Geophysics, Geosystems*, 15(5), 1783-1800.
- Schrenk, M. O., Brazelton, W. J., & Lang, S. Q. (2013). Serpentinization, carbon, and deep life. *Reviews in mineralogy and geochemistry*, 75(1), 575-606.
<https://doi.org/10.2138/rmg.2013.75.18>
- Schrenk, M. O., Kelley, D. S., Bolton, S. A., & Baross, J. A. (2004). Low archaeal diversity linked to seafloor geochemical processes at the Lost City Hydrothermal Field, Mid-Atlantic Ridge. *Environmental microbiology*, 6(10), 1086-1095.
<https://doi.org/10.1111/j.1462-2920.2004.00650.x>
- Schulte, M., Blake, D., Hoehler, T., & McCollom, T. (2006). Serpentinization and Its Implications for Life on the Early Earth and Mars. *Astrobiology*, 6(2), 364-376.
<https://doi.org/10.1089/ast.2006.6.364>
- Seyler, L. M., Brazelton, W. J., McLean, C., Putman, L., Hyer, A., Kubo, M. D., Hoehler, T., Cardace, D., & Schrenk, M. O. (2020). Carbon Assimilation Strategies in Ultrabasic Groundwater: Clues from the Integrated Study of a Serpentinization-Influenced Aquifer. *mSystems*, 5(2), e00607-00619. <https://doi.org/10.1128/mSystems.00607-19>
- Shanks, W. C., Bischoff, J. L., & Rosenbauer, R. J. (1981). Seawater sulfate reduction and sulfur isotope fractionation in basaltic systems: Interaction of seawater with fayalite and magnetite at 200–350°C. *Geochimica et cosmochimica acta*, 45(11), 1977-1995.
[https://doi.org/10.1016/0016-7037\(81\)90054-5](https://doi.org/10.1016/0016-7037(81)90054-5)

- Shervais, J. W., Kimbrough, D. L., Renne, P., Hanan, B. B., Murchey, B., Snow, C. A., Zogman Schuman, M. M., & Beaman, J. (2004). Multi-Stage Origin of the Coast Range Ophiolite, California: Implications for the Life Cycle of Supra-Subduction Zone Ophiolites. *International Geology Review*, 46(4), 289-315. <https://doi.org/10.2747/0020-6814.46.4.289>
- Shervais, J. W., Murchey, B. L., Kimbrough, D. L., Renne, P. R., & Hanan, B. (2005). Radioisotopic and biostratigraphic age relations in the Coast Range Ophiolite, Northern California: Implications for the tectonic evolution of the western Cordillera. *Geological Society of America bulletin*, 117(5-6), 633-653. <https://doi.org/10.1130/B25443.1>
- Shock, E. L., Holland, M., Meyer-Dombard, D. A., Amend, J. P., Osburn, G. R., & Fischer, T. P. (2010). Quantifying inorganic sources of geochemical energy in hydrothermal ecosystems, Yellowstone National Park, USA. *Geochimica et Cosmochimica Acta*, 74(14), 4005-4043. <http://www.sciencedirect.com/science/article/pii/S0016703710001201>
- Simoneit, B. R. T., Lein, A. Y., Peresykin, V. I., & Osipov, G. A. (2004). Composition and origin of hydrothermal petroleum and associated lipids in the sulfide deposits of the Rainbow field (Mid-Atlantic Ridge at 36°N). *Geochimica et cosmochimica acta*, 68(10), 2275-2294. <https://doi.org/10.1016/j.gca.2003.11.025>
- Simoneit, B. R. T., Summons, R. E., & Jahnke, L. L. (1998). Biomarkers as Tracers for Life on Early Earth and Mars. *Origins of life and evolution of biospheres*, 28(4), 475-483. <https://doi.org/10.1023/A:1006508012904>
- Sinninghe Damsté, J. S., Kuypers, M. M. M., Sliemers, O., Lavik, G., Schmid, M., Jørgensen, B. B., Kuenen, J. G., Strous, M., & Jetten, M. S. M. (2003). Anaerobic ammonium oxidation

- by Anammox bacteria in the Black Sea. *Nature (London)*, 422(6932), 608-611.
<https://doi.org/10.1038/nature01472>
- Sleep, N. H., Bird, D. K., & Pope, E. C. (2011). Serpentinite and the dawn of life. *Philosophical transactions. Biological sciences*, 366(1580), 2857-2869.
<https://doi.org/10.1098/rstb.2011.0129>
- Sleep, N. H., Meibom, A., Th, F., Coleman, R. G., & Bird, D. K. (2004). H₂-Rich Fluids from Serpentinization: Geochemical and Biotic Implications. *Proceedings of the National Academy of Sciences - PNAS*, 101(35), 12818-12823.
<https://doi.org/10.1073/pnas.0405289101>
- Sorokin, D. Y., & Kuenen, J. G. (2005). Haloalkaliphilic sulfur-oxidizing bacteria in soda lakes. *FEMS microbiology reviews*, 29(4), 685-702.
<https://doi.org/10.1016/j.femsre.2004.10.005>
- St-Jean, G. (2003). Automated quantitative and isotopic (¹³C) analysis of dissolved inorganic carbon and dissolved organic carbon in continuous-flow using a total organic carbon analyser. *Rapid communications in mass spectrometry*, 17(5), 419-428.
<https://doi.org/10.1002/rcm.926>
- Sturt, H. F., Summons, R. E., Smith, K., Elvert, M., & Hinrichs, K. U. (2004). Intact polar membrane lipids in prokaryotes and sediments deciphered by high-performance liquid chromatography/electrospray ionization multistage mass spectrometry--new biomarkers for biogeochemistry and microbial ecology. *Rapid Commun Mass Spectrom*, 18(6), 617-628. <https://doi.org/10.1002/rcm.1378>
- Suda, K., Ueno, Y., Yoshizaki, M., Nakamura, H., Kurokawa, K., Nishiyama, E., Yoshino, K., Hongoh, Y., Kawachi, K., Omori, S., Yamada, K., Yoshida, N., & Maruyama, S. (2014).

- Origin of methane in serpentinite-hosted hydrothermal systems: The CH₄–H₂–H₂O hydrogen isotope systematics of the Hakuba Happo hot spring. *Earth and planetary science letters*, 386, 112-125. <https://doi.org/10.1016/j.epsl.2013.11.001>
- Suhr, G. (1992). Upper mantle peridotites in the Bay of Islands Ophiolite, Newfoundland: Formation during the final stages of a spreading centre? *Tectonophysics*, 206(1), 31-53. [https://doi.org/10.1016/0040-1951\(92\)90366-E](https://doi.org/10.1016/0040-1951(92)90366-E)
- Suhr, G., & Cawood, P. A. (1993). Structural history of ophiolite obduction, Bay of Islands, Newfoundland. *Geological Society of America bulletin*, 105(3), 399-410. [https://doi.org/10.1130/0016-7606\(1993\)105](https://doi.org/10.1130/0016-7606(1993)105)
- Suzuki, S., Ishii, S., Hoshino, T., Rietze, A., Tenney, A., Morrill, P. L., Inagaki, F., Kuenen, J. G., & Nealson, K. H. (2017). Unusual metabolic diversity of hyperalkaliphilic microbial communities associated with subterranean serpentinization at The Cedars. *ISME J*, 11(11), 2584-2598. <https://doi.org/10.1038/ismej.2017.111>
- Suzuki, S., Ishii, S. i., Hoshino, T., Rietze, A., Tenney, A., Morrill, P. L., et al. (2017). Unusual metabolic diversity of hyperalkaliphilic microbial communities associated with subterranean serpentinization at The Cedars. *The ISME Journal*, 11(11), 2584-2598. <https://doi.org/10.1038/ismej.2017.111>
- Suzuki, S., Ishii, S. i., Wu, A., Cheung, A., Tenney, A., Wanger, G., Kuenen, J. G., & Nealson, K. H. (2013). Microbial diversity in The Cedars, an ultrabasic, ultrareducing, and low salinity serpentinizing ecosystem. *Proceedings of the National Academy of Sciences - PNAS*, 110(38), 15336-15341. <https://doi.org/10.1073/pnas.1302426110>
- Suzuki, S., Kuenen, J. G., Schipper, K., Van der Velde, S., Ishii, S., Wu, A., Sorokin, D. Y., Tenney, A., Meng, X. Y., Morrill, P. L., Kamagata, Y., Muyzer, G., & Nealson, K. H.

- (2014). Physiological and genomic features of highly alkaliphilic hydrogen-utilizing Betaproteobacteria from a continental serpentinizing site. *Nature communications*, 5(1), 3900-3900. <https://doi.org/10.1038/ncomms4900>
- Szponar, N. (2012). *Carbon Cycling at a Site of Present-Day Serpentinization: The Tablelands, Gros Morne National Park* Memorial University of Newfoundland].
- Szponar, N., Brazelton, W. J., Schrenk, M. O., Bower, D. M., Steele, A., & Morrill, P. L. (2013). Geochemistry of a continental site of serpentinization, the Tablelands Ophiolite, Gros Morne National Park: A Mars analogue. *Icarus (New York, N.Y. 1962)*, 224(2), 286-296. <https://doi.org/10.1016/j.icarus.2012.07.004>
- Tiago, I., Chung, A. P., & Verissimo, A. (2004). Bacterial Diversity in a Nonsaline Alkaline Environment: Heterotrophic Aerobic Populations. *Applied and Environmental Microbiology*, 70(12), 7378-7387. <https://doi.org/10.1128/AEM.70.12.7378-7387.2004>
- Twing, K. I., Brazelton, W. J., Kubo, M. D. Y., Hyer, A. J., Cardace, D., Hoehler, T. M., McCollom, T. M., & Schrenk, M. O. (2017). Serpentinization-Influenced Groundwater Harbors Extremely Low Diversity Microbial Communities Adapted to High pH. *Frontiers in Microbiology*, 8, 308-308. <https://doi.org/10.3389/fmicb.2017.00308>
- Vance, S., Harnmeijer, J., Kimura, J., Hussmann, H., Demartin, B., & Brown, J. M. (2007). Hydrothermal systems in small ocean planets. *Astrobiology*, 7(6), 987-1005. <https://doi.org/10.1089/ast.2007.0075>
- Vance, S. D., & Daswani, M. M. (2020). Serpentinite and the search for life beyond Earth. *Philosophical transactions of the Royal Society of London. Series A: Mathematical, physical, and engineering sciences*, 378(2165), 20180421-20180421. <https://doi.org/10.1098/rsta.2018.0421>

- Viviano-Beck, C. E., Murchie, S. L., Beck, A. W., & Dohm, J. M. (2017). Compositional and structural constraints on the geologic history of eastern Tharsis Rise, Mars. *Icarus (New York, N.Y. 1962)*, 284, 43-58. <https://doi.org/10.1016/j.icarus.2016.09.005>
- Volkman, J. K., Jeffrey, S. W., Nichols, P. D., Rogers, G. I., & Garland, C. D. (1989). Fatty acid and lipid composition of 10 species of microalgae used in mariculture. *Journal of experimental marine biology and ecology*, 128(3), 219-240. [https://doi.org/10.1016/0022-0981\(89\)90029-4](https://doi.org/10.1016/0022-0981(89)90029-4)
- Wallin, E. T., & Metcalf, R. V. (1998). Supra-Subduction Zone Ophiolite Formed in an Extensional Forearc: Trinity Terrane, Klamath Mountains, California. *The Journal of geology*, 106(5), 591-608. <https://doi.org/10.1086/516044>
- Wang, D., T. , Gruen, D. S., Sherwood Lollar, B., Kai-Uwe, H., Lucy, C. S., James, F. H., Alexander, N. H., John, W. P., Penny, L. M., Martin, K., Kyle, B. D., Eoghan, P. R., Chelsea, N. S., Daniel, J. R., Jeffrey, S. S., Jennifer, C. M., Harold, F. H., Michael, D. K., Dawn, C., . . . Shuhei, O. (2015). Nonequilibrium clumped isotope signals in microbial methane. *Science (American Association for the Advancement of Science)*, 348(6233), 428-431. <https://doi.org/10.1126/science.aaa4326>
- Wang, D. T., Reeves, E. P., McDermott, J. M., Seewald, J. S., & Ono, S. (2018). Clumped isotopologue constraints on the origin of methane at seafloor hot springs. *Geochimica et cosmochimica acta*, 223, 141-158. <https://doi.org/10.1016/j.gca.2017.11.030>
- White, D. C., Davis, W. M., Nickels, J. S., King, J. D., & Bobbie, R. J. (1979). Determination of the Sedimentary Microbial Biomass by Extractible Lipid Phosphate. *Oecologia*, 40(1), 51-62. <https://doi.org/10.1007/BF00388810>

- White, D. C., Stair, J. O., & Ringelberg, D. B. (1996). Quantitative comparisons of in situ microbial biodiversity by signature biomarker analysis: Microbial diversity. I. *Journal of industrial microbiology*, *17*(3-4), 185-196.
- Wilkinson, S. G. (1988). Gram-negative bacteria. In C. a. W. Ratledge, S.G. (Ed.), *Microbial Lipids* (pp. 299-457). Academic Press.
- Willers, C., Jansen van Rensburg, P. J., & Claassens, S. (2015). Phospholipid fatty acid profiling of microbial communities—a review of interpretations and recent applications. *Journal of applied microbiology*, *119*(5), 1207-1218. <https://doi.org/10.1111/jam.12902>
- Willerslev, E., Hansen, A. J., Rønn, R., Brand, T. B., Barnes, I., Wiuf, C., Gilichinsky, D., Mitchell, D., & Cooper, A. (2004). Long-term persistence of bacterial DNA. *Current biology*, *14*(1), R9-R10. <https://doi.org/10.1016/j.cub.2003.12.012>
- Williams, H. (1979). Appalachian Orogen in Canada. *Canadian journal of earth sciences*, *16*(3), 792-807. <https://doi.org/10.1139/e79-070>
- Wilson, J., Munizzi, J., & Erhardt, A. M. (2020). Preservation methods for the isotopic composition of dissolved carbon species in non-ideal conditions. *Rapid communications in mass spectrometry*, *34*(21), e8903-n/a. <https://doi.org/10.1002/rcm.8903>
- Yang, M., Yang, D., & Yu, X. (2018). Soil microbial communities and enzyme activities in sea-buckthorn (*Hippophae rhamnoides*) plantation at different ages. *PloS one*, *13*(1), e0190959-e0190959. <https://doi.org/10.1371/journal.pone.0190959>
- YSI. (2005). *Measuring ORP on YSI 6-Series Sondes: Tips, Cautions and Limitations*. <https://www.yei.com/File%20Library/Documents/Technical%20Notes/T608-Measuring-ORP-on-YSI-6-Series-Sondes-Tips-Cautions-and-Limitations.pdf>

- Zelles, L. (1999). Fatty acid patterns of phospholipids and lipopolysaccharides in the characterisation of microbial communities in soil: a review. *Biology and fertility of soils*, 29(2), 111-129. <https://doi.org/10.1007/s003740050533>
- Ziegler, S. E., Billings, S. A., Lane, C. S., Li, J., & Fogel, M. L. (2013). Warming alters routing of labile and slower-turnover carbon through distinct microbial groups in boreal forest organic soils. *Soil biology & biochemistry*, 60, 23-32. <https://doi.org/10.1016/j.soilbio.2013.01.001>
- Zhu, C., Lipp, J. S., Wörmer, L., Becker, K. W., Schröder, J., & Hinrichs, K.-U. (2013). Comprehensive glycerol ether lipid fingerprints through a novel reversed phase liquid chromatography–mass spectrometry protocol. *Organic geochemistry*, 65, 53-62. <https://doi.org/10.1016/j.orggeochem.2013.09.012>
- Zwicker, J., Birgel, D., Bach, W., Richoz, S., Smrzka, D., Grasemann, B., Gier, S., Schleper, C., Rittmann, S. K. M. R., Koşun, E., & Peckmann, J. (2018). Evidence for archaeal methanogenesis within veins at the onshore serpentinite-hosted Chimaera seeps, Turkey. *Chemical geology*, 483, 567-580. <https://doi.org/10.1016/j.chemgeo.2018.03.027>